Bergvesenet rapport nr	Intern Journal nr	Internt arkiv nr	Rapport lokalisering	Gradering
BV 3499		Boks nr 13	Nordland	**Åpen**
Kommer fra ..arkiv	Ekstern rapport nr	Oversendt fra	Fortrolig pga	Fortrolig fra dato:
Nordlandske	NGU 86.201			

Tittel

Investigation of the potential of the Tverrfjell portion of the Råna instruction for platinium group element mineralization.

Forfatter	Dato	Bedrift
Sarah-Jane Barnes	01.09. 1986	

Kommune	Fylke	Bergdistrikt	1: 50 000 kartblad	1: 250 000 kartblad
Ballangen	Nordland	Nordlandske	1331 I	

Fagområde	Dokument type	Forekomster
Geologi	Rapport	

Råstofftype	Emneord
Malm/metall	platina

Sammendrag

En betydelig likhet i krystallisasjonsrekkefølge og mineralkjemi mellom Råna-intrusjonen og Bushveld-intrusjonen (Sør-Afrika), som er verdens viktigste platina-kilde, ledet til den tanke at det kunne være en mulighet for en Merensky Reef type platinaforekomst i Tverrfjellet-delen av Råna-intrusjonen.

Etter petrologisk og kjemisk undersøkelse er konklusjonen at Tverrfjell-delen av intrusjonen ikke inneholder noen platina-forekomst, og at muligheten for en slik forekomst andre steder i intrusjonen er svært liten.

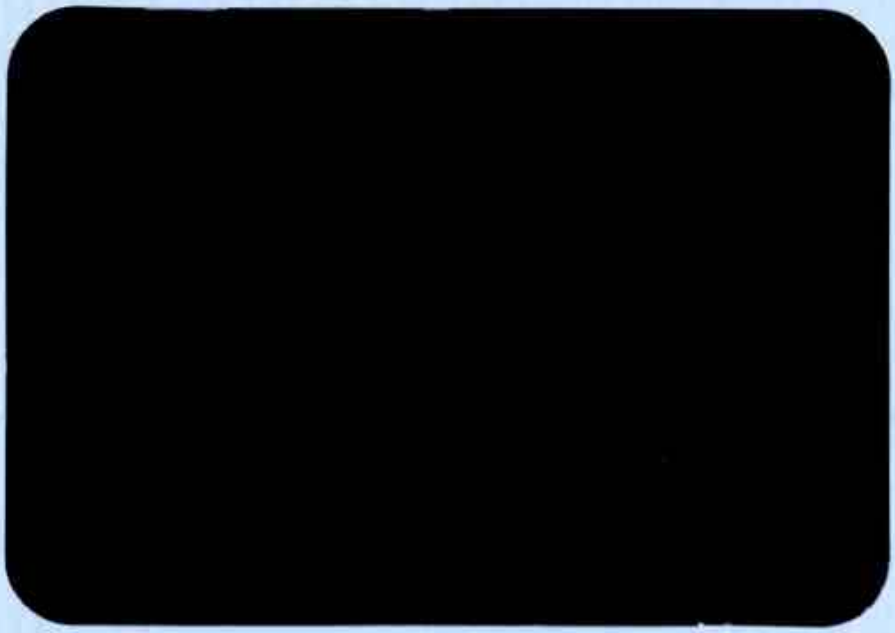

NGU

NGU-rapport nr. 86.201

Investigation of the potential of the Tverrfjell portion of the Råna intrusion for platinum group element mineralization

Norges geologiske undersøkelse

Leiv Eirikssons vei 39, Postboks 3006, 7001 Trondheim - Tlf. (07) 92 16 11
Oslokontor, Drammensveien 230, Oslo 2 - Tlf. (02) 50 25 00

Rapport nr. 86.201	ISSN 0800-3416	Åpen ~~Fortrolig~~

Tittel:
Investigation of the potential of the Tverrfjell portion of the Råna intrusion for platinum group element mineralization.

Forfatter:
Sarah-Jane Barnes

Oppdragsgiver:
LKAB, NTNF og NGU

Fylke:
Nordland

Kommune:
Ballangen

Kartbladnavn (M. 1:250 000)
Narvik

Kartbladnr. og -navn (M. 1:50 000)
1331 I Skjomen

Forekomstens navn og koordinater:
Tverrfjellet 5870-76780

Sidetall: 169 Pris: KR.500.oo

Kartbilag:

Feltarbeid utført:	Rapportdato:	Prosjektnr.:	Prosjektleder:
1984-85	01.09.86	1887.00	A. Korneliussen

Sammendrag:

En betydelig likhet i krystallisasjonsrekkefølge og mineralkjemi mellom Råna-intrusjonen og Bushveld-intrusjonen (Sør-Afrika), som er verdens viktigste platina-kilde, ledet til den tanke at det kunne være en mulighet for en Merensky Reef type platinaforekomst i Tverrfjellet-delen av Råna-intrusjonen.

Etter en petrologisk og kjemisk undersøkelse er konklusjonen at Tverrfjell-delen av intrusjonen ikke inneholder noen platina-forekomst, og at muligheten for en slik forekomst andre steder i intrusjonen er svært liten.

En sannsynlig forklaring på det lave innholdet av platina og andre edelmetaller i intrusjonen er at edelmetallene har vært oppløst i en sulfidfase som ble fjernet fra primær-magmaet før dannelse av de magmapulsene som formet de tilgjengelige deler av intrusjonen. Magmapulsene har derfor hatt et for lavt platina-innhold til å kunne danne en forekomst, selv om gunstige oppkonsentrasjons-mekanismer kan ha vært aktive i Tverrfjellet.

Emneord	fagrapport	
malmgeologi		
platina		

CONTENTS

SAMMENDRAG

Nikkelmalmen ved Bruvann i Råna-intrusjonen er ekstremt fattig på platinagruppens elementer (PGE). Dette forholdet, i tillegg til en betydelig likhet i mineralkjemi og krystallisasjons-rekkefølge mellom Råna-intrusjonen og Bushveld-intrusjonen i Sør-Afrika som med Merensky Reef er verdens, uten sammenligning, viktigste platinakilde, og Stillwater-intrusjonen i Mantana som har verdens neststørste PGE-forekopmst, antyder at det kunne være en Merensky-type forekomst et annet sted i Råna-intrusjonen. For å undersøke denne muligheten ble Tverrfjell-delen av intrusjonen valgt ut for en detaljert undersøkelse med henblikk på en slik forekomst. Området ble kartlagt i målestokk 1:5000 og ca. 150 prøver ble samlet inn langs 3 traverser.

Disse prøvene er undersøkt petrografisk. Omtrent 2000 mikrosondeanalyser av mineraler er utført. 146 av prøvene er analysert på hoved- og sporelementer, 136 på platinagruppens elementer og 46 på sjeldne jordartselementer.

Hovedkonklusjonen er som følger: Det er ingen edelmetall-forekomst i Tverrfjell-delen av Råna-intrusjonen. De høyeste platinagehaltene er 30-50 ppb mens gjennomsnittet er 6 ppb. Rekognoserende prøvetaking i to andre deler av intrusjonen, Eiterdalen og Rånbogen Ni-sulfid mineraliseringer, har også gitt lave platinagehalter. Det er derfor usannsynlig at intrusjonen inneholder noen platinaforekomst.

Når en forutsetter at edelmetallene i sin helhet inngår i sulfidmineralene, og at sulfidgehaltene er magmatiske, og sammenligner sulfidinnholdet i bergartene med mantel- eller kondritt-verdier, kan man vise at sulfidene er fattige ('depleted') på PGE sammenlignet med Ni og Cu. Begge de nevnte forutsetinger er imidlertid usikre. Istedet for å betrakte PGE-verdiene i 100 % sulfid normalisert mot mantel- eller kondritt-verdier, har en derfor i denne rapporten valgt å vurdere analyseverdiene for Cu og Ni (basemetaller) og PGE i forhold til hverandre.

Bergartene ved Bruvann, Tverrfjellet og Eiterdalen har et anomalt høyt Cu/Ir forhold (447-2380 x 1000) og ved alle disse lokaliteter, samt Rånbogen er også Ni/Ir forholdet høyt (2795-13333 x 1000). Også Cu/Pd (84-214 x 1000) og Ni/Pd (302-1200 x 1000) forholdene er svært høye sammenlignet med

tilsvarende eruptivbergarter som er beskrevet i litteraturen. Ved alle lokaliteter er Ni/Cu forholdet primitivt og Pt viser en tilsvarende opptreden som Pd. Hvis disse karakteristika er et resultat av magmatiske prosesser, så har magmapulsene som danner de synlige deler av Rånaintrusjonen vært fortynnet i platinagruppens elementer sammenlignet med basemetaller.

Bergartskjemien og mineralanalysene indikerer at primærmagmaet for Tverrfjelldelen av Rånaintrusjonen var av en primitiv olivin-tholeiitisk sammensetning med MgO-innhold i størrelsesorden 12 %. Dette magmaet har likhetstrekk med E-MORB eller oseaniske øybue-tholeitter. En mulig forklaring på det uvanlige basemetall/PGE forholdet i Råna-intrusjonen er at den delen av mantelen som smeltet og dannet primærmagmaet for intrusjonen, allerede var fortynnet i edelmetaller på grunn av en tidligere smeltebegivenhet. Imidlertid er utgangsmagmaet for Råna-intrusjonen ikke fortynnet i sterkt inkompatible elementer som Cs, Rb og lette sjeldne jordartsmetaller, og det er derfor lite sannsynlig at det er derivert fra fortynnet mantel. Isotopstudier vil kunne avklare dette spørsmålet.

En enkel oppsmelting av primitiv mantel kan ikke danne så høye basemetall/PGE forhold som det som er observert i Rånaintrusjonen. Restproduktet etter en slik begivenhet vil ha lavere basemetall/PGE forhold enn primitiv mantel. Smelting av fortynnet mantel vil derfor ikke kunne ha dannet et magma med et så høyt basemetall/PGE forhold som det som er observert.

Cu, Pt, Pd og Au inkorporeres ikke i silikatmineraler i særlig grad og silikat krystallfraksjonering vil derfor ikke forandre forholdene mellom Cu og Pt, Pd og Au. Sulfid-akkumulering senker basemetall/edelmetall forholdet. Imidlertid vil separasjon av en mindre andel sulfid før dannelsen av magmapulsene som ble intruderte til sin nåværende posisjon i Rånamassivet øke forholdet mellom basemetaller og PGE i silikatsmelten tilstrekkelig til å danne bergarter tilsvarende de som er observert ved Bruvann, Eiterdalen og Rånbogen. Det er nødvendig med både sulfid og olivin fraksjonering i primærmagmaet før dannelsen av magmapulsene som bergartene ved Tverrfjell er krystallisert fra, for å forklare basemetall/edelmetall forholdene i sulfidene på Tverrfjell.

INVESTIGATION OF THE POTENTIAL FOR PLATINUM GROUP ELEMENT MINERALIZATION IN THE TVERRFJELL PORTION OF THE RÅNA INTRUSION

Sarah-Jane Barnes

SUMMARY

Nickel sulphides from the Bruvann nickel sulphide deposit in the Råna Layered Intrusion are extremely depleted in platinum group elements (PGE). This observation, and the similarities in mineral chemistry and crystallization order between the intrusion and the Bushveld and stillwater layered intrusions led to the suggestion that there might be a Merensky Reef-like platinum deposit present elsewhere in the Råna Layered Intrusion. The Tverrfjell portion of the intrusion was selected for a detailed investigation for such a deposit. The area was mapped on a scale of 1:5000 and over 150 samples were collected along three traverses across the stratigraphy.

These samples were investigated petrographically; over 2000 microprobe analyses of the minerals were made, 146 of the samples were analysed for major and trace elements and 136 for noble metals elements and 46 for REE.

The principle conclusions of the study are as follows:
There is no noble metal deposit in this portion of the intrusion. The highest Pt values obtained were 30-50 ppb, the average was 6 ppb. Reconnaissance work at two other localities in the intrusion, Eiterdalen and Rånabogen, also indicated low Pt values. Therefore it seems unlikely that the intrusion contains any Pt deposit.

As in the case of the Bruvann rocks if the analyses are recalculated to 100 % sulphides the calculated sulphides are depleted in platinum group elements relative to Ni and Cu. The recalculation of the analyses to 100 % sulphides assumes that all the noble metals are in sulphides and that the presently observed sulphur values in the rocks represent the igneous values. Both of these assumptions are questionable, so instead of considering the 100 % sulphide normalized values, this report has considered the whole rock values for Cu and Ni (base metals) and noble metals. The whole rock compositions at Bruvann, Tverrfjell and Eiterdalen are anomalous

in terms of high Cu/Ir (447-2380 x 1000) and at all four localities in terms of Ni/Ir (2795-13333 x 1000) ratios. Similarily the Cu/Pd (84-214 x 1000) and Ni/Pd ratios (302-1200 x 1000) are very high compared with igneous rocks from the literature. At all localities the Ni/Cu ratios 3.5-6.3) are primitive. Pt exhibits a similar behaviour to Pd. If these ratios are the result of igneous processes, then the magma that formed the Råna Layered Intrusion was depleted in platinum group elements relative to base metals.

The whole rock geochemistry and mineral analyses suggest that the liquid from which the Tverrfjell rocks crystallized was a primitive olivine tholeiite with MgO content of the order of 12 %. The initial liquid has affinities with E-MORB or ocean island tholeiites. One possible reason for the unusual base to PGE ratios at Råna is that the mantle which melted to produce the Råna magma was depleted in platinum metals by a previous melting event. The initial liquid at Råna was not depleted in highly incompatible elements such as Cs, Rb and LREE and therefore it seems unlikely that it was derived from depleted mantle. However, this hypothesis cannot be ruled out entirely because the exact nature of E-MORB is still a contraversial subject. Some models suggest that E-MORB is derived from depleted mantle and then contaminated to produce the enrichment of highly incompatible elements. Isotope work will be necessary to rule out this option completely.

A single stage partial melting event of primitive mantle could not produce such high base to PGE ratios and the restite of such an event would have lower base to PGE ratios than primitive mantle, therefore melting of depleted mantle will not produce a magma with high base PGE ratios.

Cu, Pt, Pd and Au are not incorporated into silicate minerals to any large degree therefore silicate crystal fractionation will not change the Cu to Pt, Pd or Au ratios. Sulphide accumulation decreases the base to noble metal ratios, therefore cumulate processes in primitive magma will not produce rocks with high base to noble metal ratios. However, removal of a small amount of sulphide prior to the emplacement of the magma pulse to their present position would increase the base metal to PGE ratios in the silicate melt sufficiently to generate rocks similar to those observed at three of the localities. In order to account for the base metal/PGE ratios

observed at Tverrfjell sulphide and olivine fractionation prior to separation and emplacement of the magma pulse from which these rocks crystallized is necessary.

INVESTIGATION OF THE POTENTIAL FOR PLATINUM GROUP ELEMENT MINERALIZATION IN THE TVERRFJELL PORTION OF THE RÅNA INTRUSION

Sarah-Jane Barnes

1 INTRODUCTION

The Råna intrusion is a layered mafic to ultramafic intrusion located approximately 20 km southwest of Narvik in Nordland (Fig. 1).

In the northwestern portion of the intrusion (at Bruvann) there is a nickel sulphide deposit. The average Pd, Pt, Ni and Cu content in 100 % sulphides are 70 ppb, 52 ppb, 9.0 % and 2.1 % respectively (Boyd et al., 1986). These Pd and Pt values are very low when compared to Pd and Pt values from sulphides containing similar amounts of Ni and Cu (e.g. Naldrett, 1981).

The low platinum group element (PGE) values at Bruvann suggest that the magma pulse from which the nickel sulphides formed was depleted in PGE at the time of formation of these sulphides. Two possible reasons for this are: 1) that conditions during the partial melting event that produced the Råna magma generated a magma containing low concentrations of PGE or: 2) that the magma originally had a normal PGE content which was scavanged from the magma prior to its emplacement at Bruvann. This investigation will explore both possibilities.

The scavanging of PGE from the magma prior to its emplacement at Bruvann could have resulted in the formation of a PGE deposit. There are two types of economic PGE deposit.

a) Type I or PGE-dominated deposits, e.g. the Merensky and other reefs that occur within the Bushweld Complex as layers that are 1-2 m thick, containing 0.5-2 % sulphides, in a 10 km thick layered intrusion. The Merensky reef is mined principally for its PGE; average grades vary from 8 to 27 g/tonne. Three other examples of the Type I ore occur; in the Stillwater Complex of Montana, in the Lac des Isles Complex of Ontario and in the Penikat intrusion in Finland; none of these is presently mined.

Fig. 1 Simplified geological map of the Råna Layered Intrusion, modified after Boyd and Mathiesen (1979).

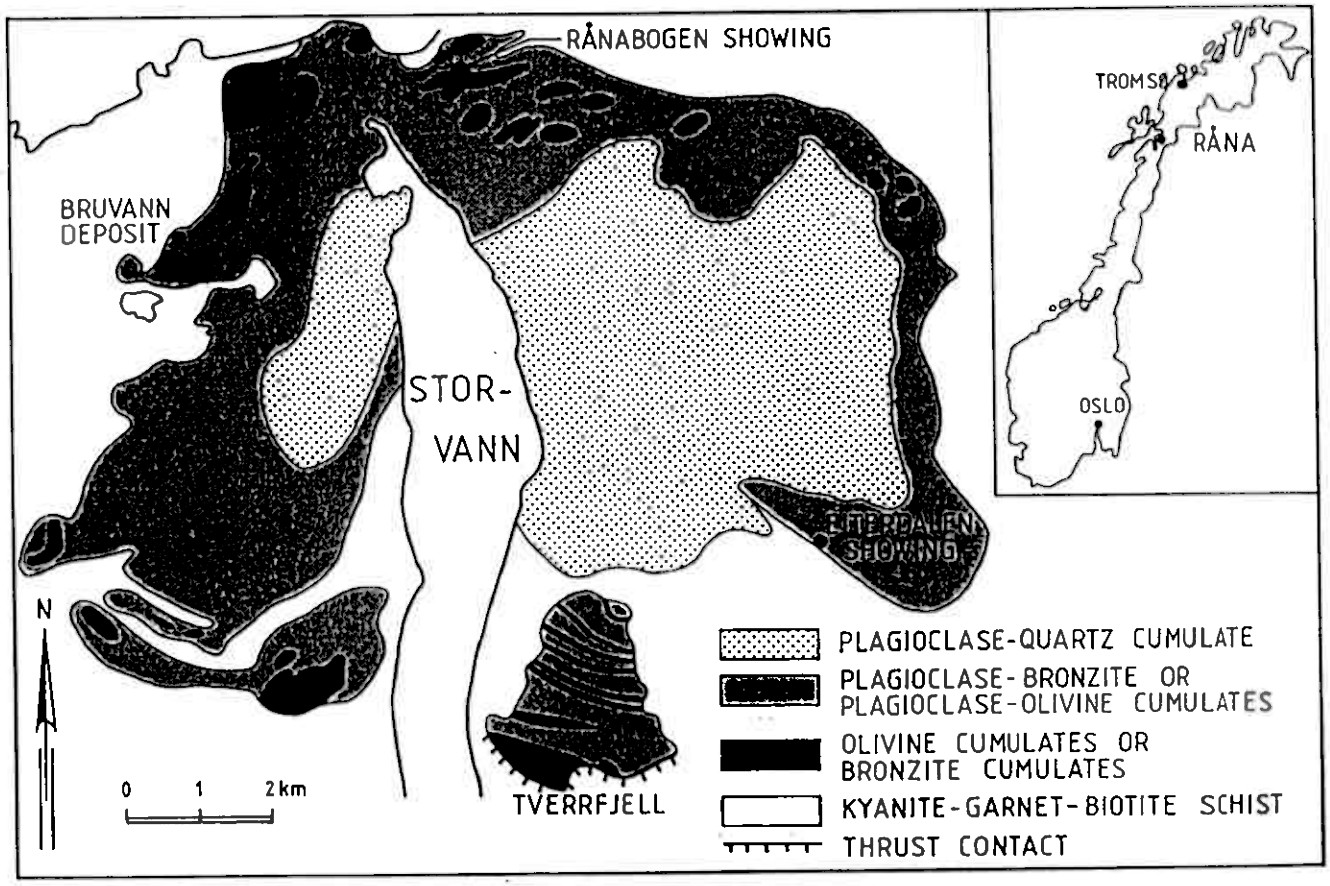

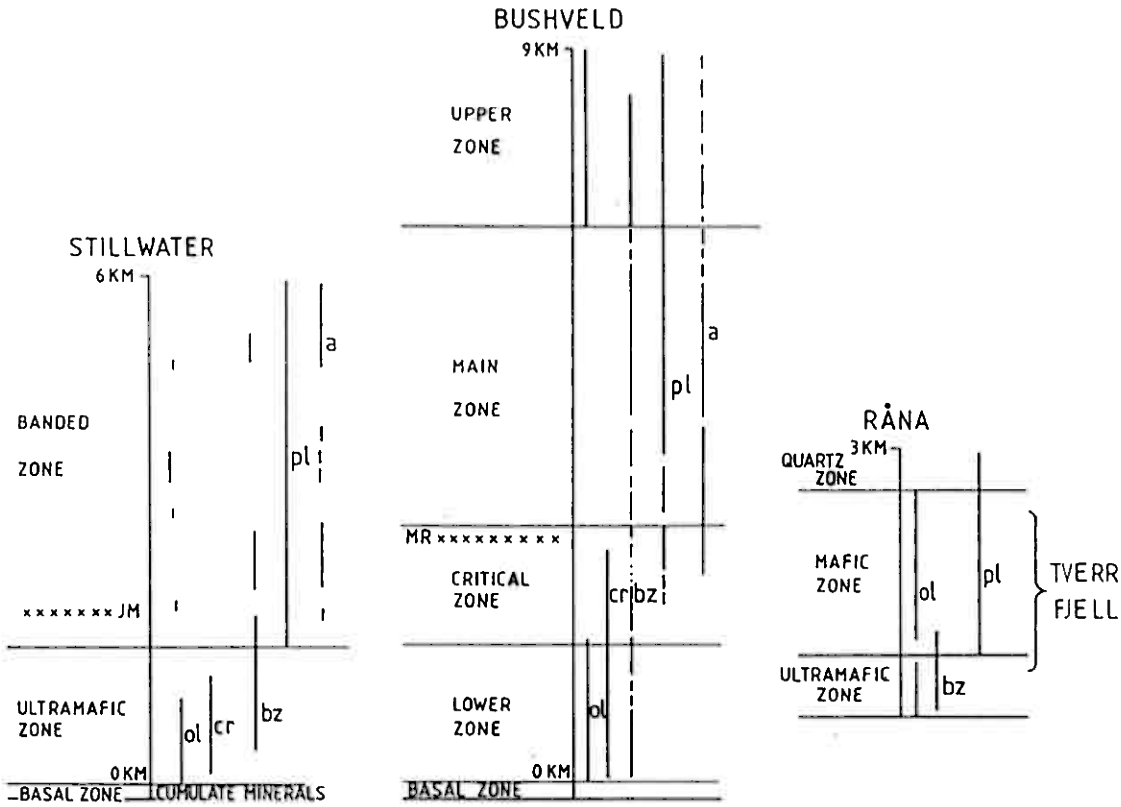

Fig. 2 Comparison of the cumulate stratigraphies of the Stillwater, Bushveld and Rana Layered intrusion. Data for Stillwater from Zientek et al. (1985); for the Bushveld von Gruenewaldt (1985) and Atkins (1969). ol=olivine, cr=chromite, bz=bronzite, pl=plagioclase, a=clinopyroxene, XXXJM=JM reef, XXXXMR = Merensky reef.

TABLE 1
COMPARISON OF THE TERMINOLOGY USED IN THIS WORK WITH THAT OF STRECKEISEN (1976)

Cumulate Minerals	Abbreviation	Streckeisen (1976)
olivine and minor chromite	oC	plagioclase harzburgite mela-olivine norite mela-olivine gabbronorite mela-troctolite
bronzite	bC	mela-norite mela-olivine norite
plagioclase and bronzite	pbC	norite olivine norite
olivine and plagioclase	opC	mela-troctolite mela-olivine gabbro olivine gabbronorite troctolite
plagioclase and olivine	poC	gabbro, olivine gabbro gabbronorite, troctolite norite

TABLE 2
CORRELATION MATRIX

	SiO2	TiO2	Al2O3	Fe2O3	MnO	MgO	CaO	Na2O	K2O	P2O5	S	Rb	Ba	Sr	Ce	Ni	Cr	V	Y	Zr	Nb	Th	Pb	Au	Se	Cs	Co	Sc	Hf	La	Ce	Sm	Eu	Tb
SiO2	1																																	
TiO2	0.332	1																																
Al2O3	0.481	-0.139	1																															
Fe2O3	-0.715	-0.009	-0.914	1																														
MnO	-0.568	0.36	-0.907	0.765	1																													
MgO	-0.668	-0.021	-0.957	0.96	0.773	1																												
CaO	0.3	-0.038	0.924	-0.919	-0.754	-0.948	1																											
Na2O	0.49	-0.029	0.902	-0.845	-0.734	-0.918	0.883	1																										
K2O	0.441	0.156	0.563	-0.583	-0.429	-0.624	0.579	0.645	1																									
P2O5	-0.156	0.672	-0.319	0.163	0.178	0.126	-0.114	-0.091	-0.021	1																								
S	-0.358	0.222	-0.512	0.586	0.425	0.523	-0.356	-0.379	-0.366	0.341	1																							
Rb	0.414	0.267	0.201	-0.278	-0.077	-0.201	0.168	0.221	0.449	0.047	-0.16	1																						
Ba	0.614	0.547	0.169	-0.347	-0.034	-0.339	0.254	0.346	0.498	-0.002	-0.215	0.484	1																					
Sr	0.331	-0.002	0.709	-0.742	-0.647	-0.749	0.739	0.716	0.466	0.017	-0.447	0.331	0.052	1																				
Ce	-0.391	0.074	-0.444	0.437	0.459	0.443	-0.457	-0.443	-0.503	0.099	0.434	-0.214	-0.195	-0.447	1																			
Ni	-0.695	-0.001	-0.098	0.632	0.359	0.882	-0.817	-0.778	-0.548	0.076	0.687	-0.248	-0.345	-0.671	0.736	1																		
Cr	-0.002	0.174	-0.591	0.401	0.411	0.319	-0.521	-0.539	-0.372	-0.102	0.263	-0.018	0.047	-0.543	0.512	0.521	1																	
V	0.548	0.419	-0.13	-0.109	0.095	-0.086	0.032	-0.094	0.085	-0.131	0.139	0.142	0.414	-0.229	0.026	-0.154	0.412	1																
Y	0.482	0.632	0.052	-0.263	-0.046	-0.255	0.261	0.304	0.368	0.107	-0.121	0.343	0.767	0.026	-0.151	-0.267	0.174	0.349	1															
Zr	0.785	0.435	0.017	-0.124	0.004	-0.171	0.158	0.179	0.281	0.272	-0.059	0.325	0.483	-0.063	-0.214	-0.158	0.461	0.267	0.744	1														
Nb	0.022	0.015	0.044	-0.015	-0.053	-0.055	0.014	0.078	0.028	-0.034	-0.048	-0.017	-0.022	0.022	0.058	-0.044	-0.107	-0.005	-0.049	-0.037	1													
Th	0.171	0.158	-0.122	0.048	0.119	0.049	-0.142	-0.104	0.014	-0.047	0.029	0.109	0.195	-0.119	0.173	0.023	0.192	0.139	0.123	0.142	0.161	1												
Pb	0.143	0.079	-0.104	0.047	0.065	0.058	-0.126	-0.178	-0.045	-0.071	0.152	-0.028	0.061	0.063	0.045	-0.029	0.066	0.158	0.116	0.017	0.132	0.344	1											
Au	0.018	-0.027	-0.025	0.048	0.027	0.041	-0.105	-0.098	-0.014	-0.112	0.238	-0.047	-0.041	-0.046	0.146	0.013	-0.026	0.073	-0.135	-0.154	0.094	0.304	0.341	1										
Se	-0.137	0.007	-0.153	0.197	0.232	0.156	-0.149	-0.115	-0.168	0.058	0.132	-0.191	-0.204	-0.054	0.092	0.111	-0.083	-0.043	-0.179	-0.134	0.318	0.121	0.014	-0.045	1									
Cs	0.098	0.078	0.187	-0.208	-0.256	-0.179	0.187	0.208	0.347	0.052	-0.162	0.134	0.039	0.313	-0.184	-0.269	-0.078	-0.016	-0.018	0.068	-0.379	-0.205	-0.125	-0.194	-0.134	1								
Co	-0.614	0.151	-0.701	0.853	0.557	0.842	-0.791	-0.729	-0.568	0.705	0.663	-0.421	-0.130	-0.343	0.745	0.745	0.356	-0.169	-0.317	-0.196	0.248	0.021	-0.032	0.079	0.361	-0.132	1							
Sc	0.723	0.301	-0.137	-0.176	0.131	-0.136	0.058	-0.063	0.117	-0.098	0.024	0.167	0.402	-0.329	-0.028	-0.265	0.367	0.795	0.568	0.315	0.133	0.232	0.295	0.101	0.011	0.015	-0.137	1						
Hf	0.124	0.263	0.093	-0.248	0.049	-0.219	0.153	0.178	0.003	-0.033	-0.291	0.271	0.591	-0.099	-0.208	-0.226	0.171	0.208	0.531	0.681	0.044	0.225	0.233	0.022	-0.096	0.068	-0.174	0.408	1					
La	0.636	0.647	0.347	-0.271	-0.214	-0.329	0.321	0.368	0.384	0.042	-0.168	-0.011	0.321	0.219	-0.312	-0.299	-0.278	-0.109	0.133	0.313	0.148	0.151	0	0.125	-0.321	-0.011	-0.096	-0.065	-0.127	1				
Ce	0.116	0.248	-0.169	-0.068	0.151	-0.042	-0.077	-0.113	0.129	-0.098	0.013	0.114	0.422	-0.335	0.149	0.466	0.563	0.619	0.618	0.563	0.062	0.151	0.2	0.042	-0.172	0.032	0.015	0.379	0.643	0.258	1			
Sm	0.111	0.283	0.304	-0.127	-0.148	-0.129	0.158	0.258	0.476	0.021	-0.214	0.173	0.616	0.017	-0.376	-0.337	-0.014	0.341	0.691	0.685	0.047	0.152	0.052	-0.037	-0.101	0.065	-0.279	0.566	0.749	0.539	0.649	1		
Eu	0.304	-0.043	0.771	-0.749	-0.524	-0.787	0.781	0.731	0.599	-0.173	-0.488	0.195	0.358	0.533	-0.661	-0.673	-0.489	0.643	0.691	0.125	0.018	0.072	0.052	-0.048	-0.031	0.121	-0.329	0.664	0.314	0.123	0.068	0.569	1	
Tb	0.336	0.204	-0.018	-0.148	0.078	-0.141	0.163	0.017	0.092	-0.036	0.016	0.029	0.486	-0.168	-0.056	-0.112	0.195	0.619	0.484	0.337	-0.032	-0.027	-0.045	0.071	-0.056	0.066	-0.068	0.613	0.142	0.998	0.672	0.647	0.714	1
Yb	0.613	0.647	-0.111	-0.153	0.123	-0.125	0.016	-0.045	0.398	-0.019	0.017	0.112	0.592	-0.349	-0.026	-0.196	0.341	0.762	0.682	0.564	0.252	0.363	0.267	0.219	-0.003	-0.011	-0.075	0.007	0.573	0.184	0.731	0.725	0.161	1
Lu	0.634	0.648	-0.131	-0.129	0.098	-0.098	-0.027	-0.064	0.171	-0.047	-0.016	0.298	0.557	-0.344	-0.005	-0.187	0.345	0.685	0.657	0.529	0.269	0.374	0.307	0.329	-0.004	-0.075	-0.053	0.015	0.191	0.169	1.701	0.658	0.123	0.542

b) Type II or Cu-Ni sulphide-dominated deposits e.g. nickel-copper sulphides at the base of differentiated mafic sills in the Noril'sk area of the U.S.S.R. The PGE are a by-product of the copper-nickel sulphide ore. There are numerous other examples of the type II deposits, the largest producer aside from the Noril'sk area being the Sudbury intrusion in Ontario.

If PGE have been removed from the magma that formed the Bruvann sulphides and formed a PGE deposit, it cannot be in the form of a large nickel sulphide body because otherwise the sulphides at Bruvann would not be so nickel-rich. This suggests a Type I deposit consisting of thin seams containing 1 to 2 % sulphides rich in PGE. In the Bushveld and Stillwater complexes these seams occur in a layered sequence of plagioclase-bronzite cumulates[1] (pbC) and plagioclase cumulates (pC) approximately 500 m above well-layered ultramafic zones. The ultramafic zones are 1 to 1.5 km thick and consist of olivine cumulates (oC), olivinebronzite cumulates (obC), and chromite cumulates (cC) (Fig. 2).

The closest analogy to this setting at Råna is the Tverrfjell portion of the intrusion (Fig. 1). At Tverrfjell, a 200 m thick ultramafic zone consisting of cyclic units of oC and bC is overlain by a 1300 m thick mafic zone of pbC and poC. Since the stratigraphy on Tverrfjell is similar to that of the Bushveld and Stillwater (Fig. 2) this area was selected for investigation for a Type I PGE deposit.

2 REGIONAL SETTING

The outcrop pattern of the Råna intrusion is elliptical and covers approximately 70 square km (Fig. 1). Geophysical evidence suggests that it is cone shaped and plunges north-northwest. At its thickest it is 3000 m thick. The body is believed to have been intruded into clastic sediments during a tensional interlude possibly within the Finnmarkian (500 m.y.) phase and at any rate before the Scandinavian (400 m.y.) phase of the Caledonide

****

[1]The terminology used in this paper is based on Irvine (1982), see Table 1 for equivalent rock names after Streckiesen (1976).

Orogeny (Boyd, in prep.). Subsequently, during the Scandinavian event it and its country rocks were emplaced into their present position as part of a nappe sequence (Boyd, in prep.). The Tverrfjell portion of the intrusion was tectonically separated from the rest of the intrusion during this event. All the contacts with country rock (biotite-garnet-kyanite schist) at Tverrfjell are tectonic. Boyd (in prep.) suggests the the body was originally saucer shaped and was subsequently modified into its present form during deformation. The tectonized nature of the intrusion makes interpretation of the original size and shape difficult.

The intrusion has been subdivided (Boyd, in prep.) into three zones:

a) Ultramafic zone, consisting of alternating harzburgite and pyroxenite layers with occasional minor norite layers.

b) Norite zone, consisting of mela- to leucocratic norite with occasional thin harzburgite layers.

c) Quartz-norite zone, consisting of gabbro-norite.

This terminology is not quite satisfactory for the Tverrfjell portion of the intrusion because the Norite zone consits of gabbros and gabbronorites, therefore instead of Norite Zone the term Mafic Zone will be used in this work. Broadly speaking the Quartz-norite zone outcrops in the central portion of the intrusion, the Norite zone rims the Quartz-norite zone and the Ultramafic zone occurs as a discontinous zone at the margins of the intrusion in the north and south. The nickel sulphide occur interstitially to cumulate olivine in the Ultramafic zone in the north-west sector of the intrusion.

3 STRATIGRAPHY

Three traverses were made across Tverrfjell (Figs. 3 and 4). There are a number of members* and groups in the body, which are distinctive mappable units and which allow correlation to be made from traverse to traverse, Fig. 5. Fig. 5 is intended to represent idealized stratigraphic columns and has been corrected for the effects of topography (assuming a constant dip

Plate 1 Layered Group of unit 1 at loc. 68. Group consists of alternating layers of bC (thicker layers) and pbC. Lense cap for scale.

Plate 2 Banded member 2 of unit 9 at loc. 17. Member consists of convoluted folded layers of oC (dark layers) and poC (light layers). Hammer handle for scale

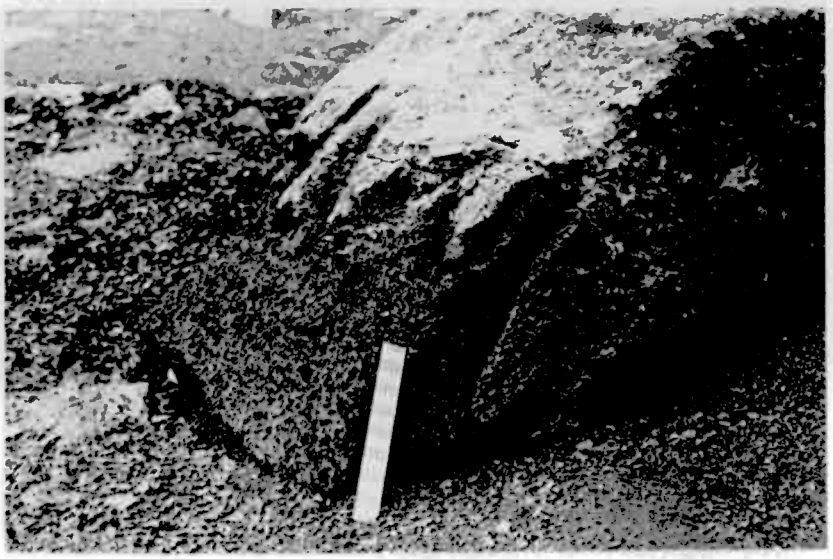

Plate 3 Lobate contact between oC and bC of unit 13 at locality 39.

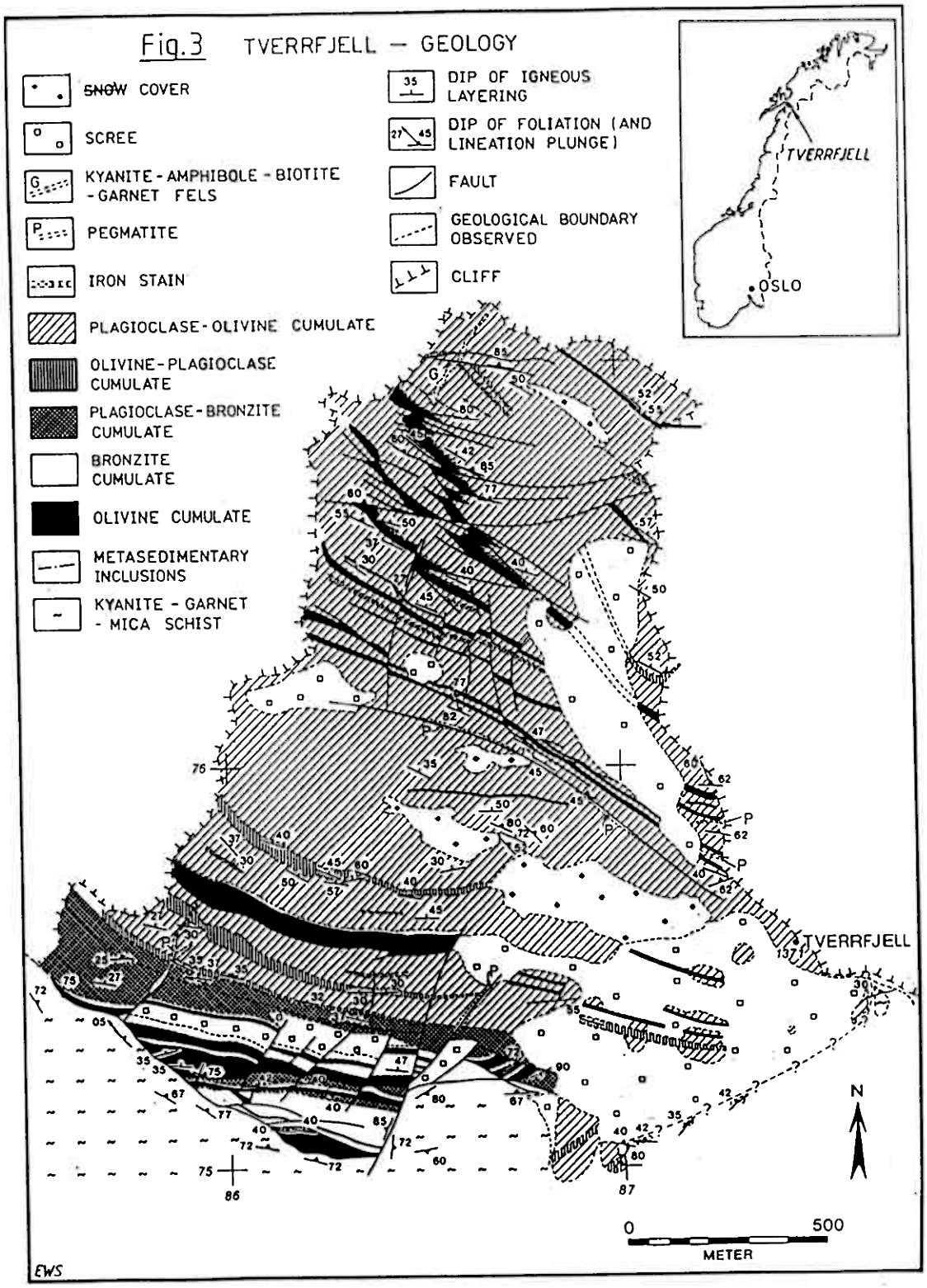
Fig.3 TVERRFJELL — GEOLOGY
SNOW COVER
SCREE
KYANITE - AMPHIBOLE - BIOTITE - GARNET FELS
PEGMATITE
IRON STAIN
PLAGIOCLASE - OLIVINE CUMULATE
OLIVINE - PLAGIOCLASE CUMULATE
PLAGIOCLASE - BRONZITE CUMULATE
BRONZITE CUMULATE
OLIVINE CUMULATE
METASEDIMENTARY INCLUSIONS
KYANITE - GARNET - MICA SCHIST
DIP OF IGNEOUS LAYERING
DIP OF FOLIATION (AND LINEATION PLUNGE)
FAULT
GEOLOGICAL BOUNDARY OBSERVED
CLIFF
TVERRFJELL
OSLO
TVERRFJELL
N
0
500
METER
EWS

Fig. 4

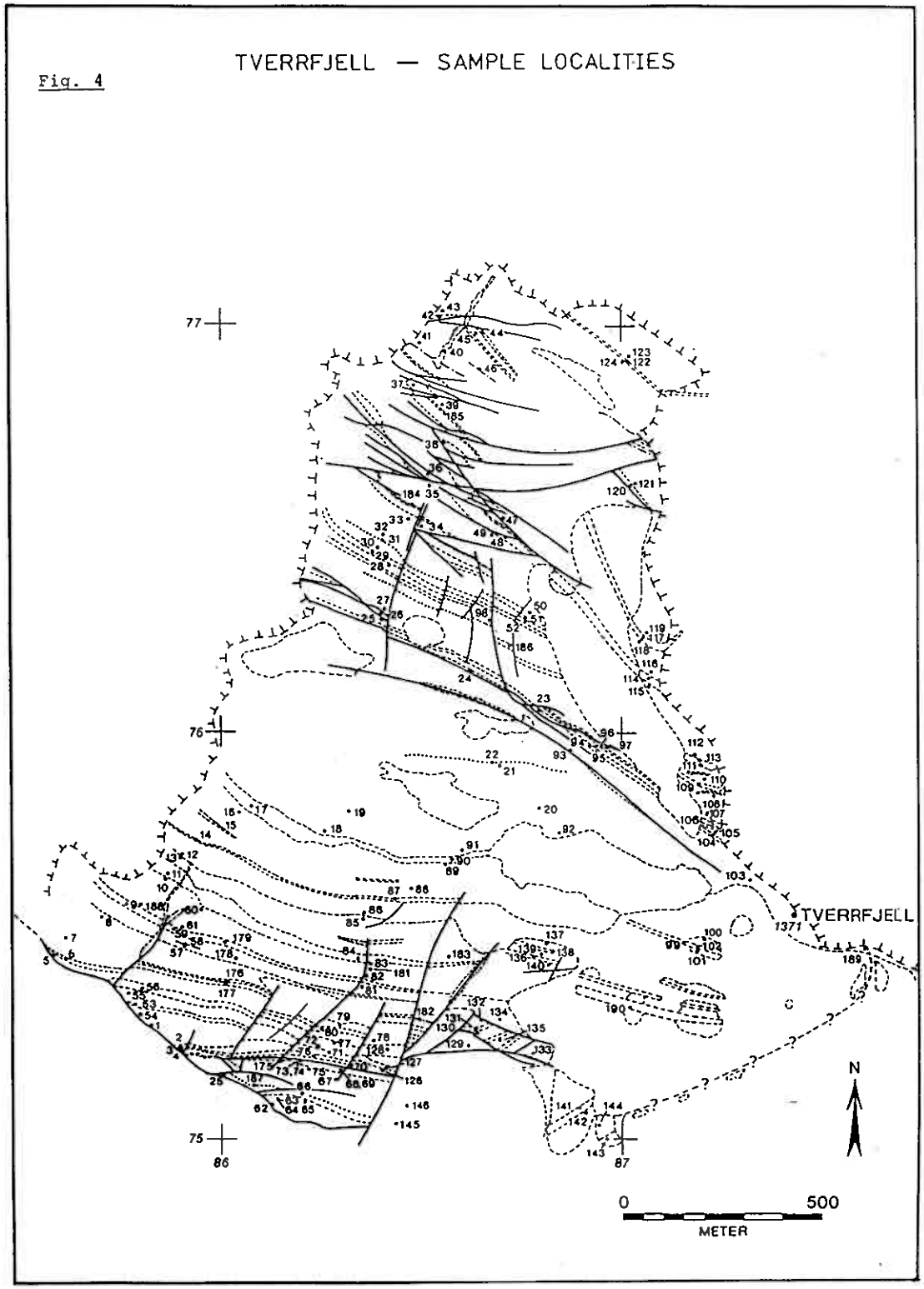
TVERRFJELL — SAMPLE LOCALITIES
TVERRFJELL
1371
N
0
500
METER

Fig. 5. Comparison of the stratigraphy on the west (w), central (c) and east (e) traverse across Tverrfjell. Legend as on Fig. 3. The thicknesses of the units have been corrected for topography and deformation but the numerous layer parallel faults and scree cover make the correlation between the central and eastern traverse a little speculative. Note that on the eastern traverse there appears to be a structural repetition of unit 14 which has been removed, and the isolated blocks of opC at localities 141 and 143 are assumed to be part of units 6 or 8.

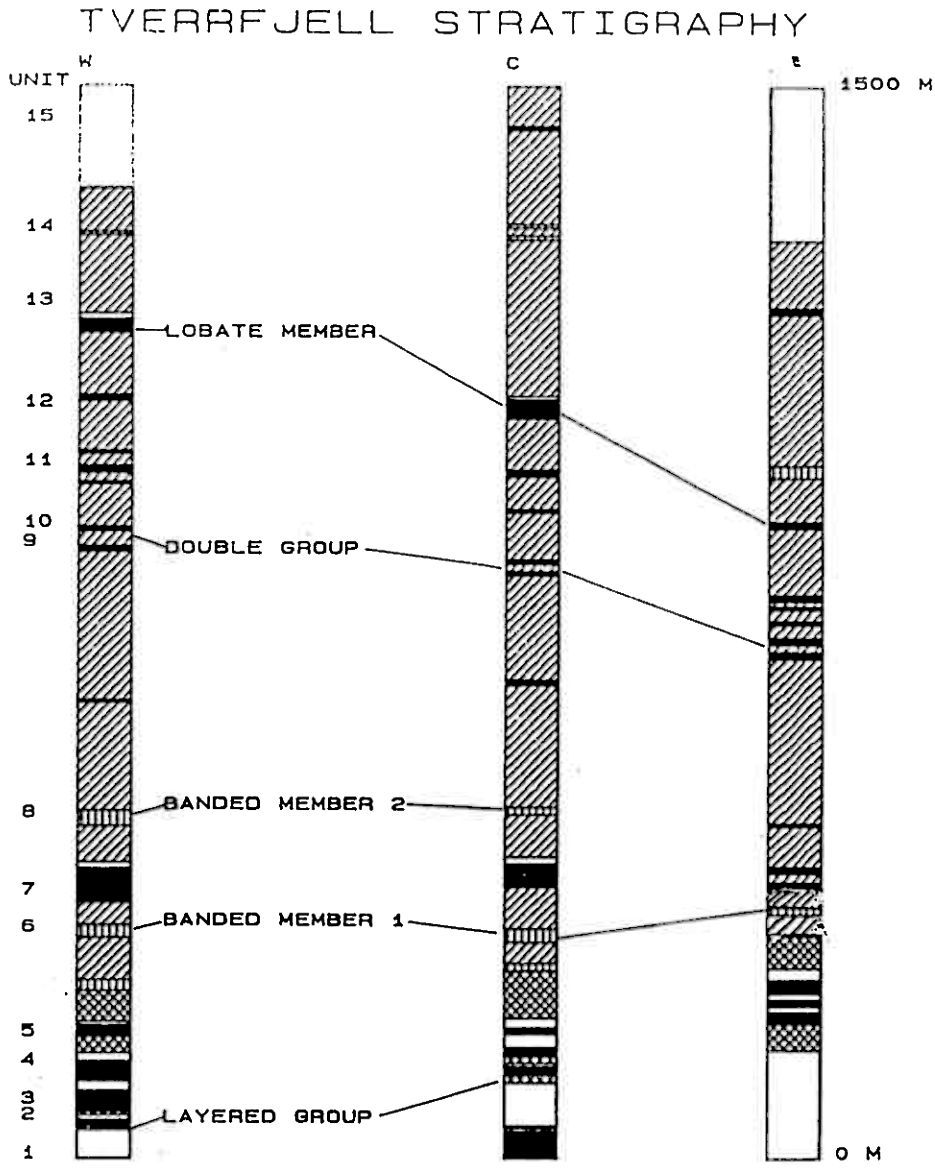

of 45°) and tectonism. The numerous sub-layer parallel faults, in the northern portion of the intrusion, make it difficult to estimate the exact original thickness of each unit.

The lowest distinctive horizon is the 'layered' group of unit 1 (Plate 1). This group consists of alternating layers of bronzite cumulate (bC) and placioclase-bronzite cumulate (pbC). The next recognizable horizons are Banded members 1 and 2 of units 6 and 8 respectively (Plate 2). These members consist of convolutedly folded oC and poC. The 'double group' formed by the oC of units 9 and 10, is present on all three traverses. Finally, the oC and the poC of unit 13 with their undulose contact form the 'lobate' member (Plate 3).

At Tverrfjell there are 15 megacylic units. The lower portions of the units 1 to 5 are oC; these are overlain by bC and pbC, except for unit 3 which has no pbC. The mafic portion of unit 5 can be subdivided into 2 macrorhythmic cycles, about 30 m and 80 m thick respectively. The lower cycle commences with melanocratic-pbC and terminates with leucocratic-pbC. Towards the top of the first cycle there is a layer of iron-stained pbC. The origin of which is discussed below. The upper cycle of unit 5 is melanocratic-pbC for the first 10 m; this is overlain by a poC in which < 10 % pyroxene is present. This layer is called the troctolite and shown as an opC to avoid confusion with other poCs which are gabbronorites. The troctolite is shown on Fig. 3 as continuous, but in fact is discontinuous and of variable thickness. It is most clearly observed on the western traverse. The poC immediately above the troctolite is the lowest unit in which clinopyroxene is the dominant pyroxene.

The lowest portions of units 6, 8 and 14 are olivine plagioclace cumulates (opC), which are overlain by poC. The remaining units have oC at the base overlain by poC. In addition in unit 7 a bC is developed between the oC and the poC. Within units 1, 8, 10 and 11 thin (<1 m), oCs are developed locally. The lack of continuity of these oCs could be due to either igneous or tectonic processes.

Units 5, 6, 10 and 11 each contain a layer of iron stained pbC or poC. The layer could be primary and may have originally contained more sulphides than the surrounding rocks. The subsequent break down of sulphides could

Plate 4 Iron stained rocks (FS) cross-cutting the trend of the igneous layering in unit 5. Photograph taken looking east from loc. 179.

Plate 5 Cross lamination defined by dark pyroxene lamellae, in the pbC of the layered group at loc. 68.

Plate 6 Flame structures in the pbC of the layered group at loc. 68.

Plate 7 Layering in the oC of unit 1 loc. 187), defined by the variations in the size of the bronzite oikiocryts in the oC.

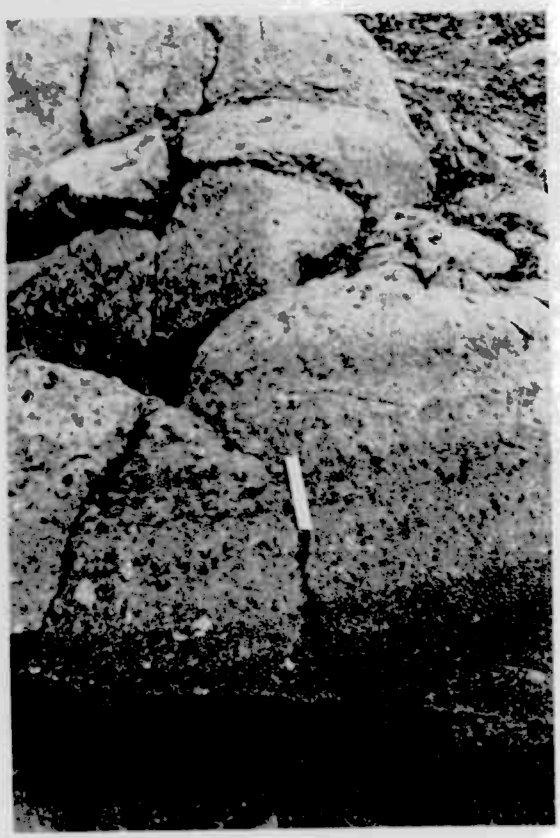

Plate 8 Gradual modal upper contact between bC and oC at loc. 187.

have released the iron. Alternatively, the iron-staining could represent the trace of faults sub-parallel to layering, which allowed fluids to enter the rock and release iron from silicate minerals. The second interpretation is favoured because the iron-stained layers cross-cut the igneous layering at a low angle (Plate 4).

The boundary between Boyd's Ultramafic and Norite Zones would be between the bC and the pbC of unit 5, although, as mentioned above, the term Mafic Zone rather than Norite Zone will be used in this work.

4 LAYERING AND LAYERS

4.1 On the Origin of Layering

There has recently been a revolution in the theory of the development of layered intrusions and therefore, in order to better appreciate the significance of the various types of layering at Tverrfjell, a summary of some of new developments is given below. At Tverrfjell there are three types of layering:

a) Layering caused by a change in rock type; a phase change. In this case the layers are the various rock types oC, bC, pbC, and poC, which together define the megacycles or units 1 to 15.

b) Layering caused by modal variations of the minerals present, where the layers are lamellae rich in pyroxene or olivine alternating with thicker massive plagioclase rich layers. Each pair defines a mesocycle and are present in almost every pbC or poC. These layers are normally planar, but in units 1 and 5 some mafic layers define cross-laminations and in units 1 and 8 the mafic layers define flame structures (Plates 5 and 6).

c) Layering caused by textural variations in the minerals, e.g. the alternation of oC layers containing coarse grained orthopyroxene with oC layers containing finer grained orthopyroxene.

Type (a) layering is the most obvious in any intrusion. Early workers e.g. Wager and Brown (1967) interpreted the megacycles as representing fresh

influxes of new magma. They suggested that as each batch of magma cooled the minerals crystallized and settled to the base of the crystal pile, producing a mafic rich cumulate and a fractionated liquid. As the liquid fractionated and cooled it reached different phase boundaries and at each one a new mineral began to crystallize. The change in rock type therefore represents a point at which the liquid reached a new phase boundary.

The idea of crystal settling has been discarded because the minerals in megacycles do not exhibit the size and density gradation that this model requires (Campbell 1978, Maaloe 1978, McBirney and Noyes 1979; amongst others). It is now suggested that the minerals crystallize in situ i.e. that the crystal pile grows from the bottom up, the liquid is displaced upwards by the growth of the crystals and possibly by double diffussive convection (Turner and Gustafson 1978). The change in rock types is interpreted as a change in liquid composition which has resulted in the crystallization of a new phase and each new megacycle requires a fresh influx of magma.

Campbell (1978) and McBirney and Noyes (1979) suggested that the origin of type (b) layering, which results from changes in modal proportions of minerals in the rocks, is due to alternation of crystallization of the minerals because of nucleation effects. Irvine (1980), on the other hand, suggested that this type of layering is due to redeposition of unconsolidated crystal mush by magmatic density currents, in a manner analogeous to the deposition of turbidites. A third suggestion (Cawthorn, p.c., 1985) is that the liquid was close to the phase boundary and that small changes in the pressure or temperature cause a change in the crystallizing phases. Finally, Boudreau (p.c., 1985) suggests that layering such as the inch-scale layering observed in the Stillwater complex is the result of metasomatic action of late intercumulate fluids.

The importance of intercumulate fluids in locally modifying mineral and rock compositions during filter pressing has been noted by many others (e.g. Irvine 1980). Recently Tait et al. (1984) showed that the intercumulate fluid could convect with the overlying magma. They suggest that differences in the cooling rate combined with magma composition affect whether the rock developes into an ortho-, meso- or adcumulate. This may be important in the development of Type (c) layering; layering due to textural differences.

4.2 Layering and Layers in Tverrfjell

Many of the thick (>2 m) oC units have moderately well developed, rhythmic, grain-size layering defined by variations in the grain-size of ortopyroxene oikiocryts (Plate 7). The boundaries of the layers are sharp. There is no whole rock compositional difference between the layers, (e.g. compare samples 63 and 64 Appendix, Table 2b). The layering arises simply due to the difference in the size of orthopyroxene oikocryts. The oikocryts are though to form from a magma close to the composition of that which crystallized the chadocryts (Wadsworth 1985). Their nucleation is delayed, possibly due to kinetic factors, and consequently the magma becomes supersaturated in the oikocrystic phase. The layering could represent waves of nucleation.

The thinner oC layers are generally planar and uniform. On the basis of the forsterite content of the olivine the units are not cryptically layered (e.g. compare samples 62 to 65 Appendix Table 3b). The upper boundaries between oC and bC are gradational modal and textural boundaries (Plate 8), whereas the lower contacts are sharp phase and textural boundaries (Plate 9).

The boundary between oC and poC in unit 13 is a sharp phase boundary which has a lobate form (Plate 3). This contact was a distinctive mappable layer and is subsequently referred to as the lobate member. The rock at the contact has the composition on an opC, (samples 184 and 185 Appendix Table 2a), but it has been metamorphosed to an amphibole fels, therefore it is not clear whether the undulous nature of this contact is igneous. It could represent an alteration zone between the oC and the poC. This interpretation is suggested by the development of amphibole fels along the joints. Similar undulous contacts from Rhum have been described by Young and Donaldson (1985) and from the Bushveld by Lee (1981); these authors ascribe them to deformation of crystal mushes. On the other hand, Butcher et al. (1985) and Robins (1982) suggest that similar contacts at Rhum and Lille Kufjord develop by metasomatic replacement of the upper unit by intercumulate liquid from the lower unit. At Tverrfjell it is not possible to decide which hypothesis holds. The other boundaries between the oC and poC, and oC and pbC are all sharp phase, modal and textural boundaries.

The bC layers are 1-2 m thick, planar units that are modally gradational with more plagioclase towards the top of the layer. The boundary between

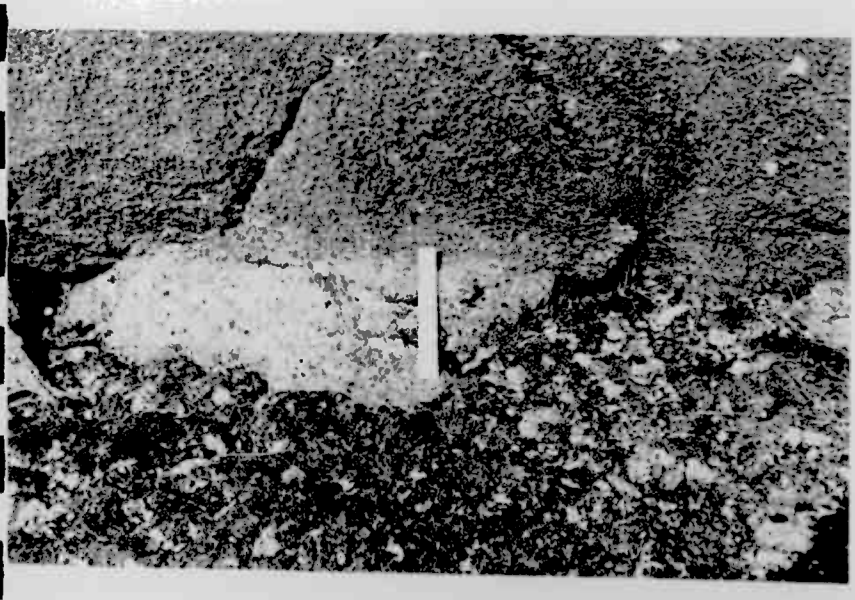

Plate 9 Sharp basal contact between oC and bC at loc. 187. Contact defined by a phase change

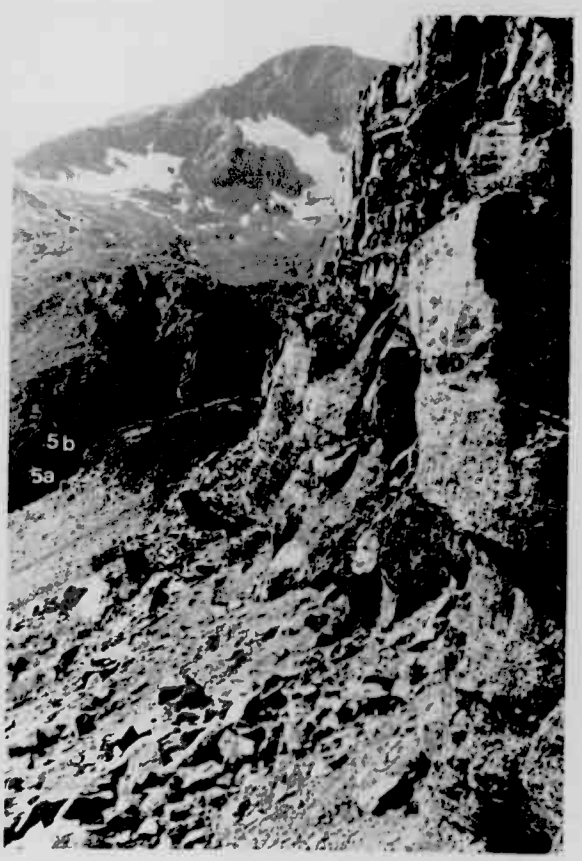

Plate 10 Looking west from loc. 179 the macro cycles of unit 5 labled 5a and 5b, are visible.

Plate 11 Wispy cross lamination, defined by dark pyroxene layers in the pbC of unit 5a at loc. 179.

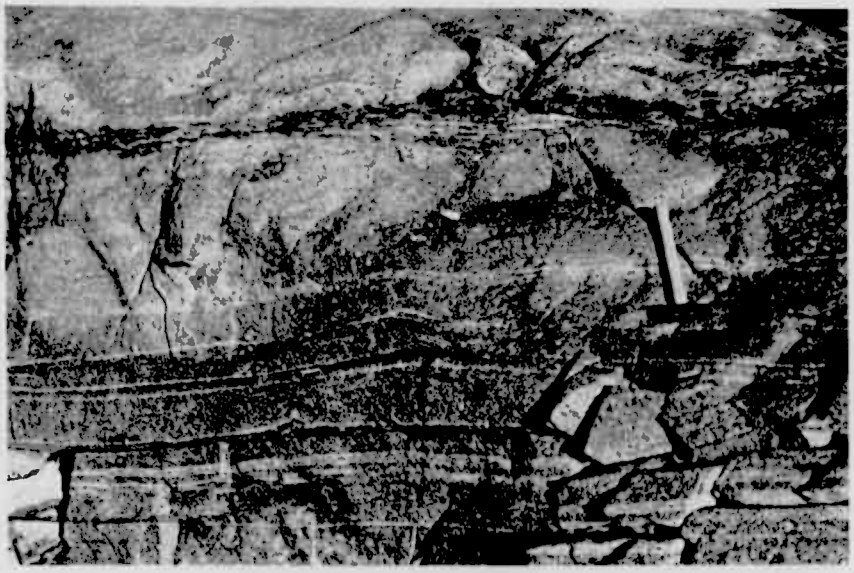

Plate 12 Mesocycles in poC of unit 9 at loc. 20

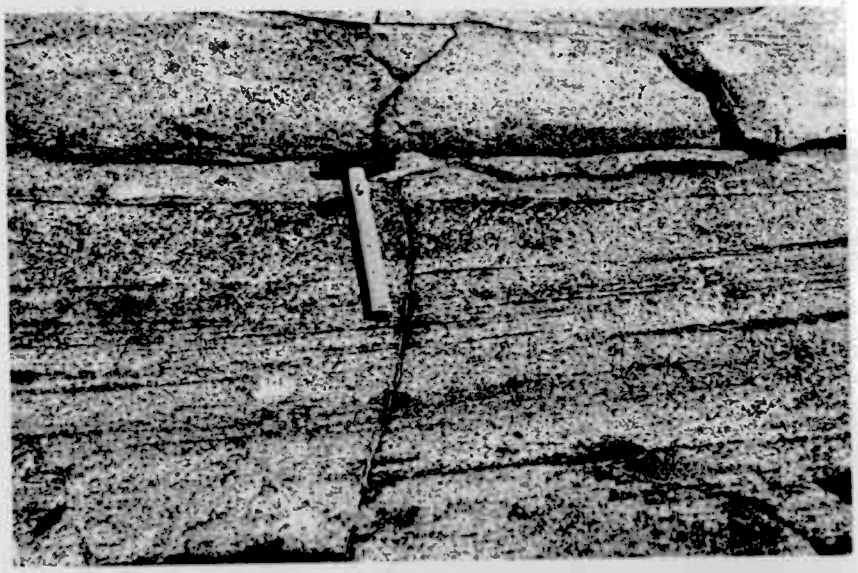

Plate 13 Wispy layering in poC, defined by olivine rich lamellae (loc. 20)

Plate 14 Flame structures in poC of unit 9 at loc. 20.

Plate 15 The undulous contact between opC and overlying poC at locality 17.

Plate 16 Crenulated schistosity in the kyanite garnet biotite schist at the contact with the intrusion (loc. 145).

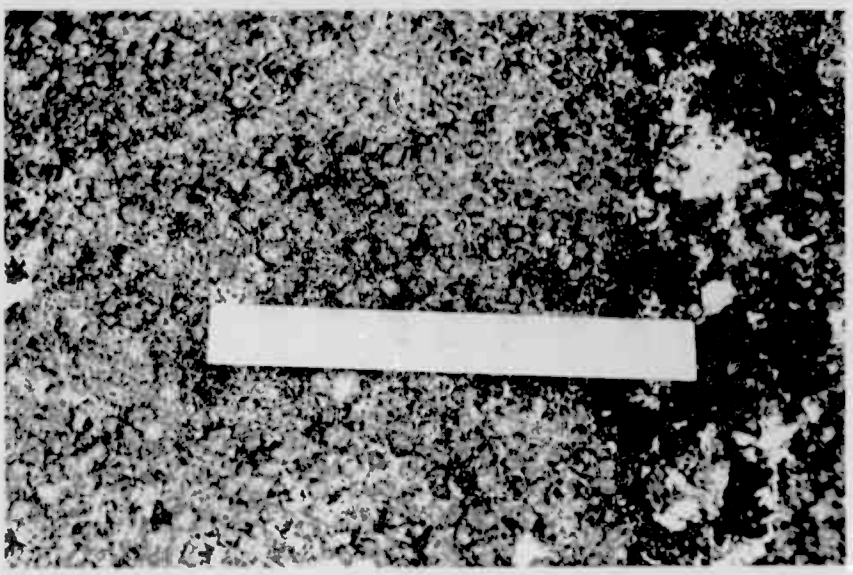

Plate 17 Garnet "dyke" at loc. 40.

the bC and pbC is a planar sharp phase and modal boundary (Plate 1).

The 'layered group' of unit 1 has a strong, rhythmic layering on the central traverse (Plate 6). The layering is defined by alternating layers (5-10 cm thick) of bC and pbC. Most bC layers are planar and uniform, the boundary between the bC and the pbC is a sharp phase and modal boundary. However, a few bC-pbC contacts are undulous and resemble soft-sediment flame structures (Plate 6). The pbC contain lamina rich in bronzite which define cross-laminated modal layering (Plate 5).

The pbC of unit 5 consists of rhythmic mesocycles with moderately well developed modal layering (Plate 4). There is an gradational increase in plagioclase and decrease in orthopyroxene, from the base to the top of each layer. The cycles are approximately 10 cm thick and planar. The boundaries between cycles are modal and grain-size boundaries. These mesocycles are part of two macrocycles (5a and 5b, Plate 10). The mesocycles at the base of unit 5 commence with melanocratic-pbC and end with an intermediate coloured pbC. The amount of bronzite in the basal pbC of each mesocycle decreases until at about 25 m into the layer the mesocycles begin with an intermediate coloured-pbC and end with leucocratic-pbC. Towards the top of unit 5a the plagioclase in the leucocratic-pbC defines a planar lamination and the cycles are thinner (5 cm) and not as well defined as in the lower portions of unit 5. In places the layering suggests cross-bedding (Plate 11). At about 30 m there is a reversal and the mesocycles again begin with melanocratic-pbC and end with an intermediate coloured-pbC (Plate 10). This reversal defines the base of unit 5b.

The poC are thick planar layers (100's m). The boundary between a poC and the oC of the overlying unit is a sharp phase, modal and textural boundary. The boundary between oC and overlying poC of the same unit is slightly more gradational and is a modal boundary. In units 12 and 13 there is an opC between the oC and the poC. The poC contains planar mesocycles 10 to 20 cm thick (Plate 12). Each cycle is modally gradational with more plagioclase towards the top of the cycle. The mesocycles define macrocycles which are 20-50 m thick. The macrocycles consist of a series of mesocycles which are more plagioclase rich up stratigraphy. Plate 12 shows part of a macrocycle, (way up topwards the top of the page). The olivine- and pyroxene-rich lamellae in the poC are planar in most rocks, but in a

few cases cross lamination (Plate 13) and flame structures were observed (Plate 14).

The opC of units 6 and 8 have been described above as the Banded Members. They consist of convoluted folded oC and poC and have undulous contacts with overlying poC (Plate 15). The convoluted folding is best developed on the western traverse especially at locality 17. The oC and poC layers in the Banded Members have gradational contacts, the folding is outlined by the oC layers which tend to be thin (0.3 to 1 m) and wispy in the upper parts of the members. The overall appearance of the members suggests soft-sediment deformation. Unit 14 is also an opC, 1-3 m thick, but it has planar contacts and no internal layering, except that on the central traverse there are two opC layers whereas on the eastern traverse there is only one. The lobate member of unit 13 may be a metamorphosed opC.

5 COUNTRY ROCKS

The country rocks at the contact are kyanite-garnet-biotite schist with an intense schistosity that has been crenulated by close minor folds (Plate 16). The intensity of the minor folding is less, away from the contact and about 50 from the contact the schistosity is planar.

Biotite-garnet-kyanite schist schlieren are also found inside the intrusion, especially in the sub-layer-parallel faults at the top of unit 8 and in units 13 and 14. The association of the sediments with large layer parallel faults could indicate that they were tectonically included in the body during deformation.

Two pods of biotite-garnet-sillimanite fels were found in the pbC of unit 5 (localities 58 and 182). These rocks could be xenoliths. There is textural evidence that they have undergone partial melting.

6 POST-INTRUSION ROCKS

Associated with many of the major faults there are quartzo-feldspathic veins. In particular, along the layer parallel fault at the top of unit 8 there is a quartzo-felspathic vein which has been mylonitized.

Plate 18 Alteration and deformation of the poC is so intense in some rocks that the poC is now a mafic gneiss (loc 93)

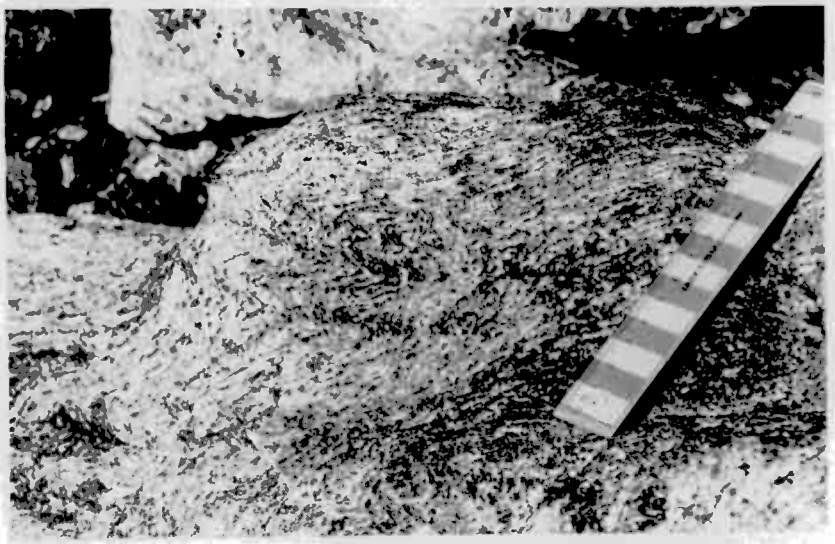

Plate 19 Crenulated mafic gneiss (loc. 39)
loc. 39

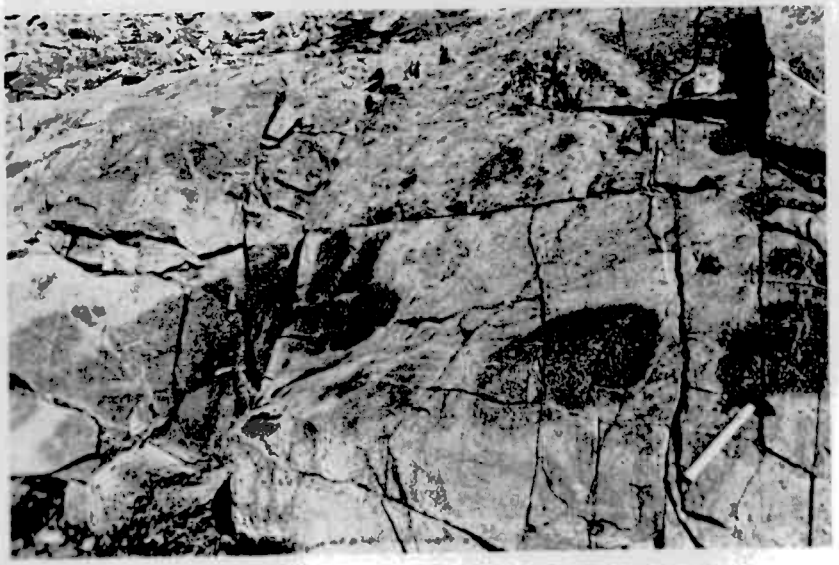

Plate 20 Alteration of poC along joints (loc. 20)

An unusual rock occurs in unit 13, and 14 (loc. 40), a kyanite-anthophyllite-cummingtonite-garnet fels. It has the form of a dyke, approximately 2 m wide and at least 150 m long. The grain size of the garnet (the principal mineral) is smallest at the edges of the dyke (1 mm) and largest in the centre (5 mm) (Plate 17). The origin of this rock is not known. I speculate that it is a metasomatic alteration of the poC, by fluids released from the sedimentary inclusions during metamorphism.

7 STRUCTURE

The primary layering strikes west to north-west and dips at about 45° north-east. The stratigraphic relationships indicate that this portion of the intrusion is the right way up and youngs to the north-east.

The contact with country rock could only be observed on the southern margin of the body where it was clearly tectonic. Therefore the oC of unit 1 is probably not the lowest oC in the Råna intrusion, but merely the lowest one to be exposed at Tverrfjell.

The main effect of deformation on Tverrfjell is the disruption of the layering by faults with two trend directions:

a) An earlier set of faults sub-parallel to the layering (west to north-west trending) and parallel to the basal thrust along which Tverrfjell was emplaced and
b) A later set perpendicular to the layering (north to north-east trending).

The earlier set of faults is more intense and has larger displacements than the later set. In particular units 13 and 14 are disrupted by these faults and up to 70 m of displacement can be measured. The rocks close to the earlier faults are no longer igneous, but metamorphic with a foliation. In places the poC in these units has been deformed and metamorphosed to a mafic gneiss (Plate 18). The development of the metamorphic minerals in the mafic rocks obliterates the igneous textures and produces a tectonic layering at about 30° to the igneous layering which is intensely folded (Plate 19). Since these faults are parallel to the basal thrust they may have formed during the emplacement of Tverrfjell into its present position.

The faults and joints perpendicular to the layering, have displacements of less than 10 m. The poCs close to the joints are altered to tremolite-chlorite fels. The joint pattern produces islands of fresh rock (brown, Plate 20), in a sea of tremolite chlorite fels (white, Plate 20). These faults may represent the brittle behaviour of the rocks when they were uplifted.

8 PETROGRAPHY

The oC are coarse-grained, poikilitic orthocumulates. The weathered surface is orange-brown and rough due to differential weathering of the 1-5 cm pyroxene oikiocryts and the 2 mm olivine chadocryts. The fresh surface consists of green-brown (pyroxene, 15% opx, 5% cpx) oikocryts and black (olivine 62%), rounded grains with white laths (intercumulus plagioclase, 15%). 0.5 % intercumulus sulphides are present in almost every sample. Figs. 6a, b and c show the variations in normative mineralogy with stratigraphic height for the western, central and eastern traverses respectively. Normative mineralogy and not modal mineralogy was used because about 15% of the samples were completely metamorphosed and do not contain any igneous minerals and about 50% of the samples contain some metamorphic minerals. Since the immediate aim of this study is to understand the igneous history of the body it was felt that the normative mineralogy would be more informative than the modal mineralogy. Where the samples are not metamorphosed the normative mineralogy and modal mineralogy agree remarkably well.

The bC is a medium grained mesocumulate. The weathered surface is beige coloured and smooth. The fresh surface consists of 2 mm blocky, apple-green cumulate orthopyroxene grains (65%), 1 mm, black, rounded olivine grains (5%), white, intercumulate plagioclase laths 2 mm long (20%) and yellow, intercumulate sulphides (1%). The remainder of the rock is made up of clinopyroxene oikocryts (7%) and opaques, but these are not visible in hand specimen.

The pbC is a medium-grained adcumulate. The fresh surface consits of 50% white interlocking plagioclase laths (2 mm), with 45% pale-green blocky orthopyroxenes (2 mm) and 5%, 4 mm ellipsoids with black olivine cores and

brown coronas. Both plagioclase and pyroxene laths show igneous alignment (Plate 21).

The poC is a medium grained, mesocumulate. The weathered surface is cream with dark green spots 5-10 mm in size. The fresh surface consists of white plagioclase (55%) laths (1-2 mm), with black olivine grains (20%) in the centre of coronas (5 mm). Pale green intercumulate pyroxene (15% cpx, 10 % opx) laths (2 mm long) occur between the plagioclase grains. The main differences between the pbC and the poC in hand specimen are the higher pyroxene to olivine ratio in the pbC and the shape of the pyroxenes. In thin section there is a clear difference in crystallization order. In the pbC, plagioclase and bronzite are cumulate and clinopyroxene encloses some of the bronzite and plagioclase grains (Plate 22). In the poC, only plagioclase and olivine are cumulate, clinopyroxene is intercumulate and orthopyroxene encloses some of the clinopyroxene grains (Plate 23).

The opC is quite variable in character. On the western traverse in units 5 and 8 it has a distinctive appearance, consisting of convoluted layers of opC and poC, (the banded members mentioned in the stratigraphic section); to the east the convoluted folding in banded member 2 becomes less distinctive. On the eastern traverse in place of the thick oC of unit 7 and the opC of unit 8 (banded unit 2) there are three thin oCs. Snow cover between the central and eastern traverse makes it difficult to tell how this transistion occurs. Banded member 1 is present on all three traverses. The opC of unit 14 is a medium grained poikolitic mesocumulate. The weathered surface is light brown, but unlike the oC the oikiocryts do not stand out. The fresh surface is mottled black with rounded grains (olivine 45%), and white laths (plagioclase 30%) enclosed in pale green oikocrysts (pyroxene, 15% cpx, 5% opx). 0.5% intercumulate sulphides are present.

9 MINERALOGY

9.1 Analytical Methods

All mineral analyses were carried out with a 4 spectometer JEOL Superprobe, at Institutt for Kontinentalsokkelundersøkelser, Trondheim SiO_2, Al_2O_3, MgO, CaO, Na_2O, K_2O, NiO and Cr_2O_3 were determined by wavelength analysis.

NiO and Cr_2O_3 were counted for 100 seconds and the other elements for 20 seconds. TiO_2, MnO and FeO were determined, simultaneously with the wave length analysis, by energy-dispersive analysis using 200 second counts. The beam diameter was 10 Mm, except for the analyses of exsolutions and intergrowths and the traverses across minerals, when a focussed beam (1-2 Mm) was used. The operating voltage was 15 KeV and the specimen current 0.5 nA. The data was reduced and ZAF corrections made by an on-line Tracor Northern computer using the computer programme MAGIC. A combination of natural and synthetic minerals was used as standards. Precision and detection limits obtained in this study are listed in Appendix Table 1. The mineral analyses in the Appendix Tables 3, 4, 5, 6 and 7 for olivine, orthopyroxene, clinopyroxene, plagioclase and chromites represent the average of the cores of 3 to 9 grains, except for the pyroxene exsolution pairs.

9.2 Olivine

In all rock types olivine occurs in two forms:

a) As 2-3 mm granular chadocryts in pyroxene oikocrysts (Plate 24)
b) As 2-3 mm subhedral grains, "free" grains; where the olivine is in contact with pyroxene the grain boundaries are straight, but in most samples where plagioclase is present there is a 2-layered corona between the olivine and the plagioclase and the olivine is embayed (Plate 25). In a few samples there are no coronas between olivine and plagioclase (Plate 26).

There appears to be no statistically significant difference in composition between the centres of the two forms of olivine (Table 3a, Appendix). The olivine in the pyroxene oikiocryts is unzoned and homogeneous (Fig. 7a). Some olivines enclosed in coronas are more forsteritic in the outer 20 Mm of the grains, but inside this they are homogeneous (Fig. 7b).

The nickel content of the olivine varies from 0.02 to 0.17% NiO. The olivines are nickel-depleted compared to olivines from other layered intrusions (Fig. 8). This nickel depletion may occur because the magma became sulphide saturated prior to olivine crystallization and the nickel would then have partitioned into the sulphide, leaving the magma depleted in

Fig. 6a. Variations in normative mineralogy on the western traverse versus height. Legend as on Fig. 3

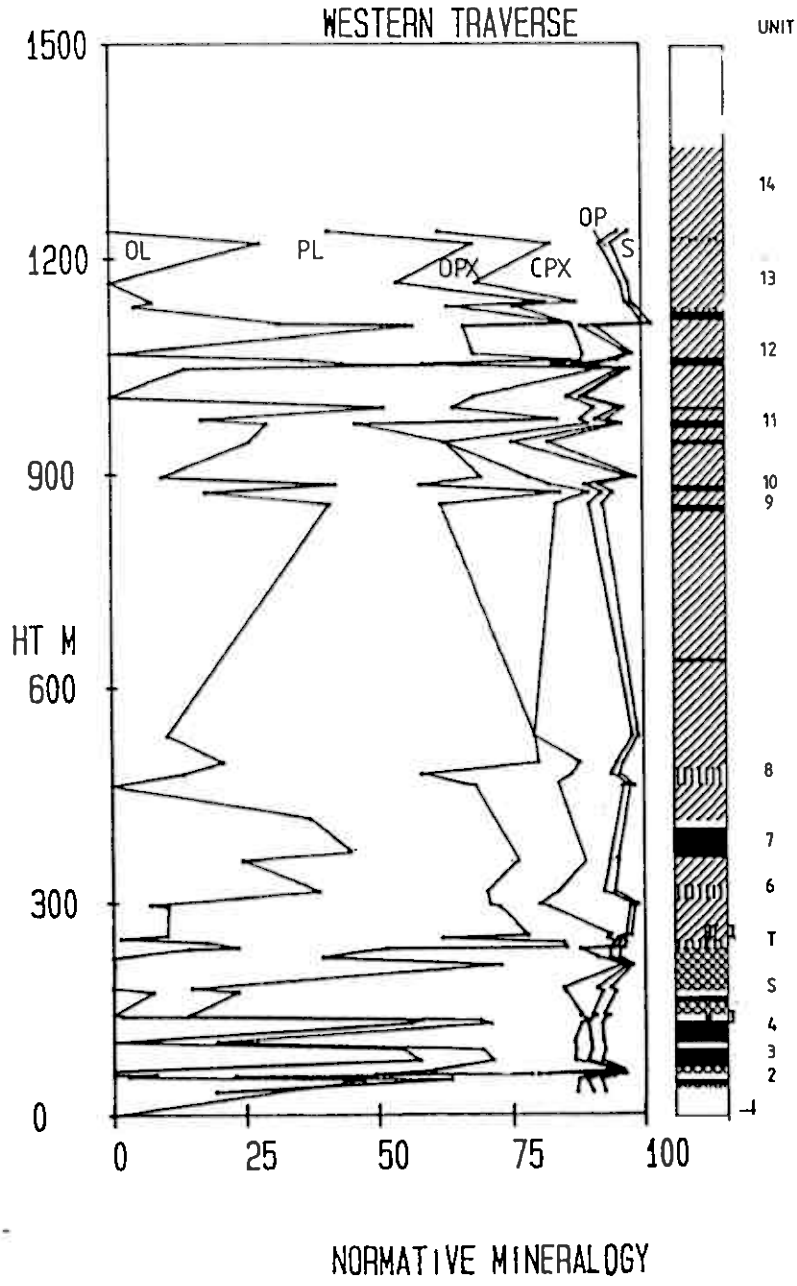

Fig. 6b. Variations in normative mineralogy versus on the central traverse versus height. Legend as on Fig. 3

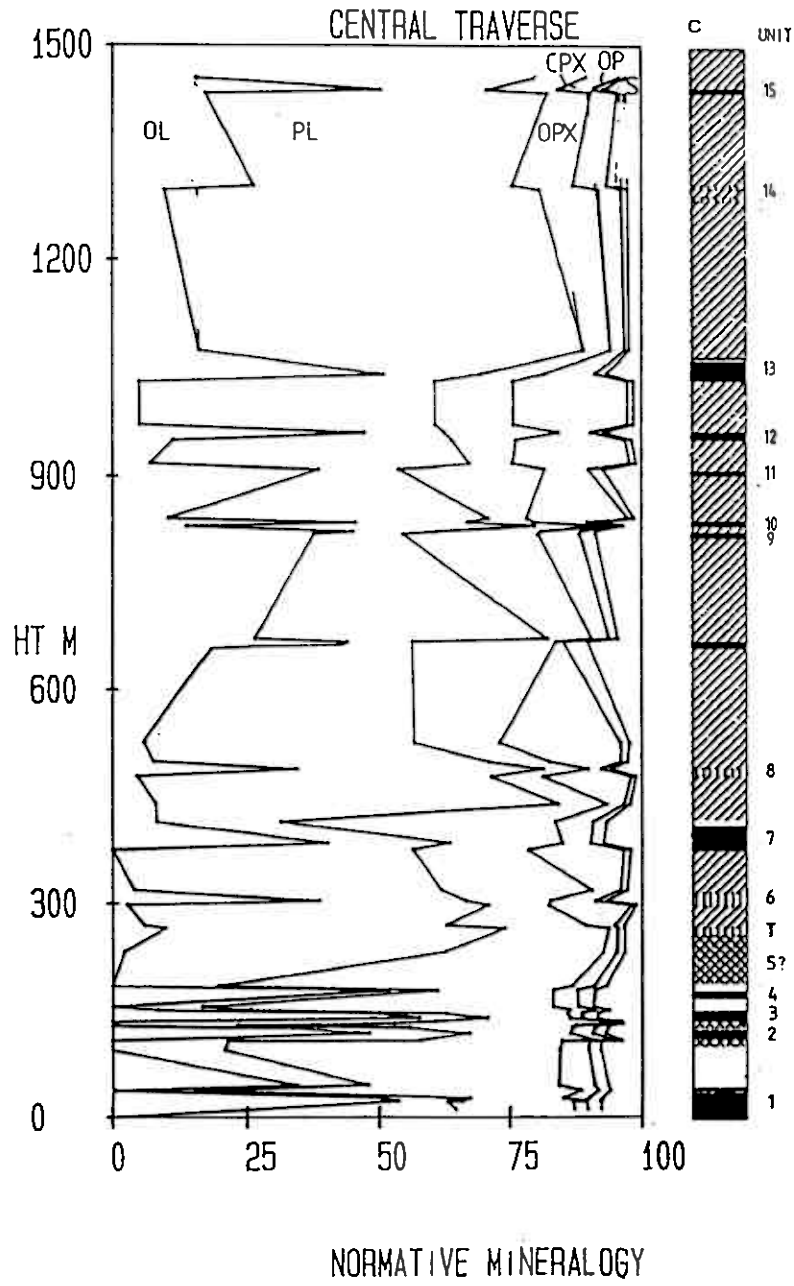

Fig. 6c. Variations in normative mineralogy versus height on the eastern traverse. Legend as on Fig. 3

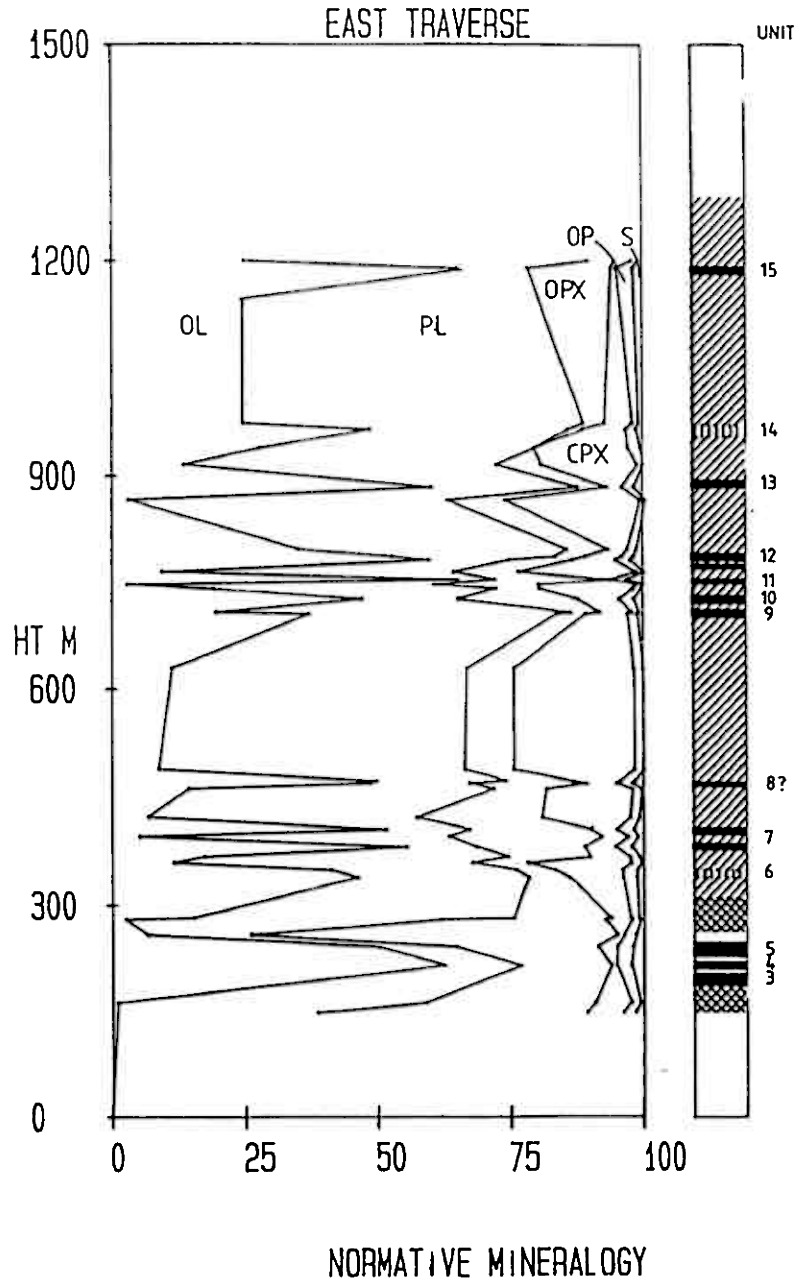

Fig. 7. Zoning profiles of the main minerals analysed by the microprobe.

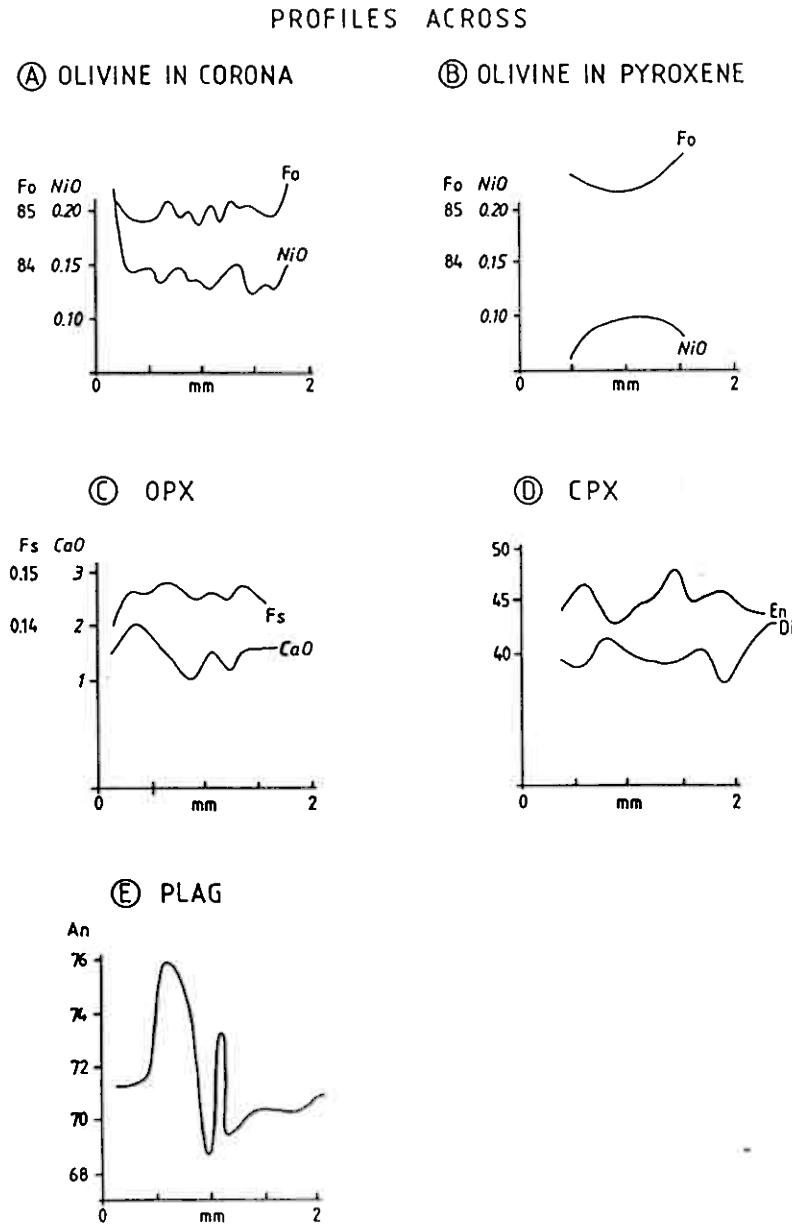

Fig. 8 MgO versus NiO for the Tverrfjell olivines, O = oikocryts, C = olivines in coronas, F=free olivines. Most of the Tverrfjell olivines are depleted in NiO relative to the field of normal layered intrusions as defined by Fleet et al. (1977).

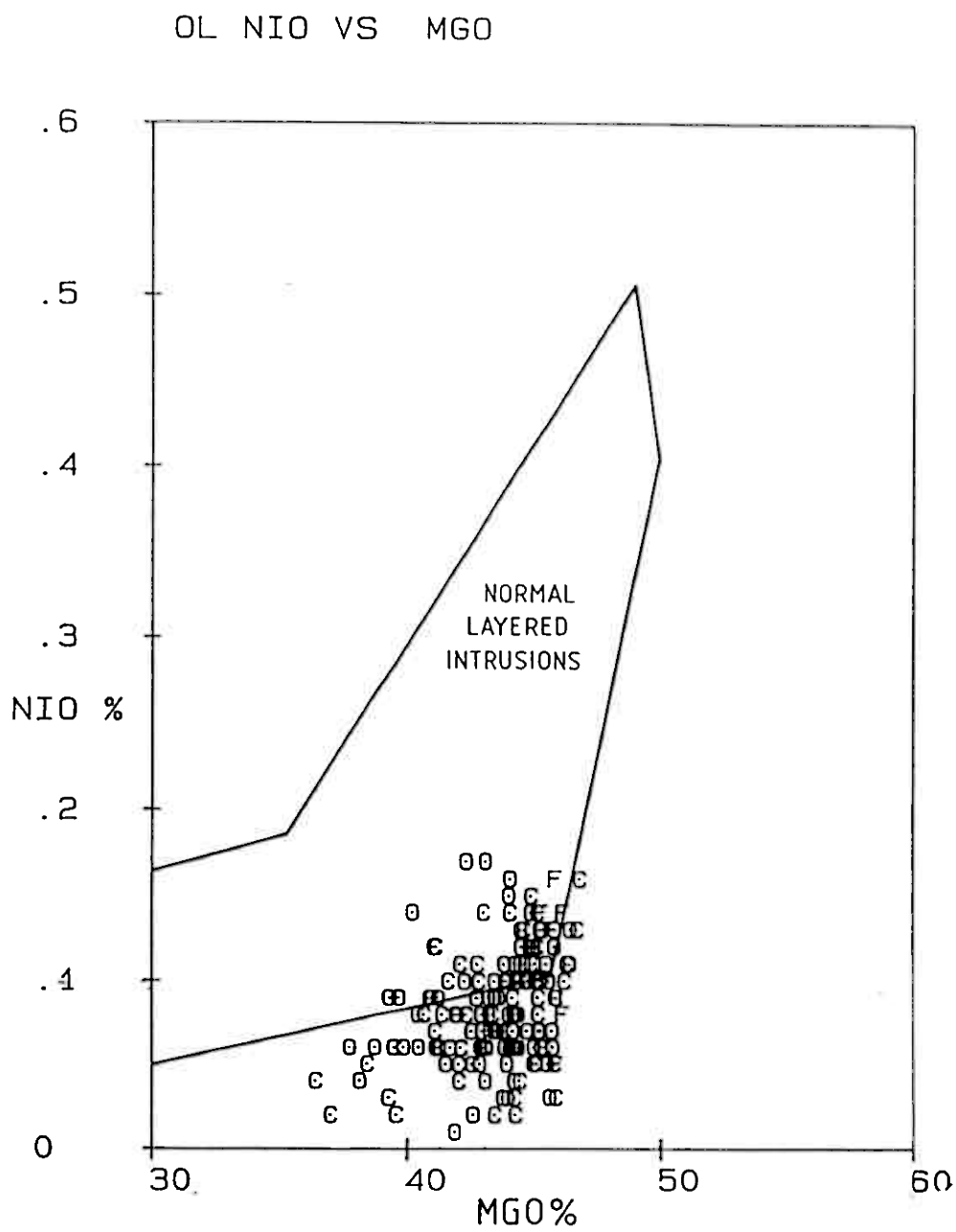

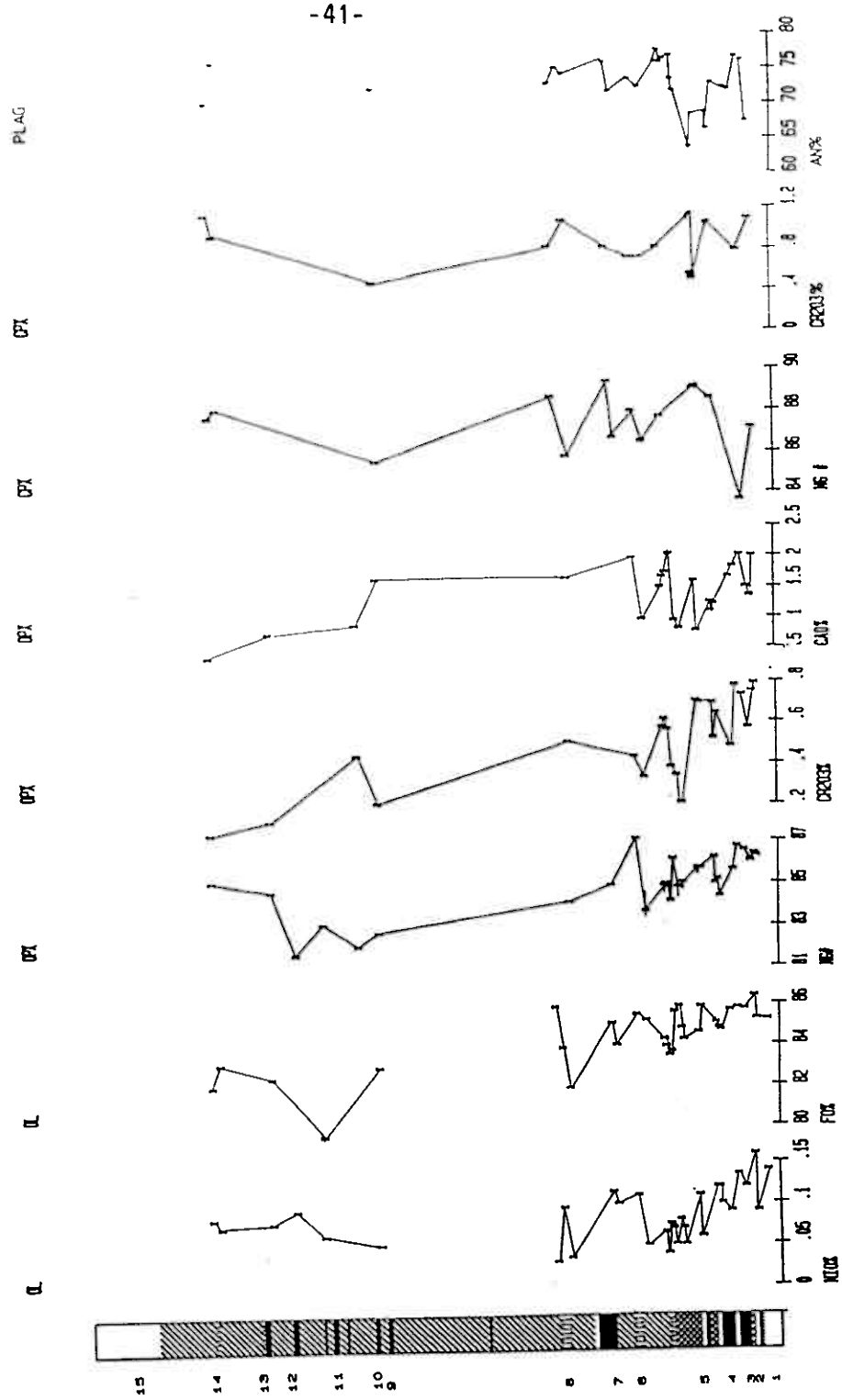

Fig. 9a Variations in mineral compositions with stratigraphic height on the western traverse. Legend as on Fig. 3. For units 1 to 6 there are depletion trends for; NiO in olivine, Mg number, Cr2O3 (Al2O3) and Wo in pyroxenes. At 6 there is a reversal of this trend. The An content of the plagioclase also falls from unit 1 to the middle of unit 5, at which point there is a reversal. The changes in mineral composition could indicate the influx of relatively unfractionated magma at the base of unit 6.

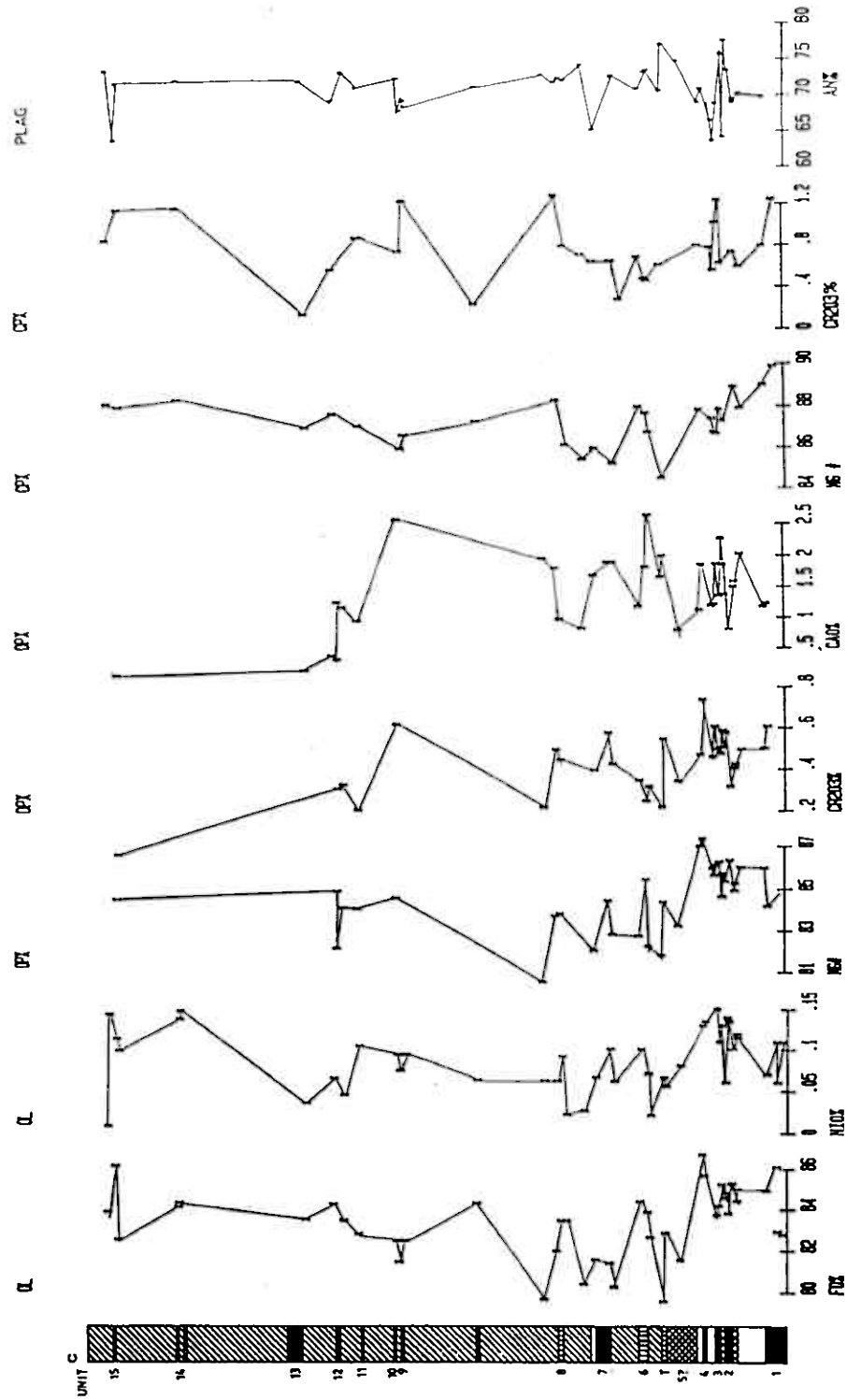

Fig. 9b Variations in mineral compositions with stratigraphic height on the central traverse. Legend as on Fig. 3. Note the trend of NiO & Fo depletion in olivine, Mg number, Cr2O3 (Al2O3) and Wo, depletion in cpx and opx from units 1 to 6. At 6 there is a reversal of this trend. The An content of the plagioclase also falls from unit 1 to the middle of unit 5, at which point there is a reversal. The changes in mineral composition could indicate the influx of relatively unfractionated magma at the base of unit 6. Similar trends can be observed for units 6 to 8, 9 to 13, possibly indicating at least 4 influxes of less fractionated magma.

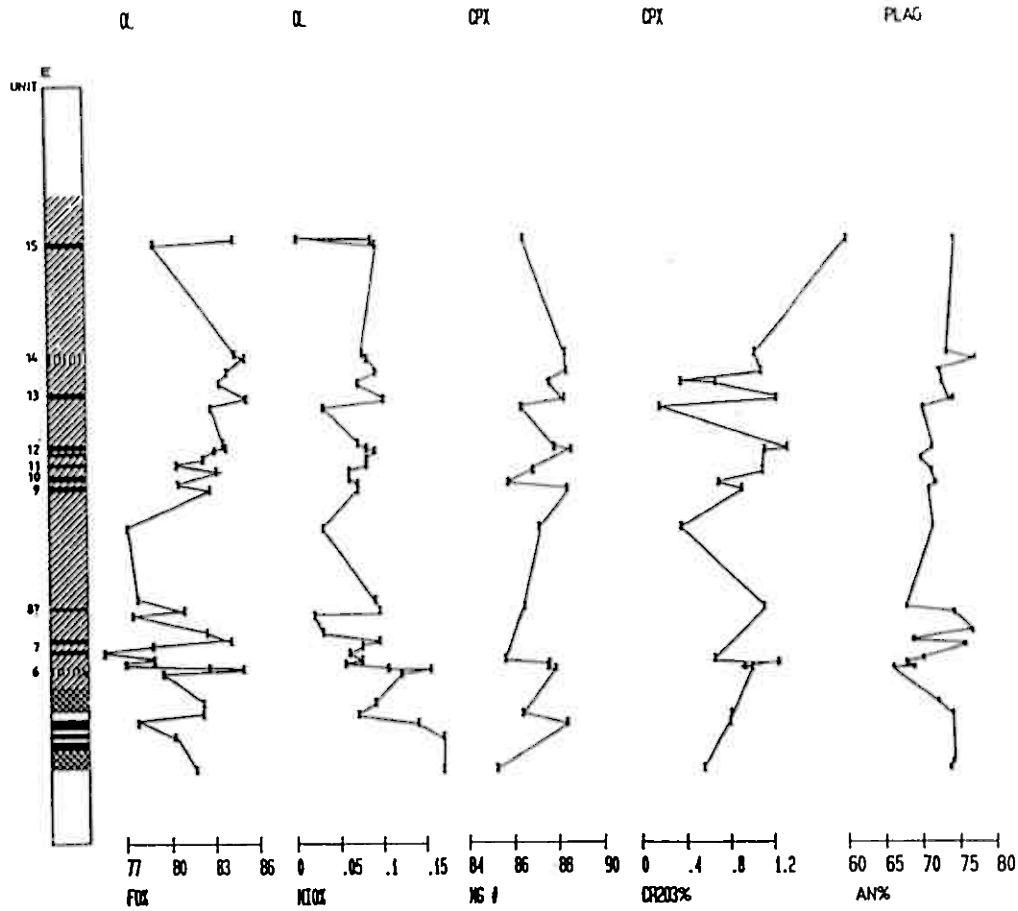

Fig. 9c Variations in mineral compositions with stratigraphic height on the eastern traverse. Legend as on Fig. 3.

Plate 21 Igneous lamination of plagioclase in pbC of Unit 5 (TV 8) Field of view 14.6 mm.

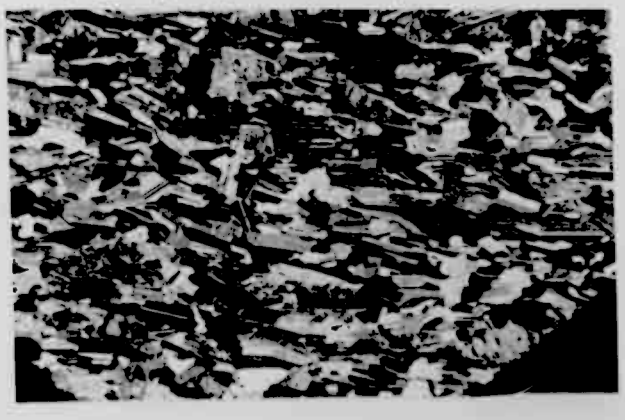

Plate 22 Cumulate bronzite (B) and plagioclase (p) partly enclosed in augite (a) in a pbC of unit 1 (Tv 74)

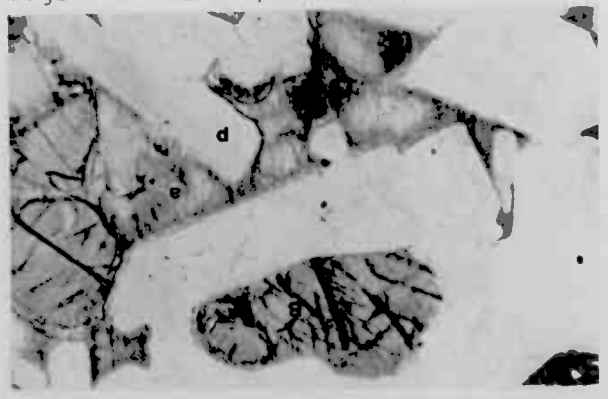

Plate 23 Cumulate plagioclase (p) enclosed in augite (a) which is in turn surrounded by bronzite (B) in a poC of unit 5 (Tv 83). Field of view 5 mm

Plate 24 Bronzite (B) oikiocryts enclosing olivine (o) and chromite (c) chadocryts in an oC of unit 3 (Tv 54) Field of view 5 mm

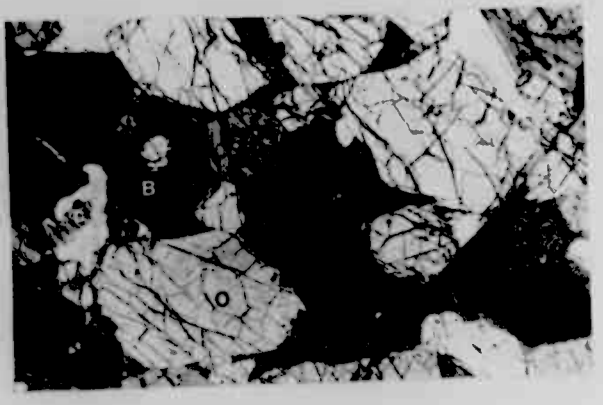

Plate 25 A two layer corona between olivine (o) and plagioclase (p). The inner shell is opx (B) and the outer shell a simplectic intergrowth of paragsite and spinel. Tv 17 an opC unit 8. Field of view 2.2 mm

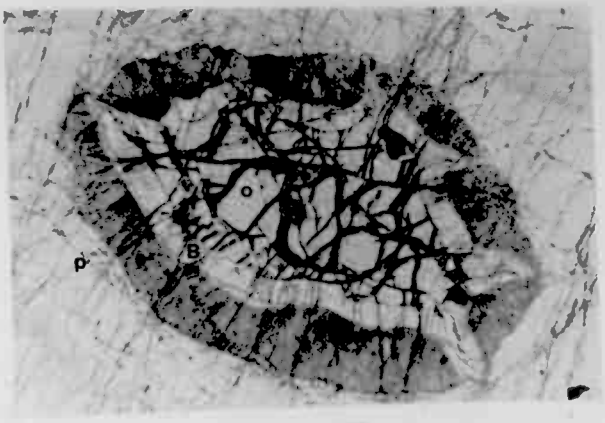

Plate 26 Olivine (o) in a plagioclase (p) oikiocryts with no corona Tv 54 an oC of unit 3. Field of view 7.2 mm

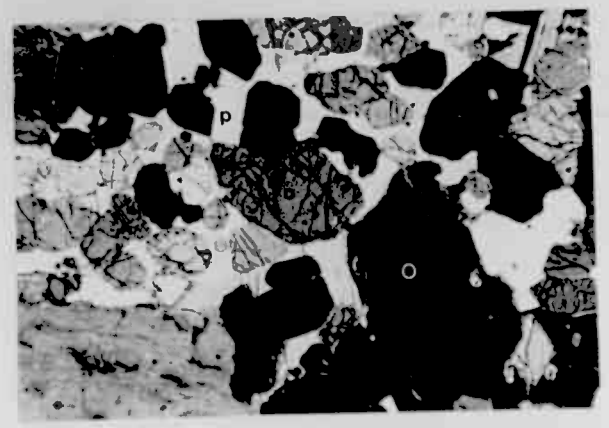

nickel. This suggestion is supported by the presence of the nickel sulphide deposit at Bruvann. In unit 1 there is no overall correlation between the nickel content of the olivine and height (Fig. 9b), but for units 2 to 6 the nickel content of the olivine in oC steadily decreases with height from 0.15 to 0.05% NiO (Figs. 9a and b). At unit 6 there is a reversal and the NiO content of the olivine in the opC is in the range 0.10-0.15% NiO. From unit 6 to unit 12 on all three traverses the nickel content of the oC olivines falls to 0.07. At unit 13 there is a reversal to high values on the eastern traverse. Insufficient olivine is preserved on the western and central traverses to determine whether this reversal is also present on these traverses.

In addition to the overall fractionation trends each individual unit exhibits a fractionation of nickel with oC olivines more enriched in nickel than the pbC or poC olivines. The nickel trends indicate that the nickel content of the initial liquid decreased for each successive unit in the Ultramafic Zone.

Irvine et al. (1983) have suggested a model for the formation of layered intrusions where the individual layers crystallize from the walls into the chamber. One of the predictions of this model is that the cumulate minerals should be more fractionated along a layer. At Tverrfjell in the units where fresh olivine was found in the oC on more than one traverse no such fractionation trend is observed (Figs. 9a, b, c).

The composition of the olivine varies between Fo72.6 and Fo87.2. Since the low forsterite values occur in oC close to the Double Group which has experienced carbonate alteration, it is believed that this alteration has effected the composition of the olivine. The range of forsterite values from samples free of carbonate alteration is Fo77 to Fo87.2. There is no overall fractionation trend in forsterite content of the olivine with height. The forsterite content of olivines in unit 1 is similar to that in the oC of unit 15, Fo85. In contrast with nickel, the relationship between Fo content of the olivine and height within each unit is complex (Fig. 9 a, b, c) and there is no clear fractionation trend. In the ultramafic zone the forsterite content of the olivine varies between Fo83 and Fo87, but there is no correlation between height, or rock type and the forsterite content of the olivine. In the Mafic Zone the Oc (excluding those samples containing

carbonate) of most units is more forsteritic than its associated mafic rocks. The fractionation trends are not as clear as those observed for nickel. A number of processes could have disturbed the olivine compositions from their igneous values, including re-equilibration with pyroxenes during cooling or during subsequent metamorphism.

The KD = (XFe/XMg)ol/(XMg/XFe)opx between olivine and igneous orthopyroxene for 71 pairs from 50 different rocks range from 1.05 to 1.2. Using the thermometry of Sack (1980), these indicat equilibration between olivine and orthopyroxene between 800 and 1000°C (Fig. 10). The KD between olivine and the orthopyroxene of the coronas for 18 pairs are 0.92-1.1, indicating equilibration between 600-800°C (Fig. 19).

The KD=(XMg/XFe)ol/(XFe/XMg)cpx for 100 pairs in 63 rocks range from 0.65-0.85 (Fig. 11). Using the thermometer proposed by Navrotsky (1979), T Co=1054/(1.987InKD-0.33)-273, these KDs indicate equilibration temperatures of 615°C - 1341°C. The mean KD is 0.75 which would indicate a mean equilibration temperature of 900°C. As Navrotsky did not propose this as a definite thermometer it is not clear whether the wide range in temperatures is real. Using the thermometer of Powell and Powell (1974) the olivine clinopyroxene pairs indicate equilibration temperatures between 900-1000°C, at 4 kb. However, this thermometer has been critisized for being insensitive (Otten, 1985).

Olivine and pyroxenes crystallize together down to 1100°C. Therefore the temperature of 800-1000°C obtained by olivine pyroxene thermometry indicate that some subsolidus re-equilibration has occurred, probably during late cooling. This subsolidus re-equilibration could account for the poor correlation between forsterite content of the olivine and stratigraphic height.

MnO content of the olivines was less than detection limit by energy dispersive analysis. About 20 samples were analysed by wavelength dispersive analysis and the MnO content of these olivines is 0.10-0.25%, which is similar to the average values determined in olivines from other ultramafic and mafic plutonic rocks, 0.13 and 0.25% (Deer et al. 1982 p. 45).

TiO_2, Al_2O_3, CaO, Na_2O, K_2O and Cr_2O_3 were also determined, but were not detected.

Fig. 10 Olivine-orthopyroxene thermometer based on Sack (1980). O = olivines in orthopyroxene oikocryts, x= olivine & orthopyroxene from a corona, + = cumulate orthopyroxene o free olivine I = olivine & orthopyroxene chadocryts in clinopyroxene oikocryts. Note that the olivine & orthopyroxenes from coronas have distinctly lower (600-800°C) equilibration temperatures than the other olivine pyroxene pairs.

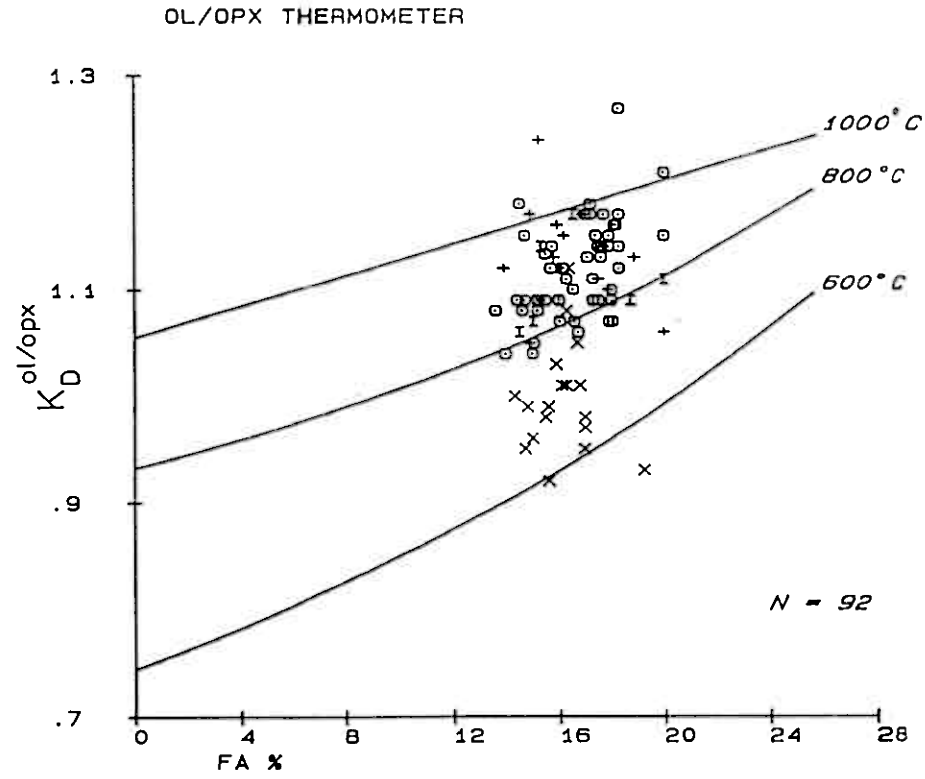

Fig. 11 (Fe/Mg) clinopyroxene versus olivine (Fe/Mg). The range in Kd's of 0.65 to 0.85 may represent extensive subsolidus re-equilibration. O = oikocryts clinopyroxenes, I = intercumulate clinopyroxenes.

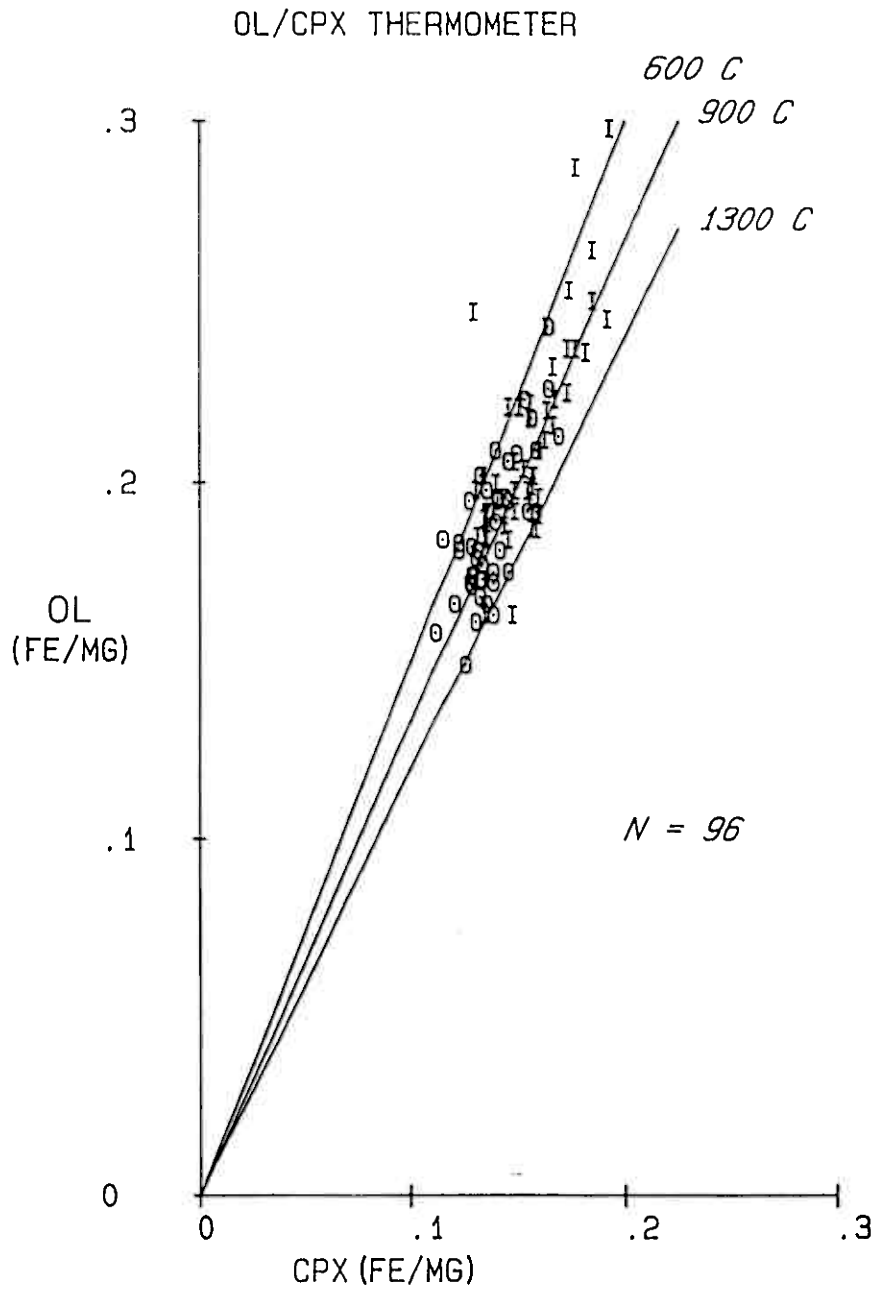

TABLE 3
ESTIMATED COMPOSITION OF MAGMA AT TVERRFJELL COMPARED WITH MAGMA COMPOSITIONS FROM THE LITERATURE.

	Tverr 1	N-MORB 2	E-MORB 3	OIT 4	Komat 5	Mantle 6
SiO2	49.41	49.1	48.4	48.0	49.72	48.9
TiO2	0.62	0.62	0.81	1.35	0.57	0.15
Al2O3	16.35	16.5	15.3	11.00	11.42	3.3
FeO	10.11	8.78	8.66	11.00	12.81	7.97
MnO	0.10	0.15	0.15	-	0.14	0.13
MgO	12.52	10.3	11.2	14.5	14.12	39.80
CaO	10.58	12.4	11.8	9.	9.49	2.64
Na2O	1.36	1.92	1.84	2	1.64	0.34
K2O	0.12	0.07	0.07	0.4	0.08	0.022
Cs	1.32	0.01	0.05	-	0.04	0.016
Rb	4.2	1	4.5	4.4	0.9	0.48
Ba	45	20	55	60	-	4.9
Zr	78	31	99	88	-	7.8
Hf	0.9	0.8	2	2.38	1.05	0.23
La	3.8	2.32	2.68	6.16	1.17	0.5
Ce	15.6	5.8	6.54	16.4	3.47	1.3
Sm	1.39	1.22	1.39	3.3	1.35	0.314
Eu	0.58	0.49	0.51	1.1	0.45	0.12
Tb	0.26	0.41	-	0.54	0.36	0.079
Yb	1.28	2.2	1.38	1.35	1.48	0.34
Lu	0.19	0.35	-	0.20	0.23	0.052
Y	16	24	24	15	14	2.9
Sc	39	34	33	21	42	10.6
V	279	140	167	-	-	84
Cr	8365	510	580	1450	1490	3000
Sr	168	127	105	213	45	15.5
Co	146	48	51	-	76	100
Ni	1121	232	262	30	250	2000
Ir	0.17	0.07	-	0.36	0.20	4
Rh	3					1.5
Pt	16	2	-	4	7	7.5
Au	17	1.8	-	-	1.7	1
Cu	627	79	81	-	52	28
S	5872	300	300	-	300	1000
Se	6.7	-	-	-	-	0.04

1. Estimate of the composition of the magma at Tverrfjell = (oC1 - 0.68xFo86)/0.32. Note that the composition is close to that of an E-MORB, except for elements that may be present in sulphides and chromite, possibly because the method used to estimate the composition of the liquid ignores the presence of cumulate chromite and sulphides.
2. Primitive N-MORB, based on; sample 527-1 from the FAMOUS area (Langmuir et al., 1977), BSVP (1981) p. 144 and olivine tholeiite DSDP-37.
3. Primitive E-MORB, based on; sample 525-2 from the FAMOUS area (Langmuir et al., 1977), BSVP (1981) p. 144.
4. Primitive ocean island tholeiite, based on; BSVP (1981) p. 181, p.173 and Crockett (1981).
5. Basaltic komatiite (Flow breccia of Fred's Flow) MacRae (1982) and ARC-9 BSVP (1981) p. 14.
6. Primitive mantle composition based on Taylor (1980), Sun (1981) and Barnes et al. (1985)

TABLE 4A
CRYSTAL FRACTIONATION MODEL FOR THE AVERAGE OF EACH ROCK TYPE

	Whole Rock oC Observed n=37	Model 1	bC Observed n=12	Model 2	pbC Observed n=12	Model 3	poC Observed n=44	Model 4
SiO2	42.53	43.57	51.44	53.46	49.35	51.04	48.22	48.72
TiO2	0.12	0.21	0.32	0.23	0.20	0.22	0.21	0.20
Al2O3	5.40	5.88	6.13	5.55	19.77	19.35	19.96	21.47
FeO	12.50	11.72	9.00	9.64	4.69	6.01	4.59	5.61
MnO	0.16	0.07	0.16	0.05	0.09	0.03	0.08	0.03
MgO	33.54	34.11	26.44	26.48	12.73	11.68	11.18	11.37
CaO	3.85	3.80	3.91	4.42	9.83	10.45	12.54	11.17
Na2O	0.20	0.49	0.34	0.43	1.37	1.37	1.68	1.54
K2O	0.03	0.04	0.07	0.03	0.11	0.04	0.13	0.06
S	2249	2000	2021	2000	1034	1111	721	666
Rb	1	1.5	2.8	1.4	3.3	1.6	2	1.4
Ba	11	16	28	15	22	17	22	15
Sr	74	60	74	57	201	198	215	274
Cu	178	124	160	120	64	62	48	55
Ni	841	1457	481	310	167	123	144	158
Y	4.5	5.7	6.8	9.3	4.9	7	6	5.3
Zr	23	28	25	26	24	29	25	26
Ir	0.055	1.48	0.06	1.5	0.07	0.7	0.06	0.6
Pt	7.1	17.45	11.6	17.7	8.88	9	6.06	7
Au	6.6	8.7	10.6	8.8	7.3	4.5	6.0	3.5

Parameters used

1. Average olivine cumulate modelled as 65% olivine and 0.5% sulphides plus 34.5% trapped liquid after 9% fractionation.
2. Average bronzite cumulate modelled as 8% olivine, 63% bronzite and 0.05% sulphides plus 28.5 % trapped liquid after a further 9% fractionation.
3. Average plagioclase bronzite cumulate modelled as 5% olivine, 22% bronzite, 43% plagioclase and 0.03% sulphide plus 29.7% trapped liquid after a furthe 9% fractionation.
4. Average plagioclase olivine cumulate modelled as 18% olivine, 51% plagioclase and 0.18% sulphides, plus 30.82% trapped liquid after 23 % fractionation.

TABLE 4B (cont)

Olvines

	oC Observed	Model5	bC Observed	Model	pbC Observed	Model	poC Observed	Model
SiO2	40.11	40.19	39.57	40.15	40.53	39.88	40.10	40.09
FeO	14.09	13.39	14.76	13.58	15.21	15.04	15.08	13.90
MnO		0.06		0.06		0.08		0.06
MgO	45.12	45.80	44.49	45.64	44.97	44.45	45.22	45.39
Ni	0.09	0.17	0.12	0.17	0.05	0.10	0.13	0.17

Orthopyroxenes

	oC Observed	Model6	bC Observed	Model	pbC Observed	Model	poC Observed	Model
SiO2	56.19	57.10	55.85	56.99	55.81	56.63	55.87	56.96
TiO2	0.29	0.06	0.23	0.06	0.25	0.07	0.13	0.06
Al2O3	2.99	0.34	2.93	0.38	2.76	0.41	1.96	0.35
FeO	8.68	8.67	8.84	8.97	9.75	10.18	10.37	9.13
MnO	<0.10	0.06	<0.10	0.04	<0.10	0.04	0.10	0.05
MgO	30.30	32.29	30.63	32.04	29.63	31.03	31.23	31.91
CaO	2.00	1.57	1.50	1.60	1.57	1.72	0.62	1.62

Clinopyroxenes

	oC Observed	Model6	bC Observed	Model	pbC None observed	poC Observed	Model
SiO2	51.37	53.95	52.45	53.43		52.73	53.25
TiO2	1.32	0.62	0.52	0.61		0.48	0.73
Al2O3	4.48	2.32	4.11	2.90		3.54	3.07
FeO	4.41	4.40	3.92	4.23		4.49	4.24
MnO	0.32	0.07	0.13	0.05		0.11	0.06
MgO	16.66	19.39	16.90	18.23		16.37	17.79
CaO	19.52	19.91	19.83	21.19		20.37	21.62
Na2O	0.56	0.06	0.59	0.23		0.39	0.01

	Plagioclase7
SiO2	50.7
Al2O3	32.09
CaO	15.08
Na2O	3.02

5. Model olivine compositions calculated using the equations of Jones (1984). The values listed here represent the average of the first and last olivine compositions crystallized for each rock type.
6. Model pyroxene compostions calculated using the equations of Nielsen and Drake (1979), opx at 1250oC, cpx 1125oC.
7. Probed composition of plagioclase used for the pbC and poC modeling

9.3 Orthopyroxene

Orthopyroxene occurs in five forms:

a) In the oC it forms 1-2 cm long, anhedral oikocryts with extremely fine (0.005 Mm) exsolution lamellae of clinopyroxene on (100). The oikocryts contain olivine and sulphides, but no plagioclase (Plate 24).
b) In the bC and pbC it forms 2-3 mm, blocky euhedral grains with straight grain boundaries and is clearly cumulate. Exsolutin lamellae similar to those in the oikocrysts are present. Also exsolutin blebs of clinopyroxene approximately 20 Mm in size are present; brown hornblende is commonly associated with these exsolutions (Plates 27 and 28). In some samples the orthopyroxene is enclosed by clinopyroxene. Where the orthopyroxene is not enclosed in clinopyroxene a narrow (10 Mm) rim of hornblende is present.
c) In the poC the orthopyroxene is intercumulate and anhedral. It encloses cumulate olivine and plagioclase grains and in some samples rims intercumulate clinopyroxene (Plate 23).
d) In any of the rock types the orthopyroxene may occur as the inner layer of the coronas that developed between olivine and plagioclase. In the coronas it grows as radial fibres around the olivine, approximately 0.2 mm long (Plate 25).
e) In the carbonate-bearing meta-oC it occurs as 0.2 mm long elongate grains with straight grain boundaries and is intergrown with dolomite or magnesite. There are no exsolution lamellae or blebs.

The igneous pyroxenes are not systematically zoned (Fig. 6c), but the presence of the exsolutions means that the grains are not homogeneous either. In order to obtain representative analyses a defocussed microprobe beam was used in analysis.

The composition of the oikocrysts and the cumulate orthopyroxene is very similar (Fig. 12 and Table 4, Appendix) and covers the range En84 Fs12.8 Di3.2 to En79 Fs 17.6 Di3.4. It has been suggested (Sparks et al. 1985, Tait 1985, Wadsworth 1985) that after the formation of the chadocryst network (in this case olivine) the magma may continue to convect through the pore space to the overlying magma. The oikocrysts nucleate on the olivine from the circulating magma. In this model the oikocrysts grow in equili-

brium with the whole silicate magma rather than with the intercumulate liquid and consequently should have a similar composition to the cumulate pyroxene. From Units 1 to 8 on the central traverse the orthopyroxenes exhibit a systematic change in composition with height. The Mg No., Al_2O_3, CaO, TiO2 and Cr_2O_3 contents of orthopyroxene of each oC decreases steadily with height and the Fs content rises (Fig. 9b, shows Mg No., Cr_2O_3 and CaO versus height). A correlation matrix (Table 4b, Appendix) indicates that the trends for Al_2O_3 and TiO_2 are the same as for Cr_2O_3). The composition of orthopyroxenes in the oCs exhibits an overall iron enrichment trend from Fs13 in Unit 1 to Fs16 in unit 8. The MnO values were not precise enough to warrant further work. Within each unit the orhtopyroxenes show a similar trend, Mg No., Cr_2O_3, CaO, Al_2O_3 and TiO_2 content of the orthopyroxenes from the oC are higher than in those orthopyroxenes from the accompanying pbC. Similar trends in orthopyroxene composition are observed in units 2 to 6 of the western traverse (Fig. 9a). Insufficient orthopyroxene is preserved on the lower part of the eastern traverse for a clear picture to emerge of the pyroxene trends.

The trends in pyroxene compositions indicate that the FeO content of the magma increased with each new cycle.

Towards the top of Unit 5 cumulate pyroxene ceases to occur in mafic rocks and the crystallization order of orthopyroxene and clinopyroxene is reversed. Both are intercumulate, but the orthopyroxene rims the clinopyroxene. In the opC of units 6, 8 and 14 clinopyroxene is the dominant pyroxene. Above Unit 5, bC occurs only in unit 7. Above Unit 8 orthopyroxene is uncommon, even in the samples from the relatively well preserved eastern traverse and no clear trends can be obtained from the few analyses available (Figs. 9a and b).

The composition of the corona pyroxenes differs from the igneous pyroxenes, they have lower TiO_2, CaO, Al_2O_3, Cr_2O_3, MnO values. The corona pyroxene composition varies from En85.5Fs14.1Wo0.2 to En80.7Fs19.5Wo0.1. It also normally has higher En content than igneous orthopyroxenes in the same rock (see Table 4b, Appendix, samples marked with cr).

The metamorphic pyroxene have a composition range similar to that of the corona pyroxene (see Table 4b, Appendix, samples marked with m), and were disinguished from them on the basis of their textures.

Fig. 12 Composition of the Tverrfjell pyroxenes plotted on the pyroxene quadilateral. Composition of pyroxenes from the Bushveld (BS), Fongen-Hyllingen (FH) and Skaergaard (SK) complexes are indicated (sources on Fig. 19). Note that the clinopyroxenes from Tverrfjell are extremely FeO poor compared with other intrusions.

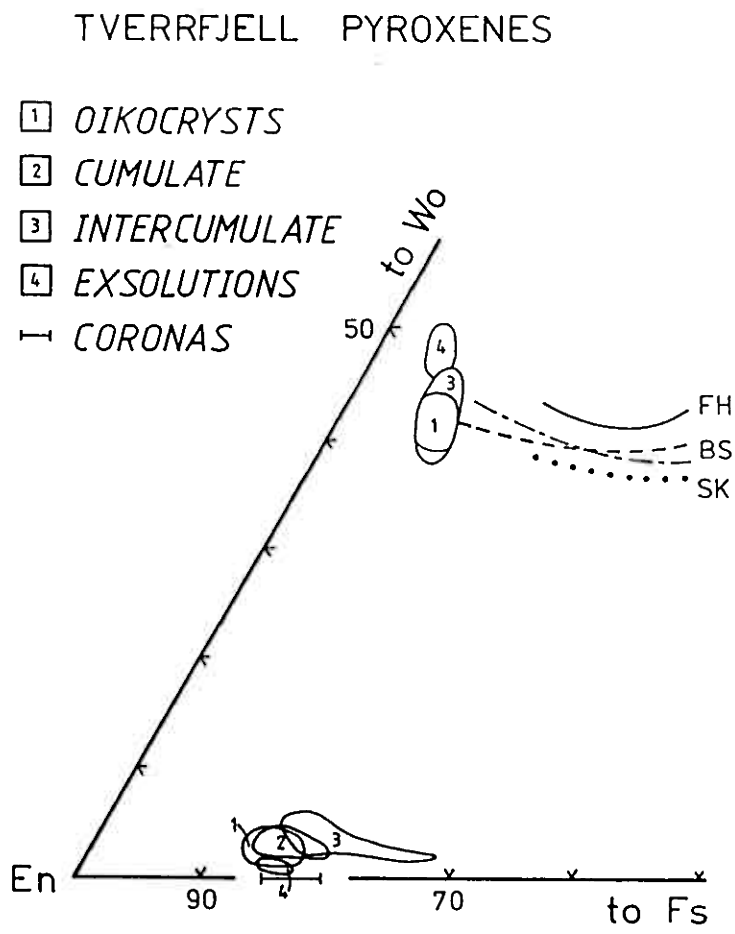

Fig. 13 Summary of results obtained for various two pyroxene thermometers. * = mean temperature, L + A = Lindsley and Andersen (1983), L + D = Lindsley and Davidson (1985), G = Gasparick (1984), N = Nickel et al. (1985), B + M = Bertran and Mercier (1985), K = Kretz (1982). Note that igneous pyroxenes yield igneous temperatures (1100 to 1300 oC) for most thermometers, but the exsolutions give subsolidus temperatures (900-1100).

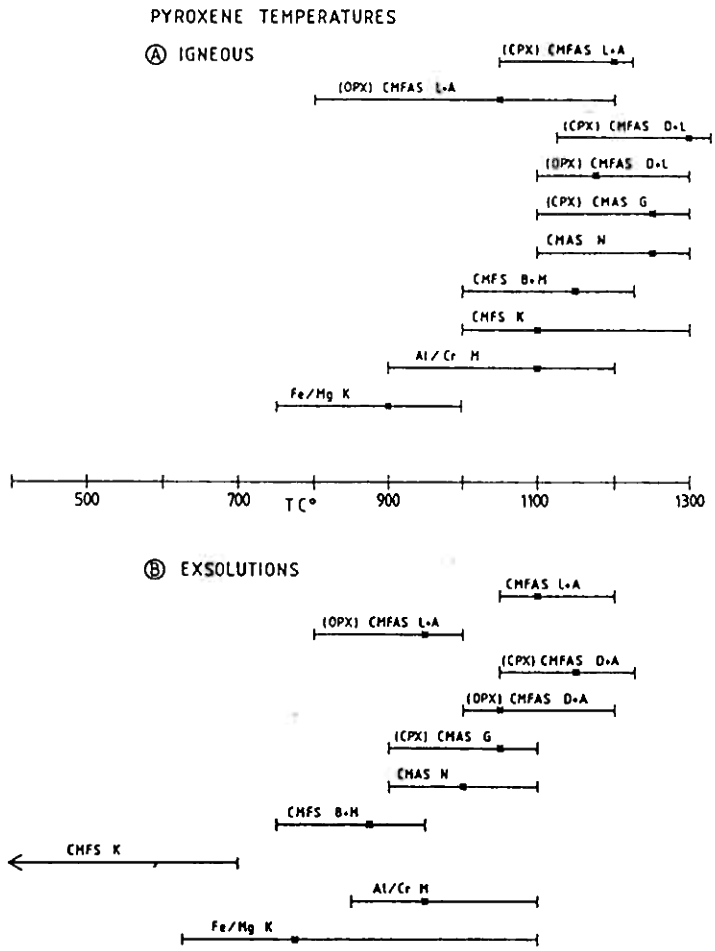

Fig. 14 Two pyroxene Al-Cr thermometer proposed by Mysen (1976). E = clinopyroxene exsolutions in orthopyroxene hosts; O = both pyroxenes oikocryts; I = both pyroxenes intercumulate C = orthopyroxene cumulate, clinopyroxene oikocryts.

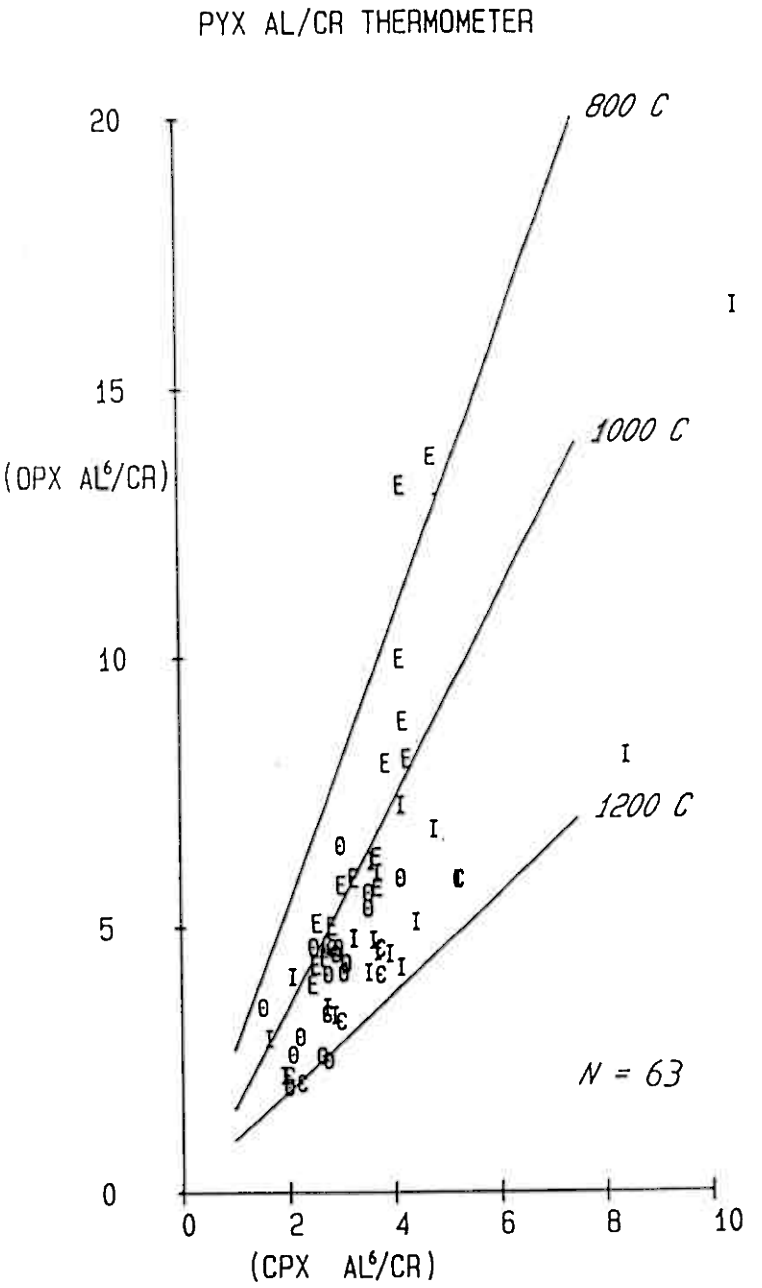

There are numerous orthopyroxene/clinopyroxene geothermometers. Fig. 13 summarizes the results, obtained for some of the more recent thermometers. For the igneous pyroxenes those thermometers that consider the system CMFAS (Ca, Mg, Fe, Al and Si) or CMAS gave similar temperatures in the range 1100 to 1300°C, with an average close to 1200°C. An exception to this was the temperatures obtained for orthopyroxene using the method of Lindslay and Anderson (1983). The orthopyroxenes gave a wide range of temperatures from 750 to 1200°C. The CMFS and Al/Cr (Fig. 14) thermometers gave slightly lower temperatures averaging at about 1150°C. Finally Kretz's (1982) Fe/Mg exchange thermometer gave the lowest temperatures, in the 750 to 1000°C range.

All of the thermometers indicate that the exsolution pyroxenes formed at 100 to 200°C lower than the igneous pyroxenes (Fig. 13 b). The CMFAS, CMAS and Al/Cr thermometers indicate equilibration temperatures in the range 900 to 1200°C with an average of 1050°C. The CMFS thermometers do not agree with one another, Kretz's (1982) thermometer gives very low results, some below 400°C.

In summary, most of the thermometers suggest that the igneous pyroxenes equilibrated in the 1000-1300°C range with an average of around 1150°C: these are close to liquidus temperatures and therefore it can be assumed that the present composition of the pyroxenes away from the exsolutions have not experienced substantial subsolidus reequilibration. The exsolutions, on the other hand, formed at subsolidus temperatures and obiously do not represent igneous compositons. The lower temperatures obtained for the Kretz Fe/Mg exchange thermometer may be a result of ignoring the other components (Ca, Al, Cr) or may be genuine. It should be remembered that all the thermometers that consider Ca tend to be dominated by the Ca concentration. Further Fe and Mg are small when compared with Ca so that these ions may continue to diffuse to lower temperatures than Ca. The difference in charge +2 versus +3 for Fe-Mg versus Al-Cr could account for the lower diffusivity of Al and Cr, hence the higher termperatures from this thermometer compared with Kretz's Fe/Mg exchange. Therefore while the Fe, Mg, Ca, Al and Cr contents of the ignous pyroxenes will be considered to be representative of igneous values the possibility that the Fe and Mg values have been disturbed cannot be ignored.

9.4 Clinopyroxenes

Three clinopyroxene morphologies are present:

a) In the oC, bC and opC the clinopyroxenes occur as subhedral oikocrysts, 1-2 cm in size, which enclose olivine and in the opC plagioclase. Most of these clinopyroxenes do not contain exsolution lamellae (Plate 22).

b) In the poC clinopyroxenes occur as intercumulate, 2-3 mm grains, the grains are frequently intergrown with, and rimmed by intercumulate orthopyroxene. The clinopyroxenes are patchy and contain orthopyroxene exsolution blebs.

c) In the bC and pbC clinopyroxene occurs as exsolution blebs up to 50 mm in size in the cumulate orthopyroxene grains (Plates 27 and 28). In many cases brown hornblende is present between the exsolution and the orthopyroxene.

The clinopyroxenes do not exhibit a systematic zonation (Fig. 6d), but exsolution patches are present. During probing an attempt was made to avoid these.

All of the clinopyroxenes are endiopsides (Fig. 13). The composition range of the oikocrysts and intercumulate grains is similar En50-55 Fs6-9 Wo38-45, the exsolutions are distinctly more Wo-rich and Fs- and En-poor En46-49, Fs4-6, Wo45-48. Compared with other layered intrusions the Tverrfjell clinopyroxenes are relatively iron-poor and aluminum-rich (Fig. 13). They are similar in Fs content to clinopyroxenes from the upper parts of the ultramafic zones of the Bushveld, Stillwater and Great Dyke intrusions, but contain approximately twice as much Al_2O_3. Otten and Senior (1985) describe similar clinopyroxenes from the ultramafic zone of the Artfjellet gabbro, of the Swedish Caledonides. They noted that only the pyroxenes of the Gross Pile Intrusion of Australia were directly comparable. However, the Gross Pile Intrusion clinopyroxenes are not as iron poor as the Tverrfjell ones. The Al_2O_3 content of clinopyroxenes has been related to the composition of the liquid and to pressure and temperature of crystallization. However, there is some debate as to which is the more important factor. On the basis of the distribution of Al between the octahedral and tetrahedral sites, the

clinopyroxenes plot in the granulite field (Fig. 14). Gasparick (1984) indicates that in the forsterite-plagioclase stability field the Al_2O_3 content of the clinopyroxenes is largely pressure dependent. Using his Fig. 6, the Tverrfjell igneous clinopyroxenes would have crystallized at 3 to 5 kb and 1100-1300°C (Fig. 18). Similarly the exsolutions indicate temperatures and pressures of 800-1000°C and pressures of 5 to 7 kb. Otten and Senior (1985, amongst others) question the use of Al_2O_3 as a geobarometer on the grounds of the large errors that can be associated with Al_2O_3 determination in the pyroxenes. Analytical errors for Al_2O_3 in this study are estimated at 5 % (Table 3), which is sufficiently small to justify the use of the geobarometer. Nickel et al. (1985) argue that the Al_2O_3 content of the pyroxenes is largely temperature dependent and use it as part of a CMAS thermometer, although they do not recommend its use in natural rocks. Finally Bertrand and Mercier (1985) suggest that the Al_2O_3 content of the clinopyroxene is not related to temperature or pressure and ignor it in their geothermometer. The answers given by Gasparick's (1984) geobarometer are geologically reasonable and have been accepted here with reservations.

On the basis of the Ti and Ca + Na content of the clinopyroxenes the magma from which they crystallized was sub-alkaline (Fig. 16). On the basis of Ti + Cr and Ca content, most of the pyroxenes plot in the "non-orogenic" field of Leterrier et al. (1982) (Fig. 17)."Non-orogenic" includes tholeiitic magmas formed at spreading zones of MOR or back-arc basin, or ocean islands or passive continental margins.

Despite the largely intercumulus nature of the clinopyroxenes they exhibit a systematic variation with height, similar to that observed for orthopyroxenes. On the western and central traverses for the first 8 units the clinopyroxenes exhibit an iron-enrichment trend. The Mg No (Fe/Fe+Mg) in oC drops from 89.9 in unit 1 to 87 in unit 8 (Fig. 8a and b). The Cr_2O_3, Al_2O_3, TiO_2, exhibit a covariance with the Mg No and steadily decrease from unit 1 to 8. (Figs. 8a and b and Table 6a). Na_2O and MnO show no systematic variations. For units 9 to 15 on the central and eastern traverse the clinopyroxenes exhibit a within unit iron-enrichment trend for units 9, and units 12 go 15. (No clinopyroxene analyses were obtained for units 10 and 11). However, there is no overall iron-enrichment trend. The Mg No of clinopyroxenes on the eastern traverse from the oC of unit 9 is similar to that of unit 14,88.2 and 88.4 respectively; correspondingly the Cr_2O_3, Al_2O_3 and TiO2 contents are similar.

Plate 27 Cumulate bronzite (B) with fine exsolution lamellae (white stripes) and clinopyroxene exsolution blebs (e) in a bC (Tv 75) of unit 1.

Plate 28 Bronzite enclosed in plagioclase oikocryts (p) in a bC (Tv 6 of unit 4). Field of view 2.2 mm

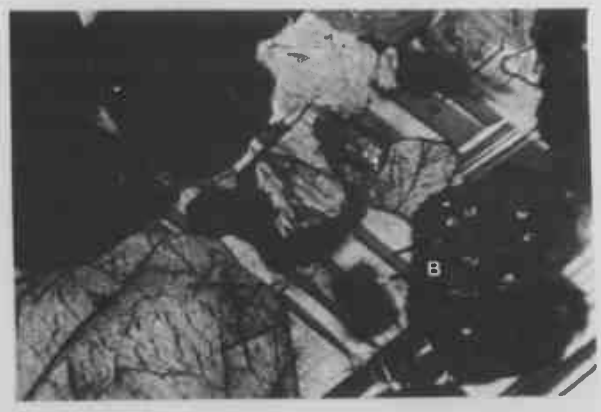

Plate 29 Chromite (c) enclosed in plagioclase (Tv 17). Field of view 3.6 mm

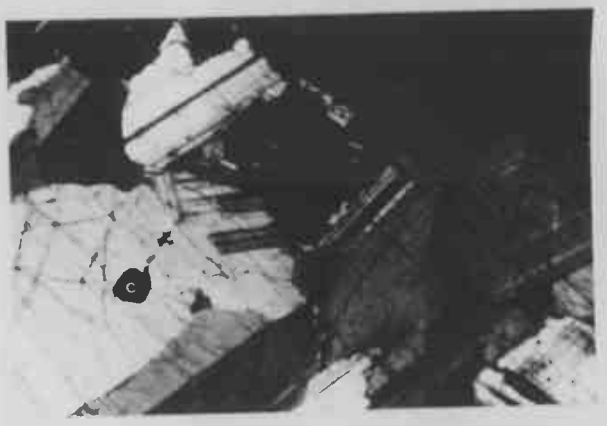

Plate 30 Chromite (c) in olivine (o) and olivine in sulphide (su). (Tv 17) Field of view 7.2 mm

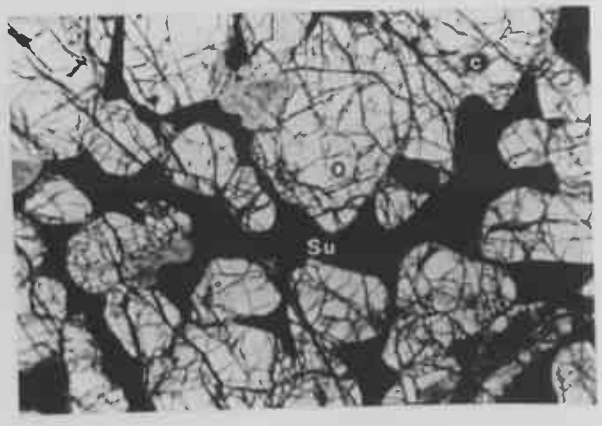

Fig. 15 Al IV versus Al VI for the Tverrfjell clinopyroxenes. E = exsolutions, O = oikocryts, I = intercumulate. Note that the clinopyroxenes plot in the Granulite field of (Aoki and Kushiro, 1968), indicating equilibration at moderate to high pressures.

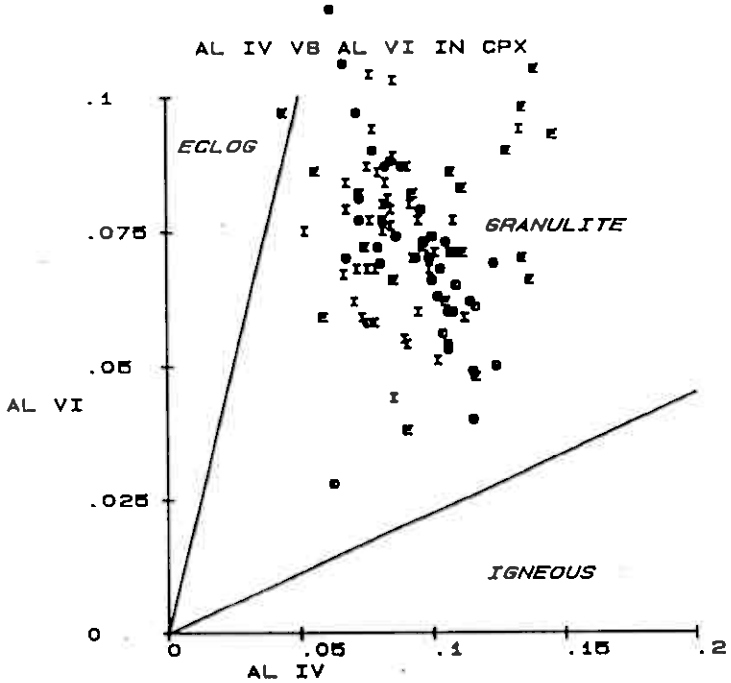

Fig. 16 Gasparick's (1984) geothermomter, geobarometer based on enstatite and Tschermakite content of the clinopyroxene. Note that the exsolutions appear to have equilibrated at lower temperatures but higher pressures than the other clinopyroxenes. Legend as on Fig. 15.

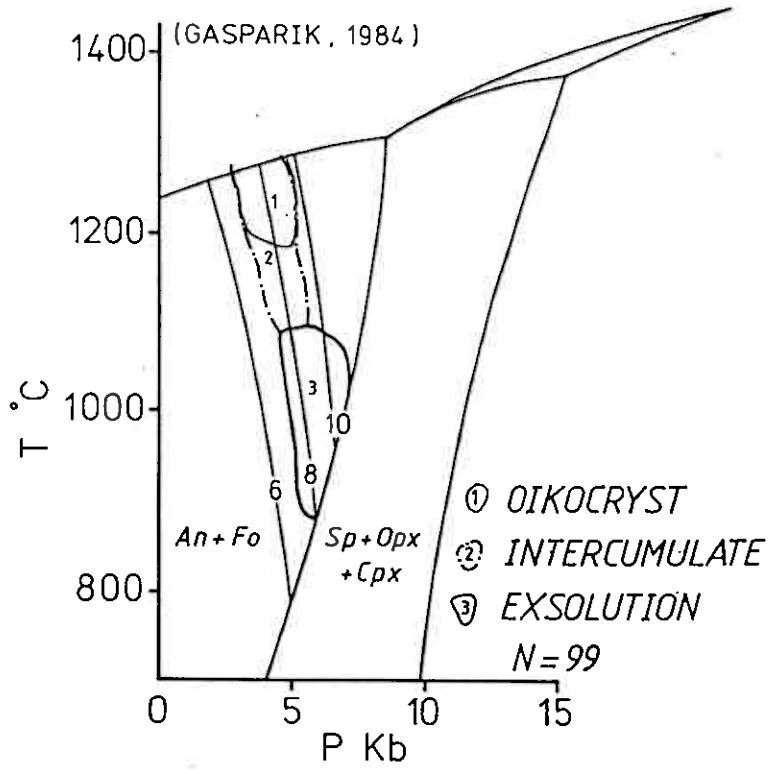

Fig. 17 Leterrier et al. (1982) diagram to distinguish clinopyroxenes from subalkaline and alkaline magmas. The clinopyroxenes from Tverrfjell fall in the sub-alkaline field. Legend as on Fig. 15.

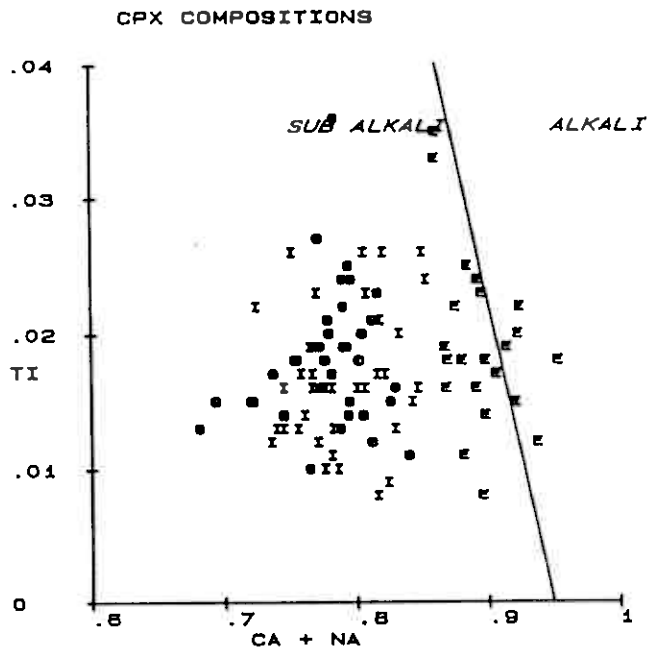

Fig. 18 Leterrier et al. (1982) diagram to distinguish clinopyroxenes from non-orogenic and orogenic environments. The clinopyroxenes from Tverrfjell fall in the non-orogenic field. This implies a tholeiitic magma formed in a spreading zone, MORB, back-arc basin, ocean island, passive continental margin.

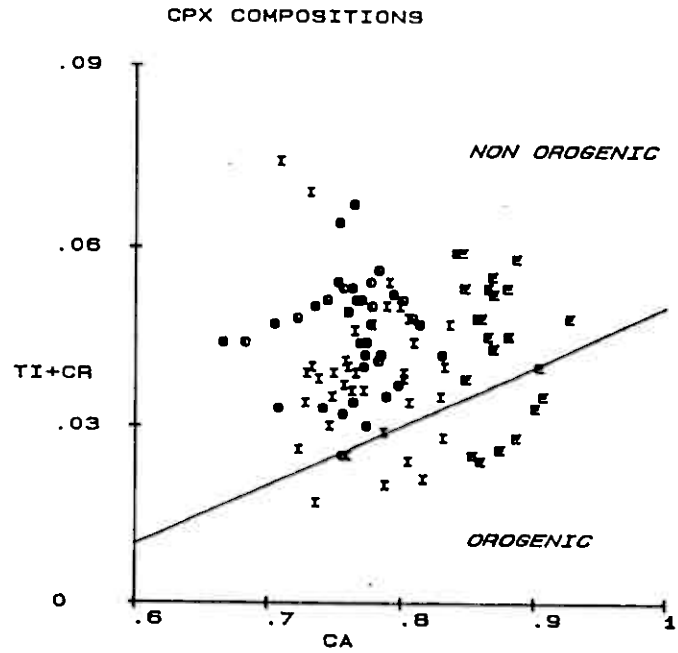

Fig. 19 Comparison of the composition of minerals from Tverrfjell with minerals from other layered intrusions. BV CZ= Bushveld, Critical Zone (Atkins, 1969, Hulbert and von Gruenewaldt, 1985; Kruger and Marsh, 1985) ST BZ = Stillwater Banded Zone (Raedeke and McCallum, 1984, Barnes and Naldrett, 1985), GD = Great Dyke, (Wilson, 1982), IN = Insizwa (Lightfoot and Naldrett, 1984), SK = Skaergaard (Brown, 1957, Brown and Vincent, 1963), FH = Fongen-Hyllingen (Wilson et al., 1981), NG = New Gabbros (Wadsworth, 1970), AR = Artfjallet (Otten and Senior, 1985),

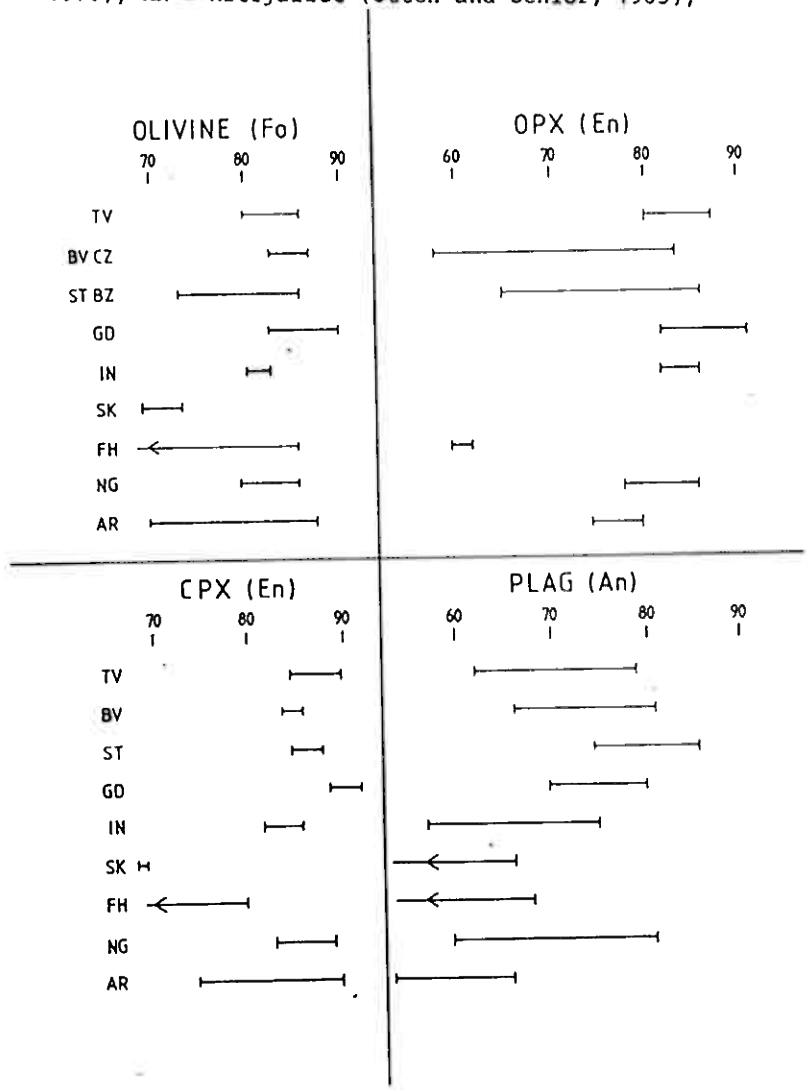

TABLE 5
MASS BALANCE CALCULATION

	Observed vol %	Wt % Norm minerals			
		ol	opx	cpx	pl
oC	9	65	12	4	15
bC	9	4	71	3	18
pbC	9	6	31	1	59
poC	23	18	10	12	61
dif=pC	50	-	26	18	59
Sum1		11	26	13	52
oC1 liq		10	26	13	52

1Sum = Ri*Mj, where Ri = weight fraction of rock type i, Mj= weight fraction of mineral j in rock type i, e.g. for olivine= 0.09*0.65 + 0.09*0.04 + 0.09*0.06 +0.23*0.14

TABLE 6
AVERAGE CHALCOPHILE AND SIDEROPHILE ELEMENT CONTENT OF ROCKS FROM THE RÅNA LAYERED INTRUSION

		Tverrfjell n=115	Brauvann n=16	Rånabogen n=7	Eiterdalen n=7	N-MORB	E-MORB	B. KOMATIITE
Ni*ppm		297	8400	4557	3447	300	300	249
Cu		110	1500	730	961	79	80	52
S		1441	54300	86300	64600	300	300	139
Ir	ppb	0.059	0.63	1.63	0.70	0.07	0.36	0.2
Pt		7.2	5	-	-	-	-	7
Pd		-	7	8	11.4	2	4	18
Au		7.3	18.4	3.4	5.6	1.8	2	2

100 % SULPHIDES

		Tverrfjell	Brauvann	Ranabogen	Eiterdalen	N-MORB£	E-MORB	KOM	Dsul/sil
Ni	%	7.6	6.85	1.96	1.97	6.0	6.0	5.00	200
Cu		2.8	1.02	0.31	0.55	1.6	1.6	1.04	200
Ir	ppb	15	4.3	6.98	4	70	360	200	1000
Pt		1862	34	-	-	2000+	4000+	7000	1000
Pd		-	47	34	65	2200	4000	18000	1000
Au		1867	126	14.6	31	1800	2000	2000	1000

* Estimated sulphide nickel
£ Calculated assuming 0.001 % sulphides segregate
+ Estimated on the basis of interpolation between Ir and Pd

TABLE 7:
AVERAGE CHALCOPHILE AND SIDEROPHILE ELEMENT CONTENT OF ROCKS FROM THE RÅNA LAYERED INTRUSION

		Tverrfjell n=115 ave.+	Range	Rånabogen n=7 ave.	Range	Eiterdalen n=7 ave.	Range
Ni	ppm	443	36 - 1615	4557	600 - 19900	3447	340 - 7730
Cu		110	3 - 320	730	138 - 2383	961	11 - 3846
Co		73	22 - 154	485	140 - 1910	337	75 - 716
S		1441	0 - 6959	86300	3504 -405816	64600	413 -163488
Ir	ppb	0.059	<0.01- 0.35	1.63	<0.3- 4.8	0.7	<0.3- 1.4
Rh		0.8	<0.5 - 6	<1	-	<1	-
Pt		7.2	<2 - 46	<10	-	<10	-
Pd		10*		8	<5 - 20	11.4	<5 - 22
Au		7.3	1 - 35	3.4	1.7- 22	5.6	1.7- 14

Also determined but not detected were Os < 2 ppb and Ru < 10 ppb. + samples <detection limit were treated as half the detection limit in calculating the averages, as 80% of the samples were above detection limit for Ir and Pd (Pt) this proceedure probably does not introduce much error however for Rh 50 % of the samples were below detection level. * Estimated on the basis of the chondrite normalized curve.

9.5 Plagioclase

Plagioclase occurs in three forms.

a) In the oC and bC it occurs as rare oikocryts, anhedral, 1-2 cm long and enclosing olivine and pyroxene (Plates 26 and 28).
b) In the pbC, opC and poC it occurs as 1 to 2 mm laths showing twinning. The grain boundaries between the plagioclase grains are bilateral (Plate 21).
c) In the pbC, opC and poC it occurs as 1 mm euhedral laths, polysynthetically twinned and enclosed in pyroxenes (Plate 22 and 23).

The plagioclase grains do not show a systematic zonation, but a wide variation in plagioclase compositions in a single grain is possible (Fig. 6e). There is no statistically significant difference between the composition of the plagioclase grains enclosed in pyroxene grains and the free grains (Table 7a). The average An content of the plagioclase is An71 and the range is An63-79.

Within most units the plagioclase shows an An depletion trend with height (Figs. 8a, b, c). Unit 5 is an important exception to this rule. On the central traverse there is an overall An depletion trend with height: the An content falls from An79 in the oC of unit 2 to An72 in the oC of unit 14. The fall in An content is not continous - there are three major reversals in the trend. From unit 2 to unit 5 the An content of the plagioclase in the oC drops from An79 to An63; just below the troctolite the An content of the plagioclase rises back up to An77. From the troctolite in units 5 to the oC of unit 9 the plagioclase again exhibits an An depletion trend to An69. There is a reversal to An72.9 in the oC of unit 11. From unit 11 to 14 the An content of the plagioclase drops to An72. On the western traverse the igneous plagioclase is present only in samples from the first 8 units. These exhibit similar trends to the plagioclase on the central traverse. On the eastern traverse there are reversals in plagioclase composition in the middle of unit 5 and at unit 13.

The plagioclase compositions at Iverrfjell cover a similar range to plagioclases from the Newer Gabbros of Scotland (Fig. 18). They are less calcic than plagioclase from the Critical Zone of the Bushveld, the Banded Zone of

the Stillwater, or the Great Dyke. They are more calcic than the Skærgård, Fongen, Artfjellet and Insizwa plagioclases (Fig. 18).

9.6 Spinels

Spinels are a small component (< 0.5 %) of the oC and opC of all units. The spinel occurs as small (0.05-0.15 mm), euhedral grains. In most samples (70 %) it is enclosed in plagioclase, but in a few samples (30 %) it is enclosed in olivine (Plates 29 and 30).

The compositional range of the spinel is chr53.6 sp29 her17.3 to chr34 sp47.8 her18.1 (Table 8). The +3 site is almost entirely occupied with Cr, Al and Ti and very little Fe+3, the Fe+3/(Cr + Al + Fe+3) ratios is 0.05-0.002. This implies that the spinels equilibrated at extremely low oxygen fugacities. Using the Fisk and Bence (1980) equation the average logfO2 at 1200°C is -14. This is close to the C/CO buffer and well below the QFM buffer. (08) is the value that most layered intrusions are thought to have equilibrated at (Haggerty, 1976). The +3 site is also unusual in its Al content; the Cr/(Cr + Al) ratio or Cr No ranges from 0.29-0.50. This is more aluminuous than spinels from other layered intrusion as can be seen on Fig. 20. The field for layered intrusions on this diagram is based on Dick and Bullen (1984) after Irvine (1967) and includes Bushveld, Great Dyke, Stillwater and Skærgård spinels. It also includes the field of Alaskan-type intrusions and komatiites. Haggerty (1979), in his review of spinels, reports spinels from the Rhum complex with Cr/(Cr + Al) ratios similar to the Tverrfjell chromites, but the Rhum chromites contain far more Fe+3. The Tverrfjell chromites have similar Cr/(Cr + Al) ratios to spinels from mantle xenoliths and abyssal tholeiites; they also have similar Fe+3 contents, but have lower Mg/(Mg+Fe) ratios or Mg No (0.3-0.5) (Fig. 20). In summary then, the Tverrfjell spinel compositions are unusual in that they resemble mantle xenoliths in the cations of the +3 site, but resemble layered intrusion in the cations of the +2 site.

The composition of a spinel is influenced by a number of factors:

a) The Si content of the melt; low Si contents lead to low Cr No (Irvine 1976). However to get Cr No as low as those observed at Tverrfjell the

Si content of the melt would have to fall sufficently for the crystallization order to be olivine, chromite, plagioclase with no orthopyroxene. This crystallization order is observed above unit 5, but half of the analysed spinels come from units where the crystallization order is olivine, chromite, orthopyroxene, plagioclase.

b) The fO2 of the melt, as logfO2 decreases to <-10 at 1200°C the Mg No of spinels from basalts decreases to about 0.33 (Roeder and Hill, 1974), which is in the correct range for the Tverrfjell spinels. However, simultaneously the Cr No increases > 0.60, which is too high for the Tverrfjell chromites.

c) Pressure of crystallization, Green et al. (1971) and Jaques and Green (1980) showed that as pressure was increased from 2 to 15 kb the Cr No of the spinels decreases from approximately 0.7 to 0.2. Eales and Marsh (1983), suggest that the increase in Al content of the chromites with pressure may simply reflect the decreasing field of plagioclase stability with pressure which increases the amount of Al that must be accomodated in the remaining phases. Haggerty (1979) points out that at the very high pressures experienced by spinel inclusions in diamonds the Cr No is high, possibly because Cr enters the tetrahedral site at these pressures. For the influence of pressure to account for the low Cr No observed in the Tverrfjell spinels, it will have to be postulated that the Tverrfjell body formed at unusually high pressures for a layered intrusion. The presence of plagioclase as a cumulate phase indicates that the pressure cannot have exceeded about 10 kb. It has been argued above that the pressure of crystallization was in the range of 3-5 kb; this is a little higher than estimates for the Bushveld and Stillwater (approximately 3 kb-Buchan et al. (1979) and Laotka (1985) respectively), but it is not clear that the pressure difference is sufficient to account for the difference in Cr No. Further, the Rhum intrusion which has chromites with similar Cr No is believed to have crystallized at 1.5-2kb (Tait 1985).

d) Post-cumulate reactions; numerous post-cumulate reactions between chromite, other cumulate minerals and magma have been suggested (Brown 1928; Thayer 1956, Irvine 1967). Henderson (1979) suggested that the low Cr No for Rhum chromites have been achieved by a postcumulate reaction

of the form:

$$2CaAl_2Si_2O_3 + (FeMg)_2SiO_4 + 2(MgFe)(Fe0.5\ Cr0.9\ Al0.6)O_4 =$$
$$\text{pl} + \text{ol} + \text{chr}$$
$$4(MgFe)(Fe0.25\ Cr0.45\ Al1.304 + Ca_2Si_5O_{12}$$
$$\text{chr} + \text{liq}$$

This is the reverse of the experimental reaction Cr-enrichment trends observed during reaction of basaltic liquid with cumulate chromites observed by Irvine (1967) and Hill and Roeder (1974). Henderson (1975) does not discuss why the reverse of the normal trend should occur. Subsequently Dunham and Wikison (1984) have argued that the low Cr No in the Rhum spinels are due to the Cr/Al ratio of the magma. This would imply that the Rhum and Tverrfjell magmas had unusual Cr/Al ratios, which seems to be a rather ad hoc solutin.

e) Sub-solidus reactions; it is fairly well established that subsolidus exchange reactions between ferromagnesian minerals and chromite lower the Mg No of the chromite (e.g. Evans and Frost 1975; Medaris 1975, Wilson 1982, Hatton and von Gruenewaldt 1985). On the basis of the Fe/Mg exchange between olivine and spinel and orthopyroxene and spinel, the spinels equilibrated at 700°C - 1200°C (Fig. 21). Since most chromite is enclosed in plagioclase this would require diffusion of Fe and Mg through the plagioclase. If the Mg No of the spinels has been lowered by sub-solidus exchange with ferromagnesian mineral then the igneous composition of the Tverrfjell spinels may have originally been in the mantle xenolith field, but still not in the layered intrusion field.

The negative correlation between Cr No and Mg No is also controversial (Fig. 20). Dick and Bullen (1984) suggest that this trend is due to olivine plus plagioclase fractionation, while Hatton and von Gruenewaldt (1985) suggest it is due to subsolidus diffusion.

In summary, the spinel compositions at Tverrfjell are unusual. The Cr Nos are lower than those normally found in layered intrusions either due to crystallization at high pressure or to crystallization from an usual magma composition. The Mg No of the spinels may have been extensively altered by subsolidus reactions. The chromites equilibrated at extremely low fO2.

Fig. 20 Cr number versus Mg number of the Tverrfjell spinels, note that the spinels fall outside the normal range of spinel compositions. Fields after Dick (and Bullen, 1984)

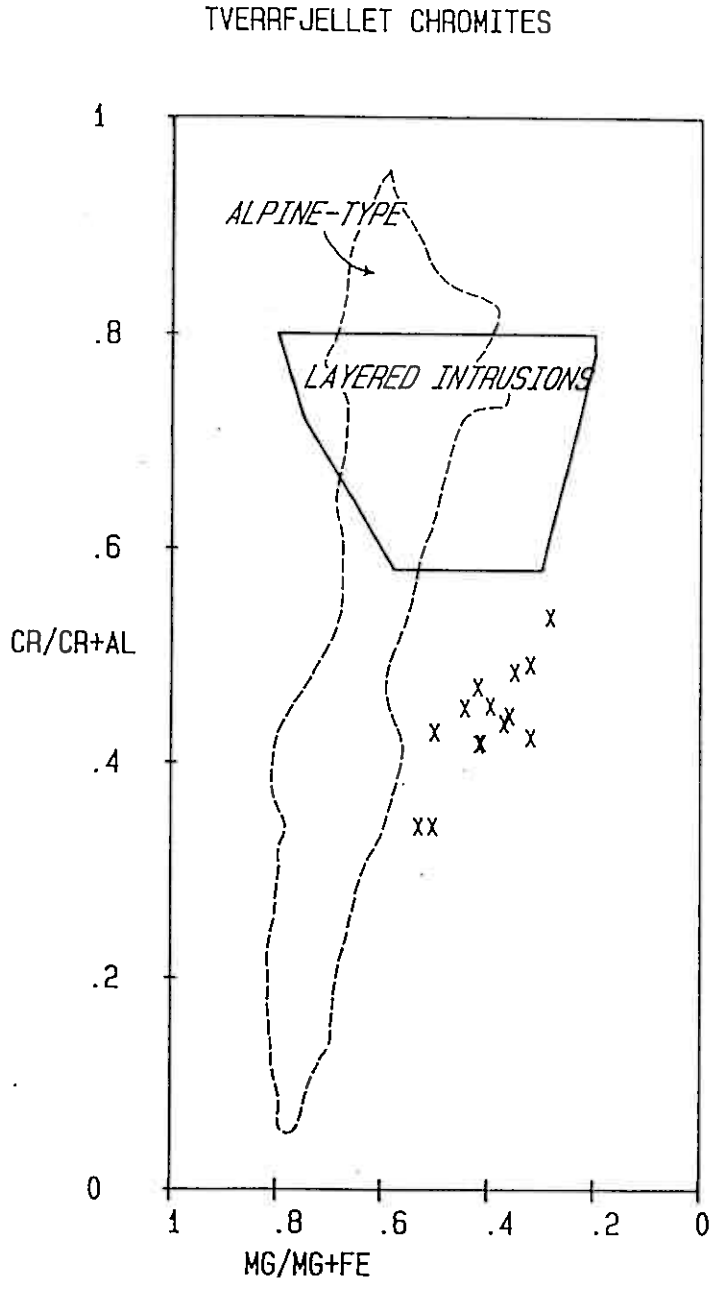

Fig. 21 Spinel olivine thermometer after Wilson (1982). The wide range of re-equilibration temperatures obtained for this thermometer is typical of layered intrusions (Deer et al., 1982, p. 58-64). O = chromite enclosed in olivine. P =chromites enclosed in plagioclase, R = chromites close to cronas.

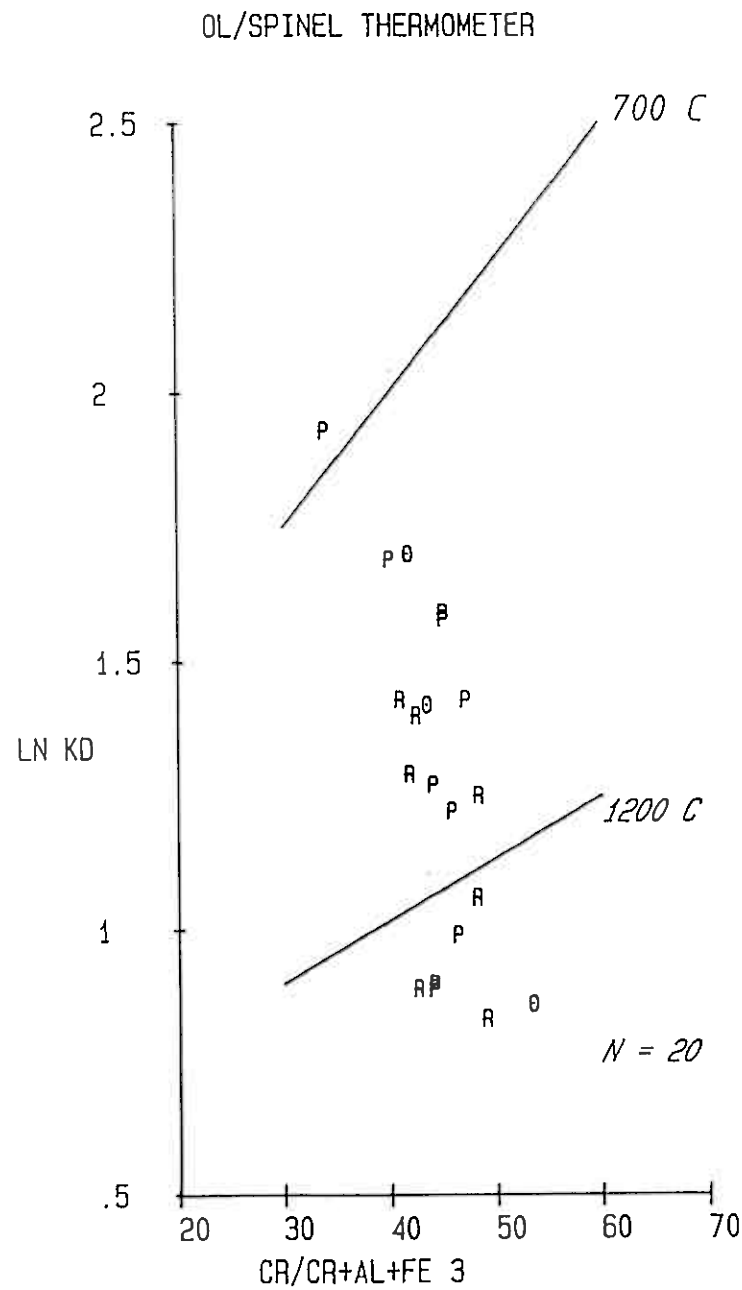

9.7 Coronas

Coronas are reaction rims that form between two minerals that are not stable together. Coronas between olivine and plagioclase are extremely common at Tverrfjell, although they are not alwas present (e.g. samples Tv 54 and 72). The coronas are approximately 0.3 mm wide and form two concentric layers of radially oriented minerals around embayed olivine grains (Plate 25). The inner shell is a 0.1 mm thick clear layer of orthopyroxene, the composition of which has been discussed in the orthopyroxene section. The outer shell is a 0.2 mm murky layer which consists of a symplectic intergrowth of clinoamphibole and spinel. Clinoamphibole predominates over spinel in a ratio approximately 10 to 1. The spinel forms vermicular intergrowths in the amphibole about 10 mm wide and 50 mm long. Precise analysis of the spinel proved impossible due to its intimate intergrowth with the clinoamphibole. The 'best' analyses obtained is defines as the one with the lowest SiO_2 and CaO contents (since spinel would not be expected to contain SiO_2 or CaO) is presented in Table 8 Appendix, Tv 12. The clinoamphibole is a pargasite. A mass-balance calculation on the spinel analysis, assuming that the spinel contains no SiO_2 and using the amphibole analysis of Tv 12, indicates that the spinel analysis is contaminated with about 56 % amphibole. The analysis was recalculated with the amphibole component removed and a passable (considering the assumptions made) pleonaste spinel analysis is obtained.

The Tverrfjell coronas are very similar to those described by Mongkoltip and Ashworth (1983) from the Newer Gabbros of Scotland. Coronas are a much studied phenomenon because both reactants and products are preserved (see Mongkoltip and Ashworth 1983 for a review). Most coronas have an inner shell of orthopyroxene, but the outer shell may consist of anhydrous products such as garnet and clinopyroxene or may contain amphibole as in the case of Tverrfjell. There is some debate as to whether the coronas represent late igneous cooling products (e.g. Griffin and Heier 1973, Mongkoltip and Ashworth 1983) or whether they are metamorphic (Esbensen 1978). In the cooling model it is suggested that the intrusions are emplaced into a regionally metamorphosed terrain at pressures between 6 and 10 kb. Olivine and plagioclase crystallize, but at pressures greater than 6 kb these two minerals are not stable together and they react to form the coronas. The pressure cannot exceed 10 kb or plagioclase would not have crystallized at all. The

metamorphic model suggests that subsequent to crystallization the intrusion experience pressures of greater than 6 kb and that the coronas develop at this time. Griffin et al. (1985) found that the Bergen and Sognefjord anorthosites have a long an complex history consisting of intrusion at 1300 Ma and less than 9kb, burial to greater than 10 kb and subsequent thrusting to the surface at 800 Ma, burial again to eclogite facies conditions at 400-500 Ma and finally reemplacement at the surface during the Caledonide Orogeny. The coronas developed during the burial to 10 kb at 870-1300 Ma.

The coronas at Tverrfjell indicate temperatures of 600-800°C (see olivine-orthopyroxene thermometer) and pressures greater than 6 kb during their formation. If the pressure estimates of 3-5 kb and temperature of crystallization of the pyroxenes at Tverrfjell 1000-1200°C are accepted, then the coronas cannot have formed at the same time. This implies that the Rana Intrusion was buried to pressures greater than 6 kb, after intrusion at 3-5 kb. At these pressures the coronas developed between olivine and plagioclase where water had access to the rock. It should be noted that in a few rocks olivine and plagioclase are in contact without development of coronas. Further, the more metamorphic minerals present in the rock, the larger are the coronas that develop.

9.8 Hornblende

Brown hornblende is developed along the exsolution planes in orthopyroxene, around the larger clinopyroxene exsolution blebs and around the rims of cumulate orthopyroxene, (analyses in Appendix, Table 8). Otten (1985) describes a similar development of hornblende in clinopyroxenes of the Artfjellet gabbro. He suggests that the hornblende formed at 900-1000°C due to "introduction of hydrous fluid from outside the gabbro". Veblen and Buseck (1981) give a comprehensive discussion of the possible mechanisms for the development of clinoamphiboles in pyroxene.

9.9 Biotite

Biotite is developed in the intercumulate material, in the corona rims and in the rims of cumulate orthopyroxene. No systematic study of this mineral was made and a single analysis is listed in the Appendix, Table 9 for interest only.

9.10 Sulphides

Sulphides are present in all rock types. They generally appear to be intercumulate (Plate 30), but this does not necessarily mean that the sulphide liquid segregated late in the magma's history. The texture presently observed indicates the order in which the minerals solidified, i.e. most silicate minerals crystallized before the sulphides. They consist of intergrowths of pyrrhotite, pentlandite and chalcopyrite. No systematic study of the variations in composition were carried out. However, based on the Ni-depleted nature of the olivines (Fig. 8) it is concluded that the sulphides segregated from the silicate magma prior to the crystallization of olivines. An alternative is that the olivine and sulphides exchanged Ni/Fe during metamorphism and hence depleted the olivine in Ni. This suggestion is rejected on the grounds that the average Kd NisulxFeol/NiolxFesul = 15 which is in the ignous range (Thompson et al. 1984). But see discussion by Fleet (1986) for an alternative point of view.

10. METAMORPHISM

The metamorphism of the intrusion is the subject of a seperate study and is beyond the scope of this report. However, the observed mineral assemblages and their implications are briefly discussed below.

10.1 Olivine Cumulates

In the olivine cumulates the first minerals to disappear are plagioclase and clinopyroxene. These are commonly replaced by an interlocking matrix of chlorite and tremolite laths 0.3 mm in length which surround xenoblastic

olivine and slightly decomposed orthopyroxene. In samples where metamorphism is a little advanced euhedral chromite and granular olivine grains are the only igneous grains in a matrix of chlorite, tremolite and dolomite (analyses in the Appendix, Tables 8 and 9). This is the most common assemblage and limits metamorphic conditions to upper amphibolite facies (Fig. 22).

In units 9 and 10 which associated with the sub-layer-parallel faults olivine is replaced by magnesite or dolomite and granular enstatite. The replacement of olivine by magnesite plus enstatite implies extremely high XCO2 conditions and temperatures of 550-600°C, at least on a local scale (Winkler 1979 Fig. 11-4).

Samples from close to the faults perpendicular to the layering and close to the basal contact have experienced some retrograde metamorphism. The olivine has been partly replaced by serpentine.

10.2 Bronzite Cumulates

Orthopyroxene is the first mineral to be affecte by metamorphism in the bronzite cumulates. In partly metamorphosed samples there is a matrix of plagioclase surrounding cumulate bronzite grains which have been partly replaced by cummingtonite (analyses in the Appendix, Table 8). The completely metamorphosed samples consist of an interlocking mat of cummingtonite and hornblende.

10.3 Plagioclase-Bronzite Cumulates

The pbC exhibit a similar alteration to the bC, but some plagioclase survives metamorphism

10.4 Plagioclase-Olivine Cumulates

In the partly metamorphosed poC the olivine in the coronas is completely replaced by orhtopyroxenes and the coronas acquire another shell consisting of pargasite plus plagioclase symplectite. In the completely metamorphosed

samples the pyroxenes and olivines are replaced by a granoblastic hornblende (analyses in Appendix, Table 8) and the plagioclase is partly recrystallized. Between the hornblende and plagioclase there is commonly a symplectite of zoisite and plagioclase.

In plagioclase-rich samples which are consequently Al_2O_3-rich, the assemblage hornblende, kyanite, zoisite and plagioclase is present. This assemblage indicates pressures greater than approximately 7 kb (Fig. 22).

10.5 Summary

Figure 22 indicates the P, T conditions recorded by the mineral assemblages in the intrusion. First, during intrusion, pressures were 3 to 5 kb. During the exsolution of the pyroxenes temperature in the intrusion were of the order of 1000°C and pressures 5 to 7 kb. During the formation of the coronas temperature were 600-800°C and pressures greater than 6 kb. During the metamorphism of the ultramafic units temperature were 600-800°C and pressures less than 13 kb. The poC indicates pressures of greater than 7 kb. Possibly all three of these events overlapped. Since the effect of the high-grade metamorphism is strongest in rocks close to the sub-layer parallel faults which probably formed during emplacement of Tverrfjell to its present position the metamorphism must have happened during or after the formation of these faults, i.e. during or after emplacement of Tverrfjell to its present position.

This suggests a model whereby the Råna intrusion was intruded into sediments at 9 to 15 km and then buried during deformation to 18 to 30 km.

11. GEOCHEMISTRY

11.1 Analytical Methods

All 147 samples from Tverrfjell were analysed for major elements and for the trace elements S, Rb, Ba, Sr, Ni,Cu, Cr, V, Y, Zr by XRF analysis at Midlands Earth Sciences Associates of Manchester. 136 samples form Tverrfjell were analysed for Pd and Rh and in addition Os, Ir, Ru, Pt and

TABLE 8:
LEGEND AND SOURCES FOR FIGS. 32 AND 33

Symbol	Rock Type	Location	Source
Ma	Mantle Nodules	World	Sun (1982);Barnes et al. (1985)
PRIMITIVE MAGMAS			
K	Komatiites	Canada	Crocket (1981)
		W. Australia	Keays et al. (1982)
Bk	Basaltic komatiites	Canada	
		W. Australia	
Morb	mid ocean ridge olivine	World basalt	BSVP (1981);Barnes et al. (1985)
Oi	ocean island basalts	World	BSVP (1981); Crocket (1981)
A	basanite	W. Australia	Mitchell and Keays (198 1)
Ct	continental olivine tholeiite	N. America	BSVP (1981); Crocket (1981)
Bc	Mg-tholeiite tholeiite	Bushveld chill	Sharpe (1982); Davis Bushveld chill and Tredoux (1985)
Sulphides-bearing komatiites			
Km	komatiites	W. Australia	Keays et al (1982)
L	komatiites	N. Ontario	Green and Naldrett (1981)
Ka	basaltic komatiite	N. Quebec	Barnes et al. (1982)
Sulphides-bearing ophiolites			
F	gabbro	Fy, Norway	Boyd and Nixon (1985)
Lf	gabbro	Lillefjell, Norway	Grnlie (1985)
Sulphides-bearing intrusions associated with continental flood basalts			
N	gabbro	Noril'sk, USSR	Smirnov (1966)
D	gabbro	Duluth, USA	Naldrett (1981)
GL	gabbro	Great Lakes, Canada	
I	picrite-gabbro	Insizwa, RSA	Lightfoot et al. (1984)
Sulphides-bearing mafic intrusions			
Ko	gabbro	Kollismaa Finland	Lahtinen (1985)
La	gabbro	La Perouse Alaska	Czamanske et al. (1981)
E	gabbro	Espedalen, Norway	Boyd and Nixone (1985)
V	gabbro	Vakkerlien,	Thompson et al. (1980)
J	gabbro	Jimberlana, W. Australia	Keays and Campbell (1981)
Hi	serpentinite	Hitura Finland	Hakli et al. (1976)
Platinium group element deposits			
UG-2	Chromitite seam	UG-2 Bushveld	Gain and Mostert (1982)
MR	gabbro-norite	Merensky reef Bushveld	Steele et al. (1975)
JM	gabbro-notite	JM reef Stillwater	Barnes and Naldrett (1985)
Ld	gabbro	Lac des Isles	Talkington and Watkinson (1984)
Hydrothermal Veins			
H	Cu-rich veins	Sudbury	Hoffman et al. (1979)
		Kambalda	Lesher and Keays (1984)
		Eretria	Economou and Naldrett (1984)

TABLE 9A: PARAMETERS USED FOR THE PARTIAL MELTING MODELLING

Degree %	Restite Minerals ol	sul	sil	Partition Coefficients sulphides				olivine					other silicates				
		wt %		Ni	Cu	Co	PGE	Ni	Cu	Co	Pd	Ir	Ni	Cu	Co	Pd	Ir
1	70	0.0913	30	250	250	50	1000	16.8	0	1	0	5	0	0	1	0	5
5	70	0.077	30	250	250	50	1000	16.8	0	1	0	5	0	0	1	0	5
10	70	0.058	30	200	200	50	1000	11.6	0	1	0	5	0	0	1	0	5
15	70	0.037	30	150	150	50	1000	7.5	0	1	0	5	0	0	1	0	5
20	70	0.0083	30	100	100	50	1000	5.4	0	1	0	5	0	0	1	0	5
25	70	-	30					3	0	1	0	5	0	0	1	0	5

TABLE 9B: MODEL COMPOSITION OF THE RÅNA ROCKS

Description	Ni ppm	Cu	Co	Ir ppb	Pt	Pd	Au
Initial melt, based on a 20% partial melt of mantle	628	135	99	1.17	26	18.7	3.7
Melt after removal 0.3% sulphides	401	86	85	0.058	1.3	0.93	0.18
Model of Eiterdalen consisiting of 17.5% sulphides 82.5% liquid F=.90	3765	807	540	0.58	13	9.3	2
Model of Ranabogen consisting of 23% sulphides 77% olivine F=.90	3952	837	616	0.58	13	9.3	1.8
Melt after removal of 15 % olivine and 0.15% sulphide	249	125	91	0.136	6.8	4.9	0.96
Model of Tverrfjell consisting of 0.39% sulphides, 30% liquid, 20% olivine and 50 % plagioclase and pyroxene	429	141	102	0.27	13	9.3	1.8

Fig. 22 Possible P-T path of the Rana Layered Intrusion.

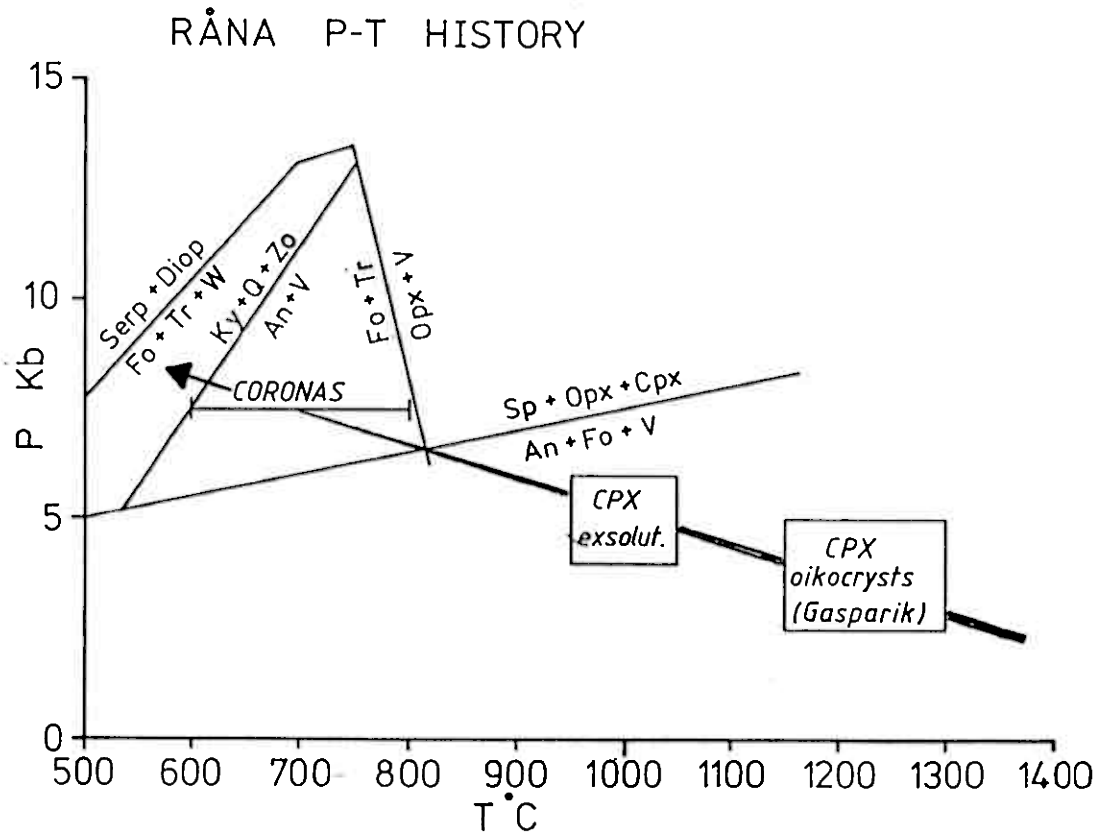

Au were obtained for 115 of these by instrumental neutron activation (INAA) after preconcentration in a nickel sulphide bead at the University of Toronto, Canada. A further 14 samples from Rånabogen and Eiterdalen were analysed for the platinum group elements in a reconnaissance study of these localities. 46 samples were analysed for REE, Hf, Cs, Sc and Co by INAA at X-RAY Assay laboratories of Toronto. Table 1 in the Appendix lists estimates for the precision of all three laboratories.

11.2 Results

Tables 2 a, b, c in the Appendix presents the chemical analyses of the Tverrfjell rocks in order of stratigraphic height on the western, central and eastern traverses respectively.

Table 2, presents a correlation matrix for the samples. Note that because the number of samples analysed for each group of elements is different the value at which r is significant is slightly different. The difference in significant r values for n=147, the number of samples analysed for major and trace elements, and for n=115, the number of samples analysed for noble metals is, however, small. Thus for the major, trace and noble elements r values of > 0.30 are significant at the 99.9 % confidence level. For the REE, Hf, Cs,Se, Sc and Co where n=46, r99.9=0.46.

The significant correlations between elements reflect mineralogical control; MgO, FeO, MnO, Co and Ni, olivine control; Al_2O_3, CaO, Na_2O, Eu and Sr, plagioclase control; SiO_2, TiO_2, Cr, V, Sc, Y and heavy rare earths elements (HREE, Lu, Yb, Tb), pyroxene control; S, Ni, Fe, Cu, Co, sulphide control; Zr, Hf, REE, Ba, K, Cs, TiO_2 and Y, trapped liquid control. Some elements e.g. Ni are associated with more than one phase, and this influence the correlation coefficients. If both phases are concentrated in the same rock type the correlation coefficients between the elements will be similar (all other factors being equal). However, if the phases are separated the correlation coefficients may be lowered. In ignous rocks it is commonly considered that the noble metals are present in the sulphides (e.g. Naldrett 1981). The correlation coefficients between S and the noble metals are therefore of interest. The correlation between Pt, Au and S is significant at the 95 % level, but there is no significant correlation between

Ir, Rh and S. The lower significance level for the correlation coefficients of Pt, Au and S, and the lack of a significant correlation coefficient between Ir, Rh and S, may reflect poor precision in determining these elements. At the extremely low levels at which the noble elements are present in these rocks the analytical error on the average Pt and Ir analysis was 50 %. Further, in many of the rocks Rh was present at less than the detection limit (values of less than detection limit are treated as half detection limit in the statistical analysis). An alternative explanation for the lack of significant correlation between Ir and S could be that Ir is not present chiefly in the sulphides. Inspection of the correlation matrix reveals only one element, besides the other noble metals, with which Ir has a significant correlation, Se. As no Ir-Se minerals are known (Cabri 1981) the meaning of this correlation is not clear; it could be fortuitous.

The mineralogical control of the elements is nicely illustrated by the mantle normalized plots for each rock type (Fig. 23). On a mantle normalized plot each element is divided by its abundance in the mantle (values used in this work are listed in Table 3, col. 6). The elements are plotted in order of decreasing incompatiblity from left to right. The compatibility of elements obviously depends on the phases that have crystallized. This varies from rock type to rock type and therefore the order of the elements on the axes could change. In this work the element order was partly determined by the crystallization order of the minerals, thus the elements related to trapped liquid are plotted first, followed by pyroxene, followed by plagioclase, followed by olivine and finally those associated with sulphide. The advantage of these mantle normalized curves is similar to that of REE curves, namely that it provides a finger-print for each rock type and deviations from the norm are easily spotted. Note that the REE are plotted as part of the mantle normalized curve and have exactly the same appearance as they would have on normal REE diagrams, where they are chondrite-normalized, except that the values are a factor of 1.4 less than on a chondrite curve. The reason for plotting the samples mantle-normalized rather than chondrite-normalized is that the concentration of metals such as Fe, Ni, Co is much greater in chrondrites than in the mantle. Mafic rocks are derived from the mantle, not chondrites and thus, if a mafic rock is chondrite normalized the values obtained for the metals are orders of magnitude less than that obtained for the other elements. Chondrite-

normalization produces an extremely jagged curve and makes comparison between rock types difficult.

The average mantle-normalized curve for each of the major rock types is illustrated in Fig. 23. The effect of the different mineral phases can be seen by comparing the curves. The oC (o) shows a relatively smooth curve steadily decreasing from Cs to Ir, with negative Rb, K, Hf and positive Sr anomalies. From Ir to Au there is a steady increase in mantle-normalized values and then a fall from Cu to S. Since olivine is the principle crystallizing phase the Cs to Fe portion of the curve probably represents the trapped liquid. On the basis of this assumption, the liquid is enriched in the highly incompatible elements, Cs to Ce, relative to the moderately incompotible elements, Sm to Ca. A similar conclusion could have been reached by considering only a REE diagram. The oC are LREE- (light rare earth element) enriched with a La/LuN (chondrite normalized ratio) of 2.5. However, by using the mantle normalized diagram many more elements can be considered and this avoids the possibility of errors due to LREE mobility or analytical problems. The R, K and Sr anomalies could be due to alteration and will be further discussed below. From Fe to Ni the curve shows a slight hump due to the presence of olivine. From Ir to S the curve should reflect the composition and proportion of sulphides present.

The bC mantle-normalized curve (B) shows a similar steady decrease from Cs to Zr to the oC, but with no Rb or K anomalies. From Zr to V the curve is much flatter than for the oC; this is because the elements from Tb to V are concentrated in pyroxenes and consequently the rock is enriched in these elements. From Cr to Fe the curve is similar to that of the oC, probably reflecting the liquid composition. From Fe to S the curve is similar to the oC curve, but at a slightly lower level in the Fe to Ni portion.

The pbC (N), poC (G) and opC have almost identical curves and will be discussed together. From Cs to Sm there is a steady fall in mantle normalized values. The presence of plagioclase produces a Eu anomaly and a peak in values from Al to Na. From Fe to Ir there is a steady decrease in values and the curves are at a lower level than for the oC or bC. The Ir to S portion of the curve is similar to the oC and bC curves.

11.3 Alteration

The three main processes that must be considered to have influenced the composition of the rocks are alteration, crystallization and partial melting. From the point of view of the economic potential of the platinum group elements, each of these processes may either enhance or deplete the PGE depending on the conditions.

All processes that have changes the composition of the samples from their igneous values are grouped together under heading 'alteration'; this thus includes mobility of elements due to late magmatic fluids, mobility during burial due to prograde metamorphism and mobility during uplift due to retrograde metamorphism.

In order for a component (or element) to be mobilized it must be soluble and be available for transport. A crude estimation of the solublity of an element in a hydrous solution is its ionic potential, (the ratio of its ionic radius/ionic charge). Those elements with a high ionic potential are the most soluble. In the case of the elements analysed in this work, Rb, K, Na, Au, Ba, Sr, Ca, Cu and S are potentially mobile (Fig. 24). However, if an element is present in a stable mineral phase then although it is capable, in itself, of being transported it may not be available for transport.

The effect of the stability of the mineral phases is well illùstrated by the difference in the behaviour of Na, Ca and Sr in the oC and the pbC or poC. Na, Cu and Sr are principaly controlled by plagioclase; plagioclase has altered to chlorite and tremolite in the metamorphosed ultramafic rocks, but in the metamorphosed mafic rocks it has merely recrystallized to form a more sodic plagioclase plus zoisite. Therefore in the ultramafic rocks, Na, Ca and Sr were released by the break-down of plagioclase during metamorphism. Large negative Na anomalies may be observed in mantle normalized curves of altered oC. (H on Fig. 25a), but no Na anomalies are observed on mantle curves of altered mafic rocks (H on Fig. 25c). On the other hand, no negative Sr and Ca anomalies are observed in either the ultramafic or mafic rocks, suggesting that little or no loss of these elements has occurred despite their release from plagioclase. This could be because one of the new phases that formed in the ultramafic rocks was a

Fig. 23 Mantle normalized curves for the four major rock types at Tverrfjell. O = oC, B = bC, N = pbC, G = poC. Note the general enrichment of highly incompatible elements Cs to Sm relative to the mildly incompatible elements Tb to Sc. La/LuN= 2.5

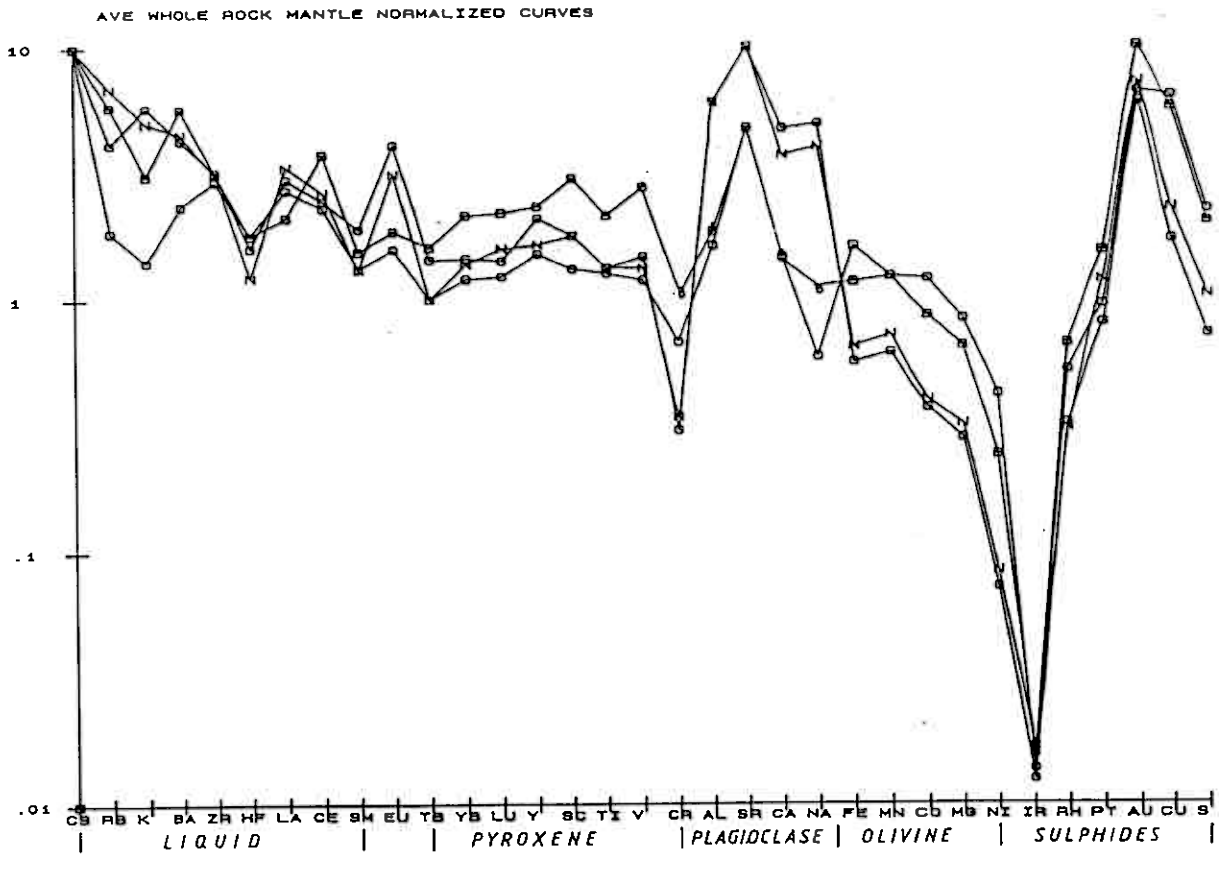

Fig. 24 Plot of ionic radius versus charge to deduce which elements are potentially mobile. Of the elements determined in this study, Cs, Rb, K, Na, Sr, Ca, Cu and S are potentially mobile.

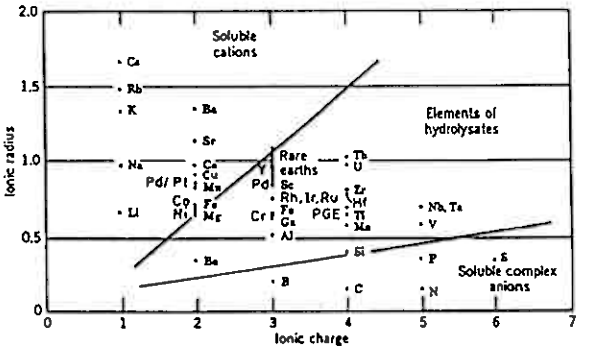

Fig.24 : Plot of ionic charge versus ionic radius to illustate the field of stability of the ions after Mason (1966)

Fig. 25a Comparison of mantle normalized curve for oC consisting largely of igneous minerals (I) with oC consisting largely of hydrous minerals (H) and oC containing carbonate minerals (C). Both the oC consisting largely of hydrous minerals and the oC containing carbonate is depleted in Rb, K, Ba and Na, in addition the oC containing carbonate is enriched in Sr.

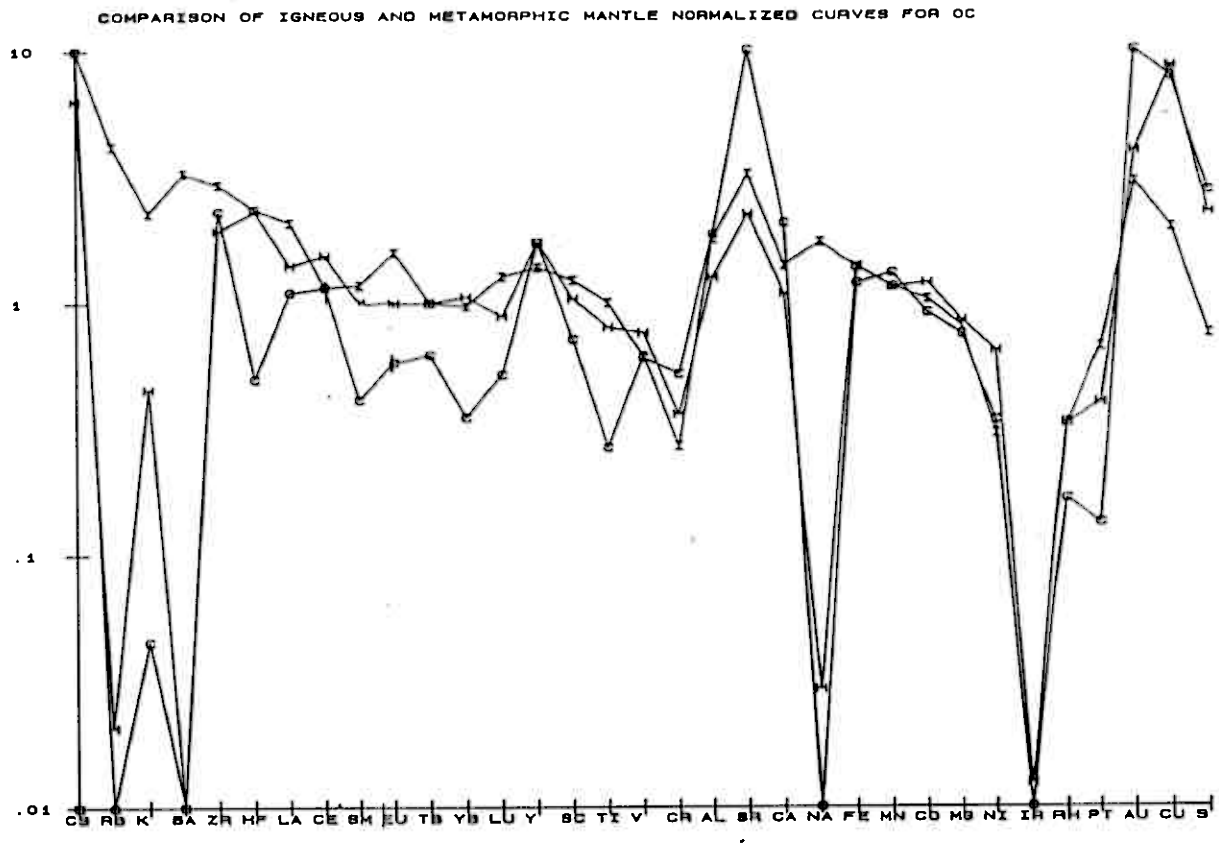

Fig. 25b Comparison of mantle normalized curves for bC consisting largely of igneous minerals (I) with bC consisting largely of amphibole (H). The amphibole rich bC is depleted in K and Na.

Fig. 25c Comparison of mantle normalized curves for poC consisting largely of igneous minerals (I) with poC containing amphibole (H). The amphibole rich poC is depleted in Rb, K and Ba.

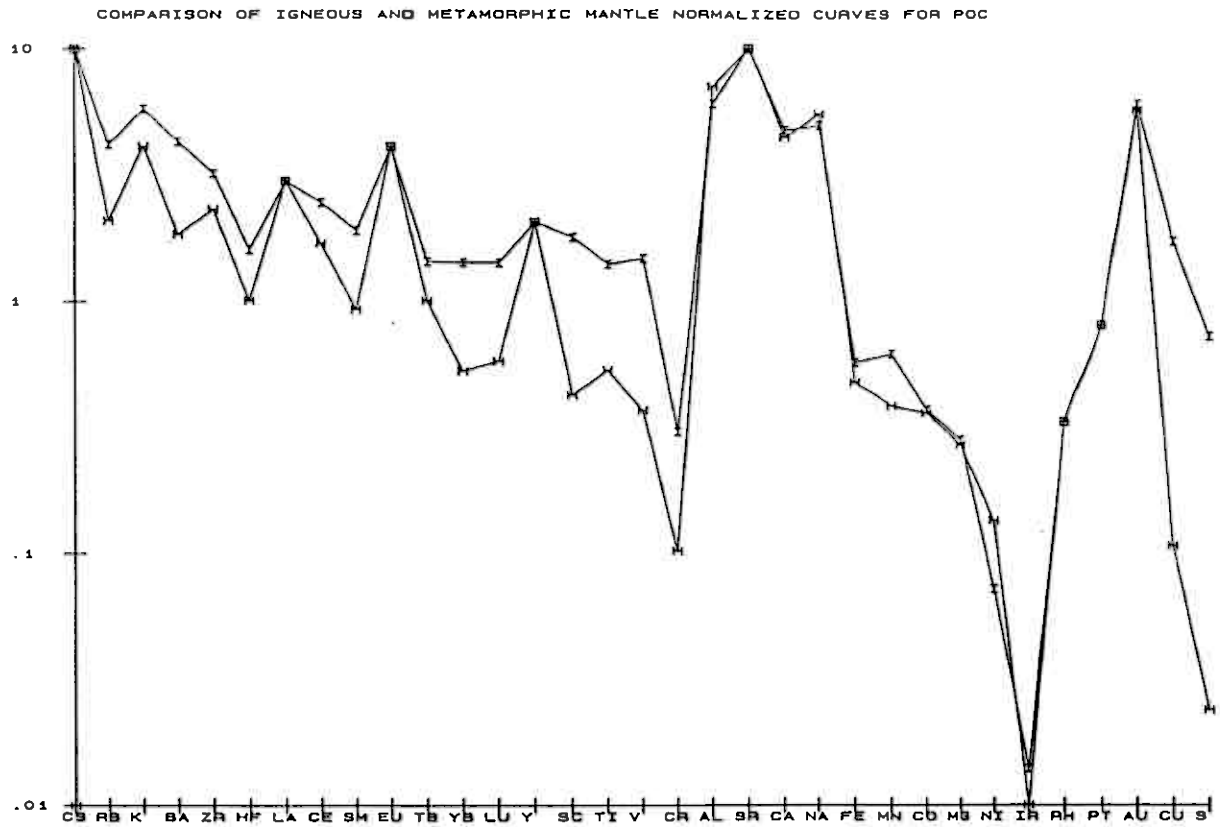

calcic amphibole and this offered a new site for the Ca and Sr and hence once again these elements were not available for transport.

An elemnt may also be enriched in a rock if a mineral phase formed for which the mineral has strong preference. Thus, positive Sr anomalies may be observed in ultramafic rocks that contain carbonate (C on Fig. 25a).

The correlation between Rb, K, Ba and Zr suggests an association with the trapped liquid phase in the rocks. These elements are probably sited in biotite. In the metamorphic form of all rock types, biotite was consumed and in most of them no K-bearing phase replaced it; consequently Rb, K and to a lesser extent Ba are depleted in the metamorphosed rocks. Metamorphic biotite is present in a few metamorphic mafic rocks and marked Rb increase is observed in these e.g. Tv 189.

Determining whether S, Cu, Au or Pt have been mobilized is a little more difficult than determining mobility in the lithophile elements, because S, Cu, Au and Pt are all potentially mobile (Fig. 24). These elements are next to each other on the mantle curve and thus there is no reference point with which to compare each individual element. Therefore the following assumptions have been made, based on samples from the literature (Barnes et al. 1985, Naldrett 1981) and on the unmetamorphosed samples of this study: the curves should be smooth and there should be a steady increase in the mantle normalized values from Ir to Au; the S to Cu ratio should be approximately 13. On the basis of these criteria most samples have not experienced alteration of the siderophile and chalcophile elements, although, a few samples are enriched in Au relative to Cu and some (in particular 3, 27, 41, 97, 126, 133, 132 140) are depleted in S. The samples depleted in S are all clearly metamorphosed, deformed and iron stained; little or no sulphide is present now and thus it is assumed that S loss has occurred.

To summarize, alteration appears to have depleted metamorphosed samples in Rb, K, Na and, in a few cases, S. In ultramafic samples containg carbonate Sr enrichment is observed. Alteration does not appear to have enriched or depleted the platinum group elements relative to their igneous values.

11.4 Crystallization

After removing the effects of alteration an estimate of the igneous composition of the rocks can be made. As these rocks are cumulates their compositions reflect the effects of crystal accumulation and fractionation. On the basis of the petrographic observations the principal mineral phases and crystallization order are; in units 1 to 5, olivine, orthopyroxene, plagioclase, clinopyroxene; in units 6 to 15 (with the exception of unit 7) the order is olivine, plagioclase, clinopyroxene and finally orthopyroxene in most samples, although orthopyroxene crystallized before clinopyroxene in a few samples. Sulphides are present in all units and rock types, but the timing of their crystallization cannot be determined on textural grounds. Ignoring the sulphides, the system can be described in terms of the tetrahedron forsterite, quartz, anorthite and diopside (Fig. 26). Crystallization paths consistent with the textural observations and the phase diagram place restrictions on the composition of the liquids from which the Tverrfjell rocks crystallized. For units 1 to 5 the liquid followed a path similar to, but necessarily identical to that shown by the cylindrical pattern (Fig. 26). For units 6 to 15 (with the exception of unit 7), the liquid (L2) contained more plagioclase component and proceeded straight from the forsterite volume to the anorthite phase boundary.

The phase relationships are a little easier to visualize on a triangular diagram and Fig. 27 shows the phase relations projected from diopside to the plagioclase-olivine-quartz surface. There are a number of differences between Fig. 26 which was intended to indicate schematically the crystallization path and Fig. 27 which is more quantitative. Firstly the samples on Fig. 27 have been recalculated into cation percentages to avoid the distortions that arise on a weight percentage plot due to the change in Fe/Mg ratio of olivine and Na/Ca ratio of plagioclase during crystallization. Secondly the phase boundaries shown on Fig. 26 are for 1 atmosphere pressure whereas those shown on Fig. 27 are for 3 and 4.5 kb., which is closer to the estimated pressure of crystallization of the Råna intrusion. It must be pointed out that the exact position of the phase boundaries is a subject of debate. Cawthorn and Davis (1983) who calculated the 3 kb. phase boundaries do not accept Irvine's (1970) 4.5 kb. phase boundaries. However, there is a general agreement on the trend. The liquid (L1) from which the oC below unit 6 (oC1) crystallized should lie along an olivine control line

Fig. 26 Phase relations in the system diopside-anorthite-quartz-forsterite, after Irvine et al. (1983). Two possible crystallization paths consistent with textures observed at Tverrfjell are shown

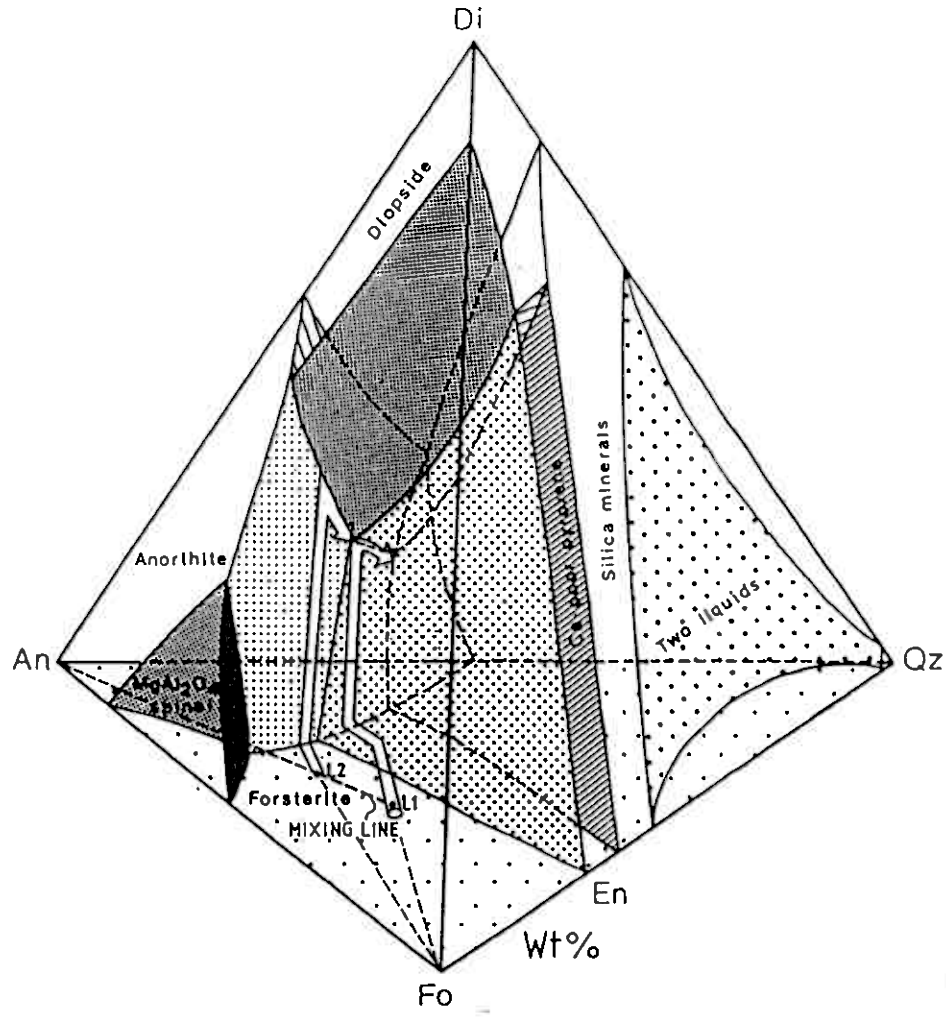

Fig. 27 pseudoternary projection from diopside to the olivine-plagioclase-quartz plane, using the method of Irvine (1970). The average and range (---) of each of the rock types at Tverrfjell is shown. L1 = the estimated composition of the liquid for units 1 to 5, L2 = a possible liquid composition for units 6 to 15 based on mixing between L1 and plagioclase cumulates (see text for further discussion)

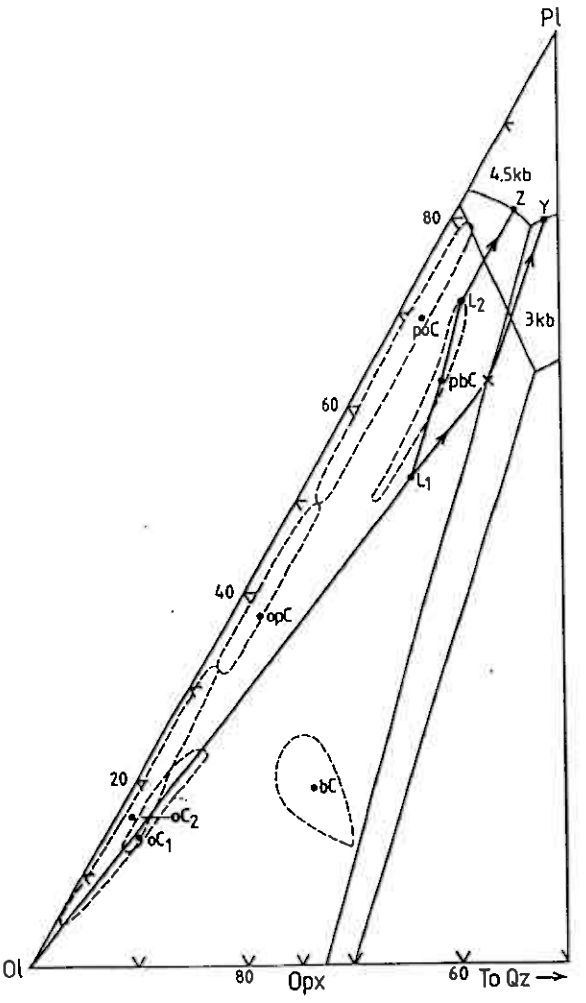

Fig. 28 Chrondrite normalized REE patterns for oC1 (x) and oC2 (o). The shape of the two patterns is similar except for the presence of a Eu anomaly in the oC2 pattern. The similarity of the REE patterns indicates that they crystallizes from liquids containing similar amounts of REE. The presence of the Eu anomaly suggests the presence of cumulate plagioclase in the oC2.

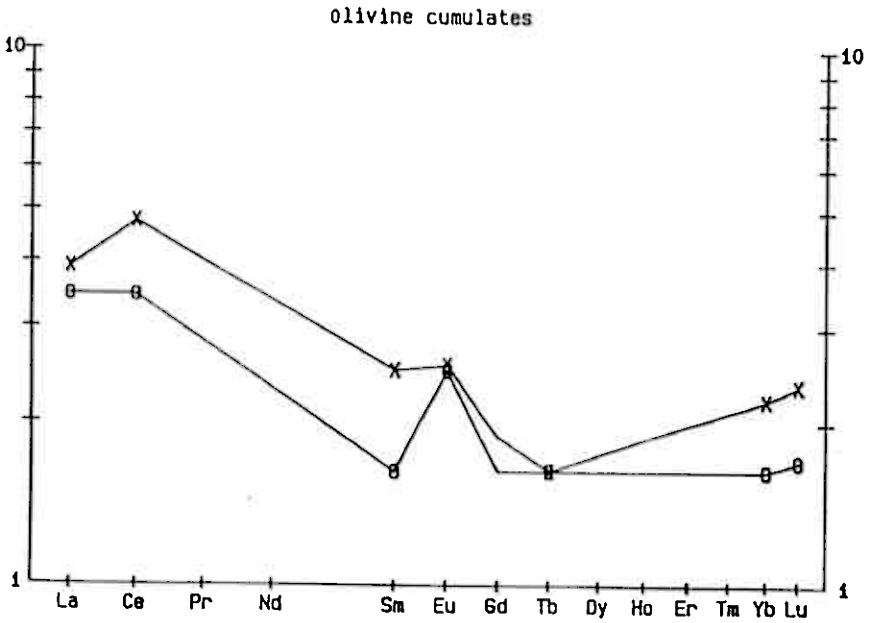

(i.e. on an extrapolation of the tie line between olivine and oC1). Estimation of the exact composition of the liquid from which Råna crystallized must be based on a number of assumptions. No chilled margins are preserved at Råna and in any event, chilled rocks are often contaminated and their exact relationship with the magma ambiguous. The composition of L1 was calculated by assuming that the average oC below unit6 represents only olivine plus trapped liquid and then subtracting the normative olivine (68 wt %) from the oC and recalculating to 100 % (Table 3, col. 1). This composition (L1) lies close to the olivine control line trough oC1 which indicates that the assumption that the oC represents mainly olivine plus trapped liquid is reasonable, since, if there were appreciable amounts of cumulate orthopyroxene or plagioclase present the calculated liquid composition would be displaced from the olivine control line towards the other cumulate minerals. The presence of cumulate plagioclase is further ruled out by the absence of a Eu anomaly in the oC1 REE pattern (X, on Fig. 28). The calculated composition of L1 assumes that all of the olivine is cumulate and does allow for the possibility of olivine overgrowths. Thus, the actual initial liquid could have had a larger olivine component; this would merely displace the liquid composition along the olivine control line towards olivine and would not be discernable on the phase diagram. The composition of olivine (Table 4 b), in equilibrium with L1 is Fo86. The most forsteritic olivine that was observed at Tverrfjell, was also Fo86, which might suggest that the initial liquid was no more MgO rich (and hence contained no more olivine) than the calculated liquid (L1). This argument ignores the possibility that re-equilibration between the olivine and trapped liquid during cooling may have occurred. Another way to test the suitability of L1 as the initial liquid at Tverrfjell is to calculate the proportions of each rock type this liquid would produce and compare it with the observed stratigraphic column. This mass balance calculation is shown in Table 5. Considering the assumptions made in such a calculation, the overall product of L1 of 9 % oC, 9 wt % bC, 9 wt % pbC, 23 wt % poC and 50 wt % pC agrees reasonably well with the observed proportions of these rock types. Therefore, L1 is a reasonable initial liquid composition.

A plausable crystallization path for the liquid would be as follows. Both the liquid and cumulates (oC1) should evolve along the olivine control line, which they clearly do (Fig. 27). When the liquid reached the orthopyroxene phase boundary at X, orthopyroxene crystallized and the liquid and

cumulates (bC) should lie along an orthopyroxene control line. Some bC do lie along the control line, but the average lies slightly to the left of the control line. This displacement may reflect the presence of a small amount of cumulate olivine in the bC. The liquid would have continued to crystallize orthopyroxene until the plagioclase phase boundary was reached at Y. It should then have crystallized both plagioclase and orthopyroxene. The product of this period of the magma history would be the pbC.

Above unit 5 the crystallization path of the magma is slightly different. Initially the liquid crystallizes only olivine and many of the oC from above unit 5 lie along the olivine-L1 control line (oC2 in Fig. 27). However, instead of bronzite, plagioclase is the second cumulate phase to form. This change in crystallization sequence could be achieved in a number of ways, two of which will be considered here. The first of these would be a change in pressure. Two sets of phase boundaries are shown in Fig. 27, one for 4.5 kb and one for 3 kb. Inspection of Fig. 27 shows that by simply changing the pressure of crystallization the crystallization order followed by a liquid of exactly the same composition can be changed from olivine, bronzite, plagioclase to olivine, plagioclase, bronzite as required. The lowering in pressure may be achieved by diapir-like rise of the intrusion through the crust or by fracturing of the country rocks and removal of some of the magma.

Another interesting possibility is a change in the liquid composition. If the liquid that crystallized the units above 5 contained more plagioclase component, for the sake of argument, composition L2, it would encounter the plagioclase phase boundary before it reached the orthopyroxene boundary. Consequently the product of the crystallization of this liquid would be opC and poC. The difference in crystallization histories for units 1 to 5 and units 6 to 15 could be due to a change in magma composition at unit 6. It was also noted that there is reversal in mineral compositions at this point (see earlier section). Noble elements reach their peak values in unit 5 (Fig. 29 a). Throughout units 1 to the top of unit 5 mineral compositions indicate a trend of iron enrichment and a normal crystallization sequence. If each unit represents an influx of new magma, the new magmas were becoming steadily more fractionated. Alternatively, if each cycle represents a double diffusive convection cell, the cells are more fractionated upwards, as they should be. The reversal of mineral compositons in unit 6

indicates that a more primitive magma was introduced. However, this is not simply a return to the original (unit 1) magma composition because the crystallization sequence changes. This magma must have more plagioclase component. The trace element signature of the oC2 (olivine cumulates above unit 5) is not statistically different in terms of incompatible elements, (e.g. Fig. 28) although it does have a Eu anomaly which indicates the presence of cumulate plagioclase. Although, the magma is more plagioclase-rich it does not have a radically different composition. The textural nature of opC of unit 6 offers a plausible explanation for the change in magma composition. OpC of unit 6 is the first banded unit. Physically it is a mixture of layers of oC and poC (plate 2). If liquid of composition L1 entered the magma chamber and mixed with the pbC of unit 5, then the composition of the liquid would be displaced towards plagioclase (Fig. 27) without changing the incompatible element ratios and the desired crystallization order would be achieved.

The situation is actually a little more complicated than this because the top of unit 5 consists of a discontinuous opC or poC (the troctolite) overlain by poC. As can be seen in Fig. 26 and 27 the presence of the poC in the upper parts of unit 5 represent a reversal in magma composition. This could be due to primitive magma from the overlying unit 6 percolating down into the semi-consolidated pbC of unit 5 and reacting with it (Fig. 29). The troctolite would then represent the reaction front, i.e. the depth to which the liquid penetrated. This model provides an explanation for the discontinuous nature of the troctolite.

The change in crystallization sequence in the middle of unit 5 is important because the highest values for Pt were obtained in units 5 to 8, which are the units where the change in crystallization order occurs. As Pt is normally present in sulphides the high values in units 5 to 8 could be due to the presence of more sulphides in these units. However, the analyses were recalculated to 100 % sulphides and replotted (Fig. 29b) and unit 5 is still enriched in Pt relative to the other units. The location of the Pt enrichment is all the more interesting since the JM and MR reefs of the Stillwater and Bushveld complexes are in a stratigraphically equivalent position, namely in the first major plagioclase cumulate overlying the ultramafic zones and in the case of the Stillwater the analogy is even more striking because the JM reef is associated with the first troctolite. It

Fig. 29a Pt versus stratigraphic hight for the western and central traverse (legend as on Fig. 1). The highest Pt values were obtained for units 5 and 8.

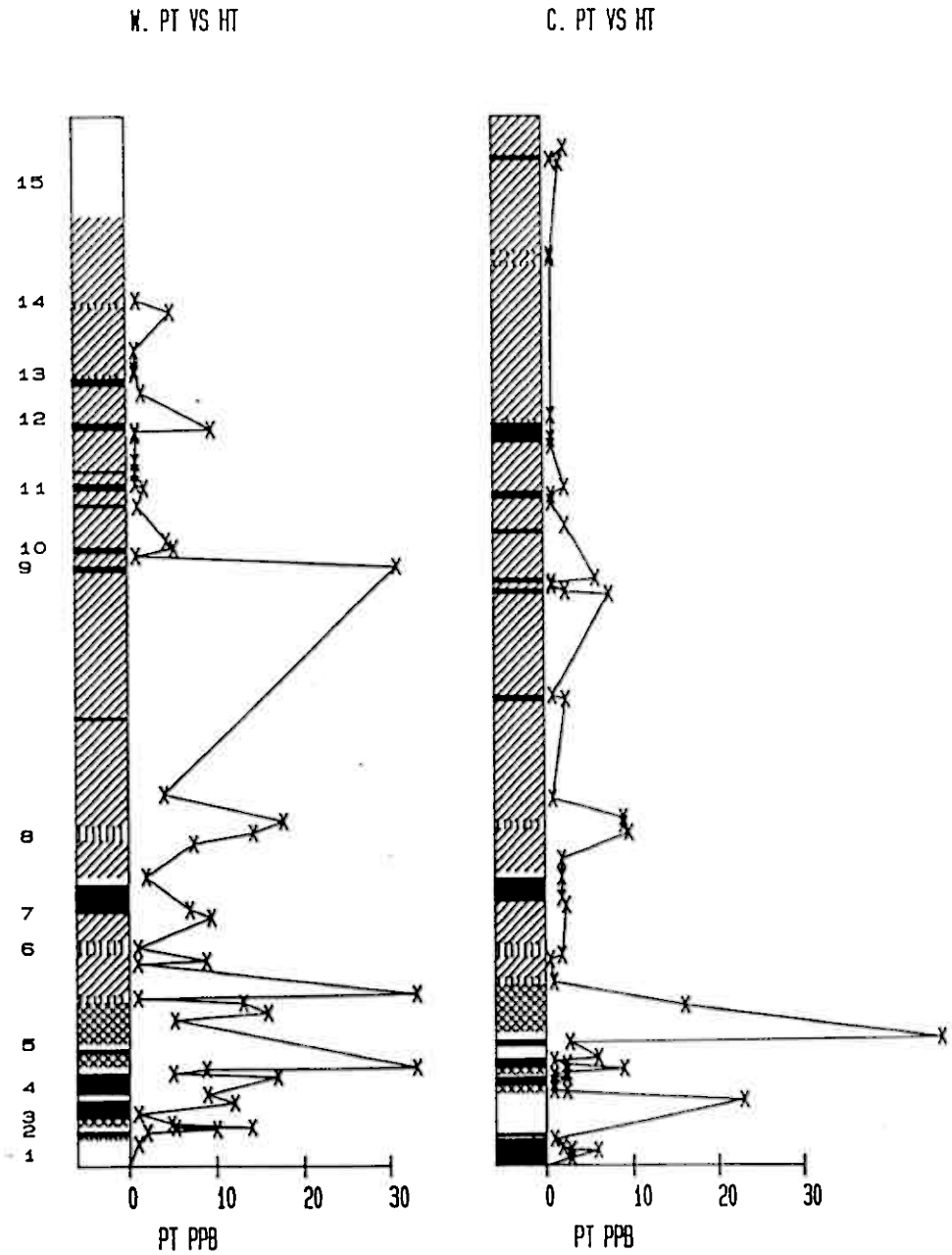

Fig. 29b Pt in 100% sulphides versus stratigraphic hight for the western and central traverse. Note that the peak for Pt values is still present in unit 5 and therefore the high Pt values obtained for the whole rock analyses was not simply due to a larger percentage of sulphides in these rocks.

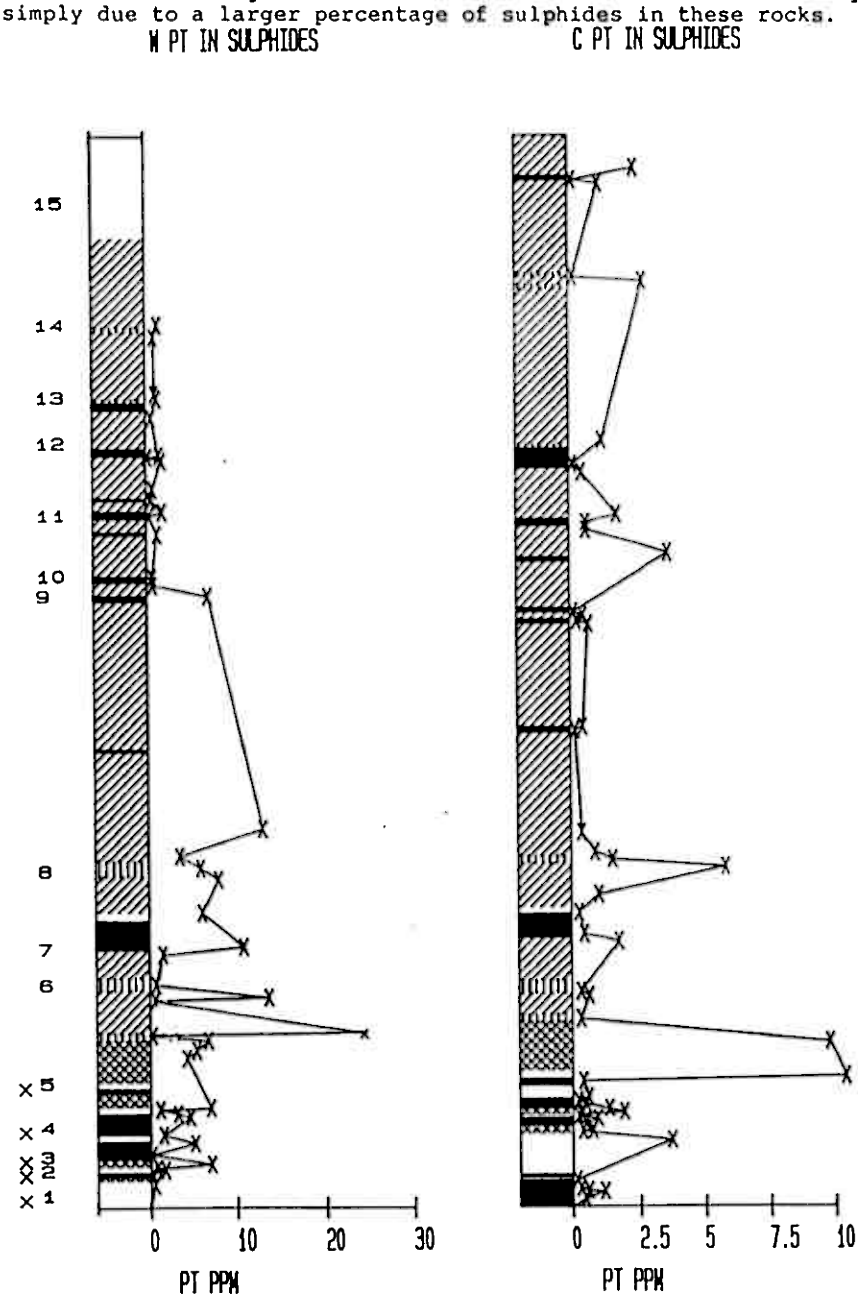

Fig. 30 Model for the formation of unit 5.

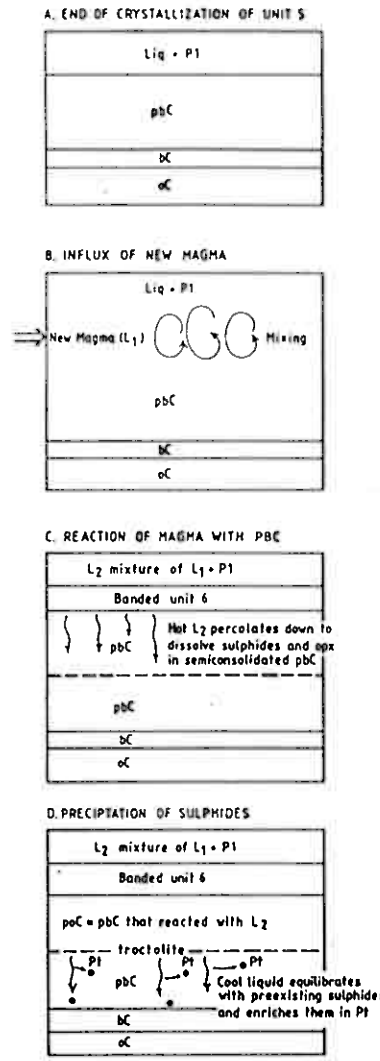

must be conceded, however that the enrichment of Pt at Råna is two orders of magnitude (50 ppb) too low to represent an economic deposit. None the less similar enrichment processes appear to have been operating in all three intrusions and it is therefore useful to try to understand the process at Råna even though no economic deposit is present.

If the change in crystallization order is due to a drop in pressure then the Pt enrichment could be due to a decrease in solubility of Pt in the magma with pressure and its consequent precipitation. This hypothesis is difficult to test, but it would suggest that there was also a decrease in pressure close to the stratigraphic height of the Pt reefs at the Bushveld and Stillwater.

On the other hand, the change in crystallization order could be due to the mixing of new magma with the pbC and the percolation of the new magma down into the underlying semi-consolidated pbC. The reaction of the new magma with the pbC could conceivably also change the solubility of Pt in the magma and cause the Pt to precipitate. If the Pt is present in sulphide, some mechanism of enriching the sulphides of unit 5 must be considered. The olivines throughout the intrusion are depleted in nickel relative to normal layered intrusions. Therefore it is assumed that sulphide saturation occurred before olivine crystallized and depleted the magma in nickel. This suggests that sulphur saturation took place before any of the silicate phases formed and it would therefore be expected that the composition of the sulphides would be similar throughout the units. On average this is true, (Table 6), but in detail and, in particular, for unit 5 it is not. This may be because sulphur solubility depends on temperature. Therefore some sulphides may segregate prior to the crystallization of the olivine, however as the temperature of the silicate magma drops more sulphides may be exsolved from the magma and thus change the composition of the average sulphide in that unit. A possible explanation for the Pt enrichment in unit 5 would be as follows (Fig. 30). Before the injection of the new magma, which formed unit 6, sulphides of normal composition developed throughout unit 5 and the lower units (Fig. 30a). When the new magma was injected and mixed with the pbC in the upper parts of unit 5 the new magma was hotter than the pbC and consequently resorbed the sulphides of pbC (Fig. 30b). This enriched the magma in Pt. As mentioned above the primitive magma percolated through the semiconsolidated pbC of unit 5 and reacted with it

(Fig. 30c). As it percolated downwards it cooled and no longer resorbed sulphides. Instead any sulphides already present in the pbC may have reacted with magma to extract the Pt that it resorbed from the higher units (Fig. 30d).

The average composition of each of the major rock types, oC, bC, pbC and poC can be numerically modelled, using the crystallization sequence outlined above and the relationship outlined by Jones et al. (1984) for equilibrium between olivine and liquid, Nielsen and Drake (1979) for equilibrium between pyroxenes and liquid and Drake (1979) for plagioclase and liquid. Using the composition of L1 as the initial liquid composition and fractionating olivine and sulphide from 9 wt % of this liquid. produced an oC very similar to the average olivine cumulate (Table 4a). The amount of liquid fractionated (9 %) was determined by the proportion of oC present in the stratigraphic column. The composition calculated for the olivine in equilibrium with the liquid is very similar to that of the probed olivine except for Ni, which is much higher in the calculated olivine composition than in the observed olivine. As pointed out earlier this may be because the sulphides segregated from the silicate liquid prior to olivine crystallization thereby depleting the magma in nickel. The oC may thus be better modelled as olivine and trapped silicate liquid plus 0.5 % sulphides liquid which the silicate liquid was carrying.

9 % of the evolved liquid was further fractionated by removal of orthopyroxene and a little olivine to produce a modelled bC very similar to the observed (Table 4a). Once again the amount of liquid fractionated was based on the proportion of the rock type present in the stratigraphic column. The calculated composition of the bronzite is similar to the probed compositions (Table 4b) except for Al_2O_3 and SiO_2. The probed compositions are higher in Al_2O_3 and lower in SiO_2 than the calculated compositions. This may be because Nielsen and Drake's equations are based on low pressure pyroxenes and Råna crystallized at moderate to high pressure. The calculated compositions of clinopyroxene are also in reasonable agreement with probed clinopyroxene compositions, although like the orthopyroxene compositions the probed compositions are richer in Al_2O_3 and poorer in SiO_2 than the modelled compositions.

The evolved liquid was further fractionated by removal of plagioclase and bronzite to produce a model composition for the pbC, that agrees reason-

ably well with observed compositions, (Table 4a). Once again the olivine, orthopyroxene and clinopyroxene compositions are close to the modelled compositions (Table 4b), but the plagioclase is not. The poor agreement between the observed plagioclase compositions and the model compositions could be either due to an inappropriate model or because the liquid composition used is incorrect. The statistical errors in the Drake model are large and the observed composition of the plagioclase lies within the error, but the equations proposed by Drake do not appear to be sensitive enough to use for modelling and therefore for the plagioclase cumulates the observed plagioclase compositions were used in the models.

After the production of the pbC, the liquid is not of a suitable composition to produce the poC. In particular it is too poor in MgO (7 %). As discussed above the poC is produced in units 6 to 15 after the oC, with no intervening bC. Therefore the liquid formed after the production of oC was used to model the poC. This may not be quite correct since, as pointed out above, the actual liquid for units 6 to 15 may in fact have been enriched in plagioclase. But since we are attempting to model the composition of a plagioclase cumulate which also naturally involves the addition of plagioclase to the liquid the processes cannot be distinguished geochemically. The chemical modelling can only indicate the total amount of plagioclase added and not the mechanism. The poC may be modelled as a mixture of plagioclase (of probed composition), olivine (of equilibrium composition, which is similar to probed composition), sulphide and trapped liquid (Table 4a). The pyroxenes in equilibrium with the liquid are close to the probed pyroxenes. In summary then, crystallization of the Tverrfjell portion of the intrusion may be modelled as forming from a tholeiitic magma containing approximately 12 % MgO, and carrying approximately 0.5 % sulphides. The oC may be modelled as a mixture of 65 % olivine, 0.5 % sulphides and approximately 34.5 % trapped liquid, the bC as a mixture of 63 % bronzite, 0.5 % sulphide, 8 % olivine and 28.5 % trapped liquid, the pbC as 43 % plagioclase, 22 % bronzite, 0.3 % sulphide and 29.7 % trapped liquid, 5 % olivine, the poC as 51 % plagioclase, 18 % olivine, 0.18 % sulphide and 30.82 % trapped liquid. In the first 5 units have crystallization order is olivine, bronzite, plagioclase, clinopyroxene, whereas in the overlying units except for unit 7, the order is olivine, plagioclase, clinopyroxene, orthopyroxene. The highest Pt values are found in the upper parts of unit 5 i.e. close to the change in crystallization order and also close to a reversal in mineral

compositions. Therefore the process that caused the change in crystallization order may also have caused Pt precipitation in the upper parts of unit 5. This process could be a change in pressure or mixing of a fresh influx of magma with the pC of unit 5.

11.5 Partial Melting

An estimate of the composition of the liquid from which the Tverrfjell portion of Råna crystallized is listed in Table 3, column 1. This is not necessarily the composition of the liquid from which the whole intrusion crystallized, because this estimate is based on the oC of units 1 to 5 at Tverrfjell. The composition of the liquid from which units below this crystallized could have been more MgO rich, but in the absence of any other means of estimating the liquid composition this estimate will be used. In terms of the major elements the liquid is an olivine tholeiite and resembles "primary ocean floor magma" such as those from the FAMOUS region or "primary ocean island magma" (Table 3 columns 2 to 4). Compared with a basaltic komatiite the estimated magma is too Al_2O_3 rich (Table 3 column 5). The resemblages between the estimated magma composition and primary oceanic magma is encouraging since the clinopyroxene analyses (see earlier section) indicated that the parental magma was one of; MORB, ocean island basalt or continental flood basalt. Further, the spinel compositions most closely resemble those found in abyssal basalts, in particular those from the FAMOUS area. Olivine and orthopyroxene analyses from all types of intrusions are similar and therefore do not help in estimating the parental composition of the magma, although they do help to estimate the FeO/MgO ratio (see crystallization section). The major element chemistry and mineral analyses indicate that the magma was primitive, possibly of MORB or ocean island affinity.

The trace elements can be used to further define the magma affinities and possibly its tectonic setting. Once again this can be most easily done with a mantle normalized curve (Fig. 31). From the mantle-normalized curve it is obvious that the estimated liquid composition does not resemble that of normal MORB for the highly incompatible elements Cs to Sm, i.e. normal MORB compositions are deplected in the highly incompatible elements such as the LREE relative to the moderately incompatible elements such as HREE. In

contrast the estimated Råna liquid is enriched in the highly incompatible elements relative to the moderately incompatible elements by a factor of about 2.5. In terms of the moderately incompatible elements, Tb to Ti, and Al to Na, the estimated magma composition and N-MORB are in reasonable agreement. The higher values for Cr and V in the estimated magma composition may be due to the presence of a small amount of cumulate chromite in the oC , because the calculated magma composition simply removed olivine from the cumulate before calculating the liquid composition. The elements Fe to Ni show a reasonable agreement with the estimated composition. However the chalcophile and siderophile elements Ni to S are enriched in the estimated composition relative to N-MORB, probably due to the presence of cumulate sulphides in the estimated liquid. Further these elements exhibit a greater degree of fractionation in the estimated liquid than in the N-MORB (Au/Ir ratio of Tverrfjell=100, Au/Ir ratio N-MORB=25). The estimated liquid composition then resembles primary N-MORB from Tb to Ni, but it is enriched in the highly incompatible elements Cs to Tb and the noble elements are more fractionated at Tverrfjell than in N-MORB.

There is a second type of MORB, known as enriched or E-MORB (Wood et al., 1979). This type of MORB, as the name implies is enriched in certain elements and these elements are the highly incompatible elements. As can be seen on the mantle normalized plot and in Table 3, column 3 primary E-MORB shows better agreement with the estimated liquid composition at Råna than the N-MORB.

As mentioned above the major elements and clinopyroxene indicate that the parental magma to Råna could have been a primitive oceanic island tholeiite. (Although the spinel compositions from Råna are too Al_2O_3-rich if compared with oceanic island spinels (BVP, 1981)). Ignoring the spinels, and considering the trace elements, the estimated liquid at Råna is depleted in the highly incompatible elements relative to primitive oceanic island tholeiites (Table 3, column 4 and Fig. 31).

It has been suggested (BVP 1981; Sun 1984, amongst others) that E-MORB is simply a mixture between N-MORB and ocean-island tholeiite. This contention is lent weight by the fact that E-MORB tends to occur close to ocean islands (BVP 1981).

The overall chemistry at Råna then suggest a magma similar to a primitive E-MORB composition. However, the geological setting of Råna namely an intrusion into graywackes at a depth of 9 to 15 km does not suggest a mid-ocean ridge setting, a seamount setting or ocean island like the Hawaian chain. Possibly the chemistry and geology can be reconsiled by suggesting that the body formed above a hot-spot in a back-arc basin, which was filling up with graywackes.

The nature and tectonic setting of the magma from which the Råna Layered Intrusion formed is of more than academic interest if the platinum group element concentrations in the magma are to be understood. The original magma composition at Råna appears to have been analogous to an olivine tholeiite possibly of E-MORB or ocean island affinities. There are few analyses of platinum group elements from ocean island tholeiites and N-MORB and none that the author is aware of, from E-MORB. However, since E-MORB has a composition intermediate between N-MORB and ocean island tholeiites for most elements its probably platinum group element content is intermediate between these. The platinum group element elements, Au, Cu and Ni are all higher and more fractionated in the estimated liquid than those observed in N-MORB or ocean island tholeiites. However, there is a component of cumulate sulphide in this estimated liquid and so direct comparison between the calculated liquid and N-MORB or ocean island values is not possible. In order to make a meaningful comparison the calues must be recalculated to 100 % sulphides, (i.e. all chalcophile and siderophile elements are multiplied by the factor 37/S). This procedure assumes that the present S values in the rocks represent igneous values and that all the platinum group elements, Au and Cu are present only in sulphides. Ni is recalculated after allowing for the Ni present in olivine.

If the composition of the sulphides from Tverrfjell, N-MORB and oceanic island tholeiites are compared (Table 15), it is seen that Tverrfjell sulphides are depleted in PGE and Au. The sulphides from Bruvann, Rånabogen and Eiterdalen are even more depleted in platinum group elements than the Tverrfjell sulphides. The generally depleted nature of all the Råna sulphides suggest that the magma from which they formed was depleted in platinum group elements. Two origins for E-MORB have been proposed, a) that it is derived from primary mantle, b) that is derived from depleted mantle which contains veins of material enriched in incompatible elements. If E-MORB is

Fig. 31 Mantle normalized curves for the estimated liquid at Tverrfjell (T), N-MORB (N), E-MORB (E) and basaltic komatiite (K). The Tverrfjell liquid most closely resembles E-MORB.

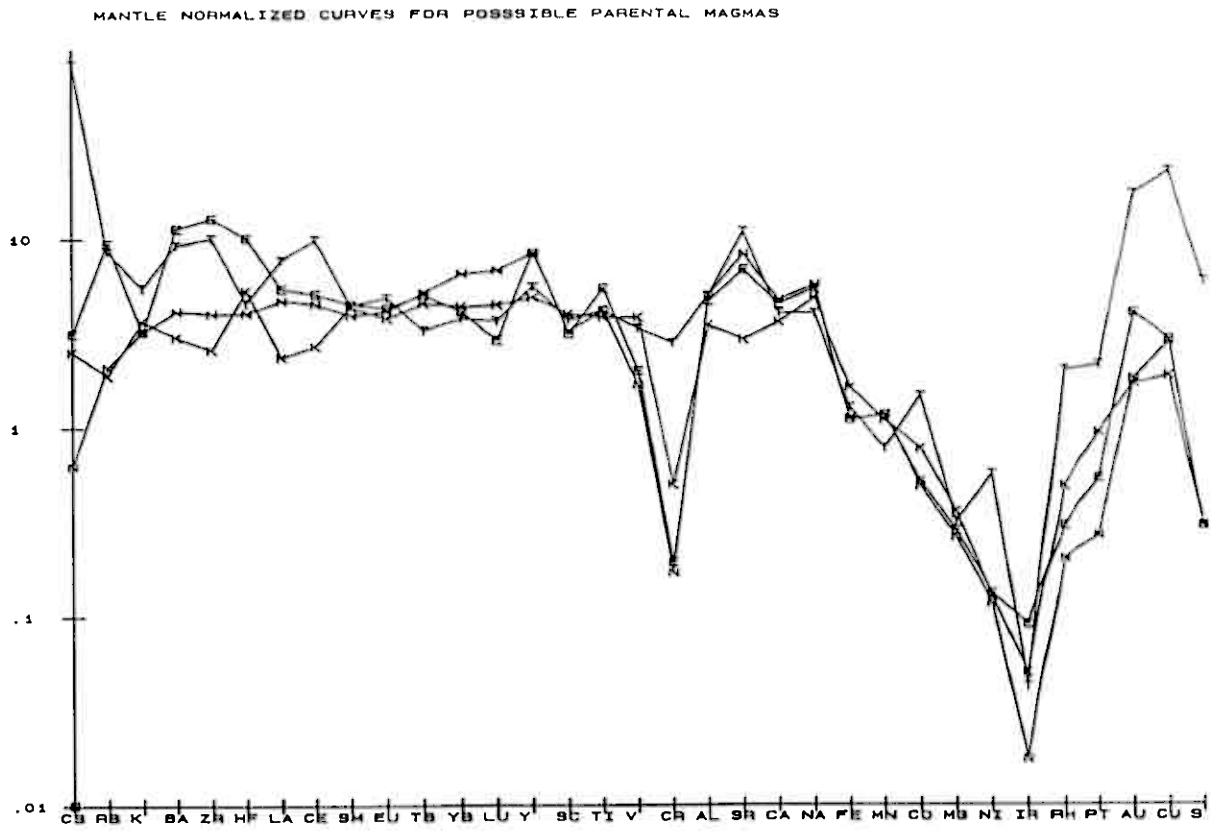

derived from fertile mantle then the Råna magma should not be depleted in PGE and its depleted nature is not a primary feature of the magma. If E-MORB is derived from depleted mantle with veins enriched in incompotible elements the levels of PGE in the source could be variable. However, since ocean island tholeiites are not depleted in PGE and E-MORB and ocean island tholeiites are thought to be derived from similar sources there is no reason to suggest that the source of the magma was depleted in PGE.

A possible mechanism of depleting the magma in PGE prior to emplacement at Råna is to fractionate a small amount of sulphides prior to the emplacement of the magma in its present position. Essentially this is the hypothesis that started the project and it will be explored below.

12. PLATINUM GROUP ELEMENTS AND GOLD

12.1 Results

Table 7 lists the average and range of noble metal values from rock at each of the 3 localities investigated. In Table 6 the noble metal values are presented after recalculation to 100 % sulphides. As discussed above these 100 % sulphide values imply that the Råna sulphides are extremely depleted in PGE. Boyd et al. (1986) have considered the noble metal values at Bruvann in terms of 100 % sulphides; similar conclusions to their would be reached if the Rånabogen, Eiterdalen and Tverrfjell analyses were normalized to 100 % sulphides. However, normalization to 100 % sulphides involves a number of assumptions which are not valid for all rock types. Firstly it assumes that all the noble elements partitioned into a Cu-Fe-Ni sulphide liquid containg 35-37 % sulphur, in the igneous phase of the rocks history and that since then, the sulphur, base and noble metal contents of the rock have not been disturbed. This may be true in sulphide-rich rocks under select metamorphic conditions. In sulphide-poor rocks, however, Rh, Pt and Pd may occur as compounds of As, Sb, Se, Hg, Te and S while Os, Ir and Au are often found in metal form: these elements may not have partitioned into a Cu-Fe-Ni sulphide liquid and may not have precipitated from the silicate magma in their present form. Secondly, during seafloor alteration and subsequent metamorphism S is mobile and hence may be either enriched or depleted relative to its igneous values. Therefore this work will consider the base and noble elements in terms of whole rock values and ratios.

Fig. 32A Pd vs Cu/Pd for various rock types and sulphide deposits. Note that the Bruvann (Bv), Ranabogen (Ra) and Eiterdalen (Et) samples have Cu/Pd ratios between 5 and 10 times that of other rock types, but the Tverrfjell (Tv) samples have normal Cu/Pd ratios. No combination of partial melting, silicate crystal fractionation or sulphide accumulation would produce the observed Cu/Pd ratios at Rana. See Table 4 for sources and legend

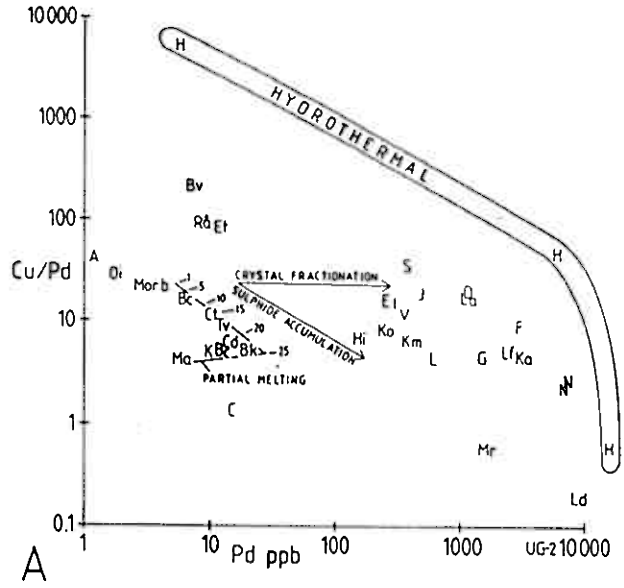

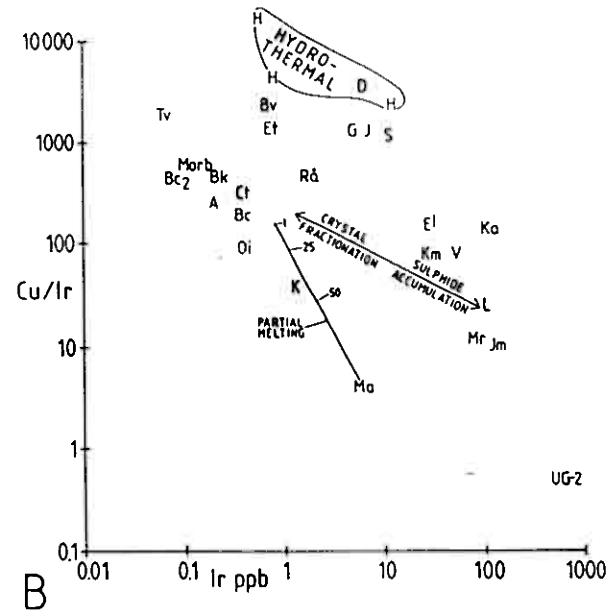

Fig. 32B Ir vs Cu/Ir for various rock types and sulphide deposits. Note that the Bruvann (Bv), Tverrfjell (Tv) and Eiterdalen (Et) samples have Cu/Ir ratios between 5 and 10 times that of other rock types.

Fig. 33A Pd vs Ni/Pd for various rock types and sulphide deposits. Note that the Bruvann (Bv), Ranabogen (Ra) and Eiterdalen (Et) samples have Ni/Pd ratios between 5 and 10 times that of other rock types, but the Tverrfjell (Tv) samples have normal Ni/Pd ratios. No combination of partial melting, silicate crystal fractionation or sulphide accumulation would produce the observed ratios at Rana.

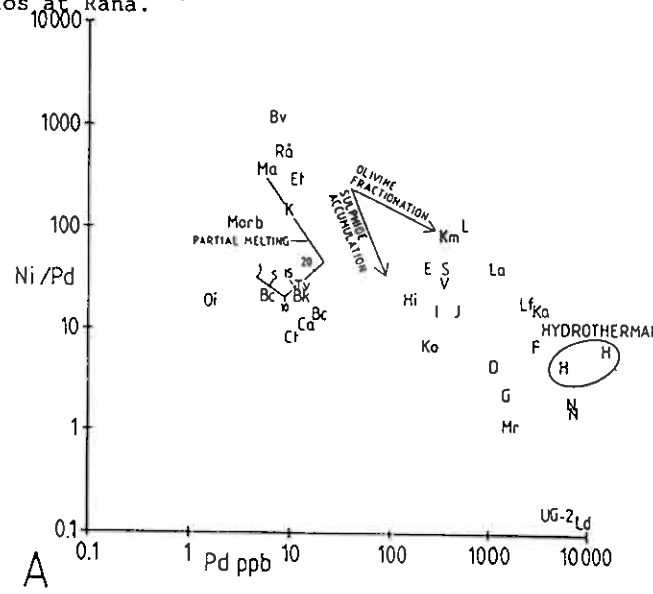

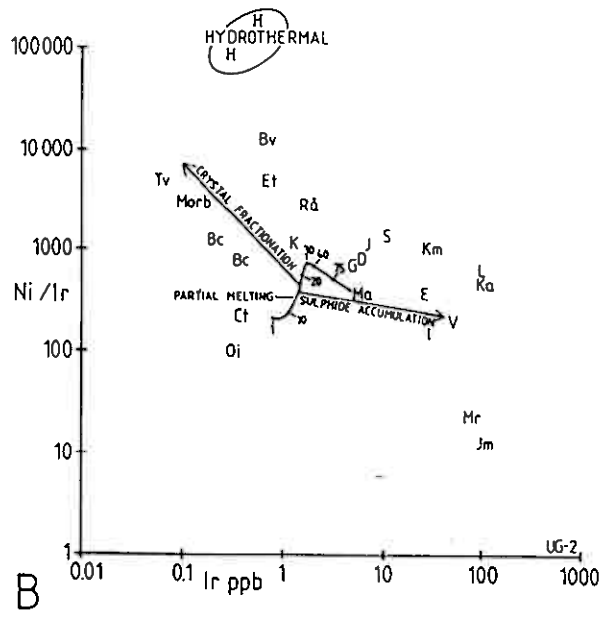

Fig. 34 Degree of partial melting versus the % sulphides in the restite. The proportions of base and noble metals released during partial melting is strongly controlled by the amount of sulphides in the melt. Assuming 350 ppm S in the mantle (Sun, 1982) and a solubility of 1550 S in the melt, (mid-point of solubilites given by Wendtland, 1982) 22% partial melting is required before all the sulphides are released.

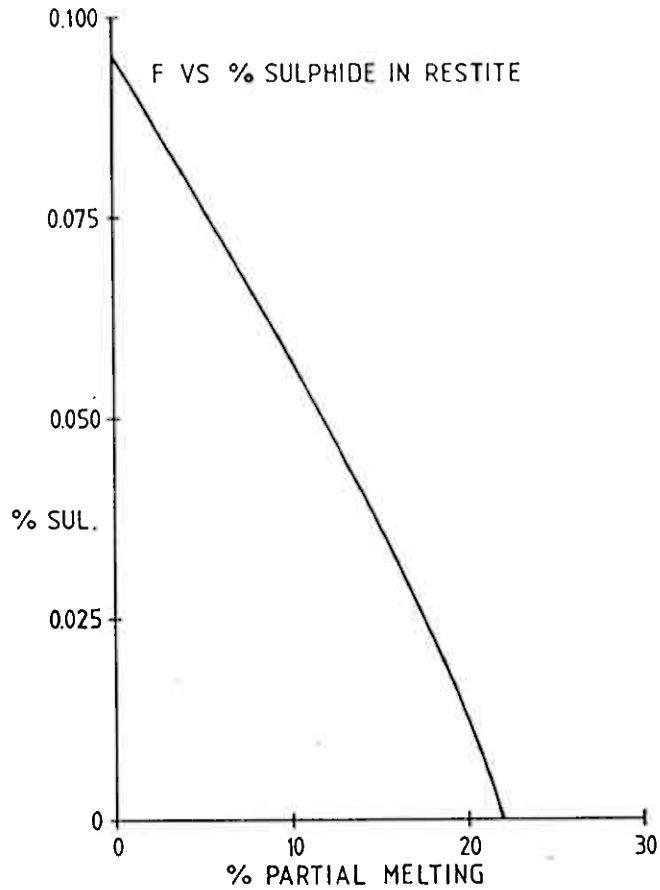

Fig. 35 A Plot of concentration of Ni, Ir, Pd, Cu in the melt versus degree of partial melting. Cu and Pd are principaly held in sulphides and hence are released to the melt as the sulphides dissolve, after all the sulphides have dissolved these elements are diluted by further partial melting by the volume effect. Ni and Ir in contrast are compatible with the restite and hence their concentrations increase with the degree of partial melting.
Fig. 35 B Plot of variations in Cu/Pd, Cu/Ir, Ni/Pd and Ni/Ir ratio with the degree of partial meling. Cu/noble element ratios are highest at low degrees of partial melting, in contrast Ni/noble element ratios are highest at high degrees of partial melting.

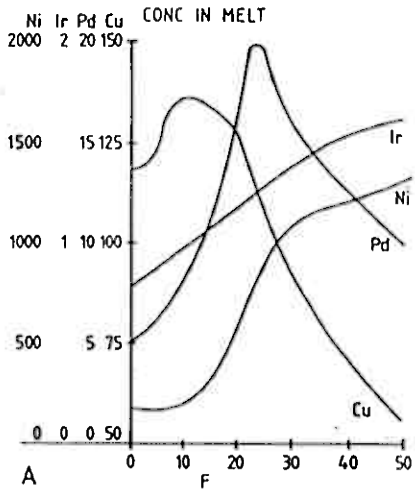

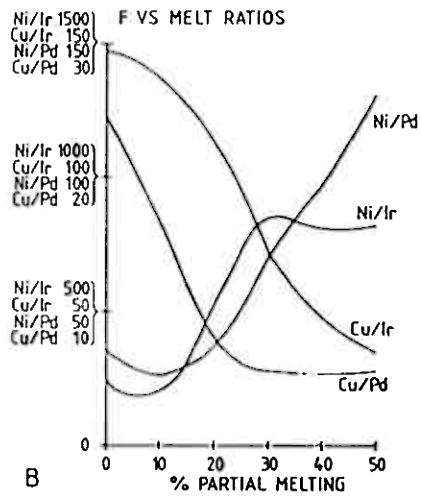

As can be seen on the plots of Cu/Pd versus Pd and Ni/Pd versus Pd (Figs. 32a and 33a) samples from the Rånabogen (Ra), Eiterdalen (Et) and Bruvann (Bv) have much higher base metal to Pd ratios than rocks and sulphide deposits reported in the literature. The samples from Tverrfjell (Tv) plot close to the continental tholeiites. (Key for the Figs. 32 and 33 in Table 8). On the Cu/Ir versus Ir and Ni/Ir versus Ir plots (Figs. 32b and 33b) the samples from Bruvann, Eiterdalen and Tverrfjell have anomalously high base metal to Ir ratios.

Most of the subsequent discussion will only consider Cu, Ni, Ir and Pd, although results for Rh, Pt and Au were also obtained for some of the samples. Broadly speaking Rh, Pt and Au should behave in a similar manner to Pd; these elements are not discussed separately because there are insufficient values from the literature to compare with and Rh and Pt were less than detection limit at two of the localities investigated.

The reason for using the plot of Cu/Pd versus Pd is to distinguish the effects of partial melting, sulphide segregation and crystal fractionation and to determine what combination of processes could have produced rocks of similar composition to those observed at Råna.

12.2 Partial Melting

The concentration of an element in a melt assuming batch partial melting is governed by the equation

$$Cl = Co/(F+D-FD) \qquad (1)$$

where Cl = concentration of the element in the liquid, Co = concentration in the source, F = The weight fraction of the solid that has melted, D = the bulk partition coefficient between the restite and liquid = E XiDi, where Xi = the weight fraction of each mineral present in the restite, Di = the partition coefficient between the mineral and the melt.

The only minerals that will retain Cu and Pd during partial melting of the mantle would be sulphides. It might be thought that all the sulphides would melt at the temperatures achieved during partial melting of the mantle

(>1100°C) and consequently that all the Cu and Pd from the mantle would be released and the partial melting equation would reduce to Cl=Co/F i.e. magmas such as alkali basalts would contain the highest concentrations of Cu and Pd. This trend is not observed (Barnes et al., 1985). This could be because although all of the sulphides melt not all the sulphur can dissolve in the silicate magma and hence there is a sulphide liquid present in the restite. This sulphide liquid will act as a host for the chalcophile elements and have been same effect as a restite. In order to solve the partial melting equation it must be decided how much sulphide liquid is left in the restite, which is governed by the equation.

$$Xs=(Co-(SxF))x2.7/(1-F) \qquad (2)$$

where Xs = the weight percentage sulphides remaining, S = the solubility of the sulphur in the magma, 2.7 converts the concentratino of S to sulphide, assuming 37 % sulphur in the sulphide. In this work S concentration in the mantle is assumed to be 0.035 %, (Sun 1982) and the solubility of sulphur in the magma 0.155 %, (the mid-point between the extremes listed by Wentlandt (1982)).

On the basis of these assumptions, at least 22 % partial melting is required to dissolve all the sulphides in the mantle (Fig. 34). Therefore at less than 22 % partial melting the concentrations of Cu and Pd and by analogy, Rh, Pt and Au in the melt are controlled by the sulphides in the restite. The peak Cu values occur around 10 % partial melting (Fig. 35 a). However, because of the high partition coefficient for Pd into sulphide the peak Pd (and by analogy Rh, Pt, Au) values are obtained once all the sulphides have dissolved and before any dilution additional melting can occur at around 22 % partial melting (Fig. 35 a).

The situation for Ni and Ir is more complex because although these elements do have high partition coefficients into sulphides, they are also compatible with other phases in the restite. The concentration of these elements in the melt have been modelled (Fig. 35 a) on the basis of the parameters listed in Table 9 a.

As a consequence of the different behaviour of the elements during partial melting the various interelement ratios change during partial melting

Fig. 35 b). Cu/Pd and Cu/Ir ratios fall rapidly from 1 to 22.5 % partial melting (at which point all of the sulphides are dissolved). After this the Cu/Pd ratio remains constant and is the same as that of the mantle (5.6) since all the Cu and Pd have been released. The Cu/Ir ratio, however, continues to fall because Ir is still being released. The Ni/Pd ratio increases very slowly from 1 to 22.5 % melting, because both Ni and Pd are continually released to the melt from sulphides; however, once all the sulphides are dissolved, the Ni/Pd ratio increases rapidly because the Pd concentrations are decreasing while the Ni concentrations are increasing. The Ni/Cu ratios (not plotted) exhibit a similar trend to the Ni/Pd ratio, except that the inflection point is at 10 %.

The results of the partial melting modelling are plotted on Figs. 32 and 33, where it can be seen that partial melting will not produce rocks with base to noble metal ratios similar to those observed at Råna. Whole rock geochemistry and mineral analysis suggest that the magma from which Råna formed was a MgO-rich tholeiite containing 12-18 % MgO (see earlier section and Boyd, in prep.); the concentrations of base and noble metals and their ratios in such a magma should be similar to those observed in a basaltic komatiite representing about 20 % partial melting, i.e. Cu/Pd = 8 x 1000 Cu/Ir = 111 x 1000, Ni/Pd = 39 x 1000, Ni/Ir = 54 x 1000. The Råna rocks have base to noble element ratios and order to two orders of magnitude higher than these.

12.3 Sulphide Segregation and Crystalliation

The rocks at Råna are cumulates that contain sulphides and since the base and noble elements have high partition coefficients into sulphides the first possibility to be considered is that sulphide accumulation has produced the high base to noble metal ratios. The concentration of an element in the cumulate during Rayleigh fractionation is governed by the equation:

$$Cc = Cl(1-F)^{(D-1)/(1-F)} \qquad (3)$$

From this equation it can be seen that the concentration of an element in the cumulate is controlled both by the degree of crystallization, i.e. how

much of the magma has crystallized and the weight fraction sulphides in the cumulate. Campbell and Naldrett (1979) have discussed in more detail the case for equilibrium crystallization of a sulphide-only cumulate. Fig. 36b shows the change in base to noble metal ratios for the cumulate with degree of crystallization assuming 23 %, 17.5 % and 0.39 % sulphides in the cumulate, these are the percentage sulphides present in average Rånabogen, Eiterdalen and Tverrfjell samples resepectively. Fig. 36b indicates that for the two localities that contain large percentages of sulphides the ratio of base to noble metals increases rapidly from 1 to 10 % crystallization and then levels out at approximately 0.95. In contrast for the low percentage of sulphides present at Tverrfjell the base to noble metal ratios are fairly constant from 1 to 10 % crystallization at about 0.2 and then increase rapidly to 0.74 at 90 % crystallization.

If only partial melting and sulphide accumulation have effected the base to noble element ratio (bm/nm) then bm/nm=bm/nm (partial melting) x bm/nm (sulphide accumulation) (4).

For the sake of developing a model it has been assumed that the ratio of base to noble metals in the Råna magma was originally close to that of a 20 % partial melt of the mantle, which can be read from Fig. 35b. The author does not wish to imply that the Råna magma ratios were exactly these, but these will be used to illustrate the point. The assumed initial magma Cu/Pd ratio is 7.2 x 1000 and the Cu/Pd ratio would be changed by a factor of approximately 0.9 by the formation of cumulates containing as much sulphide as the cumulates at Eiterdalen and Rånabogen. The observed Cu/Pd ratios at Eiterdalen and Rånabogen is 84 x 1000 and 91 x 1000 respectively, an order of magnitude higher than partial melting sulphide accumulation alone produces. At Tverrfjell the observed Cu/Pd ratio is 11 x 1000, while the calculated product of partial melting and sulphide fractionation is 7.2 x 1000 x 0.359 = 2.58 x 1000 (assuming 50 % crystallization based on whole rock geochemistry, see earlier section). Similar calculation on the other base to noble metal ratios reveal the same result, namely that sulphide accumulation decreases the bm/nm ratios.

The partition coefficients for the noble elements into sulphides are much greater than that of base metals. Sulphide accumulation tends to decrease the base to noble metal ratios as indicated schematically on Figs. 32 and

33 i.e. sulphide accumulation displaces the ratios in the opposite direction to that desired. This leads to the idea that, despite the presence of sulphides in the Råna cumulates, the Råna cumulates formed from a silicate liquid that had had sulphide liquid removed prior to its emplacement at Råna. This idea is discussed specifically for the Bruvann deposit by Boyd et al. (1986) and in the general case by Campbell and Barnes (1984) and the present work will consider the idea for Eiterdalen, Rånabogen and Tverrfjell.

During Rayleigh fractionation the concentration of an element in the melt is governed by the equation:

$$Cl = CoF^{(D-1)} \qquad (5)$$

where Cl, Co and D are defined as in equation 1 and F is the weight fraction liquid remaining.

Fig. 36a shows the change in base to noble metal ratio in the melt with the percentage sulphides removed (assuming the partition coefficients listed in Table 9b).

If the Råna rocks are the product of the three processes partial melting, sulphide removal and cumulate processes then

bm/nm = bm/nm (partial melting) x bm/nm (sulphide removal) x bm/nm (cumulate processes)

which can be rearranged to

bm/nm (sulphide removal) = bm/nm/(bm/nm (partial melting) x bm/nm (cumulate processes))

From this equation and Fig. 36a the percentage of sulphides removed from the magma prior to emplacement at Råna may be estimated, e.g. for Eiterdalen for Cu/Pd the change in base to noble metal ratio brought about by sulphide removal = 84/(7.2 x.9) = 12.9 this implies about 0.3 % sulphide removal. Thus the base and noble elements at Eiterdalen can be modelled as

having been derived from a 20 % partial melt of the mantle that experienced 0.3 % sulphide segregation prior to emplacement of the magma, followed by the formation of a cumulate containing minerals in the proportions observed in the rocks (Table 9b).

Similar calculations at Rånabogen indicate approximately 0.3 % sulphides were removed prior to emplacement of the magma at this locality. The rocks are principally olivine cumulates and in modelling them allowance was made for the presence of the olivine which increases the Ni content of the rocks. A satisfactory match between the observed and model rocks was obtained (Table 9b).

At Tverrfjell the situation is more complicated. The degree of crystallization has a marked effect on the base to noble element ratios, (Fig. 36b). On the basis of whole rock geochemistry approximately 50 % crystallization has occurred, therefore the change in base to noble metal ratios due to cumulate processes is approximately 0.35 (Fig. 36b). On the basis of this assumption, the Cu/Pd and Ni/Pd ratios indicate that approximately 0.15 % sulphides were removed from the magma prior to emplacement at Tverrfjell. In contrast the Cu/Ir and Ni/Ir ratios indicate approximately 0.5 sulphides have been remoded. Obviously both cannot have occurred and some other process has distrubed the Ir relative to the other elements at Tverrfjell.

The most obvious difference between the Tverrfjell locality and the other two is that the rocks appear to have formed from a more fractionated magma at Tverrfjell than at the other two localities, e.g. the highest forsterite contents observed in the olivines at Tverrfjell is 87 % while at Rånabogen it is 90 %. Ir tends to behave in a compatible fashion during crystallization (as originally pointed out by Crocket, 1979). If 15 % olivine were removed from the initial magma (containing approximately 18 % MgO) prior to its emplacement at Tverrfjell the MgO content of the magma would fall to 12 % and consequently the forsterite content of the olivine would fall to approximately 87 %. Possibly the Ir would be removed at the same time. A satisfactory match between the observed and modelled rocks at Tverrfjell can be obtained by assuming 0.15 % sulphide and 15 % olivine removal prior to emplacement at Tverrfjell followed by formation of a cumulate with the mineral proportions presently observed in the rocks (Table 9b).

Fig. 36 A Plot of variations in (Cu or Ni)/noble element ratios in the silicate melt with the percentage of sulphides removed.
Fig. 36 B Plot of variations in (Cu or Ni)/noble element ratios in the cumulates with the degree of crystallization of the melt. Tv = curve assuming 0.39% sulphides in the cumulate, the amount present in the average Tverrfjell sample, Et = curve assuming 17% sulphides in the cumulate, the amount present in the average Eiterdalen sample, Ra= curve assuming 23% sulphides in the cumulate as there is in the average Ranabogen sample.

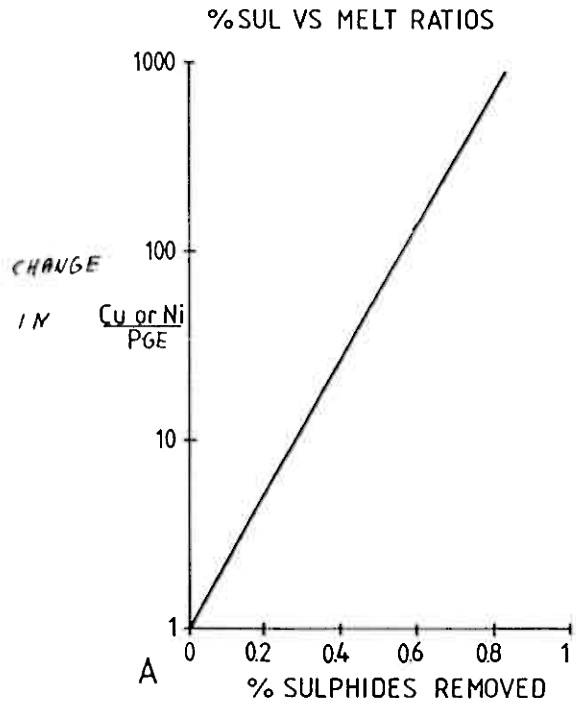

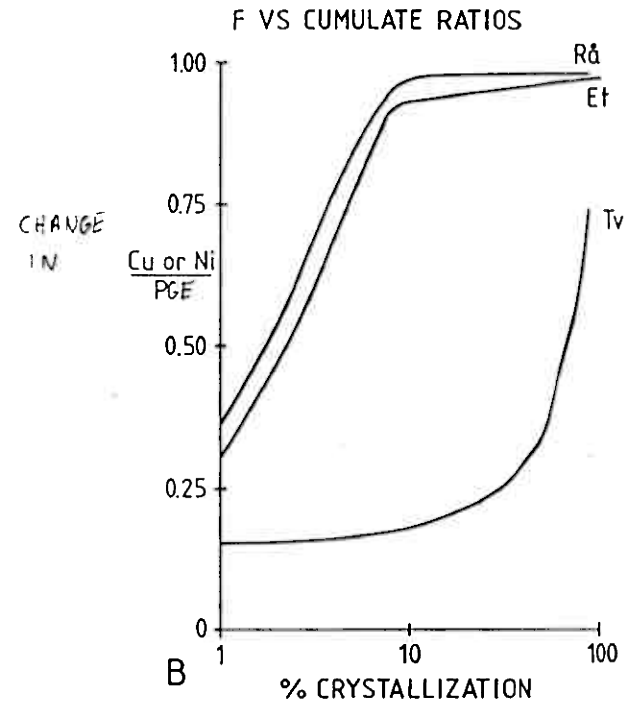

13 DISCUSSION AND CONCLUSIONS

The rocks of the Råna Layered Intrusion have unusually high base to noble metal ratios. The segregation of small amounts (0.15-0.3 %) of sulphides prior to the emplacement of the magma at Råna may account for these unusual ratios. This conclusion is supported by the olivine compositions observed at Råna; most of the olivines are depleted in nickel, (Fig. 8). This could be because the magma was depleted in nickel by the removal of sulphides prior to the formation of the olivine.

Variations in base and noble metal concentrations between the different localities at Råna may be modelled as shown in fig. 37 and Table 9b by intrusion of an MgO-rich tholeiite which has had approximately 0.15 % sulphides removed. Magma is intruded in the Eiterdalen and Rånabogen areas after removal of a further 0.2 % sulphides. Magma intruded in the Tverrfjell area after segregation of 15 % olivine.

14 Acknowledgements

This investigation was funded by LKAB by NGU and by a postdoctoral fellowship from NTNF. I would like to thank: Drs. K.S. Heier and R. Boyd for initiating the project; E.W. Sawyer and Tor-Arne Karlsen without whom no samples could have been collected and no map produced; Tony Boassen of IKU for assistance with the microprobe analyses; Astri Hemming and E.W. Sawyer for drafting the diagrams. A special thanks go to Are Korneliussen for guiding two foreigners through the logistics of living and working in Norway.

Fig. 37 Model for the developement of the Ranabogen, Eiterdalen and Tverrfjell samples.

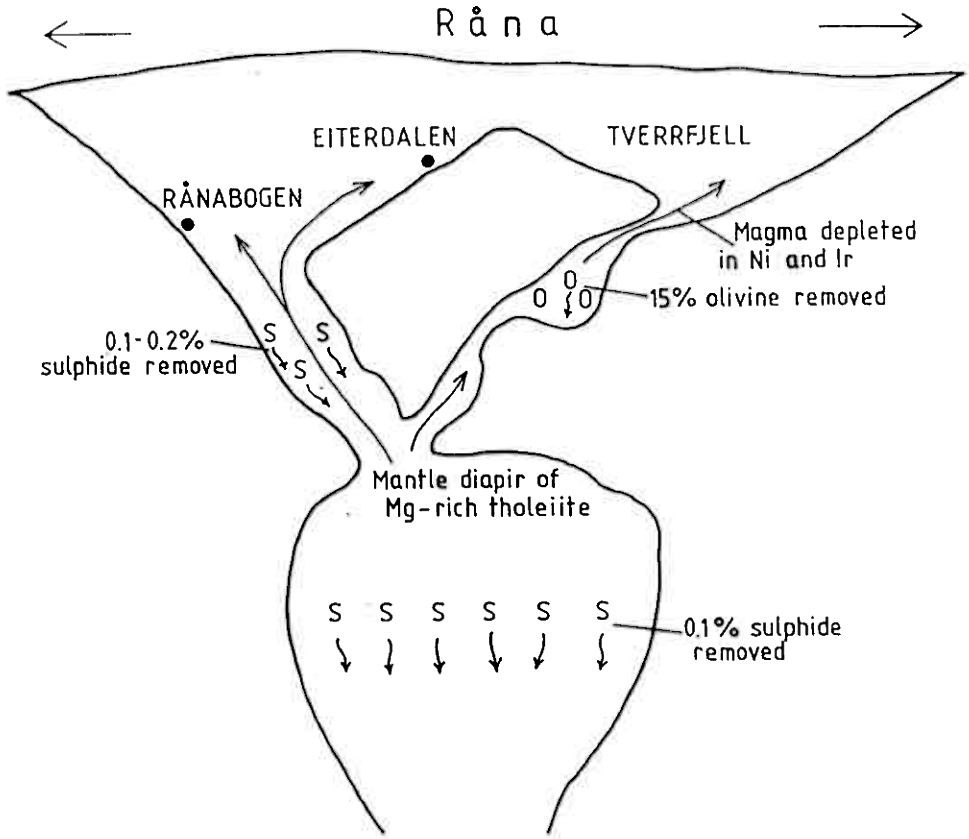

15 REFERENCES

Abbey, S. 1980: Studies in "Standard Samples" for use in the general analysis of silicate rocks and minerals. Geostandards Newsletter, 4: 163-190.

Aoki, K. and Kushiro, I. 1968: Contrib. Mineral. Petrol., 18: 326-337.

Atkins, F.B., 1969: Pyroxene of the Bushveld intrusion, South Africa. J. Petrol., 10: 222-229.

Barnes, S.-J. 1986: The platinum potential of the Tverrfjell portion of the Rana Layered Intrusion. Geol. Surv. Norway, Rep.

Barnes, S.-J. and Gorton, M.P. 1983: Trace element analysis by neutron activation with a low flux reactor (SLOWPOKE-II): Results for international reference rocks. Geostrandards Newsletters, VIII: 17-24.

Barnes, S.-J., Gorton, M.P. and Naldrett, A.J. 1983: A comparative study of olivine and clinopyroxene spinifex flows from Alexo, Abitibi Greenstone Belt, Ontario, Canada: Contr. Mineral. Petrol., 83: 293-308.

Barnes, S.-J., Naldrett, A.J. and Gorton, M.P. 1985: The origin of the fractionation of platinum group elements in terrestrial magmas: Chem. Geol. 53: 303-323.

Barnes, S.-J. and Naldrett, A.J. 1985: Geochemistry of the J-M reef of the Stillwater Complex, Minneapolis Adit Area. I Sulfide chemistry and sulfide-olivine equilibrium. Econ. Geol., 80: 627-645.

Barnes, S.-J., Coates, C.J. and Naldrett, A.J. 1982: Petrogenesis of Proterozoic nickel sulphide-komatiite association: the Katiniq Sill, Ungava, Quebec. Econ. Geol., 77: 413-429.

Barrett, F.M., Binns, R.A., Groves, D.I., Marston, R.J. and McQueen, K.G. 1977: Structural history and metamorphic modification of Archean volcanic-type nickel deposits, Yilgarn Block, Western Australia. Econ. Geol., 72: 1195-1223.

Basaltic Volcanism Study Project 1981: Pergamon Press, New York. 1286 p.

Bertrand, D.F. and Mercier, J.-C. 1985: The mutual solubility of coexisting ortho- and clinopyroxene, towards an absolute geothermometer for the natural systems. Earth Planet. Sci. Lett., 76: 109-122.

Boyd, R. (in prep.): The geology and petrology of the Råna nickelferous Layered Intrusion, Nordland. Geol. Surv. Norway.

Boyd, R. and Mathiesen, C.O. 1979: The nickel mineralization of the Råna mafic intrusion, Nordland, Norway. Can. Miner., 17: 287-298.

Boyd, R. and Nixon, F. 1985: Norwegian nickel deposits: A review. Geol. Surv. Finland, Bull. 333: 364-394.

Boyd, R., McDade, J., Millard, H.T. and Page, N. 1986: Platinum and palladium geochemistry of the Bruvann nickel-copper deposit, Råna, North Norway. IAGOD 7'th conference.

Brown, G.M., 1957: Pyroxene from the early and middle stages of fractionation of the Skaergaard intrusion, east Greenland. Mineral. Mag. 31: 511-543.

Brown, G.M., and Vincent, E.A. 1963: Pyroxene from the late stages of fractionation of the Skærgård intrusion, East Greenland. J. Petrol., 4: 175-194.

Buchanan, D.L., Noland, J. and Viljoen, E.A. 1980: Determination of silica activity in Bushveld rocks. Contrib. Mineral. Petrol., 73: 311-319.

Butcher, A.R., Young, I.M. and Faithfull, J.W. 1985: Finger structures in the Rhum Complex. Geol. Mag., 122: 491-502.

Cabri, L.J. 1981: The platinum-group minerals. Cand. Inst. Min. Metall., Spec. Iss., 23: 47-64.

Campbell, I.H. 1978: Some problems with cumulus theory. Lithos, 11: 311-323.

Campbell, I.H. and Barnes, S.-J. 1984: A model for the geochemistry of the platinum group elements in magmatic sulfide deposits. Can. Miner., 22: 151-160.

Campbell, I.H. and Naldrett, A.J. 1979: The influence of silicate: sulfide ratio on the geochemistry of the magmatic sulfides. Econ. Geol., 74: 1503-1505.

Crocket, J.H. 1979: Platinum-group elements in mafic and ultramafic rocks: a survey. Cand. Miner., 17: 391-402.

Crocket, J.H. 1981: Geochemistry of the platinum-group elements. Can. Inst. Min. Metall., Spec. Iss., 23: 47-64.

Crocket, J.H. and Chyi, L.L. 1972: Abundance of Pd, Ir, Os and Au in an alpine ultramafic pluton. 24'th Inter. Geol. Cong., Section 10: 202-209.

Czamanske, G.K., Haffty, J. and Nabba, S.W. 1981: Pt, Pd and Rh analyses and beneficiation of mineralized mafic rocks from the La Perouse Layered Gabbro, Alaska. Econ. Geol. 76, 2001-2011.

Davidson, P.M. and Lindsley, D.H. 1985: Thermodynamic analysis of quadrilateral pyroxenes. Contrib. Mineral. Petrol., 91: 390-404.

Davis, G. and Tredoux, M. 1985: The platinum-group element and gold contents of the marginal rocks and sills of the Bushveld Complex. Econ. Geol. 80. 838-8448.

Deer, W.A., Howie, R.A. and Zussman, Z. 1982: Rock-forming minerals. Orthosilicates, vol. 1A. Longman, London, 919 pp.

Dick, H.J.B. and Bullen, T. 1984: Chromian spinel as a petrographic indicator in abyssal and alpine-type peridotites and spatially associated lavas. Contrib. Mineral. Petrol., 86: 54-76.

Dunham, A.C. and Wilkinson, 1985: Sulfide droplets and the unit 11/12 chromite band, Rhum: A mineralogical study. Geol. Mag., 122: 539-548.

Economou, M.I. and Naldrett, A.J. 1984: Sulfides associated with podiform bodies of chromite at Tsangli, Eretria, Greece. Mineral. Deposita., 19: 289-297.

Esbensen, K.M. 1978: Coronites from the Fongen gabbro complex, Trondheim region, Norway: Role of water in the olivine-plagioclase reaction. N. Jb. Miner. Abh., 132: 113-135.

Evans, B.W. and Frost, B.R. 1975: Chrome-spinel in progressive metamorphism - A preliminary analysis. Geochim. Cosmochim. Acta., 39: 959-972.

Fisk, M.R. and Bence, A.E. 1980: Experimental crystallization of chrome spinel in FAMOUS basalt 527-1-1. Earth Planet. Sci. Lett., 48: 111-123.

Fleet, M.E. 1986: Geochemistry of the J-M (Howland) reef of the Stillwater Complex, Minneapolis adit area I Sulfide chemistry sulfide-olivine equilibrium. A disscussion. Econ. Geol. 81: 199-203.

Fleet, M.E., MacRae, N.D., Herzberg, C.T. 1977: Partition of nickel between olivine and sulfide. Contrib. Mineral. Petrol., 65: 191-197.

Gain, S.B. and Mostert, A.B. 1982: The geological setting of the platinoid and base metal sulfide mineralization in the Platreef of the Bushveld Complex north of Potgietersrus. Econ. Geol., 17: 1395-1404.

Gasparik, T. 1984: Two-pyroxene thermobarometry with new experimental data on the system CaO-MgO-Al_2O_3-SiO_2. Contrib. Mineral. Petrol., 87: 87-92.

Green, A.H. and Naldrett, A.J. 1981: The Langmuir volcanic peidotite-associated nickel deposits: Canadian equivalent of the Western Australian occurrences. Econ. Geol., 76: 1503-1523.

Green, D.H., Ringwood, A.E., Ware, N.G., Hibberson, W.O. and Major, A. 1971: Experimental petrology and petrogenesis of Apollo 12 basalts: In McElhinny (ed.) The Earth: its origin, structure and evolution. Academic Press: New York: 166-299.

Griffin, W.L. and Heier, K.S. 1973: Petrological implications of some corona structures. Lithos, 6: 315-335.

Griffin, W.L., Mellini, M., Oberti, R., Rossi, G. 1985: Evolution of coronas in Norwegian anorthosites: re-evaluation based on crystal-chemistry and microstructures. Contrib. Mineral. Petrol., 91: 330-339.

Grønlie, A. 1986: Platinum-group elements of the Lillefjellklumpen, North-Trøndelag. Proceedings of 7'th IAGOD conference.

Haggerty, S. 1979: Spinels. Proceedings of 2'nd. Int. Kimberlite Confr., vol. 2 The Mantle Sample. Amer. Geophys. Union.

Hakli, T.A., Hanninen, E., Vuorelainen, Y. and Papunen, H. 1976: Platinum-group minerals in the Hitura nickel deposit, Finland. Econ. Geol., 71: 1206-1213.

Hatton, C. and von Gruenewaldt, G. 1985: Chromites from the Swartkop chrome mine - an estimate of the effects of subsolidus reequilibration. Econ. Geol. 80: 911-924.

Henderson, P. 1975: Reaction trends shown by chrome-spinels of the Rhum Layered Intrusion. Geochim. Cosmochim. Acta., 39: 1035-1044.

Hill, R. and Roeder, P. 1974: The crystallization of spinel from basaltic liquid as a function of oxygen fugasity. J. Geol., 82: 709.

Hoffman, E.L., Naldrett, A.J., Van Loon, J.C., Hancock, R.G.V. and Mason, A. 1978: The determination of all the platinum-group elements and gold in rocks, ores etc: Anal. Chim. Acta., 102: 157-166.

Hoffman, E.L., Naldrett, A.J., Van Loon, J.C. and Hancock, R.G.V. 1979: The noble-metal content of ore in the Levack West and Little Stobie mines, Ontario. Can. Mineral., 17: 437-451.

Hulbert, L.J. and von Gruenewaldt, G. 1985: Textural and compositional features of chromite in the Lower and Critical Zones of the Bushveld south of Potgieterus. Econ. Geol., 80: 872-895.

Irvine, T.N. 1967: Chromian spinel as a petrological inidicator, part 2, petrological applications. Can. J. Earth Sci., 4: 71-103.

Irvine, T.N. 1976: Chromite crystallization in the join Mg_2SiO - $CaMgSi_2O_6$ - $CaAl_2Si_2O_8$-$MgCr_2O_4$ - SiO_2. Carnegie. Inst. Wash. Yb., 76: 465-472.

Irvine, T.N. 1980: Magmatic infiltration metasomatism, double-diffusive fractional crystallization and adcumulus growth in the Muskox Intrusion and other layered intrusions. In (ed.) Hargraves, R.B. Physics of Magmatic Processes. Princeton Univ. Press, New York.: 325-383.

Irvine, T.N. 1982: Terminology for layered intrusions. J. Petrol., 23: 127-162.

Irvine, T.N., Keith, D.W. and Todd, S.G. 1983: The J-M platinum-palladium reef of the Stillwater Complex, Montana II origin by double-diffusive convection magma mixing and implications for the Bushveld Complex. Econ. Geol. 78: 1287-1334.

Jaques, A.L. and Green, D.H. 1980: Anhydrous melting of peridotite at 0-15 kb. pressure and the genesis of tholeiitic basalts. Contrib. Mineral. Petrol., 73: 287-310.

Jones, J.H. 1984: Temperature and pressure independent correlations of olivine/liquid partitioning and their application to trace element partitioning. Contrib. Mineral. Petrol., 88: 126-132.

Keays, R.R. and Campbell, I.H. 1981: Precious metals in the Jimberlana Intrusion, Western Australia: Implications for genesis of platiniferous ores in layered intrusions: Econ. Geol., 76: 1118-1141.

Keays, R.R., Nickel, E.H., Groves, D.I. and McGoldrick, P.J. 1982: Iridium and palladium as discriminants of volcanic-exhalative hydrothermal and magmatic nickel sulfide mineralization: Econ. Geol., 77: 1535-1547.

Kretz, R. 1982: Trandfer and exchange equilibria in a portion of the pyroxene quadrilateral as deduced from natural and experimental data. Geochem. Cosmochim. Acta., 46: 411-421.

Kruger, F.J. and Marsh, J.S. 1985: The mineralogy, petrology and origin of the Merensky Cyclic Unit in the western Bushveld Complex. Econ. Geol., 80: 958-974.

Labotka, T.C. 1985: Petrogenesis of the metamorphic rocks beneath the Stillwater complex: Assemblages and conditions of metamorphism. Geol. Surv. Montana, Spec. Publ., 92: 70-76.

Lahtinen, J. 1985: PGE-bearing copper-nickel occurrences in the marginal series of the early Proterozoic Koillismaa Layered Intrusion, northern Finland. Geol. Surv. Finland, Bull. 333: 165-179.

Langmuir, C.H., Bender, J.F., Bence, A.E., Hanson, G.H. and Taylor, S.R. 1977: Petrogenesis of basalts from the FAMOUS area: Mid-Atlantic ridge. Earth Planet. Sci. Lett., 36: 133-156.

Lee, C. 1981: Post-depositional structures in the Bushveld Complex mafic sequence. J. Geol. Soc. Lond., 138: 327-341.

Lesher, C.M. and Keays, R.R. 1984: Metamorphically and hydrothermally mobilized Fe-Ni-Cu sulphides at Kambalda, Western Australia: In: Buchanan, D.L. and Jones, M.J., eds., Sulphide deposits in mafic and ultramafic rocks: London, Inst. Mining Metallurgy: 62-69.

Letterrier, J., Maury, R.C., Thonon, P., Girard, D. and Marchal, M. 1982: Clinopyroxene compositions as a method of identification of the magmatic affinities of paleo-volcanic series. Earth Planet. Sci. Lett., 59: 139-154.

Lightfoot, P.C. and Naldrett, A.J. 1984: Chemical variations in the Insizwa Complex, Transkei, and the nature of the parent magma. Cand. Mineral., 22: 111-123.

Lightfoot, P.C., Naldrett, A.J. & Hawkesworth, C.J. 1984: The geology and geochemistry if the Waterfall Gorge section of the Insizwa Complex with particular reference to the origin of the nickel-sulfide deposits. Economic Geology 79, 1857-1879.

Lindsley, D.H. and Andersen, D.J. 1983: A two-pyroxene thermometer. J. Geophys. Res., 88: supp. A887-906.

Maaløe, S. The origin of rhythmic layering. Mineral. Mag., 42: 337-345.

MacBirney, A.R. and Noyes, R.M. 1979: Crystallization and layering of the Skærgård Intrusion. J. Petrol., 20: 487-554.

Mason, B. 1966: Introduction to geochemistry. Wiley, New York.

Medaris, L.G. 1975: Coexisting spinel and silicates in alpine peridotite of the granulite facies. Geochim. Cosmochim. Acta., 39: 947-958.

Mitchell, R.H. and Keays, R.R. 1981: Abundance and distribution of gold, palladium and iridium in some spinel and garnet lherzolites, Implications for the nature and origin of percious metal-rich intergranular components in the upper mantle. Geochim. Cosmochim. Acta., 45: 2425-2442.

Mongkoltip, P. and Ashworth, J.R. 1983: Quantitive estimation of an open-system symplextite-forming reaction: Restricted diffusion of Al and Si in coronas around olivine. J. Petrol., 24: 635-661.

Morgan, J.W. and Baedecker 1983: Lunar Planet. Sci. Confr., XIV.

Mysen, B. 1976: Experimental determinations of some geochemical parameters relating to conditions of equilibration of the peridotites in the upper mantle. Amer. Miner., 61: 677-683.

Naldrett, A.J. 1981: Platinum-group element deposits. Can. Inst. Min. Metall., Spec. Iss., 23: 197-232.

Naldrett, A.J. and Cabri, L.J. 1976: Ultramafic and related mafic rocks: their classification and genesis with special reference to the concentration of nickel sulfides and platinum-group elements. Econ. Geol., 71: 1129-1130.

Naldrett, A.J., Duke, J.M., Lightfoot, P.C. and Thompson, J.F.H. 1984: Quantitative modelling of the segregation of magmatic sulphides: An exploration guide. Can. Inst. Mining Metal. Bull.: 1-11.

Navrotsky, A. 1979: Thermodynamics of element partitioning. Geochem. Cosmochim. Acta., 42: 887-902.

Nickel, K.G., Brey, K.G. and Kogarko, L. 1985: Orthopyroxene-clinopyroxene equilibria in the system CaO-MgO-Al_2O_3-SiO_2 (CMAS). Contrib. Mineral. Petrol., 91: 44-53.

Nielsen, R.L. and Drake, M.J. 1979: Pyroxene melt equilibria. Geochim. Cosmochim. Acta, 43: 1259-1272.

Otten, M. 1985: The subsolidus history of the Artfjellet Gabbro: A SEM study of olivine, augite and orthopyroxene. J. Petrol., 26: 488-514.

Otten, M. and Senior, A. 1985: Mineral chemistry and crystallization of the Artfjellet gabbro and dolerites (Central Swedish Caledonides). Lithos, 18: 295-310.

Powell, M. and Powell, R. 1974: An olivine-clinopyroxene geothermometer. Contrib. Mineral. Petrol., 48: 249-263.

Raedeke, L.D. and McCallum, I.S. 1984: Investigation in the Stillwater Complex Part II. Petrology and petrogenesis of the Ultramafic Series. J. Petrol., 25: 395-420.

Robins, B. 1982: Finger structure in the Lille Kufjord Layered Intrusion, Finnmark, Northern Norway. Contrib. Mineral. Petrol., 81: 290-295.

Sack, R. 1980: Some constraints on the thermodynamic mixing properties of the Fe-Mg orthopyroxenes. Contrib. Mineral. Petrol., 71: 257-269.

Sharpe, M. 1982: Noble metals in the margin rocks of the Bushveld Complex. Econ. Geol., 77: 1286-1295.

Smirnov, M.F. 1966: The structure of Noril'sk nickel-bearing intrusions and the genetic types of their sulfide ores. All-union Sci. Res. Inst. Mineral. Raw Material. (VIMS) Moscow. (In Russ).

Sparks, R.S.J., Huppert, H.E., Kerr, R.C., McKenzie, D.P. and Tait, S.R. 1985: Postcumulus processes in layered intrusions. Geol. Mag., 122: 555-568.

Steele, T.W., Levin, J., and Copelowitz, I. 1975: The preparation and certification of a reference sample of a precious metal ore: Nat. Inst. Met. Rep. 1696.

Streckeisen, A. 1976: To each plutonic rock its proper name. Earth Sci. Rev., 12: 1-33.

Sun, Shen-su 1982: Chemical composition and origin of the earth's primitive mantle. Geochim. Cosmochim. Acta., 46: 179-19 .

Sun, Shen-Su 1984: Some geochemical constraints of mantle evolution models. 27'th Inter. Geol. Congr., Moscow, v. 9: 475-508.

Tait, S.R. 1985: Fluid dynamic and geochemical evolution of cyclic unit 10, Rhum, Eastern Layered Series. Geol. Mag., 122: 469-484.

Tait, S.R., Huppert, H.E., Sparks, R.S.J. 1984: The role of compositional convection in the formation of adcumulate rocks. Lithos, 17: 139-1146.

Talkingon, R.W. and Watkinson, D.H. 1984: Trends in the distribution of the precious metals in the Lac des Iles Complex, northwestern Ontario. Cand. Mineral., 22: 125-136.

Taylor, S.R. 1980: Refractory and moderately volatile element abundance in the earth, moon and meteorites. Proc. Eleventh Lunar Planet. Sci. Confr.: 333-348.

Thompson, J.F.H., Nixon, F. and Siversten, R. 1980: The geology of Vakkerlien nickel prospect Kvikne, Norway. Geol. Surv. Finland bull. 52: 3-22.

Thompson, J.F.H., Barnes, S.-J. and Duke, M.J. 1984: The distribution of nickel and iron between olivine and magmatic sulfides in some natural assemblages. Cand. Mineral., 22: 55-66.

Turner, J.S. and Gustafson, L.B. 1978: The flow of hot saline solutions from units on the sea floor-some implications for exhalative massive sulfide and other ore deposits. Econ. Geol., 73: 1082-1100.

Veblen, R.H. and Buseck, P.R. 1981: Hydrous pyriboles and sheet silicates in pyroxenes and uralite: Intergrowth microstructures and reaction mechanisms. Amer. Mineral., 66: 1107-1134.

Von Gruenewaldt, G., Sharpe, M.R. and Hatton, C.J. 1985: The Bushveld Complex: Introduction and Review. Econ. Geol., 80: 803-813.

Wadsworth, W.J. 1970: The Aberdeenshire Layered Intrusion of north-east Scotland. Geol. Soc. S. Afr. Spec. Pub., 1: 565-575.

Wadsworth, W.J. 1985: Terminology of postcumulus processes and products in the Rhum Layered intrusion. Geol. Mag., 122: 549-554.

Wager, L.R. and Brown, G.M. 1967: Layered Igneous Rocks. Oliver and Boyd, Edinburgh.

Wendlandt, R.F. 1982: Sulphur saturation of basalt and andesite melts at high pressures and temperatures. Amer. Miner., 67: 877-885.

Wilson, A.H. 1982: The geology of the Great Dyke, Zimbabwe the ultramafic rocks. J. Petrol., 23: 240-292.

Wilson, J.R., Esbensen, K.H. and Thy, P. 1981: Igneous petrology of the synorogenic Fongen-Hyllingen Layered Basic Complex, South-Central Scandinavian Caledonides. J. Petrol., 22: 584-627.

Winkler, H.G.F. 1979: Petrogenesis of metamorphic rocks. Springer, New York.

Wood, D.A. 1979: A vaiably veined subvolcanic upper mantle-genetic significance for mid-ocean ridge basalts from geochemical evidence. Geol., 7: 499-503.

Young, I.M. and Donaldson, C.H. 1985: Formation of granular textured layers and laminae within the Rhum crystal pile. Geol. Mag., 122: 519-528.

Zientek, M.L., Czamanske, G.K. and Irvine, T.N. 1985: Stratigraphy and nomenclature for the Stillwater Complex. Geol. Surv. Montana Spec. Pub., 92: 21-32.

APPENDIX MINERAL AND WHOLE ROCK ANALYSES FROM THE RÅNA LAYERED INTRUSION.

TABLE 1
PRECISION AND DETECTION LIMITS OF ANALYSES

Microprobe Analyses IKU

	Olivine n=24	1 Sigma	Detection Limit1		Plagio n=10	1 sigma	Detection Limit1
SiO2	42.13	0.38	0.08	SiO2	51.03	0.52	0.08
FeO	7.25	0.23	0.13	Al2O3	14.38	0.65	0.06
MgO	50.22	0.68	0.13	CaO	14.38	0.33	0.05
NiO	0.35	0.025	0.03	Na2O	3.12	0.25	0.20
				K2O	0.11	0.024	0.05

	Opx n=10	1 Sigma	Detection Limit1		Cpx n=10	1 sigma	Detection Limit1
SiO2	55.67	0.52	0.08	SiO2	53.03	0.37	0.08
TiO2	0.26	0.07	0.10	TiO2	0.66	0.17	0.15
Al2O3	2.81	0.17	0.06	Al2O3	3.56	0.19	0.05
FeO	9.12	0.22	0.13	FeO	4.75	0.33	0.13
MnO	0.05	0.04	0.10	MnO	0.15	0.03	0.16
MgO	30.22	0.30	0.18	MgO	16.35	0.40	0.13
CaO	1.52	0.30	0.03	CaO	20.11	0.70	0.05
NiO	0.014	0.013	0.03	Na2O	0.42	0.06	0.2
Cr2O3	0.45	0.04	0.04	Cr2O3	0.65	0.05	0.03

Whole Rock XRF MESA

	NGU std n=4	1 sigma	Accepted value2	NIM-D	Accepted value3	BHVO
SiO2 %	59.47	0.06	58.18	38.52	38.88	50.09
TiO2	0.88	0.01	0.90	0.03	0.02	2.68
Al2O3	16.55	0.06	16.43	0.30	0.32	13.48
Fe2O3	8.02	0.05	8.23	17.07	16.97	12.31
MnO	0.09	0.007	0.10	0.22	0.22	0.18
MgO	2.49	0.07	2.38	43.19	43.56	7.20
CaO	1.91	0.02	1.96	0.27	0.28	11.31
Na2O	2.54	0.05	2.57	0.06	0.05	2.22
K2O	3.69	0.02	3.57	0.01	0.01	0.54
P2O5	0.14	0.01	-	0.01	0.02	0.28
LIO	3.85	0.05	3.76	0.00	-	0.00
Ba ppm	709.5	2.87	681	10	10	143
Cr	123	6.4	102	2872	2900	297
Cu	52.5	1.5	53.4	12	10	135
Nb	20	0	21.9	0	-	18
Ni	51	1.9	51.9	2064	2100	115
Rb	165	1.1	172	0	-	10
S	38	5.4	-	103	200?	367
Sr	85	0.7	87.7	2	3	383
V	174	4	211	41	41	321
Y	54	0.7	53.5	0	-	28
Zr	282	1.1	292	16	10?	167

INAA X-RAL

	UTA-1	Accepted Value4
Au ppb	3.7	-
Ba ppm	390	446
Ce	39	37.4
Co	27.9	25
Cr	29.7	26
Cs	1.2	0.98
Eu	1.17	1.03
Fe2O3 %	5.40	5.07
Hf ppm	2.98	3.24
La	20.4	17.9
Lu	0.24	0.22
Na2O %	3.99	3.77
Nd ppm	17.7	19.5
Rb	65	45
Sb	0.3	-
Sc	13	12.1
Se	2.4	-
Sm	3.8	3.7
Ta	0.55	0.64
Tb	0.55	0.50
Th	5.95	5.99
U	2.2	1.92

PGE ANALYSES INAA UNIVERSITY OF TORONTO

	SARM-7 1 sigma n=4		Accepted Value5	Detection Limit1
Os ppb	73	17	63	2.3
Ir	69	3	74	0.03
Ru	423	20	430	10
Rh	253	40	240	1
Pt	4093	358	3740	7.3
Pd	1495	68	1530	30
Au	356	17	310	0.03

1. Detection limit = 2.72 + 4.65sqrt(background), i.e. when the error on the 90% confidence limit is 50%
2. NGU's accpeted value (Faye pers. comm. 1985)
3. Abbey (1980)
4. University of Toronto's accepted value, (Barnes, 1983)
5. Steele et al. (1975)

TABLE 2a
CHEMICAL ANALYSES OF TVERRFJELL ROCKS, WESTERN TRAVERSE

	tv 125	tv 4	tv 3b	tv 3	tv 3c	tv 2	tv 1	tv 54
Ht m	32.4	49	54	56.7	56.7	62	76	92
SiO2 %	51.42	39.98	50.48	46.22	45.60	49.40	41.06	41.20
TiO2	0.33	0.12	0.26	0.03	0.15	0.14	0.12	0.14
Al2O3	6.10	5.22	6.68	24.67	21.59	19.96	4.58	4.95
Fe2O3	9.65	13.30	10.19	4.03	8.76	4.42	14.27	13.48
MnO	0.17	0.15	0.16	0.06	0.06	0.09	0.17	0.16
MgO	25.00	32.51	26.46	10.49	10.93	12.75	36.47	35.41
CaO	3.59	3.03	3.97	11.55	7.91	9.99	2.83	3.23
Na2O	0.32	0.24	0.38	1.32	0.88	1.10	0.35	0.25
K2O	0.30	0.02	0.05	0.15	0.16	0.05	0.02	0.04
P2O5	0.01	0.02	0.02	0.02	0.03	0.02	0.02	0.02
LOI	2.32	5.70	0.99	1.00	1.88	0.99	0.02	0.35
type	2	1	2	3	3	3	1	1
S ppm	706	3317	2208	33	6827	252	1944	865
Rb	13	1	2	4	4	1	1	<dl
Ba	45	10	22	<dl	12	14	12	10
Sr	33	56	57	292	72	190	51	55
Cu	31	302	308	16	164	63	190	85
Ni	418	1041	629	258	269	173	1004	885
Cr	3272	2021	3620	107	1205	1819	1370	1694
V	175	55	196	19	210	137	40	80
Y	7	2	6	<dl	4	2	4	5
Zr	25	18	25	18	24	19	21	21
Ir ppb	<0.01	<0.02	<0.02	0.16	0.07	0.02	0.15	0.06
Rh	<0.5	0.3	7.8	1.1	0.2	<0.5	3.3	<0.5
Pt	<2	2	10	5.3	14	4.8	<2	12
Au	5	3.8	4.6	5.9	12.6	3.4	5.7	5.4

	tv 53	tv 55	tv 5	tv 56	tv 6	Tv 177	Tv 176	tv 8
Ht m	104.1	130	135	141	143	175	180	212
SiO2 %	51.39	40.59	38.73	50.85	52.60	50.53	52.70	48.53
TiO2	0.29	0.09	0.08	0.31	0.26	0.28	0.38	0.13
Al2O3	6.60	5.21	3.73	4.22	5.07	5.16	4.84	23.97
Fe2O3	10.11	14.41	13.21	11.21	10.11	10.92	10.29	3.82
MnO	0.17	0.16	0.16	0.18	0.18	0.17	0.18	0.06
MgO	25.24	35.69	36.05	28.82	27.75	27.85	26.93	8.76
CaO	4.12	3.03	2.16	2.91	3.12	4.15	3.88	11.99
Na2O	0.29	0.16	0.01	0.18	0.19	0.39	0.35	1.56
K2O	0.04	0.04	0.01	0.01	0.01	0.07	0.06	0.10
P2O5	0.02	0.03	0.03	0.02	0.01	0.00	0.01	0.01
LOI	0.83	0.02	6.07	0.77	0.24	0.21	0.03	0.49
type	2	1	1	2	2	2	2	3
S ppm	2216	1365	588	2914	1747	nd	nd	456
Rb	1	<dl	<dl	2	1	4	4	3
Ba	25	<dl	<dl	25	17	17	23	16
Sr	56	58	49	28	182	43	40	249
Cu	34	127	40	222	153	199	163	76
Ni	355	831	734	692	462	689	497	87
Cr	2794	2356	2198	3798	3970	3673	4151	567
V	368	95	49	241	182	135	178	74
Y	6	3	2	6	4	6	7	3
Zr	23	13	16	22	19	22	24	21
Ir ppb	0.05	0.06	0.02	0.05	0.14	nd	nd	0.11
Rh	<0.5	<0.5	0.24	<0.5	1.6	nd	nd	0.6
Pt	8.9	17	5	8.8	33	nd	nd	5.2
Au	4.6	3.4	11.3	5.1	7.3	nd	nd	8.7

	tv 57	Tv 178	tv 9	tv 59	tv 61	Tv 188	tv 60	tv 10
Ht m	223	235	237	244	250	254	293	297
SiO2 %	50.60	48.40	44.54	45.27	49.02	48.47	47.48	47.79
TiO2	0.23	0.19	0.05	0.06	0.15	0.11	0.14	0.16
Al2O3	13.01	11.79	20.17	21.95	19.94	21.69	19.93	20.37
Fe2O3	7.47	8.93	6.68	5.90	5.50	4.60	4.38	3.74
MnO	0.14	0.13	0.08	0.07	0.07	0.09	0.07	0.07
MgO	19.50	21.64	15.53	12.83	13.16	11.75	11.44	9.92
CaO	6.94	6.80	10.12	10.94	10.15	10.85	13.11	13.90
Na2O	0.85	1.13	1.38	1.51	1.38	1.93	1.62	1.60
K2O	0.07	0.07	0.06	0.07	0.09	0.14	0.09	0.16
P2O5	0.02	0.00	0.02	0.02	0.02	0.01	0.00	0.01
LOI	0.62	0.70	0.75	0.29	0.37	0.79	0.62	1.35
type	3	3	6	6	4	4	4	4
S ppm	1096	nd	713	1097	4475	nd	579	243
Rb	1	3	<dl	1	2	4	1	2
Ba	24	12	<dl	<dl	15	<1	18	16
Sr	124	117	221	238	207	226	194	196
Cu	73	183	37	128	63	64	56	280
Ni	156	374	248	270	127	140	131	89
Cr	1330	1259	315	324	123	854	114	1496
V	159	123	19	28	89	54	98	146
Y	5	6	2	1	4	2	4	6
Zr	21	12	15	19	17	16	19	19
Ir ppb	0.04	nd	0.05	0.08	0.04	nd	0.05	0.04
Rh	<0.5	nd	<0.05	1	<0.5	nd	<0.5	1.1
Pt	15.9	nd	13	<2	33	nd	<2	8.9
Au	4.8	nd	10.7	27	35	nd	27	7.9

	tv 11	tv 13	tv 12	tv 14	tv 16	tv 17	tv 18	tv 19
Ht m	315	358	369	416	462	478	494	532
SiO2	43.25	44.67	44 .22	49.38	49.17	44.63	45.13	49.13
TiO2	0.09	0.08	0.11	0.12	0.21	0.12	0.10	0.25
Al2O3	10.23	16.84	6.88	22.53	22.28	15.22	18.92	21.04
Fe2O3	10.72	8.01	12.40	3.73	3.33	8.86	6.55	3.51
MnO	0.13	0.10	0.17	0.07	0.06	0.11	0.08	0.05
MgO	26.46	18.35	32.95	9.88	7.81	19.31	14.84	8.18
CaO	7.00	9.27	4.76	11.05	14.19	9.24	10.73	14.19
Na2O	0.75	1.21	0.40	1.66	1.66	1.08	1.45	1.80
K2O	0.04	0.06	0.02	0.08	0.09	0.05	0.07	0.09
P2O5	0.01	0.02	0.02	0.02	0.01	0.02	0.03	0.02
LOI	0.81	0.83	0.17	1.12	0.42	0.87	1.50	1.11
type	5	4	1	4	4	5	4	4
S ppm	4511	2308	239	121	347	886	1862	117
Rb	<dl	<dl	<dl	<dl	<dl	<dl	<dl	1
Ba	10	<dl	14	13	18	15	12	17
Sr	102	171	74	243	231	184	264	35
Cu	33	14	174	18	199	199	41	10
Ni	847	462	734	108	59	631	112	91
Cr	4280	622	2185	911	1476	930	599	1538
V	66	60	90	132	159	102	103	194
Y	3	1	3	2	6	4	3	8
Zr	17	16	16	18	20	20	18	29
Ir ppb	0.07	0.07	0.06	0.06	0.35	0.08	0.04	0.07
Rh	1.3	0.31	<0.5	0.21	0.27	0.28	0.3	0.6
Pt	<2	9.5	7	2	7.5	14.3	17.8	4.1
Au	5.0	4.4	5.3	6.12	5.7	20.9	3.9	7.4

	tv 24	tv 25	tv 26	tv 27	tv 28	tv 29	tv 30	tv 31
Ht m	859	875	886	896	945	971	977	994
SiO2 %	39.66	46.97	39.74	48.52	47.77	42.32	46.97	37.41
TiO2	0.11	0.13	0.15	0.23	0.19	0.14	0.09	0.08
Al2O3	6.95	22.42	5.31	18.48	17.87	5.25	23.37	3.87
Fe2O3	13.30	10.96	13.38	4.57	4.94	13.22	4.65	14.94
MnO	0.16	0.08	0.17	0.07	0.09	0.18	0.07	0.22
MgO	28.40	10.96	30.68	11.39	12.52	30.20	9.90	32.65
CaO	5.17	11.03	4.47	12.88	13.08	3.97	11.77	3.07
Na2O	0.00	2.08	0.00	1.85	1.45	0.03	1.99	0.00
K2O	0.17	0.16	0.02	0.32	0.10	0.01	0.08	0.01
P2O5	0.01	0.02	0.03	0.01	0.01	0.01	0.01	0.03
LOI	5.76	0.73	5.91	1.34	1.37	4.30	1.19	7.72
type	1	4	1	4	4	1	4	1
S ppm	1650	566	3328	<dl	379	2745	211	783
Rb	1	1	1	<dl	2	<dl	<dl	<dl
Ba	<dl	15	9	24	16	13	14	<dl
Sr	309	54	35	205	194	57	309	54
Cu	121	33	232	7	26	162	42	40
Ni	488	122	747	101	154	575	162	533
Cr	2539	246	3682	1629	1287	1763	533	400
V	124	36	160	192	190	165	54	50
Y	4	4	5	8	5	4	4	<dl
Zr	16	21	19	26	21	21	16	14
Ir ppb	0.04	0.09	0.02	0.06	0.02	0.05	0.03	0.07
Rh	0.48	0.22	2.1	2.5	2.4	0.23	0.75	0.31
Pt	31	<2	5.4	4.5	1.2	2	<2	<2
Au	12.7	7.1	7.6	7.1	2	5.8	3.3	2.4

	tv 32	tv 33	tv 34	tv 35	Tv184	Tv 36	tv 37	Tv 185
Ht m	1009	1048	1053	1055	1060	1069	1107	1110
SiO2	48.71	46.82	37.91	39.49	43.56	48.32	39.09	41.92
TiO2	0.13	0.06	0.13	0.16	0.07	0.18	0.08	0.04
Al2O3	23.91	24.75	1.76	5.17	15.39	21.46	3.34	15.89
Fe2O3	3.12	3.79	16.51	14.06	8.42	3.34	15.21	9.24
MnO	0.05	0.06	0.20	0.17	0.10	0.06	0.16	0.08
MgO	6.70	8.70	37.10	31.02	19.97	8.83	36.19	17.99
CaO	13.61	11.73	1.92	4.09	8.16	12.19	2.20	9.79
Na2O	0.09	2.28	0.01	0.00	1.70	1.73	0.00	2.30
K2O	0.09	0.18	0.01	0.00	0.11	0.11	0.00	0.26
P2O5	0.02	0.02	0.04	0.03	0.01	0.02	0.01	0.00
LOI	0.78	1.26	4.66	5.91	2.79	1.17	4.11	2.61
type	4	4	1	1	5	4	1	5
S ppm	555	213	2500	2459	nd	249	1096	nd
Rb	2	8	<dl	<dl	3	2	1	5
Ba	15	<dl	<dl	11	<1	17	<dl	<1
Sr	271	281	22	49	94	244	39	72
Cu	70	21	121	207	4	35	143	17
Ni	131	177	881	940	665	149	706	540
Cr	1043	79	777	3315	1179	1964	278	239
V	79	22	83	126	54	135	43	72
Y	5	3	2	4	<1	5	3	3
Zr	18	20	22	24	14	21	19	8
Ir ppb	0.03	0.06	0.07	0.03	nd	0.03	0.04	nd
Rh	0.91	0.44	<0.5	<0.5	nd	<0.5	<0.5	nd
Pt	<2	<2	<2	9.7	nd	<0.2	1.7	nd
Au	2.4	3	5.5	9.3	nd	5.4	1.6	nd

-A6-

	tv 38	tv 39	tv 41	tv 42	tv 43
Ht m	1134	1140	1167	1221	1238
SiO2 %	48.48	47.78	49.62	44.18	47.48
TiO2	0.23	0.22	0.37	0.27	0.40
Al2O3	18.76	23.20	17.62	12.72	10.43
Fe2O3	3.98	3.89	4.16	10.19	5.89
MnO	0.06	0.06	0.06	0.13	0.09
MgO	10.53	7.81	9.93	21.41	11.77
CaO	14.17	13.00	15.16	8.22	11.21
Na2O	1.51	2.20	1.16	1.08	1.97
K2O	0.12	0.16	0.08	0.11	0.18
P2O5	0.02	0.04	0.03	0.04	0.04
LOI	1.15	0.92	1.49	0.92	0.74
type	4	4	4	5	4
S ppm	296	375	<dl	2116	332
Rb	2	3	1	3	2
Ba	20	19	22	30	33
Sr	219	276	171	132	197
Cu	24	37	4	122	34
Ni	169	161	105	393	160
Cr	2151	977	1460	649	713
V	177	75	207	107	106
Y	8	5	11	7	9
Zr	29	31	38	31	38
Ir ppb	0.05	0.06	<0.01	0.09	0.04
Rh	<0.5	<0.5	<0.5	<0.5	<0.5
Pt	<2	<2	<2	5.1	1.2
Au	6.4	1.7	1	1.7	2

TABLE 2b
CHEMICAL ANALYSES OF TVERRFJELL ROCKS CENTRAL TRAVERSE

		tv 62	tv 63	tv 64	tv 65	tv 66	tv 187	tv 75	tv 73
ht	m	11	22	23	27	38	45	95	108
SiO2	%	38.45	38.50	37.85	39.01	49.57	44.08	52.29	51.90
TiO2		0.12	0.25	0.17	0.17	0.31	0.25	0.32	0.33
Al2O3		4.16	3.86	4.08	5.18	5.04	4.05	6.91	7.04
Fe2O3		12.45	12.47	12.53	12.06	9.81	11.90	9.60	9.67
MnO		0.15	0.14	0.14	0.16	0.16	0.16	0.16	0.16
MgO		33.91	33.93	34.08	31.61	27.06	31.25	24.62	24.42
CaO		2.86	2.72	2.27	3.60	3.37	3.35	4.66	4.67
Na2O		0.00	0.01	0.01	0.35	0.18	0.44	0.45	0.48
K2O		0.00	0.00	0.00	0.08	0.04	0.07	0.06	0.06
P2O5		0.02	0.03	0.03	0.01	0.03	0.01	0.02	0.03
LOI		7.79	8.17	8.58	7.90	3.93	4.48	0.42	0.50
type		1	1	1	1	2	7	2	2
S	ppm	2270	1855	1816	2339	2323	nd	2309	2431
Rb		<dl	<dl	1	2	3	4	3	4
Ba		<dl	14	<dl	23	16	9	32	34
Sr		35	16	13	65	23	41	59	61
Cu		241	196	170	217	235	177	221	216
Ni		1288	903	975	983	589	740	549	526
Cr		1085	3889	5012	2815	3578	1775	2887	2669
V		64	93	101	84	201	107	189	164
Y		5	5	6	4	7	7	6	8
Zr		15	26	26	19	25	21	30	28
Ir	ppb	<0.1	0.03	<0.1	<0.1	<0.1	nd	<0.1	<0.1
Rh		<0.5	<0.5	<0.5	<0.5	<0.5	nd	4	<0.5
Pt		3	6	3	2	<2	nd	23	<5
Au		4	4	4	3.4	7	nd	8	4
Se	ppm	3.3	2.2	2.3	1	1.4	nd	1.2	2.8
Cs		<0.2	<0.2	0.4	1.3	0.5	nd	0.6	0.8
Co		120	111	109	118	85	47	72	76
Sc		11	13	11	13	25	21	37	36
Hf		<0.2	0.46	0.18	0.27	0.36	nd	0.44	0.28
La		0.7	2.0	0.63	1.7	0.85	nd	1.08	1.12
Ce		2.8	6.4	6.3	5.4	7.6	nd	7.9	6.5
Sm		0.31	0.59	0.42	0.45	0.42	nd	0.51	0.52
Eu		0.12	0.17	0.18	0.26	0.22	nd	0.26	0.15
Tb		<0.1	0.09	<0.2	0.09	0.09	nd	0.09	0.09
Yb		0.36	0.49	0.46	0.30	0.65	nd	0.67	0.72
Lu		0.046	0.074	0.084	0.045	0.12	nd	0.10	0.12

-A8-

	tv 74	tv 70	tv 126	tv 76	tv 71	tv 127	tv 72	tv 128
ht	109	119	127	130	133	136	141	147
SiO2	51.00	41.53	44.12	51.16	48.89	49.86	40.38	41.35
TiO2	0.19	0.15	0.23	0.34	0.19	0.22	0.16	0.22
Al2O3	18.67	5.91	7.09	7.68	17.19	19.90	4.32	4.27
Fe2O3	5.40	12.24	11.86	9.58	6.19	4.94	14.78	14.64
MnO	0.09	0.15	0.16	0.17	0.09	0.09	0.17	0.17
MgO	12.88	31.91	28.89	24.45	15.68	12.13	36.47	34.68
CaO	9.63	3.70	4.39	4.77	8.82	10.02	2.70	2.76
Na2O	1.63	0.59	0.57	0.47	1.02	1.41	0.26	0.27
K2O	0.11	0.05	0.06	0.08	0.05	0.09	0.03	0.05
P2O5	0.02	0.03	0.03	0.03	0.02	0.02	0.03	0.02
LOI	0.65	3.93	2.24	0.43	0.89	0.45	0.00	0.57
type	3	1	7	2	3	7	1	1
S	483	747	978	1654	1127	484	2460	1772
Rb	2	2	1	2	2	4	1	7
Ba	19	16	24	32	17	21	17	26
Sr	199	66	77	71	185	219	53	50
Cu	61	55	97	196	96	69	273	211
Ni	162	604	590	512	179	162	1399	1111
Cr	1310	811	1432	3407	1343	1357	2455	2768
V	90	52	97	186	104	105	56	93
Y	5	4	5	8	4	5	3	6
Zr	23	23	26	29	18	22	22	25
Ir	0.01	0.02	<0.1	0.06	0.04	<0.1	0.09	<0.1
Rh	<0.5	<0.5	<0.5	<0.5	<0.5	2	<0.5	<0.5
Pt	<2	<2	<5	<2	<2	<5	9	<5
Au	4	3	4	14.5	8	5	6	6
Se	1.5	2.5	nd	1.2	2	nd	<1	nd
Cs	0.4	0.5	nd	0.7	0.6	nd	0.5	nd
Co	36	103	nd	69	46	nd	133	nd
Sc	21	13	nd	35	19	nd	11	nd
Hf	0.19	0.47	nd	0.44	<0.2	nd	0.26	nd
La	0.95	1.04	nd	1.2	1.16	nd	1.12	nd
Ce	3.8	1.88	nd	7.9	4.4	nd	6.5	nd
Sm	0.32	0.37	nd	0.55	0.26	nd	0.33	nd
Eu	0.33	0.19	nd	0.13	0.29	nd	0.17	nd
Tb	<0.1	<0.1	nd	0.09	nd	nd	0.09	nd
Yb	0.42	0.33	nd	0.79	0.40	nd	0.37	nd
Lu	0.076	0.066	nd	0.11	0.062	nd	0.05	nd

-A9-

	tv 77	tv 78	tv 80	tv 79	tv 81	tv 82	tv 181	tv 83
ht	152	157	179	185	233	266	270	298
SiO2	49.78	51.76	41.07	52.33	48.92	47.34	48.81	49.48
TiO2	0.44	0.46	0.37	0.35	0.24	0.13	0.33	0.18
Al2O3	5.46	5.51	3.05	6.49	19.63	20.88	18.08	21.68
Fe2O3	11.13	10.70	15.51	9.49	5.93	5.80	6.64	3.45
MnO	0.16	0.15	0.19	0.17	0.08	0.08	0.09	0.07
MgO	27.81	25.49	35.85	25.81	12.44	12.60	13.46	8.22
CaO	3.68	3.82	2.56	4.17	9.99	10.41	9.65	13.77
Na2O	0.46	0.36	0.22	0.44	1.50	1.58	1.75	2.03
K2O	0.08	0.08	0.08	0.05	0.18	0.12	0.09	0.11
P2O5	0.02	0.02	0.04	0.01	0.03	0.02	0.02	0.01
LOI	0.39	0.72	0.00	0.25	0.29	0.36	0.51	0.31
type	2	2	1	2	3	6	7	4
S	1767	3761	2529	1638	605	1112	nd	337
Rb	3	3	3	2	5	3	5	2
Ba	32	41	33	33	31	17	32	18
Sr	51	48	34	60	214	223	201	213
Cu	181	183	236	180	53	117	86	29
Ni	674	480	1584	439	120	180	205	44
Cr	2933	2852	2990	2802	842	681	966	814
V	194	428	113	179	114	223	80	213
Y	8	9	7	7	7	4	8	5
Zr	32	27	35	27	31	21	28	22
Ir	0.06	0.12	0.08	0.1	0.1	0.05	nd	0.06
Rh	<0.5	2.7	6.7	13	11	<0.5	nd	<0.5
Pt	<2	6.1	2.8	46	16	1	nd	0.6
Au	13.2	28	10.9	23	24.3	5	nd	6.5
Se	1.2	1.2	3.5	3	1.3	1.3	nd	2.2
Cs	0.7	0.8	<0.2	0.5	<0.2	0.4	nd	0.6
Co	84	100	135	69	38	45	47	22
Sc	34	40	18	35	17	10	19	23
Hf	0.52	0.27	0.36	0.38	0.44	0.26	nd	0.18
La	1.14	1.37	1.50	0.86	2.9	2.1	nd	1.2
Ce	6.2	6.4	6.3	4.76	5.3	3.5	nd	2.7
Sm	0.60	0.69	0.74	0.44	0.65	0.39	nd	0.48
Eu	0.22	0.25	0.27	0.34	0.51	0.42	nd	0.56
Tb	0.18	0.27	0.18	0.09	nd	0.09	nd	<0.1
Yb	0.94	1.01	0.65	0.79	0.58	0.35	nd	0.42
Lu	0.14	0.16	0.10	0.13	0.11	0.05	nd	0.06

-A10-

	tv 84	tv 183	tv 85	tv 86	tv 87	tv 88	tv 89	tv 90
ht	304	319	375	385	415	440	478	489
SiO2	42.90	50.03	49.92	42.62	48.42	46.76	48.27	43.04
TiO2	0.12	0.16	0.25	0.11	0.27	0.20	0.20	0.09
Al2O3	9.10	18.34	18.22	7.62	7.47	24.75	21.57	14.97
Fe2O3	11.83	5.68	4.89	13.02	11.86	4.20	3.48	9.85
MnO	0.14	0.10	0.10	0.19	0.17	0.15	0.12	0.08
MgO	27.11	13.39	11.02	29.03	24.50	7.95	8.70	21.11
CaO	6.37	9.68	12.95	4.92	5.30	12.70	14.25	7.63
Na2O	0.71	1.83	1.50	0.58	0.55	1.80	1.69	1.31
K2O	0.05	0.12	0.07	0.05	0.05	0.15	0.12	0.08
P2O5	0.02	0.01	0.01	0.01	0.01	0.02	0.02	0.01
LOI	0.66	2.79	0.37	0.81	0.61	0.74	0.52	0.64
type	5	7	4	1	2	4	4	5
S	2186	nd	528	1565	2583	722	611	2166
Rb	2	4	3	1	0	3	1	1
Ba	12	17	17	15	27	24	27	17
Sr	96	178	211	84	81	260	240	187
Cu	114	35	80	116	139	32	9	151
Ni	424	172	87	607	377	75	36	497
Cr	507	937	1536	985	1949	183	1416	984
V	96	161	211	97	288	49	158	36
Y	4	4	6	4	6	4	8	2
Zr	18	14	21	19	25	26	25	15
Ir	0.07	nd	0.05	0.15	0.06	0.05	0.02	0.07
Rh	0.6	nd	1	2	<0.5	<0.5	<0.5	<0.5
Pt	2	nd	2.5	2	2	2	9.6	9
Au	5.9	nd	4.2	6.7	7.2	10.4	10.3	26
Se	2	1.2	2.6	4.4	4.9	1.2	1.5	2.3
Cs	0.5	nd	0.9	<0.2	0.4	0.9	0.4	<0.2
Co	108	47	25	114	83	29	25	88
Sc	16	21	30	15	32	8	23	6
Hf	< 0.2	nd	0.46	0.17	0.26	0.35	0.43	<0.2
La	0.8	nd	1.1	1.9	0.80	1.90	1.40	1.96
Ce	3.6	nd	5.5	1.8	4.3	3.50	5.95	1.78
Sm	0.42	nd	0.62	0.34	0.38	0.57	0.64	0.26
Eu	0.27	nd	0.55	0.28	0.26	0.57	0.42	0.40
Tb	nd	nd	0.18	<0.01	0.17	0.09	0.08	<0.1
Yb	0.39	nd	0.70	0.42	0.62	0.38	0.52	0.20
Lu	0.07	nd	0.11	0.05	0.10	0.06	0.08	0.05

-A11-

	tv 91	tv 92	tv 21	tv 22	tv 23	tv 94	tv 95	tv 96
ht	499	526	668	673	819	823	831	836
SiO2	47.89	48.49	37.03	44.60	40.53	41.51	46.41	41.83
TiO2	0.22	0.35	0.88	0.09	0.20	0.16	0.15	0.18
Al2O3	20.26	16.34	4.07	17.58	5.91	5.30	20.97	7.00
Fe2O3	4.92	6.24	14.41	8.27	14.64	15.06	6.41	14.03
MnO	0.14	0.17	0.18	0.10	0.17	0.03	0.09	0.18
MgO	10.86	12.63	31.26	16.92	29.08	31.93	11.89	29.92
CaO	12.75	13.17	2.76	8.94	5.00	4.39	10.53	5.77
Na2O	1.75	1.36	0.01	1.66	0.07	0.34	1.85	0.55
K2O	0.14	0.17	0.02	0.09	0.01	0.03	0.12	0.05
P2O5	0.03	0.04	0.18	0.02	0.01	0.01	0.02	0.02
LOI	0.61	0.57	10.01	1.09	4.48	0.10	0.49	0.05
type	4	4	1	4	7	1	4	1
S	3733	916	5686	791	4031	3730	738	2696
Rb	2	4	1	2	0	0	2	1
Ba	27	38	0	20	0	9	21	12
Sr	241	184	205	194	57	62	239	87
Cu	56	45	202	150	147	274	45	157
Ni	158	102	536	390	465	876	148	478
Cr	1290	822	164	78	1503	2828	209	1374
V	131	182	34	27	139	129	45	108
Y	8	10	4	2	6	3	4	5
Zr	30	33	22	20	23	19	22	25
Ir	0.03	0.01	0.07	0.09	0.13	<0.1	0.04	0.07
Rh	<0.5	<0.5	<0.5	1.1	1	<0.5	<0.5	<0.5
Pt	9	<2	2.5	<2	7.5	<5	<2	<2
Au	3	5	6.2	6.9	3.4	5	5.9	8.9
Se	2	1.2	2.6	4.4	4.9	1.2	1.5	2.3
Cs	0.5	nd	0.9	<0.2	0.4	0.9	0.4	<0.2
Co	35	39	137	108	96	117	40	110
Sc	19	32	11	6.4	nd	18	8.5	19
Hf	0.36	0.52	<0.2	0.18	nd	0.18	0.18	0.36
La	1.60	2.2	1.2	0.90	nd	1.1	1	2.3
Ce	5.5	7.9	0.91	1.8	nd	4.5	2.7	4.5
Sm	0.67	1.02	0.26	0.26	nd	0.36	0.38	0.49
Eu	0.51	0.54	0.08	0.40	nd	0.22	0.59	0.32
Tb	0.09	0.26	<0.1	0.09	nd	0.09	<0.1	0.09
Yb	0.49	0.82	0.30	0.20	nd	0.44	0.30	0.53
Lu	0.05	0.12	0.04	0.04	nd	0.07	0.04	0.09

	tv 97	tv 186	tv 98	tv 52	tv 51	tv 50	tv 49	tv 48
ht	842	910	918	950	961	972	1031	1042
SiO2	49.51	40.26	48.53	47.63	38.59	48.20	48.20	36.98
TiO2	0.26	0.19	0.26	0.20	0.09	0.19	0.19	0.04
Al2O3	18.05	5.16	19.02	17.09	5.18	18.16	18.16	6.14
Fe2O3	4.50	13.44	4.00	5.35	12.41	4.74	4.74	10.61
MnO	0.09	0.18	0.07	0.07	0.15	0.07	0.07	0.17
MgO	11.23	29.21	10.26	13.75	30.89	11.55	11.55	29.71
CaO	12.21	4.66	14.11	13.13	4.20	13.98	13.98	5.46
Na2O	2.27	0.00	1.78	1.32	0.00	1.29	1.29	0.00
K2O	0.45	0.06	0.13	0.07	0.00	0.06	0.06	0.00
P2O5	0.02	0.01	0.02	0.02	0.01	0.02	0.02	0.01
LOI	0.86	6.92	0.52	0.39	8.19	0.59	0.59	10.77
type	4	7	4	7	1	4	4	1
S	24	nd	254	599	604	526	794	2767
Rb	12	4	3	0	0	0	0	0
Ba	31	<1	23	20	0	24	14	0
Sr	194	57	205	189	154	28	220	217
Cu	3	91	36	36	120	56	27	218
Ni	92	475	153	84	793	128	85	684
Cr	1323	1959	1715	1059	2276	869	306	1566
V	180	144	142	150	112	134	235	51
Y	8	6	8	7	2	6	3	5
Zr	25	21	27	25	17	24	21	16
Ir	0.09	nd	<0.1	0.05	<0.03	0.03	0.03	0.0
Rh	<0.5	nd	<0.5	<0.5	<0.5	<0.5	<0.5	<0.5
Pt	6	nd	<5	<2	<2	<5	<2	<2
Au	5.7	nd	5	2.24	7	6	4.3	20
Se	2.1	nd	2.9	nd	2.2	<1	1.6	1.8
Cs	2	nd	0.7	nd	2	0.7	0.8	1
Co	24	90	27	< 0	99	37	35	91
Sc	29	22	28	< 0	13	29	31	8
Hf	0.45	nd	0.36	nd	<0.2	0.18	0.26	<0.2
La	1.3	nd	1.6	nd	0.72	1.85	0.71	0.55
Ce	4.5	nd	7	nd	2.7	3.7	1.80	1.8
Sm	0.64	nd	0.81	nd	0.16	0.65	0.59	0.13
Eu	0.55	nd	0.54	nd	<0.05	0.46	0.51	0.07
Tb	0.09	nd	0.18	nd	<0.1	0.18	0.18	<0.09
Yb	0.66	nd	0.68	nd	0.22	0.61	0.55	0.12
Lu	0.10	nd	0.10	nd	0.036	0.09	0.08	0.027

-A13-

	tv 47	tv 45	tv 44	tv 124	tv 122	tv 123	tv 122	tv 123
ht	1075	1297	1303	1433	1438	1455	1438	1455
SiO2	45.86	47.41	44.79	45.96	41.10	46.70	41.10	46.70
TiO2	0.08	0.31	0.21	0.24	0.19	0.21	0.19	0.21
Al2O3	23.29	22.29	15.87	20.60	6.58	20.51	6.58	20.51
Fe2O3	4.26	4.84	8.40	5.79	12.43	5.57	12.43	5.57
MnO	0.05	0.06	0.13	0.07	0.15	0.05	0.15	0.05
MgO	10.68	9.75	18.99	12.73	32.05	12.62	32.05	12.62
CaO	11.73	11.31	9.04	10.85	4.63	11.10	4.63	11.10
Na2O	1.87	2.05	1.31	1.81	0.48	1.83	0.48	1.83
K2O	0.09	0.24	0.10	0.12	0.05	0.11	0.05	0.11
P2O5	0.01	0.04	0.02	0.03	0.03	0.03	0.03	0.03
LOI	1.12	0.76	0.58	0.82	1.85	0.54	1.85	0.54
type	4	4	5	4	1	4	7	7
S	303	135	2179	654	2517	380	2517	380
Rb	1	0	0	4	0	3	0	3
Ba	9	41	25	30	16	21	16	21
Sr	402	227	158	232	78	225	78	225
Cu	41	26	183	77	190	25	190	25
Ni	269	203	644	197	829	225	829	225
Cr	307	481	468	698	1307	333	1307	333
V	31	63	60	54	65	49	65	49
Y	6	7	2	6	5	6	5	6
Zr	18	33	28	34	24	31	24	31
Ir	0.03	0.04	0.05	0.05	0.03	<0.1	0.03	<0.1
Rh	<0.5	<0.5	<0.5	<0.5	<0.5	<0.5	<0.5	<0.5
Pt	<2	<2	1	2	<2	<5	<2	<5
Au	4.2	6.6	3.5	5.6	5	5	5	7
Se	1.5	1	3.8	1.9	1.1	1.5	1.1	1.5
Cs	1	2	1	2	<0.4	0.7	<0.4	0.7
Co	36	31	76	46	113	42	113	42
Sc	4	11	12	10	14	11	14	11
Hf	<0.2	0.43	0.28	0.4	0.27	0.27	0.27	0.27
La	1.5	2.6	1.5	1.5	1.5	1.5	1.5	1.5
Ce	2.6	6.2	3.7	4.5	2.7	2.7	2.7	2.7
Sm	0.29	0.77	0.59	0.6	0.50	0.56	0.50	0.56
Eu	0.49	0.47	0.42	0.67	0.27	0 38	0.27	0.38
Tb	<0.1	0.08	<0.1	0.09	0.09	0.09	0.09	0.09
Yb	0.18	0.53	0.43	0.44	0.43	0.40	0.43	0.40
Lu	0.03	0.088	0.06	0.06	0.07	0.07	0.07	0.07

TABLE 2c
CHEMICAL ANALYSES OF TVERRFJELL ROCKS EASTERN TRAVERSE

	tv 129	tv 133	tv 135	tv 130	tv 131	tv 132	tv 134	tv 141
ht m	148	162	215	242	259	280	282	340
SiO2 %	49.53	50.30	38.78	40.63	51.60	50.32	47.87	43.84
TiO2	0.29	0.37	0.21	0.27	0.25	0.29	0.23	0.36
Al2O3	7.52	18.59	4.90	4.97	6.62	18.78	19.37	9.94
Fe2O3	11.02	5.89	13.43	13.66	10.56	5.99	6.42	11.36
MnO	0.17	0.09	0.01	0.19	0.15	0.10	0.18	0.14
MgO	24.36	11.48	32.58	29.92	25.87	11.49	13.12	24.59
CaO	5.24	10.36	2.92	3.60	3.72	9.88	10.02	6.84
Na2O	0.55	1.63	0.01	0.00	0.28	1.80	1.63	1.07
K2O	0.09	0.09	0.01	0.00	0.03	0.10	0.18	0.14
P2O5	0.02	0.04	0.02	0.03	0.01	0.02	0.03	0.04
LOI	0.70	1.03	7.01	6.83	0.07	0.86	0.75	0.96
type	2	3	1	1	2	3	3	5
S ppm	1895	81	2675	1720	501	9	792	1145
Rb	3	7	<dl	1	2	2	5	5
Ba	33	44	<dl	16	24	32	34	36
Sr	75	216	57	77	200	234	207	115
Cu	162	31	235	151	44	16	49	101
Ni	588	124	1494	675	94	138	159	574
Cr	2224	899	1808	2142	1023	808	635	1519
V	175	120	73	85	149	119	86	94
Y	7	9	5	4	8	7	7	10
Zr	30	40	22	32	24	33	23	39
Ir	nd	0.05	0.07	nd	0.06	0.11	0.05	nd
Rh	1.2	0.4	0.4	3	1.8	0.9	0.4	1.8
Pt	nd	20	20	nd	20	<2	19	nd
Au	nd	2.79	3.7	nd	7.8	3.35	3.47	nd

	tv 143	tv 144	tv 140	tv 136	tv 139	tv 138	tv 137	tv 101
ht	350	360	368	382	396	406	423	461
SiO2	44.97	48.54	47.49	40.43	49.18	41.30	48.88	48.08
TiO2	0.45	0.46	0.27	0.20	0.33	0.29	0.32	0.31
Al2O3	10.62	17.33	18.06	4.62	18.46	5.55	16.40	18.39
Fe2O3	11.11	6.87	7.66	15.51	6.77	15.33	6.36	6.59
MnO	0.18	0.11	0.10	0.20	0.10	0.19	0.09	0.09
MgO	22.71	10.70	12.99	30.55	11.94	29.58	13.31	11.66
CaO	7.70	12.40	10.09	3.90	9.83	4.18	11.85	12.49
Na2O	1.28	1.86	1.73	0.00	1.63	0.00	1.22	1.64
K2O	0.16	0.25	0.15	0.00	0.14	0.02	0.10	0.15
P2O5	0.05	0.04	0.03	0.03	0.03	0.03	0.02	0.03
LOI	0.51	0.46	0.66	4.59	0.68	4.75	0.69	0.33
type	5	4	4	1	4	1	4	4
S	1426	484	65	2392	1483	768	3073	600
Rb	5	7	3	2	3	3	2	3
Ba	45	52	26	15	37	19	29	33
Sr	116	195	00	44	226	30	181	224
Cu	109	21	57	222	88	66	64	15
Ni	475	93	60	624	201	388	105	47
Cr	1339	578	73	1489	1022	1243	1766	914
V	118	147	95	143	145	118	228	157
Y	13	12	6	5	7	7	9	9
Zr	41	48	28	31	28	31	36	30
Ir	nd	nd	nd	0.05	nd	nd	nd	0.08
Rh	1.5	1.2	0.4	0.7	0.8	0.6	1.2	<1
Pt	nd	nd	nd	20	nd	nd	nd	11.3
Au	nd	nd	nd	3.6	nd	nd	nd	1.76

-A15-

	tv 99	tv 102	tv 100	tv 103	tv 104	tv 105	tv 106	tv 107
ht	469	472	488	629	706	708	727	742
SiO2	40.62	43.26	49.08	49.40	44.24	47.01	40.84	47.70
TiO2	0.30	0.26	0.41	0.38	0.12	0.14	0.25	0.24
Al2O3	6.49	7.66	17.96	17.40	15.20	21.35	6.18	17.25
Fe2O3	14.06	13.43	5.36	6.05	9.20	6.27	12.24	6.10
MnO	0.18	0.19	0.09	0.12	0.12	0.07	0.16	0.09
MgO	28.04	27.25	10.11	11.02	19.45	11.02	28.35	14.22
CaO	4.84	5.62	13.56	13.23	9.20	11.35	5.17	12.38
Na2O	0.00	0.74	1.86	1.88	1.14	1.98	0.00	1.48
K2O	0.02	0.07	0.15	0.18	0.06	0.10	0.01	0.08
P2O5	0.03	0.02	0.03	0.04	0.02	0.01	0.02	0.01
LOI	5.00	0.57	0.27	0.43	0.63	0.39	6.45	0.37
type	1	1	4	4	5	4	1	4
S	2405	1670	664	716	1428	924	2304	1688
Rb	<dl	3	2	4	1	<dl	<dl	2
Ba	14	28	45	44	19	21	13	24
Sr	33	94	224	214	179	256	26	189
Cu	184	126	39	22	127	58	128	125
Ni	664	536	88	58	365	164	621	348
Cr	2801	1233	1127	551	565	267	1929	1849
V	152	128	160	144	67	51	139	157
Y	6	7	12	12	4	3	5	6
Zr	38	26	38	37	21	19	26	24
Ir	nd	0.06	0.02	0.11	0.06	0.05	0.06	0.03
Rh	<1	<1	<0.7	<0.8	<1	<0.6	<1	<1
Pt	nd	<5	22	6	10	11	15	5.5
Au	nd	3.4	2.5	2.08	4.1	5.5	2.7	2.6

	tv 108	tv 109	tv 110	tv 111	tv 113	tv 112	tv 115	tv 114
ht	748	755	766	783	788	798	867	885
SiO2	50.03	40.09	49.08	41.67	42.79	44.61	49.89	40.68
TiO2	0.24	0.10	0.28	0.14	0.12	0.11	0.22	0.07
Al2O3	17.88	3.12	17.76	4.91	9.93	16.58	18.95	8.99
Fe2O3	4.51	16.79	5.19	14.93	11.52	8.51	3.75	11.86
MnO	0.09	0.20	0.09	0.18	0.17	0.12	0.06	0.14
MgO	10.51	35.14	11.58	31.85	26.90	18.83	8.86	29.36
CaO	12.54	1.38	13.75	4.29	6.50	8.91	14.81	5.15
Na2O	1.79	0.00	1.46	0.37	0.81	1.23	1.79	0.52
K2O	0.11	0.00	0.12	0.03	0.09	0.04	0.07	0.02
P2O5	0.02	0.01	0.02	0.02	0.14	0.02	0.01	0.01
LOI	1.41	2.85	0.77	0.68	0.76	0.42	0.77	2.77
type	4	1	4	1	1	4	4	1
S	600	2203	538	4392	1623	1159	718	1802
Rb	1	<dl	3	1	2	1	1	<dl
Ba	20	10	24	18	20	18	17	<dl
Sr	196	9	204	59	118	194	236	113
Cu	16	95	18	233	161	112	13	177
Ni	38	625	97	870	668	453	39	693
Cr	618	104	1686	725	1065	1027	387	1327
V	239	76	196	110	76	52	255	69
Y	8	3	9	4	3	4	7	2
Zr	20	28	29	21	15	21	23	14
Ir	0.08	0.06	0.06	nd	nd	nd	nd	<0
Rh	<1	<1	<1	<1	<1	<1	<1	<1
Pt	29	23	23	nd	nd	nd	nd	<0
Au	3.9	22.1	2	nd	nd	nd	nd	<0

-A16-

	tv 116	tv 118	tv 117	tv 119	tv 120	tv 121	tv 142	tv 189
ht	916	939	966	975	1190	1200	352	588
SiO2	47.79	47.45	43.31	46.05	38.82	45.89	45.86	54.80
TiO2	0.19	0.19	0.08	0.12	0.23	0.18	0.54	1.39
Al2O3	18.96	18.22	12.23	20.69	4.50	20.83	13.05	14.93
Fe2O3	4.70	13.05	10.06	5.58	14.58	5.70	9.91	8.86
MnO	0.09	0.07	0.13	0.08	0.19	0.06	0.13	0.15
MgO	11.69	13.05	24.66	13.32	32.77	13.44	18.42	7.08
CaO	13.30	13.32	7.87	11.05	2.72	10.63	8.88	8.60
Na2O	1.52	1.38	0.91	1.74	0.01	1.74	1.59	2.16
K2O	0.08	0.08	0.03	0.09	0.01	0.10	0.23	0.81
P2O5	0.01	0.01	0.02	0.02	0.03	0.02	0.05	0.19
LOI	0.59	0.30	0.42	0.61	6.21	0.84	0.53	0.84
type	4	4	5	4	1	4	4	4
S	591	548	1852	1012	453	544	1099	nd
Rb	2	1	2	3	<dl	1	8	29
Ba	20	14	13	9	19	17	56	202
Sr	207	176	124	208	7	235	146	180
Cu	33	30	172	81	26	39	82	17
Ni	130	129	587	290	847	209	376	35
Cr	1029	1310	984	546	971	299	1116	150
V	130	155	70	34	59	32	138	194
Y	6	7	3	3	3	6	6	6
Zr	26	25	18	22	28	24	24	39
Ir	nd	nd	<0.	nd	nd	0.11	nd	nd
Rh	<1	<1	<1	<1	<1	<1	<1	<1
Pt	nd	nd	nd	nd	nd	13.3	nd	nd
Au	nd	nd	nd	nd	nd	6.68	nd	nd

nd = not determined, dl= detection limit usually 1 to 2 ppm, also determined but not detected were Nb < 2ppm, Os < 2 ppb, Ru < 3 ppb, Pd < 20 ppb.

TABLE 3a
STATISTICS FOR OLIVINES

Element	Average	o	n=155
SiO2	40.12	0.57	
FeO	16.31	2.35	
MgO	43.49	2.06	
NiO	0.085	0.035	

Correlation matrix r99=0.25

	SiO2	FeO	MgO	NiO
SiO2	1	-.756	.705	.211
FeO	-.756	1	-.956	-.327
MgO	.705	-.956	1	.319
NiO	.211	-.327	.319	1

Comparison of analyses of the centres of olivines from coronas and olivines in pyroxene oikocrysts.

Type	Forsterite	o	n
coronas	82.68	2.41	42
oikocrysts	83.22	2.09	42

t= 1.09 therefore the two types of olivines are not significantly different.

TABLE 3b
OLIVINE ANALYSES
WESTERN TRAVERSE

	4/i	3b/f	1/i	1/cr	54/i	54/f	53/cr	55/cr
ht	49	54	76	26	92	92	109	130
SiO2	40.62	41.05	40.11	40.19	40.49	41.40	41.29	40.31
FeO	14.26	13.01	13.73	14.09	13.80	13.81	13.62	14.67
MgO	45.80	45.80	45.77	45.12	46.38	46.08	45.15	45.02
NiO	0.09	0.16	0.12	0.14	0.13	0.14	0.09	0.10
Total	100.77	100.02	100.67	99.46	100.80	101.43	100.15	100.10

	5/i	56/i	56/cr	177/i	176/cr	8/cr	178/i	57/f
ht	135	141	141	175	180	212	217	223
SiO2	40.29	40.77	40.35	40.93	40.48	40.53	40.64	40.66
FeO	14.52	14.60	13.91	13.48	14.76	15.21	14.80	13.71
MgO	44.96	44.82	45.11	45.27	44.88	44.97	45.69	46.08
NiO	0.12	0.12	0.12	0.06	0.11	0.05	0.07	0.08
Total	99.89	100.31	99.49	99.74	100.23	99.89	101.20	100.76

	57/cr	9/cr	59/i	59/cr	188/i	188/cr	60/f	60/i
ht	233	239	244	244	254	254	293	293
SiO2	39.80	40.22	40.60	40.26	40.10	40.17	39.94	40.43
FeO	13.91	15.35	15.69	15.71	14.87	15.31	14.53	14.07
MgO	45.77	43.52	44.19	43.55	45.18	44.16	45.84	45.11
NiO	0.05	0.07	0.08	0.07	0.07	0.06	0.05	0.05
Total	99.53	99.16	100.56	99.59	100.22	99.70	100.36	99.66

	11/cr	13/cr	12/i	16/i	16/cr	17/i	17/cr	18/i
ht	315	358	369	462	462	478	478	494
SiO2	41.05	40.22	40.64	39.92	40.33	40.38	40.10	40.96
FeO	13.68	15.18	14.20	16.54	17.40	14.57	15.89	14.07
MgO	44.45	43.94	43.55	42.61	42.03	44.39	42.75	45.62
NiO	0.11	0.10	0.12	0.02	0.05	0.08	0.11	0.03
Total	99.29	99.44	98.51	99.09	99.81	99.42	98.85	100.68

	18/cr	24/i	25/i	25/cr	26/i	29/i	31/i	35/i
ht	494	494	859	875	886	919	994	1055
SiO2	40.75	38.73	40.16	40.10	39.33	39.41	39.47	39.40
FeO	13.37	24.67	16.21	16.14	20.20	19.46	18.99	21.47
MgO	45.85	36.46	43.07	42.95	40.41	41.10	40.46	39.37
NiO	0.03	0.04	0.04	0.06	0.08	0.07	0.06	0.09
Total	100.00	99.90	99.48	99.25	100.02	100.04	98.98	100.33

	37/i	37/cr	42/i	43/i
ht	1107	1107	1221	1238
SiO2	40.37	39.91	40.16	39.42
FeO	16.67	16.99	16.28	17.42
MgO	43.76	42.33	43.60	43.21
NiO	0.07	0.08	0.07	0.08
Total	100.89	99.30	100.11	100.13

-A19-

CENTRAL TRAVERSE

	62/i	63/i	64/i	73/i	73/cr	74/i	70/i	70/cr
ht	11	22	23	108	108	109	119	119
SiO2	40.16	40.94	41.20	40.60	40.75	39.57	40.31	40.67
FeO	16.40	15.87	13.20	14.34	14.12	14.76	13.74	14.40
MgO	43.84	42.87	45.46	45.25	44.60	44.49	45.56	45.14
NiO	0.11	0.06	0.11	0.10	0.13	0.12	0.10	0.10
Total	100.51	99.74	99.97	100.29	99.60	98.94	99.71	100.31
	126/i	126/cr	76/f	71/i	72/i	72/f	128/i	77/i
ht	127	127	130	133	141	141	147	152
SiO2	40.10	40.32	39.94	40.41	40.74	40.63	40.24	39.68
FeO	15.08	15.91	14.56	14.74	14.20	14.25	15.23	15.45
MgO	45.23	44.07	45.24	45.00	45.79	45.64	45.04	44.08
NiO	0.13	0.14	0.14	0.06	0.13	0.13	0.11	0.16
Total	100.54	100.44	99.88	100.21	100.86	100.65	100.62	99.37
	77/cr	80/i	79/cr	80/cr	81/o	81/cr	82/i	82/cr
ht	152	179	190	179	234	234	266	266
SiO2	39.88	41.18	40.25	41.48	40.29	39.91	39.81	40.11
FeO	14.99	13.64	12.88	13.45	17.07	17.43	16.06	16.23
MgO	43.00	45.30	46.65	44.87	43.11	41.62	44.25	42.55
NiO	0.14	0.13	0.13	0.14	0.06	0.10	0.06	0.05
Total	98.01	100.25	99.91	99.94	100.53	99.06	100.18	98.94
	83/cr	84/i	84/cr	85/cr	86/i	87/i	87/cr	88/i
ht	299	310	310	375	392	424	424	440
SiO2	40.01	40.29	40.35	39.54	40.20	39.16	40.37	40.30
FeO	16.39	15.17	15.38	18.22	17.36	17.65	16.57	18.52
MgO	43.45	44.39	44.01	41.20	42.28	42.86	41.37	41.90
NiO	0.02	0.06	0.08	0.06	0.10	0.05	0.08	0.01
Total	99.87	99.91	99.82	99.02	99.94	99.72	98.39	100.73
	88/cr	89/cr	90/i	90/cr	91/i	91/cr	92/cr	21/i
ht	440	478	489	489	500	500	532	671
SiO2	40.00	40.20	40.64	40.55	39.78	39.70	39.54	39.12
FeO	18.32	15.79	15.95	15.78	16.89	17.13	19.34	20.10
MgO	42.05	44.29	43.86	45.15	43.14	42.98	42.13	39.53
NiO	0.04	0.02	0.10	0.08	0.06	0.06	0.06	0.06
Total	100.41	100.30	100.55	101.56	99.87	99.87	101.07	98.81
	22/i	22/cr	23/i	94/i	95/i	95/cr	96/i	98/i
ht	679	679	820	820	831	831	842	918
SiO2	39.69	40.97	38.76	40.02	40.16	39.89	39.83	39.66
FeO	15.04	14.68	23.54	16.67	17.46	17.77	16.34	16.23
MgO	43.94	44.71	37.05	43.63	43.43	42.54	42.73	43.44
NiO	0.05	0.07	0.02	0.09	0.07	0.07	0.09	0.10
Total	98.72	100.43	99.37	100.41	101.12	100.27	98.99	99.43
	52/cr	51/i	51/cr	50/i	50/cr	49/cr	44/i	44/cr
ht	946	968	968	973	973	1033	1304	1304
SiO2	39.47	39.98	39.79	40.41	40.22	40.23	40.15	40.39
FeO	15.88	19.53	19.11	14.84	14.75	15.77	15.17	15.04
MgO	44.45	41.05	41.38	43.84	44.07	44.27	44.48	44.86
NiO	0.04	0.12	0.09	0.06	0.06	0.03	0.13	0.14
Total	99.84	100.68	100.37	99.15	99.10	100.30	99.93	100.43
	124/i	122/i	122/cr	123/i	123/cr			
ht	1429	1440	1440	1457	1457			
SiO2	39.73	40.50	40.38	40.10	40.32			
FeO	16.50	13.46	13.47	15.08	15.91			
MgO	43.22	46.38	46.16	45.22	44.07			
NiO	0.09	0.11	0.10	0.13	0.14			
Total	99.54	100.45	100.11	100.53	100.44			

-A20-

EASTERN TRAVERSE

	129/i	135/i	130/i	131/f	134/i	142/cr	141/i	141/cr	
ht	150	215	242	259	282	340	350	350	
SiO2	39.48	39.13	39.05	39.84	39.94	39.83	40.48	40.55	
FeO	17.45	18.83	20.68	16.96	16.99	19.14	16.60	12.34	
MgO	43.09	42.34	40.22	43.24	43.41	41.14	44.03	46.77	
NiO	0.17	0.17	0.14	0.07	0.09	0.12	0.15	0.16	
Total	100.25	100.47	100.09	100.11	100.43	100.23	101.26	99.82	
	143/i	143/cr	144/i	144/cr	140/i	140/cr	136/i	139/i	
ht	352	252	360	360	368	368	382	396	
SiO2	40.47	39.81	39.50	39.15	39.55	38.60	38.80	39.18	
FeO	14.81	18.07	19.95	22.28	18.03	21.23	22.64	19.66	
MgO	44.32	42.09	39.87	38.52	41.71	39.69	38.83	41.13	
NiO	0.10	0.11	0.06	0.05	0.06	0.09	0.06	0.06	
Total	99.70	100.08	99.38	100.00	99.35	99.61	100.33	100.03	
	139/cr	138/i	138/cr	137/i	101/cr	102/i	102/o	100/i	
ht	396	406	406	423	456	467	467	483	
SiO2	38.93	39.73	39.88	39.83	39.01	40.27	39.82	39.16	
FeO	20.14	14.92	15.27	16.91	20.77	17.60	18.20	20.40	
MgO	40.97	44.68	44.17	44.00	39.60	42.81	41.22	39.69	
NiO	0.09	0.10	0.09	0.03	0.02	0.10	0.09	0.09	
Total	100.13	99.43	99.41	100.77	99.40	100.78	99.33	99.34	
	103/cr	104/i	104/cr	105/i	105/cr	106/i	107/i	109/i	
ht	630	668	668	679	679	696	712	755	
SiO2	39.77	40.93	40.47	39.52	40.74	39.56	39.66	39.33	
FeO	21.06	15.95	17.01	17.58	18.91	23.09	16.22	18.45	
MgO	39.34	44.19	42.92	42.00	41.27	37.84	44.34	41.91	
NiO	0.03	0.07	0.07	0.08	0.06	0.06	0.06	0.08	
Total	100.20	101.14	100.47	99.18	100.98	100.55	100.28	99.77	
	110/i	110/cr	111/i	113/i	112/i	115/i	114/i	114/cr	
ht	766	766	793	798	808	883	875	875	
SiO2	41.10	41.07	40.32	40.67	40.79	40.17	40.57	40.35	
FeO	16.98	16.75	16.05	15.41	15.37	16.48	14.11	14.19	
MgO	42.90	43.37	43.48	44.27	43.46	43.79	45.51	44.88	
NiO	0.08	0.08	0.09	0.08	0.07	0.03	0.05	0.15	
Total	101.06	101.27	99.94	100.43	99.69	100.47	100.24	99.57	
	116/cr	118/i	118/cr	117/i	119/i	119/cr	120/i	121/i	121/c
Ht	896	929	929	956	967	967	1118	1145	1145
SiO2	40.35	40.19	40.75	40.60	39.98	40.55	39.33	39.98	40.02
FeO	15.77	15.77	15.21	14.38	15.08	14.79	19.70	15.05	14.95
MgO	43.84	44.75	44.63	45.72	44.04	45.86	40.89	44.28	45.39
NiO	0.07	0.07	0.11	0.06	0.06	0.09	0.09	0.11	0.06
Total	100.03	100.78	100.70	100.76	99.16	101.29	100.01	99.42	100.42

i=olivine chadocryts in pyroxene oikiocryts, cr=olivines in coronas, f=free olivines. TiO2, Al2O3, MnO, CaO, Cr2O3 were also determined but were to be present at less than the detection limits, see Table 1 for detection limits.

-A21-

TABLE 4b
ORTHOPYROXENE ANALYSES
WESTERN TRAVERSE

	4/o	3b/f	3b/o	2/f	1/o	54/o	53/f	55/cr
ht m	49	54	54	62	76	92	101	130
SiO2	56.19	55.38	55.92	55.60	55.94	55.88	56.43	56.87
TiO2	0.29	0.24	0.18	0.16	0.18	0.22	0.24	0.00
Al2O3	2.99	3.06	3.22	3.19	2.99	3.02	2.48	1.38
FeO	8.68	8.84	8.30	8.83	8.50	8.44	9.01	10.60
MnO	0.00	0.14	0.07	0.13	0.11	0.04	0.16	0.00
MgO	30.30	30.15	30.33	30.24	30.35	30.59	29.85	31.71
CaO	2.00	1.98	1.61	1.49	2.01	1.82	1.65	0.15
NiO	0.01	0.03	0.04	0.01	0.04	0.02	0.02	0.02
Cr2O3	0.79	0.79	0.71	0.57	0.73	0.78	0.48	0.00
Total	101.25	100.61	100.38	100.22	100.85	100.81	100.32	100.73
type	1	2	1	2	1	1	2	3

	5/o	56/f	56/o	6/f	tv 6/e	tv 6/e	tv 6/e
ht	135	141	141	143	143	143	143
SiO2	54.73	55.80	56.22	55.85	55.10	55.28	55.10
TiO2	0.21	0.31	0.10	0.23	0.39	0.15	0.29
Al2O3	2.52	2.64	2.48	2.93	2.67	2.74	3.07
FeO	9.48	8.89	10.40	8.84	9.40	9.79	9.35
MnO	0.20	0.17	0.00	0.00	0.14	0.20	0.19
MgO	30.25	30.17	30.31	30.63	32.33	31.78	31.70
CaO	1.20	1.77	0.45	1.23	0.64	0.71	0.68
NiO	0.02	0.01	0.03	0.02	0.00	0.00	0.00
Cr2O3	0.64	0.65	0.39	0.69	0.61	0.62	0.32
Total	99.25	100.41	100.38	100.42	101.32	101.27	100.70
type	1	2	1	1	6	6	6

	177/o	177/i	176/f	176/e
ht	175	175	180	180
SiO2	55.87	55.70	54.78	55.97
TiO2	0.33	0.30	0.43	0.09
Al2O3	2.90	2.95	2.63	2.75
FeO	9.61	8.74	8.63	9.41
MnO	0.29	0.21	0.19	0.22
MgO	30.94	30.10	29.55	30.36
CaO	0.72	1.13	2.56	0.84
NiO	0.02	0.01	0.01	0.02
Cr2O3	0.61	0.77	0.82	0.58
Total	101.29	99.91	99.60	100.24
type	1	2	2	6

	176/cr	8/f	8/cr	8/e	8/e	57/f	178/o	9/cr
ht	180	212	212	212	212	223	235	239
SiO2	57.66	55.81	57.18	55.40	56.17	55.34	56.38	57.45
TiO2	0.00	0.25	0.00	0.16	0.00	0.32	0.18	0.00
Al2O3	0.87	2.76	0.76	2.01	1.70	2.75	2.42	0.71
FeO	10.10	9.76	9.75	10.89	10.44	9.73	8.95	10.61
MnO	0.18	0.00	0.00	0.15	0.18	0.00	0.20	0.09
MgO	32.73	29.63	31.84	29.02	29.76	30.03	30.75	31.11
CaO	0.05	1.57	0.09	0.31	0.91	0.91	2.00	0.09
NiO	0.02	0.01	0.01	0.00	0.00	0.00	0.03	0.00
Cr2O3	0.00	0.41	0.00	0.21	0.16	0.34	0.38	0.00
Total	101.61	100.20	99.63	98.15	99.32	99.42	101.29	100.06
type	3	2	3	6	6	2	4	3

	59/i	61/i	188/o	188/f	188/cr	60/i	11/o	12/cr
ht	244	250	254	254	254	293	315	369
SiO2	55.32	54.02	54.65	55.35	57.08	55.47	55.94	55.30
TiO2	0.39	0.30	0.37	0.46	0.00	0.11	0.20	0.00
Al2O3	2.84	2.97	3.20	2.46	0.63	2.89	2.58	0.47
FeO	9.64	9.53	8.67	10.23	9.68	10.59	8.16	10.71
MnO	0.07	0.17	0.27	0.33	0.12	0.00	0.12	0.30
MgO	29.68	29.80	28.93	29.62	32.24	29.97	30.39	33.18
CaO	1.70	1.63	2.42	1.20	0.07	0.93	1.93	0.14
NiO	0.04	0.02	0.01	0.01	0.00	0.02	0.00	0.02
Cr2O3	0.56	0.61	0.63	0.51	0.00	0.33	0.43	0.02
Total	100.24	99.05	99.05	100.17	99.82	100.31	99.75	100.14
type	4	4	1	2	3	4	1	3

	16/i	25/i	29/o	29/m	31/m	35/m	37/o	37/m
ht	462	875	919	919	994	1055	1107	1107
SiO2	55.57	55.47	54.42	56.61	57.47	57.26	55.11	57.76
TiO2	0.42	0.54	0.28	0.00	0.03	0.00	0.45	0.08
Al2O3	2.54	2.24	2.32	0.29	0.13	0.12	1.63	0.59
FeO	9.95	10.96	11.58	11.96	11.56	12.52	10.18	10.86
MnO	0.09	0.19	0.26	0.00	0.05	0.13	0.00	0.10
MgO	28.96	28.40	28.64	29.61	30.72	30.02	30.55	31.66
CaO	1.60	1.53	1.54	0.15	0.12	0.14	1.14	0.41
NiO	0.00	0.01	0.01	0.00	0.01	0.02	0.02	0.00
Cr2O3	0.50	0.19	0.84	0.00	0.00	0.02	0.12	0.07
Total	99.63	99.53	99.89	98.62	100.09	100.23	99.20	101.53
type	4	4	1	5	5	5	1	5

CENTRAL TRAVERSE

	62/m	66/f	187/o	187/f	75/f	73/o	74/f	70/o
ht	11	38	45	45	95	108	109	119
SiO2	57.90	55.66	55.29	55.65	55.03	55.32	55.08	55.56
TiO2	0.06	0.16	0.30	0.23	0.44	0.26	0.19	0.30
Al2O3	0.12	2.75	2.50	2.59	2.62	2.48	2.50	2.95
FeO	10.05	9.87	8.77	8.55	8.88	9.32	9.57	8.29
MnO	0.06	0.12	0.22	0.19	0.09	0.09	0.09	0.04
MgO	31.21	29.20	28.72	30.58	30.44	30.00	29.99	30.39
CaO	0.10	1.23	1.86	1.51	2.03	1.59	1.50	1.62
NiO	0.00	0.02	0.02	0.01	0.01	0.03	0.02	0.00
Cr2O3	0.00	0.61	0.51	0.50	0.50	0.43	0.41	0.64
Total	99.56	99.69	98.19	99.81	100.06	99.60	99.38	99.89
type	5	2	1	2	2	1	2	1

	70/cr	76/o	Tv 76/e	Tv 76/e	Tv 76/e	71/f	tv 71/e	tv 71/e
ht	119	130	130	130	130	133	101	130
SiO2	58.19	54.58	55.02	54.42	55.06	55.25	55.76	56.02
TiO2	0.00	0.21	0.09	0.12	0.00	0.24	0.20	0.00
Al2O3	0.62	2.79	2.87	2.94	3.05	2.74	3.15	2.95
FeO	9.69	9.35	10.20	10.37	10.19	8.91	10.25	10.39
MnO	0.00	0.13	0.15	0.22	0.24	0.10	0.25	0.18
MgO	32.73	30.34	31.09	31.78	32.10	29.84	31.52	31.28
CaO	0.15	1.37	1.47	0.33	0.30	1.86	0.70	0.70
NiO	0.05	0.02	0.00	0.00	0.00	0.00	0.00	0.00
Cr2O3	0.00	0.58	0.56	0.47	0.46	0.51	0.40	0.32
Total	101.45	99.41	101.45	100.65	101.40	99.50	102.23	101.84
type	3	1	6	6	6	2	6	6

-A23-

	tv/71/e	127/f	72/o	128/f	77/f	77/f
ht	130	136	141	147	152	152
SiO2	56.02	54.87	55.21	54.31	56.28	54.69
TiO2	0.00	0.37	0.62	0.34	0.32	0.25
Al2O3	2.95	2.89	2.36	2.30	2.80	2.95
FeO	10.39	9.58	8.84	8.80	9.12	8.95
MnO	0.18	0.03	0.00	0.03	0.09	0.23
MgO	31.28	29.34	30.90	30.43	29.76	30.30
CaO	0.70	2.27	1.35	1.87	1.78	1.60
NiO	0.00	0.00	0.03	0.00	0.01	0.03
Cr2O3	0.32	0.59	0.48	0.50	0.57	0.65
Total	101.84	99.99	99.80	98.65	100.81	99.75
type	6	2	1	2	2	2

	78/i	78/f	80/o	79/o	79/f	81/f	81/o	82/f
ht	157	157	179	185	185	233	233	266
SiO2	55.06	55.16	54.30	54.97	55.13	55.28	55.47	54.98
TiO2	0.27	0.24	0.32	0.12	0.15	0.12	0.18	0.56
Al2O3	2.51	2.72	3.08	2.69	2.48	3.00	2.43	2.91
FeO	9.04	8.68	8.10	8.33	8.12	10.69	10.40	9.65
MnO	0.13	0.00	0.15	0.03	0.05	0.00	0.00	0.09
MgO	29.51	31.00	31.12	30.12	31.10	29.25	28.91	28.99
CaO	1.90	1.66	1.86	1.79	1.73	1.32	1.69	2.00
NiO	0.02	0.00	0.04	0.01	0.01	0.01	0.01	0.01
Cr2O3	0.45	0.48	0.74	0.48	0.47	0.41	0.28	0.55
Total	98.89	99.94	99.71	98.54	99.24	100.08	99.37	99.74
type	2	2	1	1	2	2	1	2

	181/f	181/o	181/i	181/cr	83/o	84/o	183/f	183/o
ht	270	270	270	270	298	304	319	319
SiO2	54.63	55.80	54.89	55.64	54.89	55.26	55.69	54.90
TiO2	0.23	0.24	0.19	0.00	0.21	0.28	0.19	0.26
Al2O3	3.00	1.87	2.83	0.63	2.33	2.42	2.41	2.24
FeO	10.93	11.54	11.55	12.10	10.87	9.23	10.05	11.32
MnO	0.26	0.26	0.26	0.21	0.10	0.06	0.21	0.24
MgO	27.40	28.82	28.70	28.60	28.03	30.14	28.74	28.15
CaO	3.29	1.27	1.20	0.10	2.64	1.82	2.06	1.40
NiO	0.01	0.01	0.01	0.01	0.00	0.02	0.01	0.01
Cr2O3	0.41	0.03	0.00	0.00	0.32	0.25	0.40	0.30
Total	100.16	99.84	99.63	97.29	99.39	99.48	99.76	98.82
type	2	1	2	3	1	1	2	2

	85/i	86/o	87/i	88/cr	90/o	91/i	92/i	21/m
ht	375	385	415	440	489	499	526	668
SiO2	55.06	55.80	54.71	56.31	55.99	54.68	55.86	57.07
TiO2	0.27	0.30	0.31	0.11	0.38	0.33	0.51	0.00
Al2O3	2.53	2.48	2.39	1.39	2.55	2.51	1.94	0.24
FeO	10.80	9.80	11.12	11.00	10.48	10.22	12.20	12.58
MnO	0.03	0.08	0.03	0.02	0.12	0.03	0.02	0.00
MgO	28.91	29.55	28.20	30.05	30.10	29.10	28.00	29.56
CaO	1.89	1.89	1.68	0.83	0.98	1.80	1.95	0.10
NiO	0.01	0.01	0.01	0.02	0.00	0.00	0.00	0.00
Cr2O3	0.43	0.58	0.40	0.05	0.45	0.50	0.22	0.01
Total	99.95	100.49	98.91	99.78	101.05	99.17	100.70	99.56
type	2	1	2	3	1	4	4	5

-A24-

	96/o	186/m	98/i	52/i	51/o	51/m	50/o	50/cr
ht	836	910	918	950	961	961	972	972
SiO2	55.23	57.61	55.21	56.00	55.28	56.87	55.61	56.55
TiO2	0.00	0.07	0.00	0.00	0.20	0.00	0.20	0.00
Al2O3	2.56	0.15	1.79	2.07	1.69	0.17	1.84	1.89
FeO	9.42	12.88	10.26	10.37	11.71	12.20	9.86	10.34
MnO	0.07	0.15	0.00	0.00	0.00	0.00	0.21	0.25
MgO	28.51	29.18	29.82	30.23	29.71	30.51	30.51	30.86
CaO	2.56	0.06	0.96	1.17	0.33	0.10	1.25	0.39
NiO	0.01	0.01	0.03	0.00	0.03	0.05	0.01	0.01
Cr2O3	0.62	0.02	0.21	0.33	0.31	0.01	0.00	0.30
Total	98.98	100.13	98.28	100.17	99.26	99.91	99.49	100.59
type	1	5	4	4	1	5	1	3

	50/e	49/cr	48/m	44/m	124/cr	43/cr
ht	92	1031	1042	1303	1433	1238
SiO2	55.50	57.81	57.61	57.55	57.88	57.96
TiO2	0.28	0.00	0.00	0.00	0.03	0.05
Al2O3	1.76	0.40	0.19	0.90	0.10	0.76
FeO	11.20	10.06	12.58	10.64	10.74	10.15
MnO	0.30	0.00	0.35	0.11	0.03	0.07
MgO	31.05	31.99	30.52	31.71	32.02	31.02
CaO	0.80	0.15	0.11	0.12	0.07	0.20
NiO	0.00	0.00	0.02	0.03	0.02	0.03
Cr2O3	0.25	0.00	0.02	0.02	0.00	0.03
Total	101.14	01.40	101.08	100.89	100.41	100.27
type	6	3	5	5	3	3

EASTERN TRAVERSE

	129/i	133/o	135/o	130/o	131/f	134/f	144/o	136/o
ht	150	162	215	242	259	282	360	382
SiO2	55.06	54.91	54.92	54.09	54.70	53.63	53.97	54.36
TiO2	0.13	0.00	0.16	0.07	0.25	0.30	0.38	0.22
Al2O3	2.72	2.52	0.04	2.45	2.71	2.84	2.00	2.59
FeO	9.26	12.16	10.10	12.22	9.37	10.91	16.80	10.72
MnO	0.02	0.02	0.12	0.03	0.02	0.01	0.18	0.03
MgO	30.25	28.16	30.84	29.03	29.70	29.86	24.66	28.61
CaO	1.49	1.00	0.36	1.02	1.78	1.42	0.98	1.86
NiO	0.04	0.00	0.00	0.00	0.00	0.00	0.01	0.00
Cr2O3	0.44	0.45	0.11	0.82	0.49	0.52	0.00	0.73
Total	99.41	99.22	96.65	99.73	99.02	99.49	98.98	99.12
type	2	1	1	1	2	2	1	1

	139/f	139/o	138/o	137/f	100/o	103/o	107/cr	109/m
ht	396	396	406	423	488	629	742	755
SiO2	54.42	54.48	54.26	54.95	55.03	55.92	56.57	56.64
TiO2	0.47	0.41	0.34	0.30	0.30	0.34	0.00	0.07
Al2O3	2.04	2.42	2.42	2.46	2.10	2.08	0.28	0.15
FeO	12.50	12.15	9.00	10.00	12.23	12.20	11.15	11.44
MnO	0.03	0.03	0.01	0.02	0.02	0.06	0.10	0.02
MgO	27.46	28.17	30.59	29.45	27.54	27.85	31.24	31.24
CaO	1.80	1.75	1.58	1.90	1.46	1.55	0.10	0.11
NiO	0.00	0.00	0.00	0.00	0.00	0.00	0.00	0.00
Cr2O3	0.24	0.40	0.36	0.38	0.17	0.10	0.01	0.00
Total	98.96	99.81	98.56	99.46	98.85	100.10	99.45	99.67
type	2	1	1	2	4	4	3	5

-A25-

	111/o	115/o	116/o	118/m	115/o	116/o	118/m
ht	783	867	916	939	867	916	939
SiO2	56.36	53.77	55.87	55.81	53.77	55.87	55.81
TiO2	0.19	0.44	0.13	0.34	0.44	0.13	0.34
Al2O3	1.32	1.98	1.96	2.46	1.98	1.96	2.46
FeO	10.02	10.47	10.37	9.93	10.47	10.37	9.93
MnO	0.06	0.13	0.10	0.18	0.13	0.10	0.18
MgO	30.51	30.16	31.23	30.74	30.16	31.23	30.74
CaO	1.06	1.94	0.62	0.00	1.94	0.62	0.00
NiO	0.01	0.01	0.00	0.05	0.01	0.00	0.05
Cr2O3	0.11	0.08	0.48	0.50	0.08	0.48	0.50
Total	99.64	98.98	100.76	100.01	98.98	100.76	100.01
type	1	4	4	5	4	4	5

o=oikocryts, f=cumulate opx, i=intercumulate opx, cr=opx developed in the coronas between olivine and plagioclase, m=metamorphic opx, e=opx near cpx exsolution. Na2O and K2O were also determined, but were below detection limit. See Table 1 for detection limits

STATISTICS FOR OPI

ELEM	AVE	STD DIV	N = 100
HT	494.95	419.886	
SIO2	55.807	1.16	
TIO2	.196	.156	
AL2O3	1.95	.996	
FEO	10.211	1.331	
MNO	.063	.06	
MGO	30.093	1.236	
CAO	1.15	.742	
NIO	.013	.013	
CR2O3	.337	.259	
TOTAL	99.843	.826	

	HT	SIO2	TIO2	AL2O3	FEO	MNO	MGO	CAO
HT	0	.547	-.399	-.681	.414	-.021	.302	-.591
SIO2	0	1	-.645	-.746	.072	-.102	.641	-.725
TIO2	0	-.645	.999	.614	-.137	.186	-.501	.671
AL2O3	0	-.746	.614	.999	-.445	.131	-.47	.834
FEO	0	.072	-.137	-.445	1	-.09	-.459	-.398
MNO	0	-.102	.186	.131	-.09	.999	-.083	.129
MGO	0	.641	-.501	-.47	-.459	-.083	1	-.552
CAO	0	-.725	.671	.834	-.398	.129	-.552	.999
NIO	0	.232	-.159	-.028	-.199	.176	.341	-.221
CR2O3	0	-.62	.468	.862	-.525	.227	-.29	.738
TOTAL	0	.609	-.18	-.112	-.077	.05	.413	-.209

	NIO	CR2O3	TOTAL
HT	.118	-.613	.268
SIO2	.232	-.62	.609
TIO2	-.159	.468	-.18
AL2O3	-.028	.862	-.112
FEO	-.199	-.525	-.077
MNO	.176	.227	.05
MGO	.341	-.29	.413
CAO	-.221	.738	-.209
NIO	.999	-8E-03	.287
CR2O3	-8E-03	.999	-.023
TOTAL	.287	-.023	1

TABLE 5b
CLINOPYROXENE ANALYSES
WESTERN TRAVERSE

	4/o	1/o	56/o	Tv 6/e	Tv 6/e	Tv 6/e	177/1/oe	177/1oc
ht	49	76	141				175	175
SiO2	51.37	47.09	52.45	51.70	51.17	52.09	52.59	52.71
TiO2	1.32	4.86	0.52	0.67	0.88	0.63	0.61	0.67
Al2O3	4.48	3.67	4.11	3.83	4.75	4.55	3.92	4.06
FeO	4.41	6.09	3.92	2.25	2.90	2.38	4.08	3.79
MnO	0.32	0.13	0.13	0.08	0.11	0.04	0.15	0.12
MgO	16.66	17.30	16.90	16.13	16.33	16.13	18.19	17.56
CaO	19.52	18.70	19.83	23.78	22.26	22.66	19.70	18.90
Na2O	0.56	0.58	0.59	0.76	0.68	0.76	0.38	0.52
Cr2O3	1.10	0.80	1.07	1.06	1.10	1.01	1.16	1.13
Total	99.74	99.22	99.52	100.26	100.18	100.25	100.08	99.46
type	1	4	1	3	3	3	1	1

	177/2oe	177/2oc	177/4oe	177/o	176/o	176/o	176/o	tv 8/e
ht	175	175	175	175	180	180	180	212
SiO2	52.66	53.00	52.32	52.78	51.56	53.64	52.75	53.20
TiO2	0.49	0.55	0.55	0.63	0.59	0.68	0.57	0.41
Al2O3	4.00	3.96	3.94	4.12	3.91	4.19	3.92	3.26
FeO	4.59	4.45	3.51	4.34	3.95	3.40	4.52	2.95
MnO	0.18	0.14	0.12	0.18	0.17	0.13	0.13	0.04
MgO	17.71	18.04	16.34	18.10	16.39	16.80	17.67	15.67
CaO	16.95	17.52	20.60	18.70	20.57	19.23	18.07	21.81
Na2O	0.43	0.34	0.48	0.44	0.45	0.32	0.44	0.64
Cr2O3	1.08	1.03	1.14	1.09	1.08	1.16	1.13	0.46
Total	98.09	99.03	99.00	100.38	98.67	99.55	99.20	98.44
type	1	1	1	1	1	1	1	3

	8/e	61/i	61/i	60/i	11/o	13/i	12/e	12/i e
ht	212	254	254	293	315	358	369	369
SiO2	53.48	51.54	51.64	52.63	52.06	52.86	52.55	51.84
TiO2	0.57	0.93	0.95	0.50	0.51	0.48	0.71	0.94
Al2O3	3.33	4.13	3.93	3.66	3.73	3.65	4.09	4.11
FeO	2.84	3.92	3.91	5.02	4.20	4.88	3.48	3.21
MnO	0.00	0.20	0.10	0.14	0.15	0.14	0.19	0.14
MgO	15.28	15.15	15.76	17.87	17.01	17.64	15.75	16.14
CaO	23.13	20.00	19.80	18.66	20.04	18.93	21.79	21.08
Na2O	0.59	0.58	0.45	0.34	0.45	0.42	0.59	0.50
Cr2O3	0.65	0.83	0.83	0.73	0.73	2.00	1.20	0.50
Total	99.87	97.28	97.37	99.55	98.88	101.00	100.35	98.46
type	3	2	2	2	1	2	3	2

	12/i	16/i	17/e	18/i	25/i	42/i	43/i
ht	369	462	478	494	875	1221	1238
SiO2	52.37	51.97	52.15	51.67	52.76	52.95	52.20
TiO2	0.48	0.62	0.68	0.74	0.95	0.39	0.59
Al2O3	4.03	4.00	3.93	3.81	3.11	3.45	4.38
FeO	4.03	4.75	3.63	3.66	5.24	4.32	4.14
MnO	0.22	0.28	0.13	0.10	0.21	0.15	0.22
MgO	17.62	15.93	15.67	15.91	17.16	17.58	16.27
CaO	19.70	20.49	22.14	20.32	18.68	19.88	19.33
Na2O	0.50	0.46	0.43	0.65	0.52	0.42	0.64
Cr2O3	1.17	1.10	1.23	0.85	0.49	0.94	1.14
Total	100.12	99.60	99.99	97.71	99.12	100.08	98.91
type	2	2	3	2	2	2	2

STATISTICS FOR CPX

ELEM	AVE	STD DIV	N = 76
HT	505.868	371.635	
SIO2	52.263	.609	
TIO2	.644	.178	
AL2O3	3.769	.422	
FEO	4.449	.518	
MNO	.128	.074	
MGO	17.197	.628	
CAO	19.626	.831	
NA2O	.434	.102	
CR2O3	.88	.33	
TOTAL	99.384	.806	
TYPE	1.513	.503	

	HT	SIO2	TIO2	AL2O3	FEO	MNO	MGO	CAO
HT	0	.091	-.193	-.116	.077	-8E-03	.05	.058
SIO2	0	1	-.397	-.406	.201	.052	.331	-.256
TIO2	0	-.397	.999	.241	-.101	.116	-.381	.067
AL2O3	0	-.406	.241	1	-.349	.253	-.282	-.075
FEO	0	.201	-.101	-.349	1	-.324	.347	-.464
MNO	0	.052	.116	.253	-.324	1	-6E-03	.055
MGO	0	.331	-.381	-.282	.347	-6E-03	1	-.515
CAO	0	-.256	.067	-.075	-.464	.055	-.515	1
NA2O	0	-.293	.363	.329	-.376	.218	-.357	.112
CR2O3	0	-.147	.069	.483	-.284	.355	8E-03	-.151
TOTAL	0	.481	-.156	.01	.198	.306	.431	.071
TYPE	0	.226	-.148	-.116	.161	-.164	-.215	.16

	NA2O	CR2O3	TOTAL	TYPE
HT	-.03	.025	.132	.369
SIO2	-.293	-.147	.481	.226
TIO2	.363	.069	-.156	-.148
AL2O3	.329	.483	.01	-.116
FEO	-.376	-.284	.198	.161
MNO	.218	.355	.306	-.164
MGO	-.357	8E-03	.431	-.215
CAO	.112	-.151	.071	.16
NA2O	1	.291	-.1	-.025
CR2O3	.291	.999	.296	-.254
TOTAL	-.1	.296	.999	.071
TYPE	-.025	-.254	.071	1

CENTRAL TRAVERSE

	64/o	75/o	74/i	127/i	72/o	128/o	77/o	78/e
ht	23	95	109	136	141	147	152	157
SiO2	51.22	52.48	51.74	52.14	52.45	51.72	51.52	51.60
TiO2	0.73	0.49	0.62	0.85	0.72	0.82	0.88	0.83
Al2O3	4.03	2.11	3.86	3.99	4.18	4.04	3.90	4.48
FeO	3.60	4.51	3.86	4.52	4.35	4.73	4.77	3.01
MnO	0.16	0.13	0.10	0.01	0.20	0.03	0.14	0.00
MgO	17.80	18.21	17.19	17.23	17.44	17.06	17.34	15.88
CaO	19.95	19.59	20.37	19.34	19.44	19.66	19.62	21.79
Na20	0.60	0.40	0.37	0.36	0.58	0.59	0.50	0.56
Cr2O3	1.25	0.60	0.74	0.63	1.24	1.02	0.56	0.90
Total	99.34	98.52	98.85	99.07	100.60	99.67	99.23	99.05
type	1	1	2	2	1	1	1	3

	Tv 71/e	Tv 71/e	Tv 76/e	Tv 76/e	Tv 76/e	Tv 76/e	Tv 76/e	Tv 50/e
ht	1	1	1	1	1	1	1	1
SiO2	50.84	50.96	52.45	51.69	50.78	51.15	51.17	52.34
TiO2	0.93	0.85	0.53	0.45	0.66	0.81	0.70	0.76
Al2O3	5.02	5.38	4.19	3.88	4.73	5.61	5.71	3.00
FeO	3.59	3.74	3.12	2.76	3.12	2.31	2.32	3.07
MnO	0.14	0.10	0.10	0.01	0.12	0.10	0.03	0.12
MgO	15.31	15.12	16.30	15.88	15.94	15.46	15.35	16.55
CaO	21.81	22.06	22.47	23.02	22.07	22.81	22.56	23.21
Na20	0.70	0.85	0.84	0.97	0.84	1.10	1.02	0.47
Cr2O3	0.79	0.76	1.05	0.97	1.20	1.26	1.19	0.55
Total	99.13	99.82	101.05	99.63	99.46	100.61	100.05	100.07
type	3	3	3	3	3	3	3	3

	78/o	79/o	83/i	83/i	84/i	85/i	85/i	87/o
ht	157	185	298	298	304	375	375	415
SiO2	51.72	51.75	52.73	53.09	52.46	52.45	52.78	52.15
TiO2	0.91	0.66	0.55	0.47	0.61	0.70	0.62	0.87
Al2O3	3.72	3.96	3.35	3.29	3.39	3.77	3.59	3.46
FeO	4.51	4.28	4.43	4.98	4.48	5.23	5.30	4.78
MnO	0.15	0.17	0.13	0.21	0.16	0.03	0.03	0.02
MgO	17.36	17.15	16.57	17.66	17.70	16.69	17.08	16.28
CaO	19.80	19.93	21.26	19.50	20.20	19.26	19.16	19.84
Na20	0.48	0.55	0.32	0.35	0.56	0.24	0.55	0.32
Cr2O3	0.78	0.80	0.46	0.46	0.48	0.65	0.66	0.65
Total	99.43	99.25	99.80	100.01	100.04	99.02	99.77	98.37
type	1	1	2	2	2	2	2	1

	88/i	89/i	90/o	91/e	92/e	22/o	94/o	95/i
ht	440	478	498	499	529	673	823	831
SiO2	52.75	52.55	51.33	51.23	53.18	52.60	51.48	52.68
TiO2	0.64	0.61	1.00	1.20	0.68	0.70	0.71	0.64
Al2O3	3.09	3.90	4.08	4.20	2.76	3.55	3.83	3.87
FeO	5.32	5.04	4.12	4.36	4.32	4.66	4.64	5.07
MnO	0.02	0.01	0.28	0.01	0.03	0.10	0.01	0.03
MgO	17.30	17.38	17.23	15.40	16.33	17.76	16.71	17.27
CaO	19.34	18.66	19.14	21.40	21.82	19.32	19.66	18.95
Na20	0.31	0.48	0.52	0.40	0.48	0.39	0.47	0.59
Cr2O3	0.72	0.80	1.29	0.90	0.25	0.23	1.22	0.74
Total	99.49	99.43	98.99	99.10	99.85	99.31	98.73	99.84
type	2	2	1	3	3	1	1	2

-A28-

	98/i	50/e	50/i	Tv 50/e	49/i	44/i	122/o	123/i
ht	918	972	972	972	1031	1303	1430	1455
SiO2	52.00	52.09	52.01	52.34	53.51	52.68	51.54	52.62
TiO2	0.36	0.30	0.32	0.76	0.53	0.55	0.75	0.59
Al2O3	3.74	3.57	3.15	3.00	2.98	3.82	4.17	4.09
FeO	4.38	3.55	4.41	3.07	4.86	4.10	4.21	4.17
MnO	0.00	0.00	0.00	0.12	0.10	0.20	0.25	0.10
MgO	16.40	15.54	17.36	16.55	18.06	17.32	17.19	17.23
CaO	20.39	22.36	20.36	23.21	18.89	20.07	19.42	19.51
Na2O	0.49	0.28	0.30	0.47	0.26	0.48	0.45	0.45
Cr2O3	0.87	0.69	0.56	0.55	0.13	1.16	1.14	0.84
Total	98.63	98.38	98.47	100.07	99.32	100.38	99.12	99.60
type	2	3	2	3	3	1	2	1

	181/i	183/i	187/o
ht	270	319	45
SiO2	53.53	52.75	52.53
TiO2	0.49	0.59	0.71
Al2O3	3.47	3.84	3.57
FeO	5.68	4.03	3.77
MnO	0.14	0.16	0.11
MgO	17.24	16.39	16.98
CaO	19.30	21.32	19.68
Na2O	0.31	0.50	0.50
Cr2O3	0.61	0.69	0.80
Total	100.77	100.27	98.62
type	2	2	1

EASTERN TRAVERSE

	129/o	131/o	142/o	141/o	143/i	144/i	140/o	101/e
ht	150	259	240	350	352	360	368	461
SiO2	51.38	51.22	52.90	51.98	52.39	51.31	52.18	51.67
TiO2	0.65	0.77	0.38	0.87	0.39	0.62	0.55	0.59
Al2O3	3.80	3.67	3.21	4.15	3.98	5.29	3.47	3.64
FeO	5.40	4.93	4.24	4.28	4.56	4.35	5.46	4.15
MnO	0.01	0.02	0.20	0.12	0.13	0.17	0.02	0.03
MgO	17.27	17.32	17.85	17.12	17.70	16.98	17.97	15.54
CaO	19.30	19.40	19.33	20.64	19.61	19.67	17.97	21.32
Na2O	0.34	0.27	0.27	0.41	0.38	0.30	0.40	0.58
Cr2O3	0.55	0.80	0.79	0.99	0.92	1.23	0.65	0.75
Total	98.70	98.40	99.17	100.56	100.06	99.92	98.67	98.27
type	1	1	1	1	2	2	1	3

	102/o	103/i	103/e	104/o	105/o	107/i	110/e	111/o
ht	472	629	629	706	718	742	766	783
SiO2	51.93	52.73	53.15	51.35	53.22	51.20	52.81	51.85
TiO2	0.80	0.48	0.60	0.45	0.52	0.85	1.29	0.41
Al2O3	3.70	3.54	3.46	3.60	3.15	3.95	3.57	3.83
FeO	4.78	4.49	4.14	4.28	5.47	4.58	4.00	4.06
MnO	0.12	0.11	0.10	0.12	0.12	0.05	0.10	0.25
MgO	16.93	16.37	15.92	18.00	18.14	16.74	15.76	17.37
CaO	20.32	20.79	22.54	20.30	19.14	20.02	21.66	21.31
Na2O	0.50	0.39	0.49	0.38	0.13	0.47	0.52	0.28
Cr2O3	1.10	0.31	0.37	0.89	0.68	1.08	0.87	1.10
Total	100.18	99.21	100.77	99.37	100.57	98.94	100.58	100.46
type	1	2	3	1	1	2	3	1

-A29-

	113/o	115/i	114/o	116/i	116/i	116/i	118/i	117/o
ht	788	867	885	916	916	916	938	938
SiO2	52.22	52.47	51.81	51.12	52.04	53.03	52.97	52.10
TiO2	0.62	0.60	0.63	0.45	0.87	0.79	0.54	0.56
Al2O3	3.95	3.09	3.79	4.26	3.02	3.42	3.79	4.06
FeO	4.35	4.98	4.13	5.05	3.91	4.20	4.36	3.99
MnO	0.24	0.10	0.19	0.00	0.00	0.17	0.16	0.12
MgO	17.29	17.37	17.12	18.04	16.75	17.51	17.82	17.14
CaO	19.38	20.04	19.44	18.23	21.21	20.79	19.35	19.91
Na2O	0.51	0.38	0.44	0.38	0.47	0.45	0.35	0.50
Cr2O3	1.30	0.14	1.20	0.50	0.80	0.66	0.90	1.22
Total	99.86	99.17	98.75	98.03	99.07	101.02	100.24	99.60
type	1	2	1	2	2	2	2	1

	119/i	121/i
ht	975	1200
SiO2	52.59	52.74
TiO2	0.42	0.83
Al2O3	3.78	3.62
FeO	4.15	5.12
MnO	0.15	0.16
MgO	17.28	17.95
CaO	19.62	18.40
Na2O	0.44	0.45
Cr2O3	1.00	1.85
Total	99.43	101.12
type	2	2

o=oikocryts, i=intercumulate, e=exsolution of cpx in opx. K2O and NiO were also determined, but were below detection limit. See Table 1 for detection limits

TABLE 6a STATISTICS FOR PLAGIOCLASE

Element	Average	o	*n=136
SiO2	50.64	1.18	
Al2O3	31.61	8.96	
CaO	14.46	0.96	
Na2O	3.21	0.92	

Correlation matrix r99=0.25

	SiO2	Al2O3	CaO	Na2O
SiO2	1			
Al2O3	-.704	1		
CaO	-.823	.770	1	
Na2O	.848	-.773	-.832	1

Comparison of analyses of the centres of plagioclase enclosed in pyroxene with free plagioclase grains in the same rock

Type	Anorthite	o	n
pyroxene	71.39	3.64	12
free	71.78	1.59	12

t= 0.21 therefore the two types of plagioclases are not significantly different.

TABLE 6b
PLAGIOCLASE ANALYSES
WESTERN TRAVERSE

	3/o	2/f	1/o	54/c	54/o	53/f	55/o	56/o
ht	54	62	76	92	92	101	130	141
SiO2	52.06	49.52	49.62	50.65	50.47	50.41	50.71	51.66
Al2O3	31.21	32.09	32.61	31.52	32.70	31.98	32.46	31.17
CaO	13.40	15.59	15.69	14.16	14.94	14.82	14.85	13.57
Na2O	3.60	2.70	2.64	3.33	2.94	3.15	3.05	3.81
Total	100.27	99.90	100.56	99.66	101.05	100.36	101.07	100.21
type	1	2	1	3	1	2	1	1

	6/o	177/o	177/f	176/o	8/f	178/c	178/f	57/c
ht	143	175	175	180	221	217	217	223
SiO2	49.96	52.26	50.90	52.24	50.71	50.55	50.00	49.08
Al2O3	32.14	30.78	31.55	29.11	30.11	31.04	30.40	32.75
CaO	15.10	12.48	13.47	12.83	15.08	14.13	14.09	15.84
Na2O	3.81	3.54	3.09	4.04	3.03	3.04	3.12	2.33
Total	101.01	99.06	99.01	98.22	100.93	98.76	97.61	100.00
type	1	1	2	1	2	3	2	3

	57/f	9/f	59/c	59/f	61/f	188/f	188/c	60/c
ht	223	237	244	244	250	254	254	293
SiO2	50.33	49.14	50.35	49.48	49.97	49.58	49.92	50.61
Al2O3	32.46	32.36	32.62	32.84	32.60	32.31	32.06	32.07
CaO	15.33	15.61	15.07	15.65	15.50	14.05	15.26	14.45
Na2O	2.90	2.68	2.80	2.64	2.49	2.55	2.62	3.30
Total	101.02	99.79	100.84	100.61	100.56	98.49	99.86	100.43
type	2	2	3	2	2	2	3	3

	60/f	11/f	13/c	13/f	12/o	16/c	16/f	17/f
ht	293	315	358	358	369	462	462	478
SiO2	49.96	50.45	50.85	50.77	49.46	51.06	50.21	49.79
Al2O3	32.59	31.66	32.04	32.18	32.73	32.40	32.67	32.83
CaO	14.77	14.81	14.80	15.00	15.93	14.75	15.51	15.39
Na2O	2.95	2.99	3.18	3.39	2.83	3.12	2.69	2.82
Total	100.27	99.91	100.87	101.34	100.95	101.33	101.08	100.83
type	2	2	3	2	1	3	2	2

	18/c	18/f	25/c	42/c	43/c
ht	494	494	875	1221	1238
SiO2	51.27	49.92	50.99	50.05	51.45
Al2O3	31.69	31.58	31.65	32.47	31.60
CaO	14.59	15.58	14.56	15.35	13.87
Na2O	3.34	2.88	3.16	2.76	3.35
Total	100.89	99.96	100.36	100.63	100.27
type	3	2	3	3	3

CENTRAL TRAVERSE

	187/o	75/o	73/f	74/f	70/o	127/f	76/o	71/c
ht	45	95	108	109	119	126	130	133
SiO2	50.36	50.48	51.14	51.02	50.43	49.02	51.82	48.66
Al2O3	29.89	31.04	30.73	31.19	32.24	32.72	29.88	31.84
CaO	14.24	14.55	14.35	14.25	14.85	15.59	13.05	14.83
Na2O	3.40	3.41	3.57	3.46	2.96	2.48	4.02	2.63
Total	97.89	99.48	99.79	99.92	100.48	99.81	98.77	97.96
type	1	1	2	2	1	2	1	3

-32-

	72/o	128/o	77/o	78/c	78/f	80/o	79/o	81/c
ht	141	147	152	157	157	179	185	233
SiO2	53.46	49.82	51.82	52.66	50.15	51.81	50.77	50.04
Al2O3	28.91	31.67	30.20	30.69	32.10	32.02	31.41	32.78
CaO	11.27	13.59	13.05	12.86	14.70	14.74	14.16	15.56
Na2O	4.68	3.41	4.12	4.31	3.38	3.36	3.54	2.68
Total	98.32	98.49	99.19	100.52	100.33	101.93	99.88	101.06
type	1	1	1	3	2	1	1	3

	81/f	82/f	181/f	83/c	83/f	84/c	183/f	183/i
ht	233	266	270	298	298	304	319	319
SiO2	50.72	49.36	50.74	50.40	50.50	49.97	51.42	50.87
Al2O3	32.32	32.75	29.68	32.01	32.46	32.25	30.82	30.43
CaO	14.13	15.82	14.44	15.14	14.91	15.05	14.04	13.90
Na2O	2.89	2.63	3.35	3.10	2.95	3.07	3.26	3.14
Total	100.06	100.56	98.21	100.65	100.82	100.34	99.54	98.34
type	2	2	2	3	2	3	2	3

	85/c	85/f	87/o	88/i	88/f	89/c	89/f	90/
ht	375	375	415	440	440	478	478	489
SiO2	50.21	50.37	51.82	49.83	49.80	51.14	50.88	50.86
Al2O3	32.01	31.98	30.68	32.43	32.50	32.46	32.59	32.06
CaO	15.03	14.28	13.39	15.09	15.26	14.38	14.80	14.81
Na2O	2.98	3.15	3.95	2.89	2.92	3.13	3.10	3.12
Total	100.23	99.78	99.84	100.24	100.48	101.11	101.37	100.85
type	3	2	1	3	2	3	2	2

	91/c	91/f	92/c	22/i	22/f	94/o	95/c	95/f
ht	499	499	526	673	673	819	823	831
SiO2	49.93	50.40	50.31	50.61	51.08	50.98	51.21	51.19
Al2O3	32.09	31.99	32.40	31.82	31.48	31.55	31.98	31.48
CaO	14.92	14.38	15.00	14.69	14.24	13.90	14.23	14.03
Na2O	3.02	3.32	3.08	3.42	3.08	3.59	3.53	3.72
Total	99.96	100.09	100.79	100.54	99.88	100.02	100.95	100.42
type	3	2	3	3	2	3	3	2

	96/c	98/c	52/c	50/i	50/f	49/f	44/c	44/f
ht	836	918	950	972	972	1041	1303	1303
SiO2	50.05	50.61	49.40	50.34	50.41	50.31	50.51	51.28
Al2O3	32.01	31.59	31.86	30.76	31.84	31.88	32.19	31.97
CaO	14.59	14.21	14.54	13.36	14.38	14.81	14.86	14.28
Na2O	3.11	3.24	2.98	3.72	3.17	3.23	2.96	3.28
Total	99.76	99.65	98.78	98.18	99.80	100.23	100.52	100.81
type	3	2	3	3	2	2	3	2

	124/c	124/f	122/o	123/f	123/c
ht	1433	1433	1438	1455	1455
SiO2	49.74	50.93	51.73	49.80	50.06
Al2O3	32.24	31.97	30.61	31.61	31.77
CaO	14.90	14.38	13.22	14.86	14.68
Na2O	3.08	3.35	4.17	3.23	2.72
Total	99.96	100.63	99.73	99.50	99.23
type	3	2	1	2	3

EASTERN TRAVERSE

	129/o	133/f	131/o	134/c	134/f	142/c	142/f	141/o
ht	150	162	259	282	282	340	340	350
SiO2	49.41	50.46	50.05	50.14	49.89	50.28	58.35	51.74
Al2O3	31.59	32.12	31.45	31.12	31.84	31.99	26.90	31.45
CaO	14.66	14.56	14.76	14.23	15.36	15.12	8.66	14.29
Na2O	2.90	2.82	2.87	3.75	2.64	3.20	6.61	3.29
Total	98.56	99.96	99.13	99.24	99.73	100.59	100.52	100.77
type	1	2	1	3	2	3	2	1

-33-

	141/c	143/c	143/f	144/c	144/f	140/c	140/f	139/c
ht	350	352	352	360	360	368	368	396
SiO2	52.12	51.91	51.78	51.10	52.33	50.44	50.58	49.21
Al2O3	30.37	30.91	30.64	31.72	30.81	31.27	31.11	31.56
CaO	14.21	13.70	13.66	14.26	13.31	13.85	13.65	14.50
Na2O	3.87	3.77	4.04	3.32	3.93	3.26	3.26	2.62
Total	100.57	100.29	100.12	100.38	100.40	98.82	98.60	97.89
type	3	3	2	3	2	3	2	3
	139/f	138/c	138/f	137/f	101/f	102/c	102/f	103/c
ht	396	406	406	423	461	472	472	630
SiO2	49.66	52.12	48.99	49.28	49.57	51.86	52.99	52.81
Al2O3	31.69	30.12	31.42	32.10	31.75	30.47	30.49	29.94
CaO	14.53	12.57	14.54	15.03	14.50	14.58	13.41	13.35
Na2O	2.57	4.15	2.70	2.55	2.80	3.37	3.99	4.06
Total	98.45	98.96	97.65	98.96	98.62	100.28	100.88	100.16
type	2	2	3	2	2	3	2	3
	103/c	104/c	104/f	105/f	107/f	110/c	110/f	113/c
ht	630	706	706	718	742	766	766	788
SiO2	50.67	51.53	52.48	51.43	50.04	50.36	53.96	50.08
Al2O3	31.70	31.58	30.71	31.21	31.20	30.69	31.60	31.62
CaO	15.76	14.82	14.49	14.94	14.30	14.99	11.04	14.71
Na2O	2.47	3.30	3.41	3.28	3.22	2.89	3.26	3.23
Total	100.60	101.23	101.09	100.86	98.76	98.93	99.86	99.64
type	3	3	2	2	2	3	2	3
	113/f	115/c	114/c	114/f	116/c	116/f	118/c	118/f
ht	788	867	885	885	916	916	939	939
SiO2	51.72	50.73	49.84	49.96	50.66	50.13	50.00	50.58
Al2O3	31.06	31.17	31.81	32.30	32.42	31.29	32.32	31.63
CaO	14.31	14.35	14.66	15.09	14.82	14.66	15.06	14.55
Na2O	3.28	3.42	3.04	2.78	3.39	2.82	2.94	3.38
Total	100.37	99.67	99.35	100.13	101.29	98.90	100.32	100.14
type	2	3	3	2	3	2	3	2
	117/c	117/f	119/c	119/f	121/c	121/f		
ht	966	966	975	975	1200	1200		
SiO2	48.63	49.14	50.83	48.65	50.11	49.50		
Al2O3	32.27	32.28	32.07	32.58	32.15	31.29		
CaO	15.62	15.43	14.84	14.97	14.83	14.75		
Na2O	2.54	2.57	3.10	2.96	3.04	2.73		
Total	99.06	99.42	100.84	99.16	98.27	100.13		
type	3	2	3	2	3	2		

o=plagioclase oikiocryst, c=plagioclase chadocryst enclosed in pyroxene oikicryts, f=free or cumulate plagioclase grain. TiO2, FeO, MnO, MgO, K2O, Cr2O3 and NiO were also determined but were present at < detection level, see Table 1 for detection levels.

TABLE 7
CHROMITES

	tv 4	tv 1	tv 54	tv 55	tv 9	tv 64	tv 70	tv 90
ht	49	76	92	120	237	23	119	489
TiO2	5.99	0.33	0.63	0.83	0.51	0.80	0.09	0.73
Al2O3	30.40	29.44	26.86	25.32	31.23	29.94	38.41	30.05
Cr2O3	32.44	33.98	37.53	36.39	34.17	36.59	29.61	35.67
FeO	21.19	25.32	24.32	26.29	24.45	21.08	19.33	23.62
MnO	3.26	3.48	3.92	3.63	3.44	3.82	2.90	3.68
MgO	8.49	8.30	7.31	6.94	6.45	9.38	11.02	7.39
Total	101.77	100.85	100.57	99.40	100.25	101.61	101.36	101.14

	tv 94	tv 44	tv 141	tv 113	tv 114	tv 117	tv 114	tv 117
ht	823	1303	350	788	885	966	885	966
TiO2	1.44	1.48	0.40	0.16	0.28	0.40	0.28	0.40
Al2O3	28.96	23.31	38.95	32.12	28.48	31.79	28.48	31.79
Cr2O3	35.69	40.12	30.02	34.43	37.65	35.44	37.65	35.44
FeO	23.24	26.11	18.83	21.00	21.08	18.70	21.08	18.70
MnO	3.40	4.13	2.94	3.44	4.02	3.60	4.02	3.60
MgO	8.54	5.77	11.96	8.30	8.52	10.55	8.52	10.55
Total	101.27	100.92	103.10	99.45	100.03	100.48	100.03	100.48

Table 8:Amphiboles

	Tv 5	Tv 6	Tv 23	Tv 24	Tv 26	Tv 35	Tv 57	Tv 62
SiO2	56.60	53.36	55.09	54.71	56.28	57.87	53.05	58.02
TiO2	0.08	0.41	0.11	0.05	0.08	0.07	0.76	0.10
Al2O3	1.44	4.69	2.97	2.76	2.26	0.84	2.98	0.76
FeO	3.08	4.11	4.61	4.82	3.96	4.04	4.85	2.94
MnO	0.00	0.00	0.00	0.11	0.14	0.00	0.00	0.13
MgO	23.33	21.51	21.71	21.05	22.24	21.76	21.34	22.86
CaO	12.41	10.18	12.36	12.14	12.23	12.48	12.03	12.58
Na2O	0.50	0.47	0.63	0.73	0.54	0.06	0.38	0.27
Cr2O3	0.08	0.66	0.13	0.04	0.18	0.07	0.35	0.00
Total	97.52	95.39	97.61	96.41	97.91	97.19	95.74	97.66

	Tv 63	Tv 66	Tv 120	Tv 127	Tv 186	Tv 2	Tv 66	Tv 78
SiO2	57.23	53.86	57.83	54.40	57.20	56.36	56.94	58.95
TiO2	0.00	0.60	0.00	0.35	0.16	0.20	0.03	0.00
Al2O3	0.87	4.68	0.48	3.97	1.51	3.18	0.63	2.33
FeO	3.03	3.80	3.44	3.18	4.14	7.27	9.60	9.26
MnO	0.13	0.10	0.00	0.02	0.12	0.15	0.14	0.24
MgO	23.88	21.21	22.88	21.36	22.87	24.38	26.89	26.44
CaO	11.65	11.63	12.32	12.83	11.12	4.47	0.52	0.55
Na2O	0.23	0.91	0.05	0.33	0.39	0.33	0.50	0.04
Cr2O3	0.12	0.68	0.01	0.66	0.06	0.75	0.80	0.27
Total	97.14	97.47	97.01	97.10	97.57	97.09	96.05	98.08

	Tv 133	Tv 48	Tv 53	Tv 57	Tv 101	Tv 134	Tv 8	Tv 138
SiO2	55.28	58.73	45.17	53.24	48.87	44.32	43.91	42.35
TiO2	0.11	0.00	2.10	0.32	0.75	1.17	2.09	4.87
Al2O3	3.16	0.04	12.88	13.29	9.83	15.35	13.44	12.88
FeO	12.30	10.68	4.00	7.17	7.96	6.70	4.74	5.41
MnO	0.02	0.31	0.13	0.10	0.00	0.05	0.06	0.01
MgO	23.71	26.74	16.80	21.13	15.89	14.48	15.29	15.94
CaO	1.36	0.33	12.21	4.17	11.80	12.01	12.87	11.08
Na2O	0.21	0.04	1.59	0.75	1.18	1.78	1.80	2.70
Cr2O3	0.39	0.00	1.80	0.18	0.16	0.27	0.03	0.36
Total	96.54	96.87	96.68	100.35	96.44	96.13	94.23	95.60

	Tv 1	Tv 9	Tv 12	Tv 51	Tv 86	Tv 101	Tv 124	Tv 12
SiO2	44.48	40.02	44.08	46.37	40.68	43.11	44.11	24.77
TiO2	0.26	0.09	0.00	2.00	0.32	0.10	1.35	0.17
Al2O3	16.59	23.89	16.64	24.65	19.48	18.43	13.88	40.92
FeO	4.78	6.80	4.73	3.33	6.55	5.10	6.37	9.23
MnO	0.00	0.00	0.40	0.00	0.00	0.00	0.10	0.12
MgO	16.79	14.88	16.30	11.50	16.32	15.09	15.51	17.09
CaO	11.67	10.93	12.07	8.48	10.88	11.67	11.93	5.85
Na2O	2.77	1.88	2.70	0.75	2.55	2.37	1.98	1.56
Cr2O3	0.02	0.00	0.00	0.02	0.02	0.00	0.65	0.00
Total	97.36	98.49	96.92	97.10	96.80	95.87	95.88	99.71

	Tv 16/i	Tv 16/cr
SiO2	43.15	46.44
TiO2	2.15	0.00
Al2O3	13.21	14.85
FeO	6.39	6.36
MnO	0.05	0.13
MgO	15.92	15.93
CaO	12.26	12.29
Na2O	1.98	1.45
Cr2O3	1.67	0.00
Total	96.78	97.45

TABLE 9
MISCELLANEOUS MINERAL ANALYSES.

Chlorites

	Tv 5	Tv 21	Tv 24	Tv 26	Tv 29	Tv 31	Tv 35	Tv 62
SiO2	30.33	31.42	30.93	30.51	29.98	31.24	31.95	31.51
Al2O3	16.51	18.39	18.04	17.80	19.93	18.59	16.57	17.75
FeO	9.65	5.50	6.71	5.32	5.18	5.12	5.95	4.57
MgO	32.36	31.06	30.79	30.71	31.23	32.43	32.39	31.17
Cr2O3	0.73	0.00	0.63	1.06	0.06	0.04	1.22	0.08
Total	89.58	86.37	87.10	85.40	86.38	87.42	88.08	85.08

	Tv 63	Tv 63	Tv 23	Tv 12	Serpentine Tv 5	Tv 64
SiO2	32.39	28.62	31.90	0.00	39.87	36.81
Al2O3	16.17	10.99	17.36	63.27	1.47	0.00
FeO	4.36	16.34	5.85	16.38	3.07	5.10
MgO	32.39	31.17	30.02	19.77	40.25	41.21
Cr2O3	0.04	0.04	0.02	0.00	0.12	0.00
Total	85.35	87.16	85.15	99.42	84.78	83.12

Carbonates

	Tv 21	Tv 24	Tv 26	Tv 26	Tv 29	Tv 35	Tv 48	Tv 186
FeO	9.14	3.00	0.26	3.92	3.48	2.90	3.82	2.95
MnO	0.31	0.32	0.34	0.24	0.21	0.13	0.16	0.24
MgO	41.07	19.53	0.27	19.54	26.13	19.93	20.20	22.90
CaO	0.55	29.36	71.47	31.88	31.63	29.59	31.50	23.19
Total	51.07	52.21	72.34	55.58	61.45	52.55	55.68	49.28

Biotite

	Tv 8
SiO2	37.41
TiO2	1.25
Al2O3	18.58
FeO	7.42
MnO	0.00
MgO	19.63
CaO	0.31
Na2O	0.07
K2O	7.76
Cr2O3	0.19
NiO	0.13
Total	92.75